SIMULATION OF HEAT AND MASS TRANSFER IN A SOLAR-EXHAUST GAS GREENHOUSE DRYER FOR BLACK NIGHTSHADE SEEDS

GEORGE ONYANGO ORIDO

DOCTOR OF PHILOSOPHY

(Agricultural Processing Engineering)

JOMO KENYATTA UNIVERSITY

OF

AGRICULTURE AND TECHNOLOGY

2024

Simulation of Heat and Mass Transfer in a Solar-Exhaust Gas Greenhouse Dryer for Black Nightshade Seeds

George Onyango Orido

A Thesis Submitted in Partial Fulfilment of the Requirements for the Degree of Doctor of Philosophy in Agricultural Processing Engineering of the Jomo Kenyatta University of Agriculture and Technology

2024

DECLARATION

This thesis is my original work and has not been presented for a degree in any other university.

Signature: ……Date: …….

George Onyango Orido

This thesis has been submitted for examination with our approval as the university supervisors.

Signature: ……Date: …….

Dr. Eng. Erick K. Ronoh, PhD

JKUAT, Kenya

Signature: ……Date: …….

Dr. Patrick O. Ajwang, PhD

JKUAT, Kenya

Signature: ……Date: …….

Dr. Benson B. Gathitu, PhD

JKUAT, Kenya

DEDICATION

This work is dedicated to my wife, Mrs. Medrine Kwamboka, and my son, Wilson Ogola for giving me easy moments during my studies.

ACKNOWLEDGEMENT

To God be the glory for the mercy, grace, guidance, protection, faithfulness, strength, good health, and all the blessings that have led to my success in education and other endeavours. I am grateful for the encouragement and advice received from the Department of Agricultural and Biosystems Engineering and the entire College of Engineering and Technology, Jomo Kenyatta University of Agriculture and Technology (JKUAT). Special acknowledgement goes to the African Development Bank (AfDB) through the Ministry of Education Science and Technology (MoEST) for the financial support for this work. I would like to acknowledge the Japan International Cooperation Agency (JICA) through the AFRICA-*ai*-JAPAN Project Phase II (2022-2023) for providing financial support for this research work. I wish to sincerely thank my supervisors—Dr. Eng. Erick K. Ronoh, Dr. Eng. Patrick O. Ajwang and Dr. Benson B. Gathitu—for their continued support, guidance, and supervision.

TABLE OF CONTENTS

LIST OF TABLES

LIST OF FIGURES

LIST OF APPENDICES

ABBREVIATIONS AND ACRONYMS

AfDB	African Development Bank
AOAC	Association of Official Analytical Chemists
ASABE	American Society of Agricultural and Biological Engineers
BPNN	Back Propagation Neural Network
BMEP	Brake Mean Effective Pressure
ETSC	Evacuated Tube Solar Collector
EGR	Exhaust Gas Recirculation
EMC	Equilibrium Moisture Content
FPSC	Flat Plate Solar Collector
GAC	Ground Air Collector
GBDT	Gradient Boost Decision Tree
HRHE	Hybrid Recuperative Heat Exchanger
JKUAT	Jomo Kenyatta University of Agriculture and Technology
KMS	Kenya Meteorological Services
K-INCUD	Khwisero Integrated Community Umbrella Development
LGBM	Light Gradient Boosting Machine
LSD	Fishers Least Significant Difference
MRE	Mean Relative Error
MoEST	Ministry of Education Science and Technology
NDMA	National Drought Management Authority
NGPP	Natural Gas Processing Plant
PCM	Phase Change Material
PPCI	Partially Premixed Compression Ignition
RMSE	Root Mean Square Error
RE4Food	Renewable Energy for Food Processing
RNN	Recurrent Neural Network
RH	Relative Humidity
SGB	Stochastic Gradient Boosting
SHSM	Sensible Heat Storage Material
TIG	Tungsten Inert Gas

UNSDGs	United Nations Sustainable Development Goals
UK-AID	United Kingdom Aid
WMO	World Meteorological Organization
WLHP	Wraparound Loop Heat Pipe
Xgboost	Extreme Gradient Boosting

LIST OF NOMENCLATURES

Symbol	Description/Definition
A	Area (m^2)
$\dot{A}_{ex}$	Available thermal energy in exhaust gas (kJ/h)
A_C	The cross-sectional area (m^2)
a, b, c and n	Drying coefficients specific to each thin layer drying model
a_w	Water activity (equilibrium relative humidity)
C	Constant
C_{ex}	Specific heat capacity of exhaust gas (kJ/kg·℃)
$\dot{C}_{conv}$	Convection heat transfer rate in connectors (kW)
c_{conv}	Convection heat transfer coefficient in connectors (W/m^2·℃)
C_a	Heat capacity of air (kJ/kg·℃)
C_P	Specific heat capacity at constant pressure (kJ/kg·℃)
C_d	Coefficient of diffusivity
CN	Connectors
CN1 to CN6	Connectors numbered 1 to 6
C_{therm}	Thermal capacitance (kJ/℃)
C_r	Proportion of seeds having transverse or vertical stress cracks (%)
C_0 to C_4	Constants
D	Diameter of connector or tube components in heat exchanger (m)
DES	Diesel engine speed (rpm)
DR	Drying rate (g/g/h)
D_b	Diameter of berries
db	Dry basis
d_m	Dry mass in black nightshade seeds (kg/kg of black nightshade seeds)
E	Precision (acceptable error)
E_a	Activation energy corresponding to viability loss (Joule/mole)
F	Fraction of solar radiation
f	Friction factor
$f(t)$	Time dependent derivative

f_{CN}	Friction factor in connectors
f_{TB}	Friction factor in tubes
G_0	Initial germination of seed lot (%)
G_t	Germination after exposure time t hours (%)
$G_{t+\Delta t}$	Germination percentage at time $t + \Delta t$
GI	Germination index
G_1 and G_2	Coefficients
G	Acceleration due to gravity (m/s^2)
h	Specific enthalpy (kJ/kg)
h_{conv}	Convection heat transfer coefficient ($W/m^2 \cdot °C$)
h_a	Convection heat transfer coefficient of air ($W/m^2 \cdot °C$)
h_b	Convection heat transfer coefficient of black nightshade seeds ($W/m^2 \cdot °C$)
h_{ba}	Convection heat transfer coefficient from black nightshade seeds to air (bottom loss) = 5.7 $W/m^2 \cdot °C$
h_e	Evaporative heat transfer coefficient of black nightshade seeds ($W/m^2 \cdot °C$)
h_r	Radiative heat transfer coefficient ($W/m^2 \cdot °C$)
h_w	Convection heat transfer coefficient due to wind = 5.7+3.8υ ($W/m^2 \cdot °C$)
h_{ex}	Position of exhaust gas (m)
h_l	Total head loss (m)
h_f	Frictional head loss (m)
h_m	Minor head loss (m)
I	Solar intensity (W/m^2)
I_t	Solar intensity on horizontal surface (W/m^2)
I_i	Solar intensity on greenhouse dryer wall/roof (W/m^2)
I_{effB}	Rate of thermal energy received at black nightshade seeds surface
I_{effG}	Rate of thermal energy received at floor surface of greenhouse dryer
I_{effR}	Rate of thermal energy received by greenhouse dryer air
k, k_0, and k_1	Drying constants (h^{-1})

k	Thermal conductivity (W/m·°C)
K	Loss coefficient
KE	Kinetic energy (kJ)
KE_{ex}	Exhaust gas kinetic energy (kJ)
K_v	Constant
K_i	Constant
L	Length of connector or tube in heat exchanger (m)
L_C	Characteristic length (m)
MR	Moisture ratio
MW	Mega Watt
M	Moisture content (% db)
M_e	Equilibrium moisture content (%)
M_m	Monolayer moisture content (%)
M_t	Moisture content (% db) at time t (h)
M_i	Initial moisture content (% db)
m_d	Final mass (g) of dried sample
m_t	Dried mass (g) of sample at time t (h)
m_i	Initial/instantaneous sample mass (g)
m_{i-1}	Sample mass (g) preceding instantaneous sample mass (g)
m_{ev}	Moisture evaporated (g)
m_{ex}	Mass of exhaust gas (kg)
$\dot{m}_{ex}$	Mass flow rate of exhaust gas (kg/h)
$\dot{m}_{ex.\ in}$	Inlet mass flow rate of exhaust gas (kg/h)
$\dot{m}_{ex.\ out}$	Outlet mass flow rate of exhaust gas (kg/h)
N	Number of data points or total observations
N_c	Number of correctly predicted values
N_0	Number of observations in each set
N_t	Number of trial data
N_s	Number of seeds in a berry
N_{so}	Observed number of seeds in a berry
N_{sp}	Predicted number of seeds in a berry

n_P	Number of parameters
Nu	Nusselt number
Nu_{cn}	Nusselt number in connectors
Nu_{tb}	Nusselt number in tubes
n	Direction normal to surface area
O_i	Observed values
$\widehat{O}_i$	Average of observed values
P_i	Predicted values
$\widehat{P}_i$	Average of predicted values
P	Pressure (kN/m^2)
$P(T)$	Partial vapour pressure at temperature T (N/m^2)
Pr	Prandtl number
PM	Particulate matter
P_{ex}	Exhaust gas pressure (kN/m^2)
$P_{ex.\ in}$	Exhaust gas inlet pressure (kN/m^2)
$P_{ex.\ out}$	Exhaust gas outlet pressure (kN/m^2)
PE	Potential energy (kJ)
$PE_{ex.\ in}$	Exhaust gas inlet potential energy (kJ)
$PE_{ex.\ out}$	Exhaust gas outlet potential energy (kJ)
p_{50}	Mean viability period of seeds in days
$\dot{Q}_{ex}$	Exhaust gas volumetric flow rate (m^3/h)
$\dot{Q}_{conv}$	Convection heat transfer rate (kJ/h)
$\dot{Q}_{cond}$	Conduction heat transfer rate (kJ/h)
$\dot{Q}_e$	Rate of heat utilized to evaporate moisture ($J/m^2 \cdot s$)
R	Gas constant = 8.315 Joule/mole K
R^2	Coefficient of determination
R_{therm}	Thermal resistance
Re	Reynolds number
Re_{cn}	Reynolds number in connectors
Re_{tb}	Reynolds number in tubes
r^2	Coefficient of correlation

rpm	Revolutions per minute
r_i	Inner radius (m)
r_o	Outer radius (m)
R	Cross-correlation between x and y
SE	Standard error
S	Specific entropy (kJ/kg·°C)
S_A	Surface area (m^2)
T	Temperature (°C)
T_{amb}	Ambient temperature (°C)
T_a	Absolute temperature (K)
T_{am}	Absolute temperature during the interval Δt (K)
TB	Tubes
TB1 to TB6	Tubes numbered 1 to 6
T_{ex}	Exhaust gas temperature (°C)
T_s	Heat exchanger surface temperature (°C)
T_b	Black nightshade seeds temperature (°C)
T_r	Greenhouse dryer room air temperature (°C)
T_i	Average of black nightshade seeds and humid air temperature (°C)
T_v	Exit humid air temperature (°C)
$\dot{T}_{conv}$	Convection heat transfer rate in tubes (kW)
t_{conv}	Convection heat transfer coefficient in tubes (W/m^2·°C)
t	Drying time (h)
t_i	Instantaneous drying time (h)
t_{i-1}	Drying time (h) preceding instantaneous drying time (h)
t_v	Storage time in days for the percentage viability to fall to v
U	Overall heat loss (W/m^2·°C)
U'	Parameter for % internal uncertainty
U_{ex}	Exhaust gas total internal energy (kJ)
u_{ex}	Exhaust gas specific internal energy (kJ)
V_{ex}	Velocity of exhaust gas (m/s)
$V_{ex.\ in}$	Exhaust gas inlet velocity (m/s)

$V_{ex.\ out}$	Exhaust gas outlet velocity (m/s)
V_{cn}	Average velocity of exhaust gas in connectors (m/s)
V_{tb}	Average velocity of exhaust gas in airtight tubes (m/s)
V	Volume of greenhouse dryer (m^3)
V_{HEX}	Volume of heat exchanger (m^3)
WD	Work done (kJ)
$\dot{W}_P$	Work done by pressure forces (kJ)
$W_m = \frac{X_m}{X_{m0}}$	Dimensionless water content
X_m	Water content on dry basis (kg water/kg dry matter)
X	Characteristic dimension (m)
$\overline{X}$	Sample mean
$X - \overline{X}$	Deviation of observation from mean
x_i	Series 'x'
$\bar{x}$	Means of 'x'
$x_{predicted}$	Predicted 'x' value from model
$x_{measured}$	Measured 'x' value of variable
$y_{jexp} - y_{jcal}$	Differences between experimental and calculated data
y_i	Series 'y'
$\bar{y}$	Means of 'y'
Z	Standard variate value
Z_1 and Z_2	Constants

Greek letters

Symbol	**Definition**
ΔH	Difference in pressure head (m)
Δm	Change in mass (g)
ΔP	Difference in partial pressure head (N/m^2)
ΔT_{ex}	Temperature difference (°C)
Δt	Change in time (h)
Ω	Moisture evaporated model parameter

α	Absorptivity
β	Coefficient of volumetric expansion (1/°C)
γ	Relative humidity
ε	Emissivity
ϵ	Absolute residual error
ζ	Greenhouse dryer room air temperature model parameter
η_p	Prediction performance
λ	Latent heat of vaporization (J/kg)
μ	Dynamic viscosity ($N{\cdot}s/m^2$)
ξ	Black nightshade seeds model parameter
ϖ	Random error parameter in black nightshade seeds model
ρ	Density (kg/m^3)
ϱ	Random error parameter in greenhouse dryer room air temperature model
σ	Stefan-Boltzmann constant $= 5.6696 \times 10^{-8}\ W/m^2{\cdot}K^4$
τ	Transmissivity
χ^2	Reduced Chi-square
ψ	Derivative

Subscripts

Symbol	**Definition**
0	Initial value
a	Air
b	Black nightshade seeds
ce	Black nightshade seeds to environment
e	Above black nightshade seeds
g	Ground or Greenhouse dryer floor
g∞	Greenhouse dryer floor to underground
gr	Greenhouse dryer floor to room air
i	Greenhouse dryer wall/roof ($i = 1,2,\ldots,6$)
m	Mass
n	North wall or constant

r	Greenhouse dryer room air
v	Humid air or vent
$\|_{x=0}$	Surface of floor or greenhouse dryer
amb	Ambient
calc	Calculated
conv	Convection
cond	Conduction
crit	Critical
ex	Exhaust gas
expt	Experimental
pred	Predicted
sur	Surface
therm	Thermal

ABSTRACT

Diesel engines, used in Kenyan farms for stationary operations including milling, threshing, winnowing, and chopping of agricultural produce, generate exhaust gas which is released with heat energy to the environment. Moreover, the central problem facing farmers who produce drought resistant vegetable crops such as black nightshade in Kenya, is lack of a suitable drying method for the seeds to enhance continued biodiversity preservation. As a solution, heat energy from exhaust gas can be recovered and potentially utilized to dry black nightshade seeds. The main objective of this study was to simulate heat and mass transfer in a solar-exhaust gas greenhouse dryer for black nightshade seeds in order to predict drying time, seed and inside greenhouse dryer temperatures, and moisture evaporated from seeds. The methodology involved an experimental setup; instrumentation and data acquisition; and performance of activities within the specific objectives of the study. The results for the first specific objective showed that at optimal engine speed of 2500 rpm, exhaust gas volumetric flow rate was 0.0167 m^3/s; velocity was 8.52 m/s in connectors and 0.14 m/s in tubes, while Reynolds number was 10674 in connectors and 1368 in tubes. Consequently, 105 seconds elapsed for the 1.8 m^3 heat exchanger to be filled with 1.3 kg of exhaust gas possessing kinetic energy of 39.79 kJ in connector number six and 0.01289 kJ in the sixth tube. In addition, exhaust gas temperature of 357.36℃ at a mass flow rate of 45.07 kg/h had 16002.56 kJ/h as available energy. The maximum frictional head loss reported was 71 m in the sixth connector and 0.00225 m in tube number six. For the second specific objective, the results showed that the heat exchanger raised the dryer temperature by an hourly average of 11.78℃ in the solar-exhaust gas mode and 8.04℃ when temperature differences between inside and outside were compared in the exhaust gas mode of drying. Moreover, the rate of heat energy utilized for the three modes of drying were: solar (37.33-683.3 $J/m^2 \cdot s$), solar-exhaust gas (40.49 to 685.94 $J/m^2 \cdot s$), and exhaust gas (21.69 to 668.11 $J/m^2 \cdot s$). The convective transfer coefficients of black nightshade seeds ranged between 2.48 and 2.55 $W/m^2 \cdot ℃$ and those of evaporative heat transfer coefficients were found to be between 0.95 and 36.81 $W/m^2 \cdot ℃$. The results for the third specific objective demonstrated that in the solar mode, seeds took 11 hours to reach a final moisture content of 7.13% (db) from an initial one of 89.34% (db). In the solar-exhaust gas mode, seeds dried from an initial moisture content of 92.57% (db) to a final one of 6.07% (db) in 10 hours. In the exhaust gas mode, it took 14 hours to dry black nightshade seeds from an initial moisture content of 88.84% (db) to a final one of 9.42% (db). Further, the Page model was found suitable for solar mode with the highest coefficient of determination (R^2) of 0.9985 and the lowest root mean squared error (RMSE) of 0.0115. However, the Logarithmic model was found suitable for both solar-exhaust gas and exhaust gas modes of drying with RMSE of 0.0172 and 0.0232, and with the highest coefficient of determination (R^2) of 0.9964 and 0.9933, respectively. Based on the results for the fourth specific objective, the exhaust gas drying mode had a difference of 12.5% when its mean germination percentage was compared to the solar mode. Moreover, a 16.2% difference in means of germination percentage was recorded when the solar-exhaust gas mode of drying was compared to the exhaust gas mode. The highest mean germination percentage was recorded at 89% for exhaust gas drying mode.

Modified Giner's model predicted germination changes of black nightshade seeds more accurately than modified Sharp's model due to the higher R^2 (0.6896 > 0.6853) and lower RMSE (6.1554 < 6.4519). The activation energy in the modified Giner's model was found to be 7.034×10^3 Joule/mole through model fitting to experimental data. In conclusion, the concept of using a hybrid recuperative heat exchanger in a solar-exhaust gas greenhouse dryer was successfully applied in the recovery of exhaust gas energy from a diesel engine—heat energy that under normal circumstances is wastefully released to the environment—and it is, therefore, recommended that the solution studied in this work be extended to the recovery of waste heat energy from hammer mills operated on diesel engines in Kenya. Finally, the feasibility of exhaust gas heat energy use in drying can be expanded to seeds of other African vegetable crops.

CHAPTER ONE

INTRODUCTION

1.1 Background of the Study

Globally, international initiatives to preserve climate have been supported by several countries which are fulfilling their objectives under relevant treaties. To achieve this, large projects (Ingold, 2017) are underway to modernize global sectors of the economy including energy (Luijten, 2005), industry, agriculture (Scherr *et al*., 2012), transport as well as housing and utilities. This stresses the fact that climate conservation is a common goal for all mankind and that there is need to work and put together common to all, clear, fair, and transparent climate regulation rules to be applied globally (Jarso, 2012).

According to Shepard (2021), the latest report on the state of Africa's climate by the World Meteorological Organization (WMO), in partnership with African Union agencies, paints a grim picture of the continents ability to adapt to the increasingly frequent weather disasters. Shepard (2021) reported that the year 2020 was Africa's third warmest year on record, 0.86℃ above the average temperature in the three decades leading to 2010. It has mostly warmed slower than high latitude temperate zones, but the impact is still devastating. According to Yadoo and Cruickshank (2012), it is estimated that by 2030 the continent will be exposed to extreme heat as Africa has long been expected to be impacted by climate change.

The concerns of climate change and persistent droughts in Africa have led to the conceptualization of the current work of processing (drying) the seeds of a drought resistant vegetable crop, black nightshade (*Solanum villosum*), for biodiversity preservation. Changes in climate and weather patterns in Kenya have most often affected the optimum time for black nightshade seeds collection from the crop especially during the prolonged wet seasons at seeds harvesting (Ondieki *et al*., 2011). This is one of the challenges that affect the production of the drought resistant black nightshade.

During the wet humid weather, farmers have been forced to harvest early and allow the seeds to continue drying under a cover because rain has been proved to ruin black nightshade seeds in a short period of time. Traditionally, in the Western parts of Kenya (Ekhuya *et al*., 2018), black nightshade seeds have initially been open sun dried then placed in a ventilated package over a traditional fireplace for continued drying and preservation from borers and beetles which are repelled by the smell of soot and smoke. The current work borrowed from this practice and implemented a post-harvest processing technology of using solar-exhaust gas heat energy to dry black nightshade seeds.

Ondieki *et al*. (2011) reported that black nightshade (*Solanum villosum*) prefers low humid conditions due to lower incidence of fruit and foliar disease. In general, *Solanaceaes* such as black nightshade perform best during warm weather, flowering, and fruiting during the hot seasons. Better pollination in black nightshade translates to more seeds formed in the fruit, and therefore, larger fruit within a given species (Ekhuya *et al*., 2018). Black nightshade berries are harvested when mature and the skin is hard to resist thumbnail pressure.

The central problem facing drought resistant vegetable crops such as black nightshade in Kenya is how to dry and preserve the seeds for continued biodiversity preservation (Nakhauka, 2009). In the rural parts of Western Kenya, underdeveloped black nightshade seed systems and poor accessibility has been blamed for the low presence of black nightshade vegetable crop (Dube *et al*., 2018; Samuels, 2015). To counter this, the current work employed a new post-harvest technology to dry black nightshade seeds and strengthen the seed supply chain in Kenya. This is in line with the informal seed system channel for processing of high-quality black nightshade seeds with high germination rates which can then be shared with Kenyan farmers.

Croft (2016) reported that current seed support systems for black nightshade vegetables are informal and farmers in Western Kenya need to be provided with black nightshade seeds and technical information on processing of these seeds. According to Ndegwa and Kinyua (2018), Kenyans living in at least two thirds of land in the country fall in either arid to semi-arid zones with minimal or zero agricultural activities. It is

in these areas that a report from National Drought Management Authority (NDMA) shows the need for redress to upscale food production. To remain resilient to hostile environment, farmers in arid and semi-arid region need to embrace farming of this drought resistant vegetable crop (black nightshade), which performs well in water stressed areas.

Farmers have also learned different ways of diversifying black nightshade's use food and nutrition, medicinal, fodder a progress attributed to the ongoing sensitization of farmers from various food production stakeholders (Kamga *et al*., 2013). It is the realization of the existing benefits and markets for the produce that has led this study to dry and preserve black nightshade seeds. Dube *et al*. (2018), have advised that farmers should not stick to crops that fail. The weather is changing, and it is impossible to feed the Kenyan population if farmers cannot grow what can survive in bad weather. Growing high producing and drought resilient vegetable crops (black nightshade) is a good choice a farmer can make to escape from hunger. The proceeds from the black nightshade farming are encouraging because there is a ready market in the cities, urban and rural parts of the country (Chadha *et al*., 2006).

Kenyan economy is mainly anchored in farming, which provides more than 85% (Eichsteller *et al*., 2022) of the population jobs spread across the whole production and consumption chain. The issue of hunger will be addressed if farmers in areas such as Baringo, Kilifi, Garissa and Mandera grow crops which are drought resistant (Barrett *et al*., 2021) because these are dry areas. Presently, more than 1.3 million Kenyans (Laban *et al*., 2021) are threatened with hunger and malnutrition in the Eastern, North-Eastern, and Coastal parts of the country. Worse still, the Kenya Meteorological Services (KMS) has in the latest forecast predicted a rather dry season in most parts of the country. This will affect farming activities.

In the recent past, a lot of research interest has emerged worldwide on the utilization of exhaust gases energy for useful works (Wahile *et al*., 2020; Agudelo *et al*., 2016; Wang *et al*., 2013). The present work used a post-harvest processing technology that involved drying black nightshade seeds using solar and exhaust gas heat energy in a greenhouse dryer. Matured seed-bearing portion of the vegetable crop was dried to

maintain seed quality (germination and vigour) for subsequent planting. The current method was used to prevent mould and decay that cause damage to black nightshade seeds. This work was done to save seeds from one season to the next for continued biodiversity preservation.

Open sun drying is not feasible due to some drawback like the slowness of the process in days when radiation is below average (Jnyana *et al*., 2015). Therefore, an effective and quality drying technique using a solar-exhaust gas greenhouse dryer is essential for black nightshade seeds drying. This technique was found affordable and easily handled by rural farmers. Akhter *et al*. (2007) have demonstrated the utilization of exhaust gas heat energy from a diesel engine in a paddy dryer for rice.

Diesel engines have compression ratios ranging from 14 to 16 (Armstead & Miers, 2014). The engines achieve a high level of performance by compressing air to high pressures before injecting exceedingly small droplets of fuel into the combustion chamber. From the total heat energy supplied to the engine in the form of fuel energy, approximately, 30-40% is converted into useful mechanical work (Gaede & Meadowcroft, 2016). The heat energy which remains, around 60-70% of the fuel energy, is lost as waste heat and 30% is expelled through exhaust gases to the environment. Studies have shown that exhaust gases immediately leaving the engine can have temperatures as high as 450-600°C (Jadhao & Thombare, 2013). It is this heat energy which is lost to the environment that was of interest in this study.

1.2 Statement of the Problem

One of the problems facing drought resistant vegetable crops such as black nightshade in Kenya is how to dry and preserve the seeds for continued seasons planting (biodiversity preservation). Improper drying conditions make seeds to suffer from major retarding effects which include loss of viability, discolouration, toxin production, and fungus growth (McCormack, 2004). Complaints from small scale farmers in Western Kenya have been on how to maintain black nightshade seed quality (germination and vigour) and viability for subsequent genetic diversity preservation. The current study aimed to use, besides solar, waste heat from exhaust gas of an internal combustion stationery engine to dry black nightshade seeds. It is reported that

more than 60% of the fuel energy supplied to an internal combustion engine is lost (Jadhao & Thombare, 2013) to the environment. About 30% of fuel energy is lost in the form of heat through the exhaust system. There is a need, therefore, to develop strategies to recover waste energy from internal combustion engines of stationary agricultural machines doing milling operations for useful work drying of black nightshade seeds.

1.3 Objectives

1.3.1 Main Objective

The main objective of this study was to simulate heat and mass transfer in a solar-exhaust gas greenhouse dryer for black nightshade seeds in order to predict drying time, seed and inside greenhouse dryer temperatures, moisture evaporated from seeds and the impact of heat and mass transfer on seed drying and seed quality.

1.3.2 Specific Objectives

The specific objectives of this study were to:

(1) Establish the relationships between characteristics (fluid and thermal) of exhaust gas, and design parameters of a hybrid recuperative heat exchanger used in a solar-exhaust gas greenhouse dryer.
(2) Develop a hybrid recuperative heat exchanger and evaluate its performance using experimental temperature and moisture evaporation data.
(3) Evaluate thin layer drying models for simulating drying kinetics of black nightshade seeds in a solar-exhaust gas greenhouse dryer.
(4) Determine the influence of solar-exhaust gas greenhouse drying modes on viability of black nightshade seeds.

1.4 Research Questions

(1) How do characteristics (fluid and thermal) of exhaust gas relate to design parameters of a hybrid recuperative heat exchanger in a solar-exhaust gas greenhouse dryer?

(2) How does a developed hybrid recuperative heat exchanger perform in a solar-exhaust gas greenhouse dryer?
(3) Which thin layer drying model best describes the drying kinetics of black nightshade seeds in a solar-exhaust gas greenhouse dryer?
(4) How do drying modes in a solar-exhaust gas greenhouse dryer influence viability of black nightshade seeds?

1.5 Justification of the Study

Communities in Western Kenya have utilized black nightshade vegetables for food and valued them for their taste, nutritional qualities, and medicinal properties. With increasing demand for this vegetable crop, there is dire need for a formal reliable source of quality seeds and the need to study and develop seed processing systems for black nightshade in Kenya. It is important to properly dry black nightshade seeds to preserve genetic diversity and development of value chain. Chadha *et al*. (2006) have reported that open sun drying exposes black nightshade seeds to insects especially borers and beetles that feed on the seeds. Exposing black nightshade seeds to full sun (open sun drying) causes overheating, killing the embryos, especially in humid climates. This must be avoided as it reduces viability. Slow open sun drying may result in mould growth or premature sprouting of the seed especially when solar radiation is low. According to McCormack (2004) seeds should not be dried in the open sun, nor should they be dried anywhere where the temperature exceeds 35°C. These seeds are especially vulnerable to damage when open sun dried a practice which is unfortunately common in Western Kenya. Black nightshade seeds are blown away by wind forces when dried in unprotected open sun environment. Instead, seeds should be dried in a climate-controlled environment a solar-exhaust gas greenhouse dryer used in this work. This method dried black nightshade seeds safely and quickly when the seeds were spread out in thin layers and then stirred several times until dry. Consequently, the potential for solar drying, combined with exhaust gas heat energy utilization, is promoted through this work which contributes knowledge towards enhanced understanding of a new post-harvest processing technology for black nightshade seeds. The aspect of reduced heat being released to the environment is a win for the current study. The implementation of this work's findings has the potential impact of helping

many farmers to promote biodiversity of black nightshade vegetable crop. The current work contributes to United Nations Sustainable Development Goals (UNSDGs) number one (1) of no poverty, number two (2) of zero hunger, number eleven (11) of sustainable cities and communities and number seventeen (17) of partnership for the goals.

1.6 Scope and Limitations of the Study

This study considered Western region of Kenya, Central Rift Valley, and Central region of Kenya as its geographic scope. Black nightshade (*Solanum villosum*) seeds were obtained from Western Kenya, a low altitude area with optimal ecological requirements for the vegetable crop's growth. Design of the hybrid recuperative heat exchanger for the solar-exhaust gas greenhouse dryer was performed in Central Rift Valley (Nakuru). Development (fabrication) of the heat exchanger was carried out in Nairobi. Testing of the heat exchanger inside a solar-exhaust gas greenhouse dryer took place in Juja, Kiambu County—Central region of Kenya. Evaluating the influence of drying modes on viability of the vegetable crop's seeds was done partly in Central region of Kenya (Juja)—the location of Jomo Kenyatta University of Agriculture and Technology (JKUAT) and partly in Central Rift Valley (Nakuru)—the location of Egerton University.

This study introduced a new approach for processing black nightshade seeds and focused on drying extracted seeds from berries. The research aimed at the recovery of exhaust gas heat energy from an internal combustion diesel engine. The heat energy was used in a solar-exhaust gas greenhouse dryer when radiation was low and at night. The study focused on three drying modes: solar, solar-exhaust gas, and exhaust gas. Measurements of black nightshade seeds temperature and greenhouse dryer room air temperature were done. Changes in the seeds' mass (moisture evaporated) were recorded during drying. Relative humidity data was collected. Germination percentage data was collected for analysis and fitting of germination models. Finally, the work is linked to climate change and aimed at agriculture policy makers to address challenges related to economic and environmental sustainability of exhaust gas energy utilisation for drying.

CHAPTER TWO

LITERATURE REVIEW

2.1 Theoretical Review

2.1.1 Solar Greenhouse Drying Technology

Several attempts have been made in recent years to use solar energy for drying mainly to preserve agricultural produce and get the benefit from the energy provided by the sun (Kiburi *et al*., 2020a; Ndirangu *et al*., 2020; Ronoh *et al*., 2010). Drying is a dual process in which simultaneous heat and mass transfer lowers the moisture content by supplying thermal energy. In a study by Ndirangu *et al*. (2020), the system performance of a developed multipurpose solar-biomass greenhouse dryer improved when solar energy was backed up with biomass energy. The drying increased by about 18-19% using solar-biomass mode compared to both natural and forced convection modes. The authors recommended more tests to be undertaken to fully analyze the dryer's performance, especially in optimizing biomass use to achieve desired temperatures.

Drying is among the easiest and more affordable ways of preserving black nightshade seeds through moisture content reduction by application of heat to the seeds. The abundance of solar energy has made greenhouse solar drying a possibility in dryers designed for agricultural produce. Kiburi *et al*. (2020a) developed a solar-biomass hybrid greenhouse dryer consisting of a biomass stove and double duct heat exchanger when drying banana slices. The authors concluded with a recommendation of nighttime drying using biomass followed by daytime drying using appropriate energy mode solar or a combination of solar-biomass to save on drying time.

Ronoh *et al*. (2020) reported the importance of thin layer drying models as tools used to describe drying kinetics of agricultural produce. Improvement of drying was reported by the authors as an advantage that positively affect the design of efficient dryers thus preventing the sole reliance on experimental drying practices without considerations of the mathematics of drying kinetics. Thin layer drying of black

nightshade seeds was performed in the present work to determine the drying kinetics of the product involving simultaneous heat and mass transfer operations with an aspect of mathematical modeling of the drying process. According to Chowdhury *et al*. (2011) and Hii *et al*. (2009) thin layer drying models fall into three categories: theoretical, semi-theoretical, and empirical. Newton, Page, Logarithmic and Henderson and Pabis models are classified under semi-theoretical models which offer a compromise between theory and ease of application. Ronoh *et al*. (2020) argued that food drying kinetics is a complex phenomenon requiring simplicity for drying behaviour prediction and optimization of parameters. On prediction accuracy of thin layer drying models, the authors reported that the selection and appropriateness of a model in describing the drying behaviour of an agricultural produce may not depend on the number of constants or coefficients but on statistical indicators as supported by Onwude *et al*. (2016).

Kiburi *et al*. (2020a), while evaluating the performance and economic feasibility of a solar-biomass hybrid greenhouse dryer for drying banana slices, have reported results that showed significant difference between statistical means of drying rates of banana slices for three energy modes: solar, biomass, and solar-biomass. Further analysis, however, showed insignificant difference between drying rates of solar and solar-biomass as well as biomass and solar-biomass. The energy and exergy efficiency for solar mode have been found to be lower than those of biomass and solar-biomass modes. The payback period of the dryer has been found to be <1 year, a figure lower than the expected life of the dryer (4 years). In conclusion the study has reported that use of biomass as supplemental heat source increased annual revenue by 147.59% in reference to the solar mode only.

According to Natesan *et al*. (2020), new hybrid drying systems have been utilized and investigated by many researchers for improving the drying characteristics of products. The authors in a review of applications of thin layer modelling techniques and advances in drying of agricultural products, have classified solar dryers as active (forced convection) and passive (natural convection) types. Further classification has revealed integral-type, distributed-type, and mixed-mode dryers. Integrated type solar dryers have been reported to be available as cabinet and greenhouse solar dryers. In

the current work, a solar-exhaust heat greenhouse dryer is proposed for black nightshade seeds drying.

In a study by Ronoh *et al*. (2010), the disadvantages of open sun drying have been cited as: lack of temperature control, intensive labour, and contamination—from dust, foreign materials, rodents, and birds' droppings. The study revealed that a natural convection solar tent dryer would be a useful drying technique for safe preservation of amaranth grains. Thus, the drying technique has been utilized to enhance drying of amaranth grains in layers without significantly affecting physical, optical, and nutritive properties.

The RE4Food (Renewable Energy for Food Processing) is a collaborative project funded by UK-AID for three and a half years (2013-2016). The project has addressed research challenges associated with increasing food security and reducing reliability on fossil fuels. A solar drying technology has been introduced through this project to address the challenge of an inefficient system for food preservation. Through the project, a multipurpose solar-biomass dryer has been developed and piloted with the Khwisero Integrated Community Umbrella Development (K-INCUD) group, in Kakamega County (Kanali *et al*., 2017). In previous works, heat flow equations have been developed for various locations in a greenhouse dryer. Heat flow has been an essential determining factor of the mean state of heating and cooling within a greenhouse dryer, as the flow of energy through the greenhouse dryer is basically tied to its spatial and temporal structure and the variance of greenhouse dryer temperature, humidity, air flow, and the greenhouse dryer cover (Mishra *et al*., 2021; Chaudhari & Salve, 2014).

It is considered that the systematic flow of heat through a greenhouse dryer involves all components of the climate system, and its hydrology. Therefore, inconsistency in any one component affects the others. Similarly biases in any one component can undermine the simulation and an improved understanding of the heat flows within a greenhouse dryer. According to Kiyan *et al*. (2013), technical equipment may be used to efficiently maintain a greenhouse dryer air temperature and relative humidity at

acceptable levels during hot periods, but adequate models will be necessary to estimate the heating loads and adequately manage such control equipment.

The most used solar systems are the conventional flat plate solar collectors (FPSCs); however, payback period of these systems is considerably long when used for greenhouse dryer heating; also, the seasonal storage of solar energy is somewhat inadequate compared to daily storage (Garcia *et al*., 1998; Kurata & Takakura, 1991). In the last couple of decades, due to high efficiency and anti-freezing properties, evacuated tube solar collector (ETSC) has become the most popular design for solar water heating, and currently has more than 80% share in solar water heating market (He *et al*., 2012). It has been reported that, glass evacuated tube solar collectors have better thermal efficiencies at higher temperatures compared to the FPSCs and they are suitable for applications above 80°C (He *et al*., 2012; Tang *et al*., 2009). ETSC collect both direct and diffuse radiation like FPSCs, and they also have higher efficiencies at low incidence angles (Kalogirou, 2004).

Kiyan *et al*. (2013) posted results of simulations in a greenhouse located in Şanlıurfa/Turkey. The results of simulations performed on an annual basis have indicated that revising the existing fossil fuel system with a proposed hybrid system is economically feasible for most cases, however, it requires a slightly longer payback period than expected. On the other hand, by reducing greenhouse gas emissions significantly, it has a considerable positive environmental impact. The developed dynamic simulation method can further be used for designing heating systems for various solar greenhouses and optimizing the solar collector and thermal storage sizes.

In hybrid type, fossil fuels or biomass are used with solar energy and the drying rate is fast (Natesan *et al*., 2020). Research works have been carried out to analyze the effectiveness of various drying systems by studying the drying kinetics like moisture content, drying air temperature, air velocity, and drying rate. Kiyan *et al*. (2013) reported that solar energy is a major renewable energy source and hybrid solar systems are gaining increased academic and industrial attention due to the unique advantages they offer. Heating systems such as ground air collector (GAC), north wall storage and

movable insulation are also used for increasing greenhouse dryer air temperatures (Sethi & Sharma, 2008).

Due to increasing prices, utilization of fossil fuel is becoming expensive. As other alternatives, some farmers use renewable energy sources like solar assisted ground source heat pumps (Dai *et al*., 2015), geothermal heating systems, solar panels and biomass derived fuels for greenhouse dryer heating due to high fossil fuel prices. However, geothermal and biomass assisted greenhouse dryer heating are more site-specific solutions compared to solar based systems. The current work has necessarily proposed the utilization of exhaust gas heat energy from an internal combustion engine as an auxiliary heating source in a solar-exhaust gas greenhouse dryer. The use of exhaust gas heat and reduction in fossil fuel consumption via utilization of solar energy can help to tackle climate change due to reduction in greenhouse gas emissions. This will further reduce the impact of energy utilization on the environment. The present work considered the interaction between the heat flows in a greenhouse dryer and feedback in the climate system because heat flows of the modern-day greenhouse dryers are weather dependent. As a result, questions loom large about how the energy in the greenhouse dryer changes as global warming progresses, and a better simulation of the modern-day greenhouse dryer heating requirement is an essential first step in heat flow analysis.

The components involved in a greenhouse dryer design are the cladding material, shape, and orientation, together with the technical equipment needed to control the microclimate inside the greenhouse dryer (Choab *et al*., 2019). The greenhouse drying process has been extensively used by many farmers to protect and preserve food if possible. This widely known process is based on natural heating of the product to remove the moisture (Sangamithra *et al*., 2014). This method offers many advantages such as providing a simple design and the cost is low (Chauhan & Kumar, 2016; Perea-Moreno *et al*., 2016; Prakash *et al*., 2016; Tiwari *et al*., 2016; Lingayat *et al*., 2017). Many authors (Prakash & Kumar, 2013; Prakash & Kumar, 2014a; Sharma *et al*., 2009; Azaizia *et al*., 2017) have reported that solar greenhouse drying technology is a solution which allows the production of vegetables and fruits in hygienic and healthy conditions with nearly zero energy costs. Solar-drying technology has also been used

to dry farm products, marine products, and medicinal plants (Aritesty & Wulandani, 2014; Prakash & Kumar, 2014b).

It is beneficial to farmers to make precise predictions of hourly drying temperature for seeds in a dryer so that decisions relating to timely use of supplemental energy source are made. Greenhouse drying technique has been reported by Prakash and Kumar (2014b) as one of the proposed ways of minimising the shortcomings of open sun drying. Its suitability to perform low temperature drying of grains, fruits and vegetables has been documented under natural and forced convection modes of drying. Moreover, the technique has been proven to produce superior quality of dried products as compared to open sun drying. Product protection from rain, insects and animals is guaranteed in solar greenhouse drying. In the present study, a gabic even span roof type greenhouse dryer was developed to use solar radiation and exhaust gas energy from a diesel engine. The advantage realized from this kind of dryer has been reported by Srinivasan and Muthukumar (2021) in literature as proper mixing of inside drying air a quality synonymous with gabic even span roof type greenhouse dryers.

Kumar and Tiwari (2006) have critiqued the merits of greenhouse drying of jaggery in comparison to open sun and cabinet drying. In open sun drying the authors reported lack of controlled humidity which leads to increased drying time due to the hygroscopic nature of jaggery. High temperatures inside a cabinet dryer were cited as undesirable because they melt jaggery. Cost was further reported as a constraint with regard to cabinet drying especially when a similar volume of jaggery could be dried inside a greenhouse dryer. Reduction in drying time was mainly reported as the benefit for greenhouse drying of jaggery in a controlled environment of moderate temperature and humidity. Significantly, thermal modeling plays a role in greenhouse dryers design and development. It is used as an optimization tool for drying parameters and performance enhancement under different modes of operation. Thermal modeling is used to estimate temperatures for drying air and crops inside a greenhouse dryer. More parameters that can be estimated from thermal modeling include drying potential, drying rate, inside greenhouse relative humidity, and drying kinetics. Greenhouse drying, utilized throughout the world involves heat and mass transfer phenomenon where heat energy increases a product’s temperature in the form of sensible heat and

moisture in the product vaporizes through latent heat (Chauhan *et al*., 2017). Chauhan and Kumar (2016) evaluated coefficient of performance, heat utilization factor, convective heat transfer coefficient and coefficient of diffusivity in thermal performance analysis of a greenhouse dryer under natural convection mode.

2.1.2 Black Nightshade Vegetable Crop

Black nightshade is a species of flowering plant in the genus *Solanum*. Black nightshade (*Solanum villosum*) is a worldwide leafy herb and vegetable of arable land, gardens, rubbish tips, soil rich in nitrogen in moderately light and warm situations which occur from sea to montane levels (Edmonds and Chweya, 1997). Black nightshade is also commonly known as the red-fruit nightshade and is widely distributed in many parts of the world. The species is reported to be common in northern parts of Africa where it could well be native. It is widely distributed at altitudes of 792-3048 m above the sea level in Cameroon, Ethiopia, Kenya, Somalia, South Africa, Tanzania, and Uganda. The vernacular names of black nightshade in Kenya are: mnavu (Swahili), amanagu (Kisii), namasaka (Luhya), Kitulu (Kamba), ndunda (Taita), sochot (Keiyo), sujet (Kinandi), isusa (Maragoli), ol'momoit (Masai), soiyot (Kipsigis), managuu (Kikuyu), and osuga (Luo). Its propagation is through seeds which have a long shelf life depending on the storage conditions and the seeds moisture content the recommended being $5\pm1\%$ (Hong *et al*., 1996). Black nightshade seeds are planted in nurseries and the germination time is usually 5-7 days. The seeds sown will be in the nursery for one month from the time of sowing to transplanting. Black nightshade vegetable takes about 5 weeks from transplanting for the first harvest of the leafy vegetable to take place (Schippers, 1998).

According to Edmonds and Chweya (1997), black nightshade is an Ayurvedic herb with multiple medicinal properties. Ethnobotanical uses of black nightshade reported by the authors both in literature and herbarium material are based on beneficial properties such as: a source of food, nutritional value, medicinal value, and as a source of fodder; it is therefore of commercial value in both rural and urban settings. Throughout the world, boiled or stewed leaves and tender shoots of black nightshade are widely used as vegetables a food source during famine and in soups and sauces. In

the respective geographical ranges in Africa, the vegetable crop is used as port-herbs and the vegetative parts are boiled in water, which is discarded and replaced several times, or replaced with milk to add taste and flavor to the diet and make it delicious. Schippers (1998) has, however, reported that vitamins and other micro-nutrients are unfortunately thrown away with the discarded water, thereby reducing the nutritious value of black nightshade. In Kenya, black nightshade is used in both rural and urban areas with a good demand in Nairobi which can hardly be met by farmers from the surrounding areas such as Embu. Farmers from as far away as Kisii, South Nyanza, and Western Kenya have been reported to have made arrangements to transport their black nightshade produce to the capital city (Schippers, 1998). In the rural areas, the consumption of green leafy black nightshade is believed to result in the birth of children with dark eyes and smooth skin, therefore, the boiled leaves of the vegetable are recommended for pregnant women (Edmonds and Chweya, 1997). In addition, pregnant women who eat this vegetable are believed to recuperate well after delivery. In parts of Western Kenya, the orange ripe berries of black nightshade are frequently eaten raw as fruits. Edmonds and Chweya (1997) reported that several studies had been conducted to investigate the nutritive value of black nightshade. The authors summarized the nutritive value of the vegetable crop under nutrient per 100-g of edible portion and range of values as shown in Table 2.1.

The bruised fresh leaves of black nightshade are used externally to ease pain and reduce inflammation when applied to burns, used for ringworms, gout, and earache. In Western Kenya, black nightshade's reputation as a good gargle and mouthwash has been reported (Schippers, 1998; Edmonds & Chweya, 1997). The raw fruits of the vegetable crop when chewed and swallowed will treat stomach ulcers, general abdominal pain, and stomach-ache. Children who have developed crooked teeth may have infusions of leaves and seeds rubbed onto their gums to ease pain. Pounded leaves and fruits form an infusion used against tonsilitis, muscular and joint pains associated with malarial fever and arthritis. Cattle, sheep, and goats in Kenya are known to feed on black nightshade vegetable as fodder and browse. Macerated leaves and berries produce a dye and ink source used to colour sisal and baskets. This commercial value is realized because black nightshade is a useful source of colorants, the pigment is present in high concentration, it is vigorous and easy to grow. Most women from

Western Kenya have benefitted from the sale of the vegetable crop in both rural and urban markets (Schippers, 1998).

Table 2.1: Nutritive Value of Black Nightshade Per 100 G of Fresh Shoots or Leaves

Nutrient	Measure	Range of values
Water	%	83 - 91
Crude protein	g	2.8 - 5.8
Crude fibre	g	0.6 - 1.4
Fat	g	0.8
Carbohydrates	g	3.3 - 5.0
Calories	kcal	38
Etheral Extract	g	38 - 44
Total Ash	g	3.3 - 8.8
Iron	mg	1.0 - 4.2
Calcium	mg	90 - 442
Phosphorus	mg	75
Beta-Carotene	mg	1.7 - 11.6
Ascorbic Acid	mg	20 - 158
Oxalate	mg	58.8 - 98.5
Nitrate-N	mg	29 - 400
Total Phenolocs	mg	63.3 - 73.4

Source: Edmonds and Chweya (1997)

Black nightshade seed drying is a normal part of the seed maturation process. These seeds must dry down to minimum moisture content before they can germinate. Low black nightshade seed moisture content is a pre-requisite for long-term storage and is the most important factor affecting longevity. Black nightshade seeds lose viability and vigour during processing and storage mainly because of high seed moisture content greater than 84%. In the current work, a drying technology for black nightshade seeds is recommended to use solar-exhaust heat. This technology is proposed to have more control on drying parameters such as air flow rate, drying

temperatures, and relative humidity as opposed to open sun drying. High seed moisture causes several problems: moisture increases the respiration rate of seeds, which in turn raises seed temperature. For example, in large-scale commercial seed storage, respiring seeds may generate enough heat to kill the seeds quickly, or to even start a fire if not dried sufficiently. Small-scale growers are not likely to have such an extreme condition, but seed longevity will, nevertheless be affected. Mould growth is encouraged by moisture and will damage the seeds either slowly or quickly, depending on the moisture content of the seeds. Some moulds that do not grow well at room temperature may grow well at low temperatures causing damage to seed in cold environments. In such a case there may be no visual sign of damage. Unless seeds' moisture content is 8% and below, insects such as borers and beetles can breed on the seeds causing rapid destruction in a short period.

According to Dube *et al*. (2017), feeding the quickly growing population in Kenya remains a challenge and as the demand for food increases, climate change, on the other hand, poses more challenges to agricultural productivity, implying that the provision of sufficient quantities and qualities of food is threatened. Black nightshade vegetable is resilient to adverse weather conditions and is naturally rich in nutrients including vitamins A and C, iron, protein, and other micronutrients. There is need for research on seeds and development of seed systems for black nightshade vegetable crop. Preparation and processing methods for black nightshade vegetable products like cakes or flour is needed to increase its consumption, particularly among the young, elite, and urban dwellers.

2.1.3 Diesel Engine and Heat Exchangers

Heat exchangers are generally built of a bundle of round tubes mounted in a cylindrical shell with the tube axis parallel to that of the shell as described by Janssens and Cloudt (2013). One of the fluids flows inside the tubes, the other flows across and along the tubes. The major components of a heat exchanger are tubes (or tube bundle), shell, front-end head, rear-end head, baffles, and tube sheets (Morales *et al*., 2012). A variety of different internal constructions are used, depending on the desired heat transfer and pressure drop performance and the methods employed to reduce thermal stresses, to

prevent leakages, to provide for ease of cleaning, to contain operating pressures and temperatures, to control corrosion, and to accommodate highly asymmetric flows (Rubaiyat & Bari, 2010). The three most common types are: fixed tube sheet design, U-tube design, and floating-head type. In all three types, the front-end head is stationary while the rear-end head can be either stationary or floating, depending on the thermal stresses in the shell, tube, or tube sheet, due to temperature differences because of heat transfer.

Commercial waste heat recovery devices include, among others, recuperators and radiation or convective hybrid recuperators. Recuperators are also known as flat plate air-to-air heat-exchangers (Ogulata, 2004), in which heat exchange takes place between flue gases and air through metallic or ceramic walls. Duct or tubes carry the air for combustion to be pre-heated and the other side contains waste heat stream. The simplest configuration for a recuperator is the metallic radiation recuperator, which consists of two concentric lengths of metal tubing. The inner tube carries the hot exhaust gases while the external annulus carries the combustion air from the atmosphere to the air inlets of the furnace burners. The hot gases are cooled by the incoming combustion air which now carries additional energy into the combustion chamber. Studies have reported that additional energy does not have to be supplied by fuel (Karamarkovic *et al*., 2013; Ogulata, 2004; Maruoka *et al*., 2004). Consequently, less fuel is burned for a given furnace loading. The saving in fuel also means a decrease in combustion air and therefore stack losses are decreased not only by lowering the stack gas temperatures but also by discharging smaller quantities of exhaust gas as reviewed in studies that have used recuperators in steel making industry and rotary kilns (Karamarkovic *et al*., 2013; Maruoka *et al*., 2004). In a radiation recuperator a substantial portion of the heat transfer from the hot gases to the surface of the inner tube takes place by radiative heat transfer. The cold air in the annulus, however, is almost transparent to infrared radiation so that only convection heat transfer takes place to the incoming air. For maximum effectiveness of heat transfer, combinations of radiation and convective designs have been used (Ogulata, 2004), although they are more expensive but less bulky than simple metallic radiation recuperators.

Quoilin *et al*. (2011) have recommended further research on heat exchangers' thermal performance and pressure drop. The authors have further proposed more research on the effect of mass flow rate on friction factor and effectiveness of heat exchangers in the analysis of heat transfer. Several studies are dedicated to assessing the dynamic performance of single-phase heat exchangers as well as to two-phase ones (Feru *et al*., 2014; Morales *et al*., 2012; Quoilin *et al*., 2011), and the assessment of the impact of heat exchanger parameters on performance and effectiveness in a system still remains unclear. Sathiamurthi (2011) has concluded that waste heat is heat energy, which is generated in a process by way of fuel combustion or chemical reaction, and then dumped into the environment even though it could still be reused for some useful and economic purpose. This heat energy depends in part on the temperature of the waste heat gases and mass flow rate of exhaust gas (Kruiswyk, 2008).

2.1.4 Exhaust Gas Heat Energy as a Supplement to Solar Radiation

Energy demand is on the increase in Sub-Saharan Africa. This has necessitated the introduction of ways to fully utilize the available solar energy. One of the solutions to the energy demand increase is to supplement solar energy with heat energy recoverable from exhaust gas of diesel engines commonly used in the region for milling operations. Previous studies in a solar-biomass greenhouse dryer had variations of temperature, relative humidity, and solar radiation with time of the day reported by Kiburi *et al*. (2020a). The authors have reported average inside greenhouse dryer temperatures above 50°C when the dryer was on solar mode and drying was on a considered ideal period when the weather conditions were most suitable for the mode.

Cai *et al*. (2022) have proposed a gradient boost decision tree (GBDT) model based on a newly-developed light gradient boosting machine (LGBM) algorithm to model the internal temperature of a greenhouse. To compare the predictive accuracy, back propagation neural network (BPNN) model, recurrent neural network (RNN) model, two GBDT algorithms, extreme gradient boosting (Xgboost), and stochastic gradient boosting (SGB) were introduced as adaptive cross validation methods to improve the LGBM model performance and self-adaptive ability. The results in the study by Cai *et*

al. (2022) suggest that the LGBM has the best fitting ability for the temperature curves as well as the fastest training speed among all algorithms.

Manzela *et al*. (2010) have presented an experimental study on an ammonia-water absorption refrigeration system using the exhaust of an internal combustion engine as an energy source. The results from this previous study suggest that the cooling capacity can be highly improved for a dedicated system based on the calculated exhaust gas energy availability. Alklaibi and Lior (2021) in a study to utilize waste heat from internal combustion engines for power augmentation and refrigeration have found that the influence of integration of heat recovery systems on the engine emissions were negligible and the associated increase of the engine back pressure was found to be below the manufacturers' permissible value. In the study, the payback period of using waste heat recovery with diesel engines was found to be 2-6 years. Moreover, the authors have recommended a comprehensive economic feasibility analysis to consider the ongoing efforts for lowering carbon emissions, future carbon taxes on emissions, and potential changes in the cost of fuel, as well as studies that ensure long-term high-performance and robustness of the required waste heat recovery heat exchangers.

Lin *et al*. (2022) have applied a top-down energy efficiency analysis to develop a societal waste heat accounting model to quantify the amount of waste heat potential in China. The results from this study revealed that waste heat occupies 42% of the total primary energy inputs, and 26% of the primary energy and carbon emissions can be theoretically saved by utilizing waste heat. Further, the results in the study showed that the industry sector has a wide range of waste heat temperatures, mostly above 300℃. A recommendation from the study encouraged scholars to focus on the utilization of low-temperature waste heat, which is 66% of the total. López-Flores *et al*. (2022) have proposed a methodology for efficient, accurate, and sustainable waste heat recovery, where the energy needs of an industrial plant allow the installation of thermal engines (steam Rankine cycle, organic Rankine cycle, and absorption refrigeration cycle). The results from the study show that with the methodology, it is possible to find the optimal operating conditions of the thermal engines and solutions that allow the use of different fuels.

Toneatti *et al*. (2022) have proposed an innovative solution for recovering embedded energy from waste generated in a cruise ship. In detail, the authors have studied feasibility of an absorption plant's ability to exploit the residual energy of the flue gas of the ship's incinerator. The proposal from the authors is to use the recovered energy to control the temperature of the refrigerated store-rooms; operating simultaneously with, or in place of the existing compression vapors system already installed, to allow the reduction of CO_2 emissions and of fuel consumption. Siddiqui *et al*. (2021) have analysed a cooling-power cogeneration system driven by the exhaust gas heat of a homogeneous charge compression ignition engine fueled by wet-ethanol. The results from the study, computed for R134a, R290, and R600a working fluids, show that increase in turbocharged pressure ratio from 2.5 to 3.5 raises the thermal efficiency of the cooling-power cogeneration from 47.87% to 50.09% when R134a is used as a working fluid.

Khaliq *et al*. (2021), by establishing a thermodynamic model, conducted the simulation and parametric analyses of a proposed system where a natural gas-fueled homogenous charge compression ignition engine was coupled to an exhaust gas operated turbine driven two-phase ejector cycle to generate power and cooling energy, simultaneously. In the study, the results from the analyses of the two-phase ejector cooling cycle using three working fluids, R717, R290, and R600a, reveal that the thermal efficiency of the engine is increased from 47.44% to 49.94%, and for the R600a operated combined cycle, it is increased from 60.05% to 63.26% when the equivalence ratio is promoted from 0.3 to 0.6.

Previous authors (Thakar *et al*., 2018) have reported exhaust gas temperatures of 220-370℃ from a single cylinder diesel engine used in rural areas for agricultural purposes and this heat energy if not harvested for useful work is unjustifiably lost to the environment. A comparative study by Pati *et al*. (2015) utilized the concept of waste heat recovery in a biomass operated natural convection dryer for sliced ginger. The biomass dryer had sensible heat storage material (SHSM) and phase change material (PCM). The authors' observation was a reduction in the consumption of biomass and melting time of PCM due to the use of waste heat.

2.1.5 Waste Heat Recovery for Useful Work

In the agriculture sector, diesel engines are used for both mobile and stationary farm operations due to their improved specific power output, durability, fuel economy, and reliability. Early research conducted by Wang *et al*. (2004) successfully applied energy from the exhaust gas of a diesel engine to drive an adsorptive ice maker. A new concept based on heat pipe technology has been introduced to effectively harness waste heat generated in nuclear power reactors for sea water desalination (Jouhara *et al*., 2009). Recent advances in waste heat recovery from engines have been documented by Wang *et al*. (2015) with a proposal of a resorption system combined with an energy storage function to recover waste heat from vehicles. The authors analysed possible phase change materials (PCMs) for energy storage function with the consideration that the melting point of PCM should be lower than the exhaust gas temperature of 250°C (Wang *et al*., 2015).

Heat-pipe based heat exchangers have been potentially applied in cooling data-centres with achievable energy savings of up to 75% (Jouhara & Meskimmon, 2014). In an analysis of the integration of a trigeneration scheme within a Natural Gas Processing Plant (NGPP) that uses waste heat from gas turbine exhaust gas, Popli *et al*. (2012) found that the trigeneration system could recover 79.7 MW of gas turbine waste. In the steel industry, a flat heat pipe (FHP) heat exchanger has been used in recovery of residual heat to significantly reduce production costs and greenhouse gas emissions (Jouhara *et al*., 2017a). Alklaibi (2017) has reported results indicating that for maximal efficiency, use of heat from a gas turbine exhaust gas and air bottoming exhaust air is best performed by an absorption system in a cogeneration plant. In the ceramics industry, Jouhara *et al*. (2021b) designed, manufactured, and installed a heat pipe heat exchanger (HPHE) system on a roller hearth kiln and managed to recover up to 100 kW at steady state without cross contamination or excess fouling. A comprehensive review of state-of-the-art applications, materials and performance of heat pipe devices has been documented by Jouhara *et al*. (2017b) and the popularity of heat pipes as passive heat transfer technologies due to their high efficiency was reported.

In a study by Liu *et al*. (2013) aimed at engine exhaust gas energy recovery through direct and indirect means, results have shown that direct recovery bottom cycle through secondary expansion suits diesel engines at full load with high boost pressure. Notwithstanding, indirect recovery bottom cycles have a substantial applied range with their exhaust gas energy recovery potential higher compared to direct recovery means. Jouhara *et al*. (2018) have reviewed waste heat recovery techniques such as direct contact condensation recovery, indirect contact condensation recovery, transport membrane condensation and the use of units such as heat pumps, heat recovery steam generators, heat pipe systems, organic Rankine cycles, including the Kalina cycle, that recover and exchange waste heat with potential energy content. Organic Rankine cycle power units have been recently used in the recovery of waste heat from proton exchange membrane fuel cell system in a study by Wilberforce and Muhammad, (2023) while Mahmoud *et al*. (2023) investigated use of a ground-cooled organic Rankine cycle for waste heat recovery from a diesel generator.

The composition of diesel engine exhaust gas includes carbon monoxide (CO), hydrocarbons (HC), nitrogen oxides (NOx), and particulate matter (PM). Jouhara and Olabi (2018) have advocated the need for solutions to reduce the production of greenhouse gases and also lower the level of global warming through development and utilization of waste heat technologies. An experimental study by Zhang *et al*. (2022) was conducted to further improve understanding of injection strategies on engine performance and NOx emission of 17.4 g/kWh was reported. In a similar study by Zheng *et al*. (2018), it was reported that ethanol shows potential for reducing NOx emissions to less than 1.5 g/kWh. In comparison to composition of air, exhaust gas from a diesel engine have higher concentrations of water vapor (H_2O) and carbon dioxide (CO_2) which are the main combustion products. By comparison, concentrations of pollutants from a diesel engine are small, therefore, to determine physical properties of diesel exhaust gas, they are neglected. Zhang *et al*. (2023) have directly supplied compressed air to a stationary diesel engine to investigate soot emissions which increased with increasing intake pressure and decreased with increasing intake temperature. The authors compared thermal efficiency of supplied compressed air to a diesel engine against a hybrid system consisting of compressed air engine and a baseline diesel engine.

In another study by Zheng *et al*. (2015), combustion and emissions of a single-cylinder diesel engine have been investigated under high exhaust gas recirculation of 46% with two-stage injection strategies (pilot-main and main-post). In their conclusion, the authors reported that NOx emissions decrease first and then increased with increasing pilot-main interval. However, carbon monoxide increased with increasing pilot-main interval while NOx emissions decreased with increasing main-post interval. De Poures *et al*. (2022) have attempted to minimize emissions of a single-cylinder diesel engine by using waste cooking oil and C8 oxygenate blends. Pan *et al*. (2019) have established that smoke and nitrogen oxide could be minimized simultaneously using exhaust gas recirculation. Dhahad *et al*. (2019) have reported 4.3 g/kWh as the maximum CO level achieved at an engine speed of 1000 rpm and 1 bar engine load for ultra-low sulfur diesel use. At similar engine speed and pressure, 4.7 g/kWh of CO level was reported when diesel-water emulsion was used. Minimum CO levels were reported as 2.9 and 2.34 g/kWh at 2250 rpm and 625 bars for ultra-low sulfur diesel and diesel-water emulsion use, respectively (Dhahad *et al*., 2019).

Chaichan 2018 used 85% bioethanol and 15% unleaded gasoline as E85-diesel blend in a partially premixed compression ignition (PPCI) engine and reported increased CO and HC concentrations. PPCI combustion caused significant improvement in NOx-PM trade-off and cooled exhaust gas recirculation (EGR) addition significantly expanded the engine torque range. Maize has been the main staple crop of Kenya for both urban and rural populations. According to De Groote and Kimenju (2008), Kenyan consumers strongly prefer white milled maize whose preparation for lunch and dinner is dished as *ugali* (a stiff, boiled preparation). Food security has depended on ensuring adequate supplies of maize to be milled by diesel operated engines that power *posho* mills in Kenya. These engines, mostly used in milling operations, lose 30% of their fuel energy through exhaust emissions in the form of heat to the environment. There is a need, therefore, to develop strategies to recover exhaust gas heat energy from these stationary diesel engines on milling operations and the solution as provided in the current work is to structurally design heat exchangers to recover heat energy from exhaust gas generated by the engines. According to Tavousi *et al*. (2023), it is imperative to design efficient heat exchangers that are simpler, cheaper to

manufacture, have higher rates of heat transfer, and low in pressure drop, to meet the growing need for more energy.

In advanced systems, wraparound loop heat pipes (WLHP) charged with R134a as the working fluid are used for heat energy recovery because of their overall effective thermal resistances which is as low as 0.048℃/W (Jouhara & Ezzuddin, 2013). Heat exchangers are classified according to the degree of surface compactness, heat transfer mechanisms, transfer processes, flow arrangements, construction features, and the number of fluids. An exploration and review by Jouhara *et al*. (2018) revealed the operation and performance of common waste heat recovery technologies such as recuperators, regenerators, including furnace regenerators and rotary regenerators or heat wheels, passive air preheaters, regenerative and recuperative burners, plate heat exchangers and economizers and units such as waste heat boilers and run around coil (RAC).

Uses of new emerging technologies for direct heat to power conversion such as thermoelectric, piezoelectric, thermionic, and thermophoto voltaic power generation techniques have been discussed in detail by Jouhara *et al*. (2018). Nevertheless, thermal energy storage and management problems were encountered in the current study and proposed solutions lie in the design of solar harvester systems, use of phase change materials (PCM), and mechanisms of storage (sensible heat, latent heat, and sorption heat) as reported by a number of authors (Adesusi *et al*., 2023; Tawalbeh *et al*., 2023; Alamayreh *et al*., 2023; Jouhara *et al*., 2020). Different types of PCM such as wax, salt hydrate and salt hydrate mixtures have been investigated for their heat capacity and results showed that wax was the most suitable PCM (Hathal *et al*., 2023). In the present study, the floor of the greenhouse dryer was painted black to optimize the absorption of solar rays because according to Murr *et al*. (2023), for black bodies the absorptivity and emissivity are approximately equal and close to one.

2.1.6 Influence of Drying Temperature on Germination

Seeds are the reproductive units of higher plants, and they have a significant place in agriculture and plant diversity maintenance (El-Maarouf-Bouteau, 2022). Moreover, investigating how seed germination of multiple species in an ecosystem responds to

environmental conditions is crucial for understanding the mechanisms for community structure and biodiversity maintenance (Yi *et al*., 2019). It is important for seed scientists to be aware of areas on which to focus their research to support the work of the genebanks in conserving and making available plant genetic resources (Whitehouse *et al*., 2020). Bakhtavar *et al*. (2019) have recommended that seeds must be dried to safe moisture limits before storage and the dryness should be maintained throughout the supply chain. Previous studies have been undertaken to examine the effect of drying on viability, the water absorption pattern, laboratory and field germination and seedling growth on seeds of three citrus species, one of its allied genus and a hybrid (Saipari *et al*., 1998). In vegetable crops like black nightshade, high yield and growth are primarily associated with seedling health and early emergence which induces a potential to cope with various biotic and abiotic stresses (Waqas *et al*., 2019). As long as the soil moisture requirements are met, germination can be achieved in one day and rainfall rather than temperature will be extremely limiting for seed germination in future climate scenarios (Dantas *et al*., 2020). Important parameters that influence seeds' germination and seedlings' emergence consist of environmental factors such as soil temperature, soil water potential, exposure to light, fluctuating temperatures, nitrates concentration, soil pH, and the gaseous environment of the soil (Travlos *et al*., 2020).

One of the traditional and economical drying methods for seeds is to leave them in the field to be dried and another is to extract the seeds as proposed by Degwale *et al*. (2023) then expose them to direct sunlight through open sun drying. In the present work, three methods of drying: solar, solar-exhaust gas, and exhaust gas have been introduced in a greenhouse dryer. Greenhouse drying has significant advantages over in-field and open sun drying such as early harvesting options, yield and quality benefits, and reduced threat of weather damage (Jittanit *et al*., 2009). It is for these reasons that the three modes of drying were studied for black nightshade seeds. Seed quality is characterized by germination percentage and physical purity. Determination of key traits in seeds such as dormancy and viability is important, therefore, researchers like Krichen *et al*. (2023) have introduced a modelling approach to identify the cardinal temperature of germination of needle grass, considering dormancy and viability after exposure to salinity and drought conditions experienced in North Africa

due to desertification. A state-of-the-art multichannel imaging method introduced by ElMasry *et al*. (2022) has been recommended for monitoring germination and vigour in actual growing environments; and its applicability was reported to be critically important in identifying vigorous seeds that can tolerate abiotic and biotic stress under different conditions of the environment. According to Reed *et al*. (2022), elevated temperature during seed development can delay germination and reduce seed vigour in crops such as cereals, legumes, and vegetable crops (black nightshade). Reed *et al* (2022) have argued that in the coming decades, maintaining a steady food supply for the increasing world population will require high yielding crop plants which can be productive under increasingly variable conditions. Black nightshade vegetable crop has been reported to have the ability to withstand the potential impact of climate change in addition to combatting malnutrition and contributing to Africa's food supply (Moreno *et al*., 2022). However, some authors have treated it as one of the worst weeds in crop fields (Ma *et al*., 2021) while others have promoted its cultivation through improved seeds germination by priming treatments (Poovizhi & Sujatha, 2020) because of its economic and medicinal importance. Khaeim *et al*. (2022), have conducted a study that provides essential information regarding germination requirements and investigates tolerance to a range of environmental temperatures and drought stresses. The authors in their conclusion declared that dry weight could indicate seedling development, because dry matter accumulation is consistent with the physical measurement of seedling growth. Furthermore, Khaeim *et al*. (2022), affirmed that different seed and seedling densities present no significant difference; thus, using a lower seed density is recommended for lab examination.

To inhibit microorganisms and prevent germination during storage, seeds must be dried to safe moisture level. In the agriculture sector, low black nightshade seeds quality due to delayed or improper drying is a problem to farmers. Chao *et al*. (2022) have also shown a literature gap and reported that currently, the effects of different drying methods on bioactive compounds, antioxidant capacity and antityrosinase activity of seed-used pumpkin by-products are not clear, therefore, this influenced their selection for an optimal drying method to acquire particularly anticipated quality for dehydrated seed-used pumpkin by-products. A study on lentils by Najib *et al*. (2022) revealed a knowledge gap on preparation of plant-based ingredients from germinated

lentils using microwave-assisted infrared drying process. Lack of reported data necessitated Najib *et al*. (2022) to carry out a comprehensive comparison of three lentil varieties in hydration, germination, and dehydration behaviour. Huang *et al*. (2020) aimed to determine the optimum drying temperature for rice seeds according to their initial moisture content, and to elucidate the mechanism mediating the effects of drying temperature and initial moisture content on seed vigor of rice. The authors reported that drying temperature, drying rate, and seed temperature showed extremely significant negative correlations with germination energy, germination rate, germination index, and vigor index (Huang *et al*., 2020). For a single seed population of each of four species of grain legume studied by Covell *et al*. (1986), positive linear relationships were shown between temperature and rate of germination for different fractions of each population, from a base temperature, at which germination rate was zero, to an optimum temperature, at which germination rate was maximal. Subsequently, Ellis *et al*. (1987) reported that a screening procedure which required information on the progress of germination at only four temperatures was able to define the response of the rate of seed germination to sub- and supra-optimal temperatures for whole seed populations of each of five bean genotypes. Aflakpui *et al*. (1998) have also reported that positive linear relationships were established between the rate (reciprocal of time taken) of germination of 90% of the final germination percentage and temperature up to the respective optimal temperatures.

In a recent study, Ismaili *et al*. (2023) have determined optimal germination conditions for *Stachys mouretti*, an endemic species of Morocco considered rare and threatened. The researchers aimed to conserve and valorize the plant whose seeds were collected then subjected to alternating temperatures which had a significant effect on germination capacity. A recent methodology used to investigate the impact of temperature on germination of perennial ryegrass has been reported by Javaid *et al*. (2022) and in their study, twenty seeds were placed uniformly in a Petri plate, lined with filter paper beneath the seed, moistened with distilled water of three millilitres and then retained in an incubator at constant temperatures of 20, 25, 30 and 35°C for fifteen days. Javaid *et al*. (2022) concluded that temperature had a significant impact on seed germination of perennial ryegrass with optimum temperature for its germination as 25°C. Xie *et al*. (2022) explored the suitability of radio frequency

combined hot air drying and found that the technique reduced germination rate by 27.8% as compared to pulsed vacuum drying which maintained good germination rates when peanut pods used for seeds were dried. Coradi *et al*. (2020) in a study aimed at evaluating the associations of drying temperature with storage systems and conditions as a strategy for preserving the quality of maize grain postharvest on laboratory and field scales reported that an increase in temperature accelerated the reduction in grain moisture but increased deterioration. Baskin *et al*. (2006) have pointed out the mistakes made in seed germination ecology, problems in determining the kind of dormancy and in extrapolating data to the field situation. The authors emphasized that even if treatments that seeds might experience in nature are effective in promoting germination, it is not safe to assume that they play an important role in nature (Baskin *et al*., 2006). In a study to determine the influences of temperatures on seed germination rate in Himalayan elm, the thermal time both at sub and supra-optimal temperatures increased linearly as the values of the percentile germination increased in all three seed sources but the seeds germinated at supra-optimal temperatures required less thermal time to germinate than at sub-optimal temperatures (Phartyal *et al*., 2003).

Maturity of seeds, dryer design, drying time, moisture content, and species or variety are the factors which affect seeds response to hot air drying (Jittanit *et al*., 2009). High quality seeds tolerate stressful planting conditions and result in uniform stand which allows better secondary tillage operations, therefore, there is a need to maintain the quality through new methods of drying to ensure germinability. According to De Vitis *et al*. (2020), in order to ensure that a seed lot of good quality (high seed viability) reaches the storage facilities, standard practices must be followed starting from seed collection and during postharvest seed management, prior to storing seeds. De Vitis *et al*. (2020) have documented a compendium of best practices, tools, and standards for the steps between postharvest seed handling and seed storage for applications in restoration. Restoration studies by Budelsky and Galatowitsch (1999) have shown particular interest in the potential influence of storage condition and duration (seed history) on seed response to different germination conditions with uniqueness in considering the effects of storage condition, storage duration, germination temperature, and germination moisture simultaneously for *carex* seeds to determine

the optimum treatment combination for maintaining viability and stimulating germination. The proximate implications of the research by Budelsky and Galatowitsch (1999) include recommendations for seed producers regarding the best storage conditions for maintaining seed viability after collection, the efficacy of short-term stratification on germination of stored seed, optimum conditions for growth chamber or greenhouse germination, and timing of seed dispersal in restorations and creations. Harrington (1959) in a summary pointed out that seeds reach a peak of vigor and germination at the moment of full maturity and that man can only attempt to keep them as close to this peak as possible by proper harvesting and milling and by drying seed to safe moisture levels for storage until needed.

2.2 Empirical review

2.2.1 Seed drying technology

Thin layer drying models (Equations 2.1-2.7) shown in Table 2.2 have been used to describe the rate of moisture removal in drying of agricultural products because of their high level of accuracy. In Table 2.2, MR is moisture ratio; a, b, c and n are drying coefficients specific to each model; k, k_0, and k_1 are drying constants (h^{-1}); t is drying time (h). Seed drying is the process of removing moisture from a seed. The reduction of seed moisture content should be done to a safe limit for the purposes of maintaining viability and vigour during storage. Seed quality is known to deteriorate fast due to mould growth, heating, and enhanced microbial activity. Jittanit *et al.* (2010) have reported 40℃ as a clearly safe drying temperature for corn, rice, and wheat seeds with initial moisture content of 20-25% wet basis. Accordingly, the seeds have been dried to a moisture content of 18% wet basis at 40-80℃ in a fluidized bed dryer and spouted bed dryer. Two-stage drying concept has been proved feasible in the study when the seeds were further dried to a moisture content of 14% wet basis at an air temperature of 18-30℃ and a relative humidity of 60-70% by an in-store dryer.

Table 2.2: Thin Layer Drying Models Used to Describe Drying Kinetics

Model	Equation	Equation Number	Citations
Newton	$MR = exp(-kt)$	(2.1)	(Kaya & Oydin, 2009)
Page	$MR = exp(-kt^n)$	(2.2)	(Kaya & Oydin, 2009; Ronoh *et al*., 2010)
Modified Page	$MR = exp[-(kt)^n]$	(2.3)	(Kaya & Oydin, 2009; Ronoh *et al*., 2010)
Henderson and Pabis	$MR = a \cdot exp(-kt)$	(2.4)	(Kaya & Oydin, 2009)
Logarithmic	$MR = a \cdot exp(-kt) + c$	(2.5)	(Kaya & Oydin, 2009; Ronoh *et al*., 2010)
Wang and Singh	$MR = 1 + a \cdot t + b \cdot t^2$	(2.6)	(Kaya & Oydin, 2009; Ronoh *et al*., 2010)
Two term exponential	$MR = a \cdot exp(-k_0 t) + b \cdot exp(-k_1 t)$	(2.7)	(Kaya & Oydin, 2009)

Elimination of moisture from a seed is in two stages. Initially, moisture from seed is removed from the surface by drying air. Secondly, this causes an imbalance in moisture potential on surface of seed and inner portion of seed which leads to migration of moisture from inner organ to surface. In a related study to determine moisture distribution in rice kernel during tempering drying, Dong *et al*. (2009) have concluded that moisture contents of internal layers of kernels always decreased in whole intermittent drying while that of outer layers of kernels decreased during drying periods and increased during tempering periods. The previous study has compared intermittent drying of long-grain and short-grain rough rice and moisture content distributions within rice kernel have been estimated by a simplified sphere drying model. This migration of moisture to surface is slower as compared to evaporation

thus a moisture gradient is developed in kernel. Removal of moisture from seed depends upon relative humidity and environmental temperature surrounding seed. When relative humidity of seed is higher than that of atmosphere, moisture is eliminated from seed. Care should be taken to minimize and or prevent oxidation, decomposition, and volatilization while drying because when these processes take place at high temperature there will be more loss of dry weight of seed. Moreover, high moisture seeds should be dried at low temperature.

When the rate of moisture loss from seed to surrounding atmosphere is equal to rate of moisture gained by seed from atmosphere, seed is said to be in equilibrium with environment. Equilibrium moisture content models (Equations 2.8-2.12) shown in Table 2.3, such as modified Chung-Pfost, modified Halsey, modified Oswin, modified Henderson, and Guggenheim-Anderson-de Boer have been used in previous studies to compare and fit experimental values using statistical modelling analysis (San Marin *et al*., 2001; Iguaz & Virseda, 2007; Mitrevski *et al*., 2015; Mohite *et al*., 2016). Initial seed moisture content of 18-30% require a recommended maximum drying temperature of 32.2℃ compared to 43.3℃ for moisture contents below 10%. However, initial seed moisture contents of 10-18% will need 42.2℃ because the greater the seed moisture content the lower should be the maximum recommended drying temperature (McCormack, 2004).

In Table 2.3, *A*, *B* and *C* are equation coefficients; M_e is equilibrium moisture content in % (dry basis); T is temperature (℃); a_w is water activity (equilibrium relative humidity) in decimal. Chen (1988) has reported that modified Chung-Pfost, modified Halsey, modified Henderson, and modified Oswin equations have been successfully used among others to model grains and seeds sorption equilibria data. American Society of Agricultural Engineers (ASAE, 1996) has also recommended these four equations with three parameters as documented in American Society of Agricultural Engineers (ASAE) standard D245.5. Van der Berg (1984), Weisser (1985), Wolf *et al*. (1985) and Speiss and Wolf (1987) have recognized GAB equation as the most satisfactory theoretical equation, and it has been recommended as the standard model for use in food laboratories. GAB equation has also been successfully used by many

authors to model sorption isotherms of grains (Sopade & Ajisegiri, 1994; San Marin *et al*., 2001; Tolaba *et al*., 2004; Pagano & Mascheroni, 2005).

Table 2.3: Equations for Modelling Equilibrium Desorption Isotherms

Model	Equation	Equation Number	Citations
Modified Henderson	$M_e = \left[-\frac{\ln(1-a_w)}{A\cdot(T+B)}\right]^{\frac{1}{C}}$	(2.8)	(Henderson, 1952; Thompson *et al*., 1968)
Modified Chung-Pfost	$M_e = -\frac{1}{C}\ln\left[\left(-\frac{T+B}{A}\right)\ln a_w\right]$	(2.9)	(Chung & Pfost, 1967)
Modified Halsey	$M_e = \left[-\frac{exp(A+B\cdot T)}{\ln a_w}\right]^{\frac{1}{C}}$	(2.10)	(Halsey, 1948; Chirife & Iglesias, 1978)
Modified Oswin	$M_e = (A+B\cdot T)\cdot\left(\frac{a_w}{1-a_w}\right)^{\frac{1}{C}}$	(2.11)	(Oswin, 1946; Chen, 1988)
Modified GAB	$M_e = \frac{A\cdot B\cdot\left(\frac{C}{T}\right)\cdot a_w}{(1-B\cdot a_w)\left[1-B\cdot a_w+\left(\frac{C}{T}\right)\cdot B\cdot a_w\right]}$	(2.12)	(Anderson, 1946; De Boer, 1953; Guggenheim, 1966; Jayas & Mazza, 1993)

The original GAB equation proposed by Anderson (1946), De Boer (1953), and Guggenheim (1966) does not incorporate a temperature term, and the determination of the effect of temperature using the model usually involves the evaluation of up to six constants (Aviara *et al*., 2004). Jayas and Mazza (1993) have developed a modified GAB model that incorporates the effect of temperature and has been successfully used to fit sorption equilibrium data of some grains and seeds. According to Sun (1999),

Aviara *et al*. (2004), and Aviara *et al*. (2006) the five isotherm equations include three parameters which have been shown to produce similar good estimations for sorption equilibria data than equations that include more parameters.

The moisture content corresponding to saturation of all primary adsorption sites by one water molecule is known as the monolayer moisture content (Jayendra *et al*., 2005) and it has been reported (Rockland, 1969) as the lower limit of moisture in dehydrated food. The application of BET equation (Brunauer *et al*., 1938) to the experimental data on equilibrium moisture relationships of food has been used to obtain the monolayer moisture content as shown in Equation (2.13), where M_m is monolayer moisture content, M_e is equilibrium moisture content, a_w is water activity, and C is equation coefficient.

$$\frac{a_w}{(1-a_w)\cdot M_e} = \frac{1}{M_m \cdot C} + \frac{(C-1)\cdot a_w}{M_m \cdot C} \tag{2.13}$$

Seeds are dried in stages with heated air passing through the dryer. Tempering period also known as equilibrium period is important as it shortens drying time. Accordingly, during drying, seed surface moisture is removed, and internal moisture moves towards the surface slower than evaporation. This phenomenon leads a moisture gradient to develop in the kernel because the outside part of seed becomes drier than inside as evaporation rate is decreased. Moreover, tempering moisture concentration equalizes in the kernel then evaporation of surface moisture becomes as rapid as at the start of drying. A study by Liu *et al*. (2020) which has primarily focused on the effects of tempering time and seed size on the modification of lentils using infrared heating, has reported findings from the research which are meaningful for utilization of infrared heating to process lentil seeds for development of novel food ingredient.

According to Sun and Woods, (1997a, 1997b) a deep knowledge of the relationship between the equilibrium moisture content and equilibrium relative humidity is of primary importance to fully describe the drying process. A review carried out by Iguaz and Virseda (2007) has revealed two basic techniques, including manometric and gravimetric methods that have been used to determine moisture sorption isotherms of foods and agricultural products. Static gravimetric technique involves the utilization

of saturated salt solutions or sulphuric acid dilutions at different concentrations to maintain constant relative humidity in enclosed still moist air at a certain temperature. Gravimetric technique has been preferred and recommended by several authors to obtain complete sorption isotherms (Gal, 1981; Speiss & Wolf, 1987).

Chirife and Iglesias (1978) have reviewed more than twenty different equations for modelling sorption isotherms of different agricultural materials. The authors have found that each model had some success in predicting equilibrium moisture content data for a given product and a given range of relative humidities and temperatures. Chen and Morey (1989), Sun and Woods (1994), Sun and Byrne (1998), and Basunia and Abe (2001) have reiterated the need to select the most appropriate sorption isotherm equation for a specific crop and range of relative humidities and temperatures.

Many authors have reviewed the importance of moisture content as the most widely used control parameter for drying processes (Samapundo *et al*., 2007; Oliveira *et al*., 2009). Therefore, an understanding of the relationship between water activity and moisture content is necessary to achieve optimal storage stability for black nightshade seeds. It is apparent that knowledge of sorption isotherms is important for several reasons including, design and optimization of drying equipment, evaluation of air and product interface state in drying process simulation, and determination of drying limit at given air conditions (Simal *et al*., 2007). Adsorption or desorption are the two ways in which an isotherm curve can be obtained. Additionally, adsorption and desorption processes are not fully reversible, and the system has hysteresis. Consequently, by determining whether moisture levels within the product are increasing or decreasing a distinction must be made between the isotherms. Agricultural products are exposed to a range of temperatures during storage and processing. Water activity changes with temperature which affect sorption isotherm, mobility of the water molecules, and the dynamic equilibrium between the vapor and adsorbed phases (Al-Muhtaseb *et al*., 2004).

2.2.2 Model Verification and Validation

In research work, validity of developed models are tested using several statistical indicators including, cross correlation equation, root mean square error (RMSE), reduced Chi-square (χ^2), absolute residual error (ϵ), and prediction performance (η_p) which have previously been used by a number of researchers (Rolke & Gongora, 2021; Ndeda *et al*., 2013; Ronoh *et al*., 2010; Kilcik, 2005) for predicted and measured values of variables. Jobst *et al*. (2021) have reported that the test of RMSE provides information on the short-term performance of a studied model as it allows a term-by-term comparison of the actual deviation between the predicted and measured values of variables. The authors have further recommended that a zero value of RMSE is ideal.

Model testing, accreditation, certification, and credibility are activities that primarily deal with the measurements and assessment of accuracy of models and simulations. Verification of a model is substantiating that the model is transformed from one form into another, as intended, with enough accuracy. Model verification deals with building the model in the best way possible. The accuracy of transforming a problem formulation into a model specification or the accuracy of converting a model representation from a micro flowchart form into an executable computer program is assessed in model verification. Jiang *et al*. (2014), have presented Tsmart, a self-contained toolkit to address how to model local synchronous components and asynchronous communication between components in a single framework. The tool has ensured the correctness of a model and maintained the consistency between the model and the implementation of the system.

Previous works (Sun, 1999; Basunia & Abe, 2001; Tolaba *et al*., 2004; Iguaz & Virseda, 2007) have recommended the following equations to evaluate the ability of each isotherm model to fit experimental data: the mean relative percent error (MRE) in Equation (2.14), the standard error (SE) in Equation (2.15) and the coefficient of correlation between the experimental and predicted data (r^2) in Equation (2.16).

$$MRE = \frac{100}{N}\sum_{j=1}^{N}\left|\frac{y_{jcal} - y_{jexp}}{y_{jexp}}\right| \tag{2.14}$$

$$SE = \sqrt{\sum_{j=1}^{N} \frac{\left(y_{jcal} - y_{jexp}\right)^2}{N - n_p}} \tag{2.15}$$

$$r^2 = \frac{S_t - SCE}{S_t} \tag{2.16}$$

The parameters of Equation (2.16) are further evaluated as given in Equations (2.17) to (2.19).

$$S_t = \sqrt{\frac{\sum_{j=1}^{N}\left(\bar{y} - y_j\right)^2}{n - 1}} \tag{2.17}$$

$$\bar{y} = \frac{\sum_{j=1}^{N} y_j}{N} \tag{2.18}$$

$$SCE = \sum_{j=1}^{N}\left(y_{jcal} - y_{jexp}\right)^2 \tag{2.19}$$

Equations (2.14) to (2.19) show that, residuals are the differences between experimental and calculated data $\left(y_{jexp} - y_{jcal}\right)$; N is number of data points; n_P is number of parameters. Aviara *et al*. (2004) have reported that plots of residuals against experimental values are important to evaluate the fitting of the different equations to experimental data and if the residuals are uniformly scattered around the horizontal value of zero, showing no systematic tendency towards a clear pattern, a model is considered acceptable.

Model validation confirms that the model, within its domain of applicability, behaves with acceptable accuracy consistent with the modeling and simulation objectives. Model validation deals with building the right model. Model testing is finding out whether inaccuracies or errors exist in the model. In model testing, the model is subjected to test data or test cases to determine if it functions properly. It is noted that Daniels (2003) has argued that the coefficient of determination (R^2) in nonlinear regression should not be used as a measure of goodness of fit, because it represents the ratio between the residual deviances for the model under comparison and for a model

with an intercept. Daniels (2003) further reported that some non-linear models do not have an intercept and, therefore, the R^2 value is not meaningful and can also assume values outside the range from 0 to 1.

The cross-correlation equation given by Ndeda *et al*. (2013) and Kilcik (2005) has been used in previous works as given in Equation (2.20).

$$r = \frac{\sum_i [(x_i - \bar{x})(y_i - \bar{y})]}{\sqrt{\sum_i (x_i - \bar{x})^2}\,[\sum_i (y_i - \bar{y})^2]} \tag{2.20}$$

In Equation (2.20), for any two series x_i and y_i $(i = 0,1,2,3,\ldots\ldots n-1)$; r is the cross-correlation between x and y; $\bar{x}$ and $\bar{y}$ are the means of the corresponding series. Popular statistical indicators used to validate models are: RMSE, reduced Chi-square (χ^2), absolute residual error (ϵ), and prediction performance (η_p) as shown in Equations (2.21) to (2.24) (Ndeda *et al*., 2013; Rolke & Gongora, 2021; Ronoh *et al*., 2010).

$$RMSE = \left[\frac{1}{N}\sum \left(x_{predicted} - x_{measured}\right)^2\right]^{\frac{1}{2}} \tag{2.21}$$

$$\chi^2 = \sum \left[\frac{\left(x_{measured} - x_{predicted}\right)^2}{x_{predicted}}\right] \tag{2.22}$$

$$\varepsilon\ \% = \left|\frac{x_{predicted} - x_{measured}}{x_{measured}} \times 100\right| \tag{2.23}$$

$$\eta_p\ \% = 100 \times \frac{N_c}{N_t} \tag{2.24}$$

In Equations (2.21) to (2.24) $x_{predicted}$ is the predicted value from the models; $x_{measured}$ is the measured value of the variable; and N is the total number of observations; N_c is the number of correctly predicted values; and N_t is the number of trial data.

On the whole, however, a test is devised, and testing is conducted to perform either validation or verification or both. Some tests are devised to evaluate the behavioural accuracy, that is, validity of the model, and some tests are intended to judge the accuracy of model change from one form into another (verification). Accreditation is the official certification that a model or simulation is acceptable for use for a specific purpose.

2.3 Summary of Literature and Research Gaps

Previous works have recommended more tests to be undertaken to fully analyze greenhouse dryers' performance, especially in optimizing biomass use to achieve desired temperatures. The current work has, therefore, introduced a new heat energy source (exhaust gas) to supplement the heat requirements of a greenhouse dryer when solar radiation is low and at night. Technical equipment may be used to efficiently maintain a greenhouse dryer air temperature and relative humidity at acceptable levels during hot periods, but adequate models will be necessary to estimate the heating loads and adequately manage such control equipment.

The present work, therefore, developed such models for prediction of temperature and moisture evaporation. It is considered that heat flows of the modern-day greenhouse dryers are weather dependent. As a result, questions loom large about how the energy in the greenhouse dryer changes as global warming progresses, and a better simulation of the modern-day greenhouse dryer's heat transfer is an essential first step in heat flow analysis. The present work considered the interaction between the heat flows in a greenhouse dryer and feedback in the climate system.

One of the goals of the current study was to determine drying time of black nightshade seeds when exposed to three modes of drying: solar, solar-exhaust gas, and exhaust gas modes. Towards achieving this goal, use of mathematical models is inevitable. These models act as powerful tools in describing the complex processes that are involved during drying. The development of a proper model to simulate black nightshade seeds drying process requires knowledge of its thin layer drying models and moisture desorption isotherms at drying temperatures. Limited studies have been conducted on fluid and thermal characteristics of diesel engine generated exhaust gas

when used as a working fluid in a hybrid recuperative heat exchanger to provide supplemental heat energy for drying of agricultural produce. Moreover, limited studies have been conducted on thin layer drying of black nightshade seeds.

Justifiably, there is need to study the effect of drying modes on quality characteristics of the seeds because drying is an energy intensive process requiring harvested seeds with an initial moisture content of 88-93% to be dried to an equilibrium moisture content (EMC) of 5±1% (Hong *et al*., 1996) by using energy in a solar-exhaust gas greenhouse dryer an alternative for Kenyan farmers rather than open sun drying. Finally, from the above reviewed literature and to the best of the authors knowledge it is evident that published studies on use of exhaust gas energy to dry black nightshade seeds are limited with no clear consensus on recommended temperatures and drying methods' influence on viability of black nightshade seeds.

In addition, knowledge of seed germination response of species to environmental conditions is still scarce at the community level (Yi *et al*., 2019). The present study, therefore, focused on drying behaviour and germination of black nightshade seeds subjected to solar, solar-exhaust gas and exhaust gas modes of drying in a greenhouse dryer. Drying experiments and standard germination tests were conducted to generate data to be fitted to two commonly used germination models to allow for selection of the best model to describe germination experimental data.

The hypothesis proposed for this research was that germination percentage for the three drying modes was the same. The overall goal of this research was to determine the influence of the drying modes on the viability of black nightshade seeds. Specifically, the authors asked the question: how will the drying modes influence viability of black nightshade seeds? To comprehensively address the research gaps, a hybrid recuperative heat exchanger (HRHE) was developed to recover exhaust gas heat energy from a stationary diesel engine and the energy was utilized as a supplement in a solar greenhouse dryer when radiation was low and at night. As a new contribution from the current work, an HRHE was introduced as a strategy to recover exhaust gas heat energy from a stationary diesel engine to heat drying air in a modified solar-exhaust gas greenhouse dryer. The expected output from this study was quicker and

continuous drying of black nightshade seeds in a solar-exhaust gas greenhouse dryer when radiation was low during the day and during nighttime when there was no solar radiation. The benefit of the heat exchanger in the whole system was to transfer heat energy from exhaust gas released by a diesel engine to the greenhouse dryer inside environment for drying purposes.

As a justification, the present work was chosen to promote the conservation of black nightshade crop through seeds drying to recommended conditions to improve germination and subsequently to preserve the biodiversity of the beneficial vegetable crop—black nightshade has been reported to have larvicidal activity against *Stegomyia aegypti*, a common vector of dengue fever according to Chowdhury *et al*. (2008). The previous study concluded that *Solanum villosum* offers promise as a potential bio control agent against *Stegomyia aegypti* particularly in its markedly larvicidal effect. The use of black nightshade extract or isolated bioactive phytochemical has been recommended in stagnant water bodies for the control of mosquitoes which act as communicable diseases' vectors. However, the main objective of the current work was to recover heat energy from exhaust gas of a stationary diesel engine doing milling operations and then to utilize the energy to heat a fluid stream of drying air in a solar-exhaust gas greenhouse dryer for black nightshade seeds.

The drying technique used in the current work was fast on solar-exhaust gas mode, protected black nightshade seeds from exposure to the environment and prevented contamination due to dust and insects. Black nightshade seeds are small in size and can easily be blown away by the actions of wind if not dried in a protected environment—solar-exhaust gas greenhouse dryer—as has been performed in this study. Heat energy from a diesel engine generated exhaust gas was a supplemental source during nighttime phase of drying and daytime when solar radiation was low. Exposure of black nightshade seeds to full sun should be avoided, as this can cause overheating, killing the embryos, especially in humid climates.

The current study was further conducted to develop mathematical models that were used to predict responses of black nightshade seeds temperature, moisture evaporated and greenhouse dryer room air temperature during greenhouse drying of the seeds. The

study hypothesized that there is no difference in the means between predicted and experimental observations of the responses. The choice of an experimental design involved the selection of a tentative empirical model to describe the results. The model was a quantitative relationship (equation) between the response and important design factors (drying time and experimental data).

2.4 Conceptual Framework

The conceptual framework linking independent and dependent variables in this study is shown in Figure 2.1.

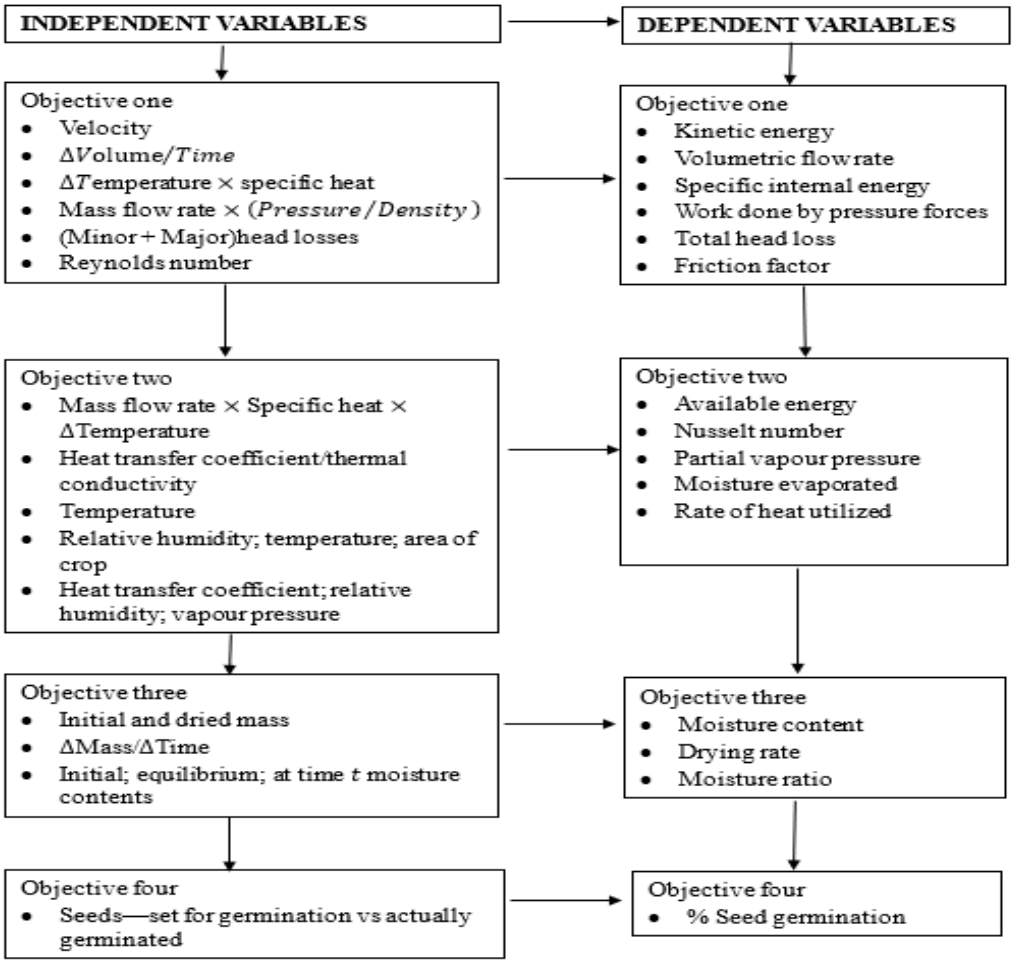

Figure 2.1: Conceptual Framework for the Study

CHAPTER THREE

MATERIALS AND METHODS

3.1 Description of Study Site and System Layout

Field experiments were set up at the Department of Agricultural and Biosystems Engineering, Jomo Kenyatta University of Agriculture and Technology (JKUAT), Kenya. The latitude and longitude of the University are $1^{\circ}5'20.8''$S and $37^{\circ}0'30''$E, while the altitude is 1527 m above the sea level. The mean annual temperature is 19.85℃ with a mean annual maximum temperature of 24.91℃ and a mean annual minimum temperature of 14.79℃. The relative humidity range from 15-80%. The climate for the study site is considered warm and temperate with an annual bimodal rainfall of 1014 mm characterized by cold rainy seasons occurring from April to August and October to December each year.

The solar-exhaust gas environment in this study is an example of a dynamic system such that its response is predictable when subjected to a defined input (introduction of heat energy from the sun and diesel engine generated exhaust gas). To explain the system used in the present work, an internal combustion engine using diesel produces exhaust gas which is channeled to a hybrid recuperative heat exchanger for energy recovery. The heat exchanger system is at a steady state when the pressure of exhaust gas immediately leaving the engine is increased, forcing the gas through a connector of 0.05 m diameter into a tube of 0.39 m diameter.

A series of six connectors and six tubes are arranged to compose the heat exchanger as shown in Plate B.10 such that the mass of exhaust gas is increased in the tubes leading to an increase in pressure, and the exit pipe of the heat exchanger is open to the atmosphere leading to a zero-gauge pressure. In two ways, energy is added to or subtracted from the hybrid recuperative heat exchanger designed and developed for the current study. Energy in the form of exhaust gas internal energy, kinetic energy, and potential energy is transported into or out of the hybrid recuperative heat exchanger through its boundaries (inlet and outlet). In addition, energy is transferred to the hybrid recuperative heat exchanger surface in the form of heat when the dryer is

operated on solar-exhaust gas mode. The properties of the solar-exhaust gas system, that is, density of exhaust gas, temperature of drying air and that of the working fluid, change due to transport of mass. Heat transfer processes in this dynamic system involve the transport of energy from the exhaust gas to a hybrid recuperative heat exchanger surface. In this study, the analyses of fluid and thermal systems of the solar-exhaust gas dryer use the assumption of lumped parameter such that all dependent variables and properties are constant in relation to space and size with time being the independent variable.

Exhaust gas fluid properties include density and viscosity, and thermal properties are conductivity and specific heat. However, unpredictable changes in the solar-exhaust gas input necessitates the introduction of a feedback control system designed to provide a stable desired response to control temperature. The output variable for the solar-exhaust gas system is the temperature of the dryer environment where the drying of products takes place. A change in the input leads to a dynamic response from the solar-exhaust gas system in the form of a change in its inside temperature. The greenhouse dryer had dimensions of 8 m long, 4 m wide, and 3.6 m high. It was glazed with an ultraviolet polythene film of 0.2 mm as a thickness. The solar-exhaust gas greenhouse dryer used in this study is shown in Plate B.1 (outside view) and Plate B.2 (inside view).

The dryer was of a standard peak even span positioned in an east-west orientation to make full use of the available yearly solar energy. The installation based on the east-west orientation has been reported by Ronoh *et al*. (2020) as the preferred longer axis orientation for latitudes less than 40°. The floor of the dryer was painted black, acted as a heat sink, and increased the conversion of light into heat. Four drying trays, two on the right and two on the left were fabricated inside the dryer to measure 6 m long by 1 m wide with a spacing of 0.3 m between the two levels of drying. Food-grade plastic mesh screen (green in colour) held the drying products in position during the experiment.

Samples of freshly harvested black nightshade berries shown in Plate B.3 were collected from Western Kenya. Black nightshade seeds were extracted from the berries

by a fermentation process (Ekhuya *et al*., 2018; Schippers, 1998; Edmonds & Chweya, 1997) where the seeds with the pulp were left to ferment for three days. The seeds were then separated, thoroughly washed with water, and dried in the solar-exhaust gas hybrid greenhouse dryer. The seeds were evenly spread in thin layers on the drying trays as shown in Plate B.4. Galvanized iron connectors increased the structural strength of the hybrid recuperative heat exchanger while unions and sockets formed the plumbing system. The heat exchanger provided heat energy to surrounding air of the dryer environment below the drying trays.

3.2 Instrumentation and Data Acquisition

To study the variation of temperature and relative humidity profiles inside and outside the solar-exhaust gas greenhouse dryer, twenty-six (AM2301A, China) temperature and relative humidity composite sensors with calibrated digital signal output were used. The sensors performance based on temperature characteristics were resolution ratio of 0.1℃, accuracy of ±0.5℃, measuring range of -40-80℃ and repeatability of 0.2℃. Based on humidity characteristics, the sensors performance was resolution of 0.1%, extended measuring range with a minimum of 0% and a maximum of 99.9%, accuracy of ±0.3%, repeatability of ±1%, and hysterisis of ±0.3%. Twenty-four of the sensors were placed at the desired locations inside the dryer while one RH sensor and another temperature sensor were placed outside the solar-exhaust gas greenhouse dryer. Surface temperatures of connectors and tubes of the hybrid-recuperative heat exchanger were measured using twelve (DS18B20, China) programmable resolution 1-wire digital thermometers with operating temperature range of -55℃ to +125℃ (±0.1). With reference to the solar-exhaust gas greenhouse dryer, inside and outside radiations were measured using two (MAX44009, China) ambient light sensors with digital outputs ideal for applications and operations in the dryer. The (AM2301A, China), (DS18B20, China), and (MAX44009, China) sensors were programmed to record data in a microcontroller (ATmega2560, Italy). The Arduino Mega microcontroller was equipped with a 2 GB microSD card for data storage of the drying experiments conducted between July 2022 and January 2023—the ideal period to perform experiments when the weather conditions were most suitable for solar mode, solar-exhaust gas mode, and exhaust gas mode. Mass of black nightshade seeds was

recorded after one hour interval until no further change in mass occurred using a strain gauge based digital weighing scale (D-72336 Balingen, Germany) with a precision of $\pm$0.001 g as shown in Plate B.5.

3.3 Establishing the Relationships between Characteristics (Fluid and Thermal) of Exhaust Gas, and Design Parameters of a Hybrid Recuperative Heat Exchanger

To mathematically model a dynamic system like the solar-exhaust gas dryer used in the present work, appropriate equations for conservation of mass, energy, and Bernoulli's equation derived from conservation of momentum are established for control volume analysis. Equations for friction losses, and compressible flows are customized for exhaust gas flow in the system of the hybrid recuperative heat exchanger pipe geometry. In addition, laws for heat transfer mechanisms are set for the thermal system. Diesel engine generated exhaust gas is treated as a compressible fluid such as an ideal gas with an approximately constant density of 0.7487 kg/m^3 for a wide range of exhaust gas temperatures. In the present work, the hybrid recuperative heat exchanger is a dynamic thermal system. When exhaust gas from the diesel engine flows inside the heat exchanger with a surface temperature at ambient, transient thermal behaviour occurs as heat is transferred to the heat exchanger surface until a steady state is reached. A transient response occurs as the surface temperature of the heat exchanger gradually approaches the temperature of the exhaust gas flowing inside it. The heat exchanger has a capacity for accumulating internal energy due to the transfer of heat from the exhaust gas before it dissipates this energy in the form of heat to the solar-exhaust gas dryer environment.

3.3.1 Principle of Work and Energy as Applied to Modelling Exhaust Gas Flow

The work and energy principle was derived by taking the dot product of Newton's second law of motion. Both sides of the resulting equation were integrated while considering the path of motion of exhaust gas from the inlet to the outlet of the hybrid recuperative heat exchanger. The general form of the principle of work and energy was expressed in Equation (3.1).

$$KE_2 \quad = \quad KE_1 + WD_{1\rightarrow 2} \tag{3.1}$$

In Equation (3.1), KE_2 is the kinetic energy of the exhaust gas at heat exchanger outlet, KE_1 is the kinetic energy at inlet, $WD_{1\rightarrow 2}$ is the work done by all external forces as the exhaust gas moves from the inlet denoted by 1 to the outlet denoted by 2, in the heat exchanger. The potential energy function, PE, was defined for both conservative and non-conservative forces where conservative forces had their work dependent on the initial and final positions of the exhaust gas and non-conservative forces had their work dependent on the path of motion of the exhaust gas as it flowed through the heat exchanger. In both cases, the potential energy function was defined so that the work done was expressed as a difference in potential energies as shown in Equation (3.2) where PE_1 is the potential energy of the exhaust gas at heat exchanger inlet, PE_2 is the potential energy at outlet.

$$WD_{1\rightarrow 2} \quad = \quad PE_1 - PE_2 \tag{3.2}$$

Consequently, the total work was represented using Equation (3.3). In the equation, conservative forces were denoted by C, and non-conservative forces were denoted by NC.

$$WD_{1\rightarrow 2} \quad = \quad (WD_{1\rightarrow 2})_C + (WD_{1\rightarrow 2})_{NC} \tag{3.3}$$

The total energy in the exhaust gas was the sum of kinetic and potential energies which for a conservative system was a constant and satisfied the principle of conservation of energy as shown in Equation (3.4).

$$KE_{ex} + PE_{ex} \quad = \quad Constant \tag{3.4}$$

In Equation (3.4), KE_{ex} is the exhaust gas kinetic energy and PE_{ex} is the exhaust gas potential energy. For the purposes of direct application, Equation (3.4) was used to develop its equivalence as shown in Equation (3.5).

$$\begin{aligned} &\frac{1}{2}\, m_{ex} V_{ex}^2 \\ &+ m_{ex}.g.h_{ex} \end{aligned} \quad = \quad Constant \tag{3.5}$$

In Equation (3.5), m_{ex} is the mass of exhaust gas, V_{ex} is the exhaust gas velocity, g is the acceleration due to gravity, and h_{ex} is the position of exhaust gas in relation to the exhaust gas manifold. In the current application the potential energy was insignificant.

3.3.2 Conservation of Exhaust Gas Mass Analysis in the Heat Exchanger

The control volume form of conservation of mass in a hybrid recuperative heat exchanger in which exhaust gas flows was given in Equation (3.6).

$$\begin{pmatrix} Rate\ at\ which \\ mass\ enters \\ heat\ exchanger \end{pmatrix} - \begin{pmatrix} Rate\ at\ which \\ mass\ leaves \\ heat\ exchanger \end{pmatrix} = \begin{pmatrix} Rate\ at\ which \\ mass\ accumulates\ in \\ heat\ exchanger \end{pmatrix} \quad (3.6)$$

Mass enters and leaves the heat exchanger through its boundaries (inlet and outlet). The rate at which mass crossed the boundary of the heat exchanger was the mass flow rate of exhaust gas, $\dot{m}_{ex}$. If m_{ex} is the total mass of exhaust gas in the heat exchanger at any instant, Equation (3.6) is written as Equation (3.7).

$$\dot{m}_{ex.\ in} - \dot{m}_{ex.\ out} = \frac{dm_{ex}}{dt} \quad (3.7)$$

The total mass of exhaust gas in the heat exchanger at any instant was as given in Equation (3.8).

$$m_{ex} = \int \rho_{ex} dV_{HEX} \quad (3.8)$$

In Equation (3.8), ρ_{ex} is the mass density of exhaust gas and V_{HEX} is the volume of the heat exchanger. The mass flow rate of exhaust gas was written as shown in Equation (3.9).

$$\dot{m}_{ex} = \rho_{ex} \cdot \dot{Q}_{ex} \quad (3.9)$$

In Equation (3.9), $\dot{Q}_{ex}$ is the volumetric flow rate of exhaust gas. Using Equation (3.8) and Equation (3.9) in Equation (3.7) yields Equation (3.10).

$$\rho_{ex.\ in} \cdot \dot{Q}_{ex.\ in} - \rho_{ex.\ out} \cdot \dot{Q}_{ex.\ out} = \frac{d}{dt}\left(\int \rho_{ex} dV_{HEX}\right) \quad (3.10)$$

Exhaust gas entering the heat exchanger was assumed to be of a constant species, homogenous, and the density did not vary with time so that, $\rho_{ex} = \rho_{ex.\ in} = \rho_{ex.\ out}$. Consequently, Equation (3.10) reduced to Equation (3.11).

$$\dot{Q}_{ex.\ in} - \dot{Q}_{ex.\ out} = \frac{dV_{HEX}}{dt} \quad (3.11)$$

3.3.3 Modeling Total Energy in the Hybrid Recuperative Heat Exchanger

The total energy in the control volume (hybrid recuperative heat exchanger) in the current work was given by Equation (3.12).

$$E_{HEX} = U_{ex} + KE_{ex} + PE_{ex} + E_{other} \quad (3.12)$$

In Equation (3.12), E_{HEX} is the total energy in the heat exchanger, U_{ex} is the internal energy of all particles in the heat exchanger, KE_{ex} is the exhaust gas kinetic energy, PE_{ex} is the exhaust gas potential energy, and E_{other} represents other forms of energy such as energy stored in the components and energy associated with any reactions within the heat exchanger. The potential energy in the exhaust and other forms of energy were insignificant in our control volume, therefore, Equation (3.12) was reduced to Equation (3.13).

$$E_{HEX} = U_{ex} + KE_{ex} \quad (3.13)$$

To obtain the total internal energy, the specific energy (the energy per unit mass, u_{ex} , over the control volume) was integrated as shown in Equation (3.14).

$$U_{ex} = \int u_{ex}\, dm_{ex} = \int u_{ex}\, \rho_{ex} dV_{HEX} \quad (3.14)$$

In Equation (3.14), m_{ex} is the mass of exhaust gas, ρ_{ex} is the mass density of exhaust gas and V_{HEX} is the volume of the heat exchanger. The internal energy was the energy associated with the random motion of exhaust gas molecules and thus was a function of temperature. The specific internal energy associated with the exhaust gas flow was given by Equation (3.15).

$$u_{ex} = C_{ex}T_{ex} \tag{3.15}$$

In Equation (3.15), C_{ex} is the specific heat capacity of exhaust gas and T_{ex} is the temperature of the diesel engine generated exhaust gas. Using these definitions, Equation (3.13) was rewritten as Equation (3.16).

$$E_{HEX} = \int (KE_{ex} + u_{ex}\rho_{ex})dV_{HEX} \tag{3.16}$$

The form of the energy equation for the heat exchanger as a control volume was summarized in Equation (3.17).

$$\begin{pmatrix} Rate\ at\ which\ energy\ is\ transferred\ into\ the\ heat\ exchanger\ through\ its\ boundaries \end{pmatrix} - \begin{pmatrix} Rate\ at\ which\ energy\ is\ transferred\ out\ of\ the\ heat\ exchanger\ through\ its\ boundaries \end{pmatrix} + \begin{pmatrix} \text{Rate of convection heat transfer to the surface of the heat exchanger} \end{pmatrix} = \begin{pmatrix} Rate\ at\ which\ energy\ accumulates\ within\ the\ heat\ exchanger \end{pmatrix} \tag{3.17}$$

The hybrid recuperative heat exchanger used in the current study had one inlet and one outlet, therefore, Equation (3.17) was rewritten as Equation (3.18).

$$\dot{m}_{ex.\ in}(u_{ex} + KE_{ex})_{in} - \dot{m}_{ex.\ out}(u_{ex} + KE_{ex})_{out} + \dot{Q}_{conv} = \frac{d}{dt}\left[\int (KE_{ex} + u_{ex}\rho_{ex})dV_{HEX}\right] \tag{3.18}$$

In Equation (3.18), $\dot{m}_{ex.\ in}$ is the mass flow rate of exhaust gas at the inlet of the heat exchanger, $\dot{m}_{ex.\ out}$ is the mass flow rate at the outlet and $\dot{Q}_{conv}$ is the rate of convection heat transfer to the surface of the heat exchanger. Assuming steady flow of exhaust gases, the rate of work done by pressure forces was given by Equation (3.19).

$$\dot{W}_P = \left(\dot{m}_{ex}\frac{P_{ex}}{\rho_{ex}}\right)_{in} - \left(\dot{m}_{ex}\frac{P_{ex}}{\rho_{ex}}\right)_{out} \quad (3.19)$$

In Equation (3.19), $\dot{W}_P$ is the work done by pressure forces, and P_{ex} is the exhaust gas pressure. Using Equation (3.19) in Equation (3.18) resulted in Equation (3.20), which was the form of the energy equation for the hybrid recuperative heat exchanger with one inlet and one outlet as utilized in the present work.

$$\dot{m}_{ex.\ in}\left(u_{ex} + \frac{P_{ex}}{\rho_{ex}} + KE_{ex}\right)_{in} - \dot{m}_{ex.\ out}\left(u_{ex} + \frac{P_{ex}}{\rho_{ex}} + KE_{ex}\right)_{out} + \dot{Q}_{conv} = \frac{d}{dt}\left[\int (KE_{ex} + u_{ex}\rho_{ex})dV_{HEX}\right] \quad (3.20)$$

3.3.4 Application of Bernoulli's Equation for Gas Flow in the Heat Exchanger

For the flow of exhaust gas in the hybrid recuperative heat exchanger, Equation (3.21) was applied.

$$\frac{P_{ex.\ in}}{\rho_{ex}} + \frac{V_{ex.\ in}^2}{2} + PE_{ex.\ in} = \frac{P_{ex.\ out}}{\rho_{ex}} + \frac{V_{ex.\ out}^2}{2} + PE_{ex.\ out} \quad (3.21)$$

In Equation (3.21), $P_{ex.\ in}$ and $P_{ex.\ out}$ are the inlet and outlet pressures of exhaust gas, $V_{ex.\ in}$ and $V_{ex.\ out}$ are the inlet and outlet velocities of exhaust gas, $PE_{ex.\ in}$ and $PE_{ex.\ out}$ are the inlet and outlet potential energies, and ρ_{ex} is the exhaust gas density. In the present work, the exhaust gas potential energy was insignificant, therefore, Equation (3.21) reduced to Equation (3.22).

$$\frac{P_{ex.\ in}}{\rho_{ex}} + \frac{V_{ex.\ in}^2}{2} = \frac{P_{ex.\ out}}{\rho_{ex}} + \frac{V_{ex.\ out}^2}{2} \quad (3.22)$$

Under the assumptions of steady flow, the hybrid recuperative heat exchanger energy equation represented by Equation (3.20) reduced to Equation (3.23).

$$\dot{m}_{ex.\ in}\left(u_{ex}+\frac{P_{ex}}{\rho_{ex}}+KE_{ex}\right)_{in}-\dot{m}_{ex.\ out}\left(u_{ex}+\frac{P_{ex}}{\rho_{ex}}+KE_{ex}\right)_{out}+\dot{Q}_{conv}=0 \tag{3.23}$$

For steady flow of exhaust gas, there is no mass accumulation within the heat exchanger, such that, $\dot{m}_{ex}=\dot{m}_{ex.\ in}=\dot{m}_{ex.\ out}$. Dividing Equation (3.23) by $\dot{m}_{ex}$ and defining $q_{ex}=\dot{Q}_{conv}/\dot{m}_{ex}$, Equation (3.23) reduced to Equation (3.24).

$$\left(u_{ex}+\frac{P_{ex}}{\rho_{ex}}+KE_{ex}\right)_{in}-\left(u_{ex}+\frac{P_{ex}}{\rho_{ex}}+KE_{ex}\right)_{out}+q_{ex}=0 \tag{3.24}$$

If the following three equations are applied to Equation (3.24):

$$q_{ex} \;=\; u_{ex.\ out}-u_{ex.\ in} \tag{3.25}$$

$$(KE_{ex})_{in} \;=\; \frac{V_{ex.\ in}^2}{2} \tag{3.26}$$

$$(KE_{ex})_{out} \;=\; \frac{V_{ex.\ out}^2}{2} \tag{3.27}$$

It followed that Equation (3.24) reduced to Bernoulli's equation as defined in Equation (3.22), which was applicable for the flow of exhaust gas in the hybrid recuperative heat exchanger used in the current work. Equation (3.25) implied that heat transferred to the heat exchanger led to an increase of internal energy. In addition, Equation (3.22) involved the term $(P_{ex.\ in}-P_{ex.\ out})/\rho_{ex}$ which is the gauge pressure and exposing the exhaust gas flow to the open atmosphere made the gauge pressure to be zero.

3.3.5 Determination of Losses in the Heat Exchanger Pipe Flow System

The total head loss in the hybrid recuperative heat exchanger piping system was given using Equation (3.28).

$$h_l \;=\; h_f+h_m \tag{3.28}$$

In Equation (3.28), h_l is the total head loss, h_f is the head loss due to friction (major head losses), and h_m is the sum of all minor head losses due to elbows, unions, sockets, and connectors used in the piping system. Connectors caused sudden contraction in the hybrid recuperative heat exchanger. Minor head losses were expressed in the form of Equation (3.29).

$$h_m = K\frac{V_{ex}^2}{2g} \tag{3.29}$$

In Equation (3.29), K is a loss coefficient, V_{ex} is the exhaust gas velocity, and g is the acceleration due to gravity. The frictional head loss in the heat exchanger piping system was dependent on the geometry of the pipe as well as the flow properties and it was expressed in the form of Equation (3.30).

$$h_f = f\frac{L}{D}\frac{V_{ex}^2}{2g} \tag{3.30}$$

In Equation (3.30), f is the friction factor, L is either the length of a tube or connector, and D is either the diameter of a tube or connector. The friction factor was defined as a function of two dimensionless parameters expressed in Equation (3.31).

$$f = function\left(Re, \frac{\varepsilon}{D}\right) \tag{3.31}$$

In Equation (3.31) ε/D is the ratio of the pipe's roughness to its diameter. The Reynolds number, Re was defined as expressed in Equation (3.32).

$$Re = \frac{\rho_{ex} \cdot V_{ex} \cdot D}{\mu_{ex}} \tag{3.32}$$

In Equation (3.32), Re is the dimensionless Reynolds number, ρ_{ex} is the diesel engine exhaust gas density, and μ_{ex} is the dynamic viscosity of exhaust gas. For laminar flow in tubes of the heat exchanger, analytical methods were used to show that the friction factor was expressed as shown in Equation (3.33).

$$f = \frac{64}{Re} \tag{3.33}$$

Noting that the velocity of exhaust gas in a circular pipe was related to the volumetric flow rate, Equation (3.34) was expressed as:

$$V_{ex} = \frac{4Q_{ex}}{\pi D^2} \tag{3.34}$$

The substitution of Equations (3.32) and (3.33) into Equation (3.30) led to Equation (3.35), which was used for laminar flows in tubes.

$$h_f = \frac{128 \cdot \mu_{ex} \cdot L}{\rho_{ex} \cdot g \cdot \pi \cdot D^4} Q_{ex} \tag{3.35}$$

The Colebrook equation provided a quantitative fit to empirical data for a pressure drop in the heat exchanger pipe system and it was used as an empirical method to quantify Equation (3.31) for turbulent flows in connectors as expressed in Equation (3.36).

$$\frac{1}{\sqrt{f}} = -2.0\, log\left(\frac{\varepsilon}{3.7D} + \frac{2.51}{Re\sqrt{f}}\right) \tag{3.36}$$

Consequently, because it was not possible to solve Equation (3.36) in closed form to determine the friction factor after having obtained the values of Reynolds number and the ratio of the pipe's roughness to its diameter, the friction factor was obtained by referring to the Moody diagram (Moody, 1944), a chart that provided curves of friction factors versus Reynolds number for different values of the ratio of the pipe's roughness to its diameter. Galvanized iron, an ideal metal for fabrication and welding using tungsten inert gas (TIG) welding technique was used to fabricate the hybrid recuperative heat exchanger. From the Moody diagram, the ratio of pipe's roughness to its diameter for galvanized iron connectors of 50 mm diameter was found to be 0.003 and for the tubes of 390 mm the ratio was 0.0004. In this study, major head losses due to friction were determined and reported, while minor head losses in the piping system were considered insignificant.

3.3.6 Thermal Modeling of the Hybrid Recuperative Heat Exchanger System

Internal energy was accumulated in the heat exchanger before it was dissipated to the solar-exhaust gas greenhouse dryer environment. The thermal capacitance of the heat exchanger was defined as expressed in Equation (3.37).

$$C_{therm} = \frac{dU_{ex}}{dT_{ex}} \tag{3.37}$$

In Equation (3.37), C_{therm} is the thermal capacitance of the heat exchanger, U_{ex} is the total internal energy in the exhaust gas, and T_{ex} is the exhaust gas temperature. The heat transfer to the heat exchanger surface from the exhaust gas was resisted with a thermal resistance defined in Equation (3.38).

$$R_{therm} = \frac{\Delta T_{ex}}{\dot{Q}_{conv}} \tag{3.38}$$

In Equation (3.38), R_{therm} is the thermal resistance, ΔT_{ex} is the temperature difference between the exhaust gas and heat exchanger surface, and $\dot{Q}_{conv}$ is the convective heat transfer rate between them. When the temperature of the heat exchanger surface and exhaust gas were equal, thermal equilibrium occurred, the heat transfer ceased, and the heat exchanger stopped absorbing energy. The total internal energy, U_{ex} , was a product of the mass of exhaust gas, m_{ex} , and the specific internal energy, u_{ex}. From Equation (3.15), the specific internal energy was equal to the specific heat capacity of exhaust gas, C_{ex} , times the temperature, T_{ex}. The application of Equation (3.37) led to the thermal capacitance of the heat exchanger as expressed in Equation (3.39).

$$C_{therm} = m_{ex} \cdot C_{ex} \tag{3.39}$$

The transient behaviour of the heat exchanger was modeled by applying conservation of energy to the exhaust gas. Energy, in the form of heat, was transferred to the surface of the heat exchanger and the rate of change of internal energy was equal to the rate at which heat was transferred to the heat exchanger surface as defined in Equation (3.40).

$$\frac{dU_{ex}}{dt} = \dot{Q}_{conv} \tag{3.40}$$

With the assumption of constant specific heat and using Equation (3.38), Equation (3.40) became as expressed in Equation (3.41).

$$m_{ex}C_{ex}\frac{dT_{ex}}{dt} = -\frac{1}{R_{therm}}(T_{ex} - T_s) \tag{3.41}$$

In Equation (3.41), T_s is the heat exchanger surface temperature. Equation (3.41) was rearranged and expressed as Equation (3.42) which is a first order differential equation.

$$m_{ex}C_{ex}\frac{dT_{ex}}{dt} + \frac{1}{R_{therm}}T_{ex} = \frac{1}{R_{therm}}T_s \tag{3.42}$$

In as much as conduction heat transfer in the current work was insignificant because the inside and outside heat exchanger surface temperatures were assumed to be the same over a 1.6 mm thickness of galvanized iron making tubes and connectors, the rate of heat transfer through conduction could be modeled by Fourier's law of conduction as expressed in Equation (3.43).

$$\frac{\dot{Q}_{cond}}{S_A} = -k\frac{\partial T_{ex}}{\partial n} \tag{3.43}$$

In Equation (3.43), $\dot{Q}_{cond}$ is the conduction heat transfer rate, S_A is the surface area, k is the thermal conductivity and, n is the direction normal to the area through which heat is transferred. The resistance due to conduction in the annular cylindrical heat exchanger of length, L , inner radius, r_i , and outer radius, r_o , which was made of galvanized iron of thermal conductivity, k , could be modeled as expressed in Equation (3.44).

$$R_{therm} = \frac{1}{2\pi kL}\ln\left(\frac{r_o}{r_i}\right) \tag{3.44}$$

Convection heat transfer occurred between the moving exhaust gas at high temperature and the heat exchanger surface at rest. A thermal boundary layer, as a thin region near the heat exchanger surface, existed with a temperature gradient, therefore, the rate of

convection heat transfer per unit area was modeled by Newton's law of cooling as expressed in Equation (3.45).

$$\frac{\dot{Q}_{conv}}{S_A} = h_{conv}(T_{ex} - T_s) \quad (3.45)$$

In Equation (3.45), $\dot{Q}_{conv}$ is the convection heat transfer rate, and h_{conv} is the convection heat transfer coefficient.

3.4 Developing a Hybrid Recuperative Heat Exchanger and Evaluating its Performance Using Experimental Temperature and Moisture Evaporation Data

3.4.1 Heat Exchanger Development

The heat exchanger setup involved the use of a naturally aspirated diesel engine (R175A, China). This type of engine is commonly used to power a stationary milling machine on the farm. The basic parameters of the R175A engine are listed in Table A.1. To provide boundary conditions for performance calculation, a steady state heat balance was carried out in the Thermofluids laboratory at JKUAT on a test engine shown in Plate B.6. The engine had similar specifications to the R175A and the experimental data under the benchmark operating condition point of 2500 rpm and mean effective pressure of 576 kN/m^2 were obtained. Previously, Zhang *et al*. (2022) selected an operating condition of 1.5 MPa brake mean effective pressure (BMEP) and 1500 rpm engine speed when conducting experiments of injection strategies on engine performance. In the current study, the single cylinder compression ignition engine running on diesel fuel was tested for engine speed, DES (rpm); exhaust gas temperature, T_{ex} (°C); exhaust gas mass flow rate, $\dot{m}_{ex}$ (kg/h); exhaust gas volumetric flow rate, Q_{ex} (m^3/s); exhaust gas velocity in connectors, V_{cn} (m/s); and exhaust gas velocity in tubes, V_{tb} (m/s). Five other exhaust gas properties corresponding to engine speed were computed based on relevant fluid and thermal equations for heat transfer mechanism.

Some of the assumptions made when diesel exhaust gas was used as a working fluid in the heat exchanger included: the existence of steady operating conditions, negligible potential energy, and use of air properties for exhaust gas. The heat exchanger was named HRHE based on the construction and the counterflow configuration. It has separate flow paths for exhaust gas and drying air. The two fluids flow simultaneously through the heat exchanger as heat is exchanged across the wall separating the flow paths. In the solar-exhaust gas greenhouse dryer environment, the inlet air from outside was allowed to flow from one direction, pick up moisture from the drying product and exit in an opposite direction. The heat exchanger ran across the greenhouse dryer environment to entirely cover it. Exhaust gas was channeled to flow through the tubular heat exchanger and allowed to exit at one end. The greenhouse dryer environment was heated through convective heat transfer from exhaust gas, through the heat exchanger surface and to the dryer environment. Table A.2, adapted from Perry and Green (1997) shows the physical properties of air at a pressure of 101.13 kPa.

To assess exhaust gas thermal energy available in a diesel engine in the thermofluids laboratory, modern convenient emission measurement system research tools were used. Temperature sensors of type K thermocouples (RTD type-PT100) capable of transmitting temperature data in the range of 0-1200℃ were used with a software for engine performance analysis as presented in Plate B.7. Besides temperature measurements, exhaust gas mass flow rate was measured using a pitot tube flow sensor (mass flow rate meter) which was part of a portable exhaust gas analyzer. The mass flow rate of the exhaust gas was computed based on Bernoulli and flow continuity equations using the pitot tube as indicated in Equation (3.46). Large changes in pressure differences reflected small changes in the flow because of the square root relationship, therefore, four pressure difference sensors were incorporated with ranges that span more than two orders of magnitude to overcome the problem of a limited dynamic range associated with flow meters based on differential pressure.

$$\dot{m}_{ex} = K(Re) \times A\sqrt{\rho_{ex}(P_{HIGH} - P_{LOW})} \quad (3.46)$$

In Equation (3.46), $\dot{m}_{ex}$ is exhaust gas mass flow rate, $K(Re)$ is discharge coefficient for flow tube assembly as a function of Reynolds number, A is physical cross-sectional area of flow tube assembly, ρ_{ex} is density of exhaust gas, and $(P_{HIGH} - P_{LOW})$ is differential pressure. To determine the available energy in the exhaust gas, the relationship presented in Equation (3.47) was used.

$$\dot{A}_{ex} = \dot{m}_{ex} C_{ex} \Delta T_{ex} \quad (3.47)$$

In Equation (3.47), $\dot{A}_{ex}$ is available thermal energy in the exhaust gas, $\dot{m}_{ex}$ is mass flow rate of exhaust gas, C_{ex} is specific heat capacity of exhaust gas, and ΔT_{ex} is change in temperature of exhaust gas in comparison with the ambient temperature. For calculations of the available exhaust gas thermal energy, the specific heat capacity of exhaust gas was adopted as 1.0683 kJ/kg·℃ an average value of the specific heat capacities of air, at constant pressure, for all the temperature ranges in Table A.2. The need to recover energy from exhaust gas led to the conceptualization of a heat exchanger. Heat transfer in the separating wall of the heat exchanger was evaluated based on the analysis of the non-dimensional Nusselt number presented in Equation (3.48) and Equation (3.49). The working fluid inside the heat exchanger tube was exhaust gas from a diesel engine. The temperature difference between diesel engine exhaust gas and the wall surface of the heat exchanger was large. Consequently, the Sieder and Tate equation was used to evaluate Nusselt number for turbulent flow in connectors of the heat exchanger as expressed in Equation (3.49). For the fully developed laminar flow in airtight cylindrical tubes of the heat exchanger where Reynolds number was less than 2000, Nusselt number was used as 3.66.

$$Nu = \frac{h_{conv} \cdot L_C}{k} \quad (3.48)$$

$$Nu = 0.027 \cdot Re^{0.8} \cdot Pr^{\frac{1}{3}} \cdot \left(\frac{\mu_{ex}}{\mu_{sur}}\right)^{0.14} \quad (3.49)$$

In Equation (3.48), Nu is Nusselt number, h_{conv} is convection heat transfer coefficient, L_C is characteristic length and k is thermal conductivity. In Equation (3.49), Nu is Nusselt number, Re is dimensionless Reynolds number, Pr is Prandtl number, μ_{ex} is dynamic viscosity of exhaust gas, μ_{sur} is dynamic viscosity of air at the surface of the heat exchanger wall material. Prandtl number was adapted from Rapp (2016) and used

as 0.72. The dynamic viscosity of air at the surface of the heat exchanger wall material was used as 1.85×10^{-5} N·s/m^2. The average velocity of exhaust gas as it flows through the connectors and tube was determined from Equation (3.50).

$$V_{ex} = \frac{\dot{m}_{ex}}{\rho_{ex} \cdot A_C} \tag{3.50}$$

In Equation (3.50), V_{ex} is average velocity of exhaust gas, $\dot{m}_{ex}$ is mass flow rate of exhaust gas, ρ_{ex} is exhaust gas density, and A_C is cross-sectional area through which exhaust gas flows. For computation of the average velocities of exhaust gas through connectors and airtight tubes of the heat exchanger, density of exhaust gas was adopted as 0.7487 kg/m^3, an average value of the densities of air at constant pressure. To determine whether diesel engine exhaust gas was in laminar or turbulent flow, Reynolds number was used as defined in Equation (3.51).

$$Re = \frac{\rho_{ex} \cdot V_{ex} \cdot D}{\mu_{ex}} \tag{3.51}$$

In Equation (3.51), Re is dimensionless Reynolds number, ρ_{ex} is diesel engine exhaust gas density, V_{ex} is average velocity of exhaust gas, D is diameter of connector or airtight cylindrical tube, and μ_{ex} is dynamic viscosity of exhaust gas. Classification of diesel engine exhaust gas flow through the heat exchanger was done according to Menon (2014) where three main flow regimes have been reported as laminar flow with Reynolds number less than 2000, critical flow with Reynolds number greater than 2000 but less than 4000 and turbulent flow with Reynolds number greater than 4000. For calculations of Reynolds number, the dynamic viscosity of exhaust gas was adopted as 2.987×10^{-5} N·s/m^2 an average value of the dynamic viscosities of air, at constant pressure. The flow of exhaust gas through the heat exchanger was based on forced convection, such that a motion was generated by the action of a running diesel engine. The equation for the rate of convection heat transfer to the surface of the heat exchanger is given in Equation (3.52).

$$\dot{Q}_{conv} = h_{conv} S_A (T_{ex} - T_s) \tag{3.52}$$

In Equation (3.52), $\dot{Q}_{conv}$ is convection heat transfer rate, h_{conv} is convection heat transfer coefficient, S_A is surface area, T_s is surface temperature, and T_{ex} is exhaust gas temperature. This study introduced galvanized iron plates, sockets, unions, and connectors as the chosen materials of fabrication for the heat exchanger because of their availability, affordability, good ductility, and weldability—galvanized iron is ideal for metal fabrication and welding using tungsten inert gas (TIG) welding technique. The properties of galvanized iron that makes it suitable for this work are listed in Table A.3.

The heat exchanger was designed to have circular surfaces on both front and back faces. Rolled plates were used to form cylindrical portions. The geometry of the heat exchanger was considered cylindrical with straight horizontal portions to allow for effective use of available sizes of galvanized iron materials. In the design, back pressure on exhaust system was considered. It was necessary to periodically lower and increase back pressure interchangeably to achieve the right amount and allow expulsion of exhaust gas from manifold. A galvanized iron pipe connector of 5 cm diameter (Sawant *et al*., 2018; Kesgin, 2015) was connected to the diesel engine exhaust manifold to lower back pressure and allow exhaust gas to leave the engine. The length of the first connector, CN1, was guided by proximity of exhaust manifold to first tube, TB1, and width of dryer. The engine was operated at optimal speed, surface temperature of connector was measured, and velocity of exhaust gas was determined. Temperature of exhaust gas leaving a connector was measured and compared to ambient temperature with the objective to obtain an exit exhaust gas temperature desired at $\pm$1-2℃ above ambient temperature. Tubular part of the heat exchanger was made larger in diameter (39 cm) as compared to a connector's (5 cm) to create the circular geometry which allowed more flow of the working fluid thereby increasing retention time and total heat transfer as shown in Plate B.8. The diameter of tube was guided by height between floor and lower drying tray of dryer. To further lower back pressure, TB1 was introduced and connected as part of heat exchanger. Repeatedly, surface temperature, exhaust gas velocity and temperature at exit of tube were measured and recorded. A series of connectors (CN1-CN6), designed to increase back pressure, and tubes (TB1-TB6) designed to reduce back pressure formed the heat exchanger. They were developed and introduced in the dryer. Temperature inside the

dryer was measured and compared to those of outside environment as a measure of performance and benefit of HRHE.

3.4.2 Energy Balance Models for Drying Black Nightshade Seeds

Considering black nightshade seeds drying, solar radiation is converted to thermal energy. According to Jain and Tiwari (2004b) solar radiation falling on the seeds' surface is partly absorbed to evaporate moisture from it to the surrounding air. Plastic cover used in the dryer produces a greenhouse effect by trapping solar energy in the form of thermal heat expressed in Equation (3.53) where with respect to greenhouse cover, I_i is solar intensity (W/m^2), A_i is area (m^2) and τ_i is transmissivity.

$$Thermal\ heat\ within\ cover \quad = \quad \sum I_i A_i \tau_i \tag{3.53}$$

A fraction of trapped energy is received partly by black nightshade seeds and partly by the floor and exposed tray area as shown in Equation (3.54) and (3.55) while the remaining solar radiation will heat the enclosed air inside the solar-exhaust gas greenhouse dryer as shown in Equation (3.56) where α is absorptivity and for Equations (3.54) - (3.56), F is fraction of solar radiation.

$$\begin{matrix} Radiation\ received\ by \\ black\ nightshade\ seeds \end{matrix} \quad = \quad F_b \sum I_i A_i \tau_i \tag{3.54}$$

$$\begin{matrix} Radiation\ received\ by \\ floor\ and\ tray\ area \end{matrix} \quad = \quad (1 - F_n) \sum I_i A_i \tau_i \tag{3.55}$$

$$Remaining\ solar\ radiation \quad = \quad (1 - F_n)(1 - F_b)(1 - \alpha_g) \sum I_i A_i \tau_i \tag{3.56}$$

To write the energy balance equations, the assumptions made were: thin layer drying is adopted, heat capacity of greenhouse dryer cover and wall material is neglected, no stratification in greenhouse dryer air temperature, absorptivity of air is neglected, and greenhouse dryer is east-west oriented. Thermal models for prediction of black nightshade seeds temperature and moisture evaporation were developed using energy balance equations for forced convection drying system in a solar-exhaust gas greenhouse dryer. For the energy balance equation (Chauhan *et al*., 2018a; Chauhan *et al*., 2018b; Chauhan & Kumar, 2018; Chauhan *et al*., 2017; Kumar & Tiwari, 2006; Jain &Tiwari, 2004b) at black nightshade seeds surface, the form is expressed in Equation (3.57) which is then rewritten as Equation (3.58).

$$\begin{bmatrix} Rate\ of\ thermal\ energy\ received\ at\ black\ nightshade\ seeds\ surface \end{bmatrix} = \begin{bmatrix} Rate\ of\ thermal\ energy\ stored\ by\ black\ nightshade\ seeds \end{bmatrix} + \begin{bmatrix} Rate\ of\ thermal\ energy\ lost\ due\ to\ convection\ loss \end{bmatrix} + \begin{bmatrix} Rate\ of\ thermal\ energy\ lost\ due\ to\ evaporation\ loss \end{bmatrix} \tag{3.57}$$

$$(1-F_n)F_b\alpha_b\sum I_iA_i\tau_i = M_bC_b\frac{dT_b}{dt} + h_b(T_b-T_r)A_b + 0.016h_b[P(T_b) - \gamma_rP(T_r)]A_b \tag{3.58}$$

In Equation (3.58), F_n is the fraction of solar radiation falling on tray area, F_b is the fraction of solar radiation falling on black nightshade seeds, α_b is the absorptivity of black nightshade seeds, I_i is the solar intensity on greenhouse dryer walls/roof, A_i is the area of greenhouse dryer walls/roof, τ_i is the transmissivity of greenhouse dryer walls/roof, M_b is the moisture content of black nightshade seeds, C_b is the specific heat capacity of black nightshade seeds, T_b is the temperature of black nightshade seeds, h_b is the convective heat transfer coefficient of black nightshade seeds, T_r is the greenhouse dryer room air temperature, A_b is the surface area of black nightshade

seeds, P is the vapour pressure, and γ_r is the relative humidity of greenhouse dryer room air. The energy balance equation (Chauhan *et al*., 2018a; Chauhan *et al*., 2018b; Chauhan & Kumar, 2018; Chauhan *et al*., 2017; Kumar & Tiwari, 2006; Jain &Tiwari, 2004b) at ground surface is summarized in the form of Equation (3.59) which is then rewritten as Equation (3.60).

$$\begin{bmatrix} Rate\ of\ thermal \\ energy \\ received\ at \\ floor \\ surface \end{bmatrix} = \begin{bmatrix} Rate\ of\ thermal \\ energy\ lost \\ inside\ the \\ ground\ due \\ to\ conduction \\ loss \end{bmatrix} + \begin{bmatrix} Rate\ of\ thermal \\ energy\ lost \\ from\ floor \\ to\ greenhouse \\ dryer\ air \\ due\ to \\ convection\ and \\ radiation\ losses \end{bmatrix} \tag{3.59}$$

$$(1-F_n)(1-F_b)\alpha_g \sum I_i A_i \tau_i = h_{g\infty}(T|_{x=0} - T_\infty)A_g + h_{gr}(T|_{x=0} - T_r)(A_g - A_b) \tag{3.60}$$

In Equation (3.60), F_n is the fraction of solar radiation falling on tray area, F_b is the fraction of solar radiation falling on black nightshade seeds, α_g is the absorptivity of greenhouse dryer floor surface, I_i is the solar intensity on greenhouse dryer walls/roof, A_i is the area of greenhouse dryer walls/roof, τ_i is the transmissivity of greenhouse dryer walls/roof, $h_{g\infty}$ is the convective heat transfer coefficient of greenhouse dryer floor to underground, $T|_{x=0}$ is the temperature of greenhouse dryer floor surface, T_∞ is the underground temperature, h_{gr} is the convective heat transfer coefficient of greenhouse dryer floor to room air, T_r is the greenhouse dryer room air temperature, A_b is the surface area of black nightshade seeds, and A_g is the area of greenhouse dryer floor surface. The energy balance equation (Chauhan *et al*., 2018a; Chauhan *et al*., 2018b; Chauhan & Kumar, 2018; Chauhan *et al*., 2017; Kumar & Tiwari, 2006; Jain &Tiwari, 2004b) at greenhouse dryer chamber is written by using the number of air

exchange per hour and is summarized in the form of Equation (3.61) which is then rewritten as Equation (3.62).

In Equation (3.62), F_n is the fraction of solar radiation falling on tray area, F_b is the fraction of solar radiation falling on black nightshade seeds, α_g is the absorptivity of greenhouse dryer floor surface, I_i is the solar intensity on greenhouse dryer walls/roof, A_i is the area of greenhouse dryer walls/roof, τ_i is the transmissivity of greenhouse dryer walls/roof, h_b is the convective heat transfer coefficient of black nightshade seeds, T_b is the temperature of black nightshade seeds, T_r is the greenhouse dryer room air temperature, A_b is the surface area of black nightshade seeds, P is the vapour pressure, γ_r is the relative humidity of greenhouse dryer room air, h_{gr} is the convective heat transfer coefficient of greenhouse dryer floor to room air, $T|_{x=0}$ is the temperature of greenhouse dryer floor surface, A_g is the area of greenhouse dryer floor surface, T_a is the ambient temperature, and U_i is the overall heat loss on greenhouse dryer walls/roof.

$$
\begin{gathered}
[Rate\ of\ thermal\ energy\ recieved\ by\ greenhouse\ dryer\ air] \\
+ \\
\begin{bmatrix} Rate\ of\ thermal\ energy\ received\ from\ black\ nightshade\ seeds \\ due\ to\ convection\ loss \end{bmatrix} \\
+ \\
\begin{bmatrix} Rate\ of\ thermal\ energy\ received\ due\ to\ evaporation\ loss \\ from\ black\ nightshade\ seeds \end{bmatrix} \\
+ \\
\begin{bmatrix} Rate\ of\ thermal\ energy\ received\ from\ greenhouse\ dryer\ floor \\ due\ to\ conduction\ and\ radiation\ losses \end{bmatrix} \\
= \\
\begin{bmatrix} Rate\ of\ thermal\ energy\ lost\ to\ the\ ambient\ air \\ by\ forced\ ventilation \end{bmatrix} \\
+ \\
\begin{bmatrix} Rate\ of\ overal\ heat\ loss\ from\ greenhouse\ dryer\ air \\ to\ ambient\ air\ through\ canopy\ cover \end{bmatrix}
\end{gathered}
\tag{3.61}
$$

$$
(1-F_n)(1-F_b)(1-\alpha_g)\sum I_i A_i \tau_i \quad + \quad h_b(T_b - T_r)A_b \qquad +
$$

$$0.016h_b[P(T_b) - \gamma_r P(T_r)]A_b + h_{gr}(T|_{x=0} - T_r)(A_g - A_b) = 0.33NV(T_r - T_a) + \sum U_i A_i (T_r - T_a) \quad (3.62)$$

3.4.3 Solution of Energy Balance Models

Two approximations are used to solve the mathematical models given in Equation (3.57) – (3.62). First, it is noted that black nightshade seeds area, A_b, reduces with moisture reduction due to shrinkage which leads to a change in absorption of solar energy during drying process. Using shrinkage ratio as a function of moisture ratio allows for approximation of the value of A_b as shown in Equation (3.63) and Equation (3.64) (Nguyen *et al*., 2018; Ratti, 1994).

$$\frac{A_b}{A_{b0}} = 0.339 + 1.246W_m - 1.385W_m^2 + 0.792W_m^3 \quad (3.63)$$

$$W_m = \frac{X_m}{X_{m0}} \quad (3.64)$$

The second approximation is based on linearization of partial vapour pressure, as shown in Equation (3.65), over small temperature ranges between 25-55℃ in which solar drying mostly occurs.

$$P(T) = G_1 T + G_2 \quad (3.65)$$

If I_{effB} is the rate of thermal energy received at black nightshade seeds surface, I_{effG} is the rate of thermal energy received at floor surface of greenhouse dryer, and I_{effR} is the rate of thermal energy received by greenhouse dryer air, then their expressions and use are as shown in Equations (3.66) – (3.68).

$$I_{effB} = (1 - F_n)F_b\alpha_b \sum I_i A_i \tau_i \quad (3.66)$$

$$I_{effG} = (1 - F_n)(1 - F_b)\alpha_g \sum I_i A_i \tau_i \tag{3.67}$$

$$I_{effR} = (1 - F_n)(1 - F_b)(1 - \alpha_g) \sum I_i A_i \tau_i \tag{3.68}$$

Similarly, Equations (3.69) – (3.73) are expressed and used in the following formats to solve the mathematical models.

$$H_g = \left[1 + \frac{h_{g\infty} A_g}{h_{gr}(A_g - A_b)}\right]^{-1} \tag{3.69}$$

$$UA_{g\infty} = \left[\frac{1}{h_{gr}(A_g - A_b)} + \frac{1}{h_{g\infty} A_g)}\right]^{-1} \tag{3.70}$$

$$P(T) = exp\left[25.317 - \frac{5144}{T + 273.15}\right] \tag{3.71}$$

$$h_{be} = h_b + h_r \tag{3.72}$$

$$h_r = \frac{\varepsilon\sigma[(T_b + 273.15)^4 - (T_v + 273.15)^4]}{T_b - T_v} \tag{3.73}$$

With the help of Equations (3.65), (3.67) - (3.70), Equation (3.62) is simplified to determine the greenhouse dryer room temperature under forced convection mode for values of black nightshade seeds temperature and ambient temperature as given in Equation (3.74).

$$T_r = \frac{I_{effR} + h_b A_b T_b + 0.016(G_1 T_b + R_2 - \gamma_r G_2) + H_g I_{effG} + \left[(UA)_{g\infty} + 0.33NV + \sum U_i A_i\right] T_a}{h_b A_b + 0.016 h_b \gamma_r G_1 + (UA)_{g\infty} + 0.33NV + \sum U_i A_i} \quad (3.74)$$

Substituting linear expression of partial vapour pressure in Equations (3.58) and (3.62) and combining the resultant equations, a form of a first order differential equation is produced for black nightshade seeds temperature as shown in Equation (3.75).

$$\frac{dT_b}{dt} + \psi T_b = f(t) \quad (3.75)$$

In Equation (3.75), the derivative, ψ and the time dependent derivative, $f(t)$ are determined using Equation (3.76) and (3.77).

$$\psi = \frac{h_b A_b (1 + 0.016 G_1)}{M_b C_b} \quad (3.76)$$

$$f(t) = \frac{I_{effB} + h_b A_b [T_r - 0.016\{G_2 - \gamma_r (G_1 T_r + G_2)\}]}{M_b C_b} \quad (3.77)$$

Once the value of the greenhouse dryer room air temperature, T_r is known, with the help of Equation (3.58), black nightshade seeds temperature, T_b can be determined using Equation (3.75) and the rate of moisture evaporation is evaluated using the expression in Equation (3.78).

$$m_{ev} = 0.016 \frac{h_b}{\lambda} [(G_1 T_b + G_2) - \gamma_r (G_1 T_r + G_2)] A_b t \quad (3.78)$$

3.4.4 Convective Heat Transfer Coefficient for Black Nightshade Seeds

The Nusselt number is a function of Reynolds and Prandtl numbers for forced convection (Jain and Tiwari, 2004a) as expressed in Equation (3.79).

$$Nu = \frac{h_b X}{K_v} = C(RePr)^n \tag{3.79}$$

The hourly data of relative humidity inside the solar-exhaust gas greenhouse dryer, black nightshade surface temperature, inside the dryer air temperature and mass of black nightshade seeds were recorded during the experiment. The moisture evaporated, m_{ev} was calculated by taking the difference of mass of black nightshade seeds between two consecutive readings at one-hour intervals. The convective heat transfer coefficient of black nightshade seeds, h_b under forced convection mode of drying was defined as shown in Equation (3.80) (Tiwari *et al*., 2004).

$$h_b = \frac{K_v}{X} C(RePr)^n \tag{3.80}$$

The rate of heat utilized to evaporate moisture was given as shown in Equation (3.81) (Tiwari *et al*., 2004).

$$\dot{Q}_e = 0.016 h_b [P(T_b) - \gamma_r P(T_r)] \tag{3.81}$$

On substituting h_b from Equation (3.80), Equation (3.81) becomes Equation (3.82).

$$\dot{Q}_e = 0.016 \frac{K_v}{X} C(RePr)^n [P(T_b) - \gamma_r P(T_r)] \tag{3.82}$$

Evaporation moisture was determined by dividing Equation (3.82) by the latent heat of vaporization, λ and multiplying by the area of black nightshade seeds drying tray, A_b and the time interval, t as expressed in Equation (3.83) which is similar to the form of Equation (3.78).

$$m_{ev} = \frac{\dot{Q}_e}{\lambda} A_b t = 0.016 \frac{K_v}{X\lambda} C(RePr)^n [P(T_b) - \gamma_r P(T_r)] A_b t \tag{3.83}$$

Let Equation (3.84) be expressed as:

$$Z = 0.016 \frac{K_v}{X\lambda} [P(T_b) - \gamma_r P(T_r)] A_b t \tag{3.84}$$

It follows that Equation (3.83) will reduce to Equation (3.85):

$$\frac{m_{ev}}{Z} = C(RePr)^n \tag{3.85}$$

Taking logarithms on both sides Equation (3.85) is written as shown in Equation (3.86).

$$\ln\left[\frac{m_{ev}}{Z}\right] = \ln C + n \ln(RePr) \tag{3.86}$$

This is in the form of a linear equation as expressed in Equation (3.87).

$$y = mx + c \tag{3.87}$$

The parts of Equation (3.87) are represented as follows:

$y = \ln\left[\frac{m_{ev}}{Z}\right]$, $m = n$, $x = \ln(RePr)$, $c = \ln C$, and $C = e^c$

The following polynomial expressions shown in Equation (3.88) – (3.92) have been used according to Anwar and Tiwari (2001) to determine density (ρ_v), viscosity (μ_v), specific heat (C_v) and thermal conductivity (k_v) of humid air. The physical properties of humid air were then used in computation of Reynolds number (Re) and Prandtl number (Pr).

$$\rho_v = \frac{353.44}{(T_i + 273.15)} \tag{3.88}$$

$$\mu_v = 1.718 \times 10^{-5} + (4.620 \times 10^{-8} T_i) \tag{3.89}$$

$$C_v = 999.2 + 0.1434 T_i + (1.101 \times 10^{-4} T_i^2) - (6.7581 \times 10^{-8} T_i^3) \tag{3.90}$$

$$k_v = 0.0244 + (0.6773 \times 10^{-4} T_i) \tag{3.91}$$

$$T_i = \frac{(T_b + T_v)}{2} \tag{3.92}$$

Measured data of black nightshade seeds temperature (T_b), exit humid air temperature (T_v), and exit humid air relative humidity (γ_v) were recorded. The weight of black nightshade seeds was precisely recorded during the drying period. Calculated data of moisture evaporated (m_{ev}) during drying, results of Equation (3.84) representing (Z), Reynolds number (Re), and Prandtl number (Pr) were tabulated. The values of y and x in Equation (3.87) which correspond to Equation (3.86) were evaluated for different time intervals and the constants C and n were obtained by linear regression analysis and used to evaluate the convective heat transfer coefficient of black nightshade seeds (h_b). The evaporative heat transfer coefficient (h_e) was then evaluated using Equation (3.93) (Tiwari *et al*., 2004).

$$h_e = 16.273 \times 10^{-3} h_b \left(\frac{P(T_b) - \gamma_r P(T_r)}{T_b - T_r} \right) \tag{3.93}$$

From Jain and Tiwari (2004b), constant values of parameters used in modelling were adopted as follows: latent heat of vapourization (λ) as 2.26×10^6J/kg, humid air velocity (v) as 0.01 m/s, and black nightshade seeds absorptivity (α_b) as 0.6.

3.4.5 Proposed Simulation Models for Evaluation of Temperature and Moisture Evaporated

Equations (3.53) to (3.93) reveal that greenhouse drying is complex and is under the influence of external variables in interaction with one another. The need for simple models to describe responses obtained from controlled black nightshade seeds drying experiments is therefore emphasized considering deterministic effects as given in Equations (3.94) to (3.96).

$$T_{b-pred} = f(t, \xi) \tag{3.94}$$

$$T_{r-pred} = f(t, \zeta) \tag{3.95}$$

$$m_{ev-pred} = f(t, \Omega) \tag{3.96}$$

In Equations (3.94) to (3.96), predicted black nightshade seeds temperature (T_b), greenhouse dryer room air temperature (T_r), and moisture evaporated from black nightshade seeds (m_{ev}) are obtained as a result of a stimulus (predictor) known as drying time (t) according to a response function (f) based on a number of parameters which are indicated by the Greek letters (ξ), (ζ), and (Ω), respectively. Introducing stochastic effects of experimental error while considering the Gaussian probability density function (PDF) and cumulative distribution function (CDF), the relationship between predicted and experimental data is given in Equations (3.97) to (3.99).

$$T_{b-pred} \neq T_{b-expt} \tag{3.97}$$

$$T_{r-pred} \neq T_{r-expt} \tag{3.98}$$

$$m_{ev-pred} \neq m_{ev-expt} \tag{3.99}$$

Experimental data for (T_b), (T_r) and (m_{ev}) were collected for each drying time in solar, solar-exhaust gas, and exhaust gas modes of drying. Both experimental data and drying time were treated as stimuli for predicted data of (T_b), (T_r) and (m_{ev}). According to biological mechanism of black nightshade seeds drying process the response functions (f) were empirically selected as non-linear second order equations for predicting (T_b) and (T_r) following the Galilean process (Finocchiaro, 2012) by posing the hypothesis in the form of mathematical models given in Equation (3.100) and (3.101). Moreover, for moisture evaporated from black nightshade seeds (m_{ev}), the response function (f)

was selected as an exponential decay equation given in Equation (3.102). Equations (3.100) to (3.102) have taken into account the interactions between one stimulus and the other.

$$T_{b-pred} = \xi_0 + \xi_1 t + \xi_2 T_{b-expt} + \xi_3 t T_{b-expt} + \xi_4 t^2 + \xi_5 \left(T_{b-expt}\right)^2 + \varpi \tag{3.100}$$

$$T_{r-pred} = \zeta_0 + \zeta_1 t + \zeta_2 T_{r-expt} + \zeta_3 t T_{b-expt} + \zeta_4 t^2 + \zeta_5 \left(T_{r-expt}\right)^2 + \varrho \tag{3.101}$$

$$m_{ev-pred} = \Omega_0 \left(1 - exp(-\Omega_1 (t)^{\Omega_2})\right) + \Omega_3 \left(1 - exp\left(-\Omega_4 \left(m_{ev-expt}\right)^{\Omega_5}\right)\right) \tag{3.102}$$

Experimental data used in the modeling process of Equations (3.100) to (3.102) were divided into three data sets: training, validation, and testing. To fully specify the response functions (f), values of parameters (ξ), (ζ), and (Ω) were found through curve fitting in R statistical software.

3.4.6 Internal Uncertainty Analysis

To validate the experimental error, the percent internal uncertainty was determined using Equation (3.103) (Chauhan & Kumar, 2016; Anwar & Tiwari, 2001).

$$\%\ internal\ uncertainty = \left[\frac{U'}{mean\ total\ number\ of\ observations} \times 100\right] \tag{3.103}$$

The parameter (U') for % internal uncertainty evaluation is found as shown in Equation (3.104).

$$U' = \frac{\sqrt{\sigma_1^2 + \sigma_2^2 + \cdots + \sigma_N^2}}{N} \tag{3.104}$$

The standard deviation (σ) is given as expressed in Equation (3.105).

$$\sigma = \sqrt{\frac{\sum(X - \bar{X})^2}{N_O}} \tag{3.105}$$

In Equation (3.104) and Equation (3.105) ($X - \bar{X}$) is the deviation of observations from the mean, (N) is the number of data sets, and (N_O) is the number of observations in each set.

3.5 Evaluating Thin Layer Drying Models for Simulating Drying Kinetics of Black Nightshade Seeds

3.5.1 Drying Characteristics of Black Nightshade Seeds

The initial moisture content was determined according to Feldsine *et al*. (2002) on Association of Official Analytical Chemists (AOAC) method of analysis. 50 g of black nightshade seeds were placed in a moisture dish and both weights were taken. The seeds sample and moisture dish were placed in an oven and temperatures set at 105℃. The samples were removed and placed in a desiccator. The final mass was obtained after cooling. A constant mass was measured and recorded. Moisture content (% db) at any given drying time t (hours) was obtained using Equation (3.106).

$$M = \frac{m_i - m_t}{m_t} \times 100 \tag{3.106}$$

In Equation (3.106), M is moisture content in (% db); m_i is initial mass of sample (g); and m_t is dried mass of sample (g) at time t (hours). Ronoh *et al*. (2020) and Uluko *et al*. (2006) have reported that the relationship between drying time and moisture content is based on Newton model of thin layer drying for the material under varying relative humidity like in solar-exhaust gas greenhouse drying. The instantaneous drying rate of black nightshade seeds was computed using Equation (3.107) where DR is the drying rate (g/g/h), Δm is change in mass (g), Δt is change in time (h), m_{i-1} is the sample mass (g) preceding a given instantaneous sample mass, m_i (g), t_{i-1} is the

drying time (h) preceding a given instantaneous drying time, t_i (h), and m_d is the final mass (g) of dried sample.

$$DR = \frac{\Delta m}{\Delta t} = \frac{m_{i-1} - m_i}{m_d(t_{i-1} - t_i)} \tag{3.107}$$

The moisture ratio at different drying time was computed using Equation (3.108) from the data for moisture content of black nightshade seeds. Equation (3.108) is based on the theory of thin layer drying and MR is moisture ratio; M_t is the moisture content (% db) at time t in hours; M_e is equilibrium moisture content (%), M_i is initial moisture content (% db).

$$MR = \frac{M_t - M_e}{M_i - M_e} \tag{3.108}$$

Simulation of the drying process of black nightshade seeds in a solar-exhaust gas greenhouse dryer was done by the application of thin layer drying models described such as Newton model, Page model, Logarithmic model and Henderson and Pabis model. These models were considered for use in this study because they have been widely used for thin layer drying prediction.

3.5.2 Models Validation

Models' validation was a necessary step to examine the thin layer drying models used in this work. The initial scrutiny involved studying the values predicted by the models with those observed as experimental data. First, the performance of the models was measured in terms of root mean squared error (RMSE) which according to Hodson (2022) is considered an excellent general purpose error metric for numerical predictions and optimal for normal (Gaussian) errors as given in Equation (3.109), where n is the number of observations available for analysis, P_i are the predicted values of the variable and O_i are the observed values.

$$RMSE = \sqrt{\frac{1}{n}\sum_{i=1}^{n}(P_i - O_i)^2} \tag{3.109}$$

A low RMSE value meant that the predicted values were close to the real values and that the model could well predict the observations (Hodson, 2022). Secondly, plotting of the residuals against the predictions of a model was done as a standard through which the model could be validated statistically because it was used as a measure of the distribution of errors. The interpretation of residual plots led to the acceptance or non-acceptance of the thin layer drying model. Generally, if the right model was used to determine the quality of fit, the residuals had a low band width and were close to the residual line. A model with residuals plot indicating a high band width was not accepted because it could not best describe the drying behaviour of black nightshade seeds.

3.5.3 Data Analysis

Microsoft 365 Excel software was used as a computational and graphical tool. Statistical analyses were carried out using R, version 4.1.3 (R Core Team, 2023). Curve fitting to experimental data for thin layer drying models was performed using *mosaic* collection of packages in R language (Pruim *et al*., 2017). R Scripts and console outputs for coefficients, constants and RMSE in the three modes of drying were produced.

3.6 Determining the Influence of Solar-Exhaust Gas Greenhouse Drying Modes on Viability of Black Nightshade Seeds

3.6.1 Sampling Procedure

The technique adopted in selecting black nightshade berries, for diameter and seeds number determination as quantitative parameter and qualitative variable, respectively, involved the sample design and size. A finite type of accessible population was considered with Western Kenya as the geographical sampling unit. To represent the accessible population under study, comprehensively and reliably, the sampling frame was defined as the source list composed of mature black nightshade berries from the vegetable crops within Western Kenya. The berries were deemed mature for harvesting when they were still held by the plant and their colour had turned orange from green to signify that they had ripened. In this study, diameter of black nightshade berries was

treated as a quantitative parameter characteristic to the accessible black nightshade berries' population on the one hand and seeds number in a berry was a qualitative variable dependent on the diameter and characteristic to the sample of black nightshade berries drawn from the accessible population on the other hand. To denote the number of black nightshade berries to be selected from the accessible population to constitute a sample, an optimum sample size that fulfilled the requirements of representativeness, reliability and flexibility was used. The sample procedure constituting the sample design was chosen to result in the smallest sampling error. The disproportionate sampling design was used as expressed in Equation (3.110).

$$\frac{n_1}{N_1\sigma_1} = \frac{n_2}{N_2\sigma_2} = \frac{n_3}{N_3\sigma_3} = \cdots \ldots \ldots \ldots = \frac{n_k}{N_k\sigma_k} \tag{3.110}$$

In Equation (3.110), n_1, n_2, n_3,…., n_k denote the sample sizes of k strata; N_1, N_2, N_3,…., N_k denote the accessible black nightshade berries' population sizes of k strata; and σ_1, σ_2, σ_3,…., σ_k denote the standard deviations of the berries' diameters of k strata. From Equation (3.110), the allocation of the subsample sizes for each stratum was computed as expressed in Equation (3.111).

$$n_i = \frac{nN_i\sigma_i}{N_1\sigma_1 + N_2\sigma_2 + N_3\sigma_3 + \cdots \ldots \ldots + N_k\sigma_k} \tag{3.111}$$

The confidence interval for the accessible black nightshade berries' population mean (μ), was given by Equation (3.112).

$$\mu \geq \bar{X} \pm Z\frac{\sigma}{\sqrt{n}} \tag{3.112}$$

In Equation (3.112), $\bar{X}$ is the sample mean, Z is the value of the standard variate at a given confidence level, n is the sample size and σ is the population standard deviation. The difference between the population mean (μ), and the sample mean ($\bar{X}$), was termed the acceptable error (E), which was computed as expressed in Equation (3.113).

$$E = \left(Z\frac{\sigma}{\sqrt{n}}\right)\sqrt{\frac{(N-n)}{(N-1)}} \tag{3.113}$$

In Equation (3.113), N is the size of the finite accessible black nightshade berries' population and other terms are as defined previously in Equation (3.112). Ripe black nightshade berries were plucked from buds of mature plants and placed in a sealed container. Plucking was done by the action of fingers to prevent unnecessary physical damage to the ripe berries that would have led to loss of seeds. A micrometer screw gauge was used to measure the diameter of the round berries. In order to measure the diameter, berries were placed between the jaws of the micrometer screw gauge and the thimble was rotated using a ratchet until each berry was secured. To read the results from the micrometer screw gauge, the first significant figure was taken from the last graduation showing on the sleeve directly to the left of the revolving thimble. An additional half scale division of 0.5 mm was included if the mark below the main scale was visible between the thimble and the main scale division on the sleeve. The remaining two significant figures—hundredths of a millimeter—were taken directly from the thimble opposite the main scale. The thimble had to line up with the main scale for the hundredths of a millimeter reading to be taken. To count the number of seeds within a berry, a sample of black nightshade berry was placed on a spot in the middle of a circular absorbent paper and with the application of thumb pressure, it was smashed to extract the seeds from the concentration of soluble solids contained in the berry fruit. The pulp and skin of the black nightshade berry were then separated from the seeds, to allow the latter to be counted. A sample of 40 berries were evaluated in this manner. The data was used in an analysis to determine the relationship between black nightshade berry seed count and size across the largest diameter to the nearest 0.01 mm with a micrometer screw gauge.

3.6.2 Standard Germination Test

Experiments were conducted in order to accomplish the above specific objective of this study. The experiments involved seed sample collection, drying experiments, seeds quality tests and models fitting. Black nightshade seeds were dried under solar, solar-exhaust gas, and exhaust gas drying modes so that the influence of the drying conditions on the seed viability could be determined. Initial moisture content of black nightshade seeds was determined, and the seeds were dried to a final moisture content and measurements taken. A standard germination test for viability was conducted for

the samples collected from the drying experiments. The objective was to determine the seed quality in terms of germination percentage (the percentage of seeds that develop into normal seedlings) under normal environmental planting conditions within a period of time. Seed samples were kept in aluminium containers under ambient conditions overnight to be in equilibrium with ambient temperature and reduce seeds stress. The standard germination test was conducted by placing seed samples on moist soil. Six replications of 30 seeds were performed for each drying mode. The seeds that had root and shoots longer than 2 mm were considered as germinated seeds and were counted after 7 days. Thereafter, the numbers obtained were converted to percentages. Germination tests were carried out in accordance with the criteria established in the rules for testing seed (International Seed Testing Association, 1985). The percentage germinated black nightshade seeds were calculated using Equation (3.114) as reported by Akowuah *et al*. (2018).

$$\%\ Germination = \frac{Number\ of\ seeds\ germinated}{Number\ of\ seeds\ set\ for\ germination} \tag{3.114}$$

3.6.3 Germination Modelling

To predict the percentage viability of seeds during storage after a given period of time, the relationship between temperature, moisture content and mean viability is used as given in Equation (3.115) (Roberts, 1972).

$$log\ p_{50} = K_v - C_1 M - C_2 T \tag{3.115}$$

In Equation (3.115), p_{50} is mean viability period in days (time taken for 50% of the seeds to die), M is moisture content (% db), T is temperature (℃), K_v, C_1 and C_2 are constants. Equation (3.116) (Ellis & Roberts, 1980; Sharp, 1982) is used to model the effect of time, temperature, and moisture content on the storage life of seeds.

$$t_v = (K_i - v)10^{(C_1 - C_2 logM - C_3 T - C_4 T^2)} \quad (3.116)$$

In Equation (3.116), t_v is storage time in days for the percentage viability to fall to v, C_1, C_2, C_3, and C_4 are constants which vary for different crops and are independent of initial seed quality, K_i is a constant specific to each seed lot and is a measure of initial seed quality. The change in seed germination which is a function of the resultant temperature from heat balance and moisture content for any time step is estimated using the modified Sharp's model presented in Equation (3.117) (Jittanit *et al*., 2009).

$$G_t = G_0 - \frac{t}{10^{(C_0 - C_1 logM_i - C_2 T - C_3 T^2)}} \quad (3.117)$$

In Equation (3.117), G_t is germination of seed after t hours of exposure (%), G_0 is initial germination of seed lot (%), M_i is initial moisture content of seeds (% db), T is temperature (°C), C_0, C_1, C_2, and C_3 are constants. Equation (3.118) is the modified Giner's model (Giner *et al*., 1991) and is used to estimate germination (G_t) of seeds with initial germination (G_0) after an exposure time (t), during which grain moisture (M_i) and absolute temperature (T_a) are kept constant.

$$\frac{G_t}{G_0} = exp\left[-\left(exp\left(-\frac{E_a}{RT_a} + Z_1 + Z_2 M_i\right)\right)t\right] \quad (3.118)$$

To fit experimental data over a succession of time intervals (Δt), Equation (3.119) (Giner *et al*., 1991) is used with grain moisture and temperature deemed constant.

$$\frac{G_{t+\Delta t}}{G_t} = exp\left[-\left(exp\left(-\frac{E_a}{RT_{am}} + Z_1 + Z_2 M_m\right)\right)\Delta t\right] \quad (3.119)$$

In Equation (3.119), G_t is germination percentage at time t, $G_{t+\Delta t}$ is germination percentage at time $t + \Delta t$, M_m is mean grain moisture content during the interval Δt (db, decimal), T_{am} is absolute temperature during the interval Δt (K), E_a is activation energy corresponding to viability loss (Joule/mole), R is gas constant, and Z_1 and Z_2 are constants of the model. Equation (3.120) (Thuy *et al*., 1999) which is a polynomial relationship between stress cracks and germination of seeds is used to find germination percentage of seeds.

$$G = -0.0211c_r^2 + 2.051C_r + 48.577 \tag{3.120}$$

In Equation (3.120), G is germination percentage of seed and C_r is proportion of seeds having transverse or vertical stress cracks (%). To validate the models' performance against experimental data, firstly, the coefficient of determination was defined by Equation (3.121), where P_i were the predicted values of the variable, O_i were the observed values, $\hat{P}_i$ was an estimate of the average response, $\hat{O}_i$ was the average of observations made and n was the number of elements of data from the experiment.

$$R^2 = \frac{\sum_{i=1}^{n}\left(P_i - \hat{P}_i\right)^2}{\sum_{i=1}^{n}(O_i - \bar{O}_i)^2} \tag{3.121}$$

Secondly, the performance of the model was measured in terms of RMSE as given in Equation (3.109). Finally, plotting of the residuals against the independent variable was done as a standard through which the regression model could be validated statistically because it was used as a measure of the distribution of errors.

CHAPTER FOUR

RESULTS AND DISCUSSION

4.1 Establishment of the Relationships between Characteristics (Fluid and Thermal) of Exhaust Gas, and Design Parameters of a Hybrid Recuperative Heat Exchanger

Table A.4 shows the connector and tube distances from the diesel engine exhaust manifold, volumes and mass of exhaust gas contained therein. Connectors were denoted by CN1 to CN6 while tubes were denoted by TB1 to TB6. For the computation of the exhaust gas mass through connectors and airtight tubes of the hybrid-recuperative heat exchanger, the density of exhaust gas was adopted as 0.7487 kg/m^3. Table A.5 shows the time taken in seconds by exhaust gas to fill connectors and tubes of the hybrid-recuperative heat exchanger.

It has been shown in Table A.5 that at the volumetric flow rate of 0.0167 m^3/s corresponding to the diesel engine speed of 2500 rpm, it took 105 seconds for exhaust gas from the engine to fill the hybrid-recuperative heat exchanger. The stated speed of 2500 rpm was the desired optimized operation speed for the diesel engine used in the current work. Accordingly, it took 0.25 seconds for exhaust gas to fill the first connector (CN1) which was 2.1 m away from the exhaust manifold and 18 seconds to fill tube number one (TB1) with a volume of 0.3 m^3 at 4.6 m away from the exhaust manifold. The mass of the exhaust gas in TB1 was 0.2 kg at the stated conditions with reference to Table A.4.

Plots of volumetric flow rates of exhaust gas against time taken to fill connectors and tubes of the hybrid-recuperative heat exchanger are shown in Figure 4.1 and Figure 4.2 for connectors and tubes respectively. The asymptotic relationship between time to fill connectors and tubes and volumetric flow rates was true for both figures. The time taken to fill connectors and tubes decreases with an increase in volumetric flow rate; however, it does not get to zero seconds value. Preliminary results of diesel engine generated exhaust gas properties corresponding to engine speed are tabulated in Table A.6 for temperatures, mass and volumetric flow rates, velocities, Reynolds and Nusselt

numbers in connectors and tubes, and available energy. Results from Table A.6 show that for all the volumetric flow rates, Reynolds number in the tubes were below the value of 2000 and this indicated fully developed laminar flows in the tubes.

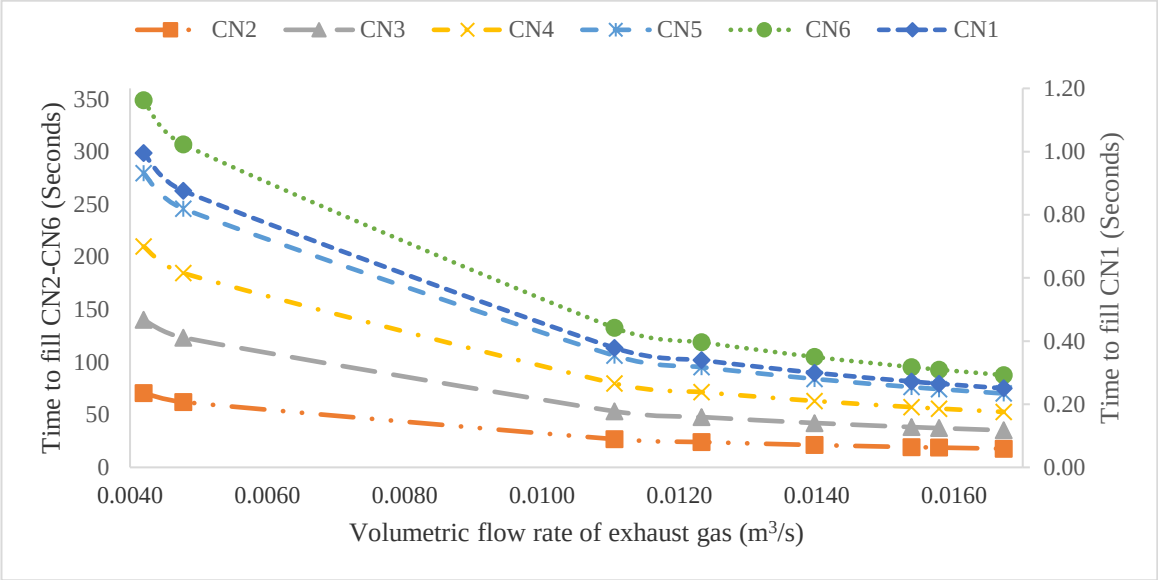

Figure 4.1: Variation of Time to Fill Connectors with Volumetric Flow Rates

Critical flow was observed at Reynolds numbers of 2681 and 3048 when exhaust gas flowed through connectors. Higher Reynolds numbers of between 7055 and 10674 in connectors were attributed to high volumetric flow rates of exhaust gas which ranged from 0.0111 to 0.0167 m^3/s. The classifications of flows in the current study are in tandem with a publication by Menon (2014) in which Reynolds numbers have been used to classify flows as laminar, critical, and turbulent.

The results of kinetic energy of exhaust gas and the variations within connectors and tubes of the hybrid recuperative heat exchanger are as shown in Table A.7. At the optimal diesel engine operation speed of 2500 rpm, the plotted variations of kinetic energy within connectors are shown in Figure 4.3 while Figure 4.4 shows the same variations within the tubes of the heat exchanger. Comparatively, the kinetic energy of exhaust gas within connectors was higher than that of tubes because it was dependent on the velocity of the gas as it flowed through the hybrid recuperative heat exchanger. When the diesel engine was operated at 2500 rpm exhaust gas velocity through

connectors were found to be 8.52 m/s and 0.14 m/s through the tubes of the heat exchanger.

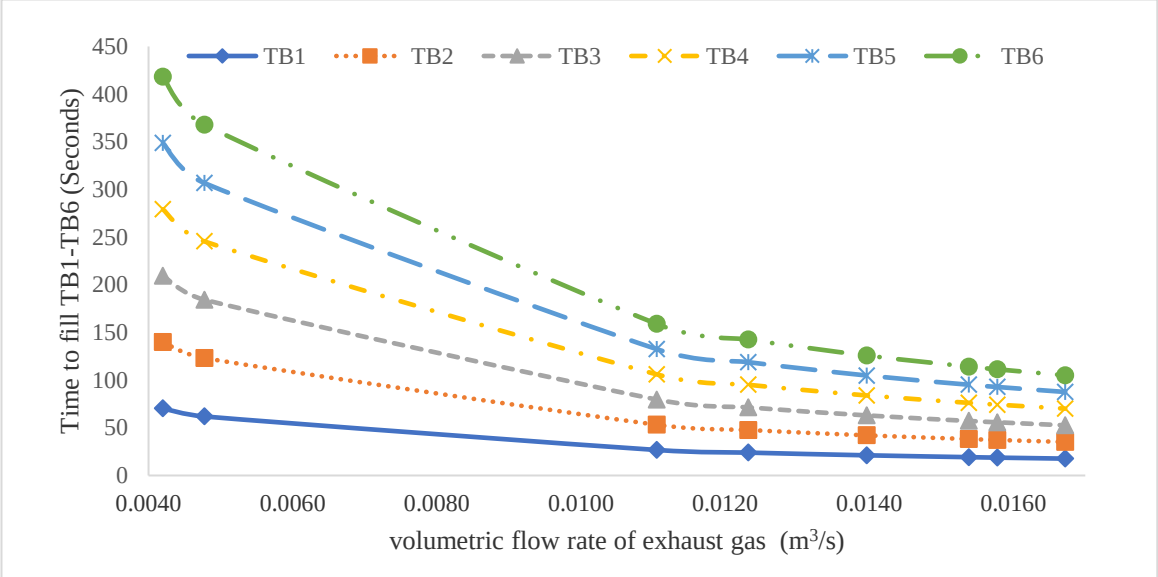

Figure 4.2: Variation of Time to Fill Tubes with Volumetric Flow Rates

The increase in kinetic energy from connector number one (CN1) to six (CN6) and from tube number one (TB1) to six (TB6) was attributed to increasing mass of exhaust gas from 0.003 to 1.1 kg in connectors and 0.2 to 1.3 kg in tubes. Mass of exhaust gas as a function of density and volume depended on the longitudinal distance from the diesel engine exhaust manifold. Connector number six (CN6) and tube number six (TB6) both had the highest amount of kinetic energy with 39.79 kJ corresponding to CN6 and 0.01289 kJ relating to TB6.

Both represented 90% of the total kinetic energy of exhaust gas in either case. The kinetic energy in connector number one (CN1) was insignificant because it represented about 0% of the total kinetic energy in the connector system. The general variations of kinetic energy with exhaust gas velocities in tubes and connectors of the hybrid recuperative heat exchanger are plotted in Figure 4.5 and Figure 4.6. The general trend is that kinetic energy increases with increase in velocity. A similar observation was made within tubes and connectors as their longitudinal distance from exhaust manifold increased.

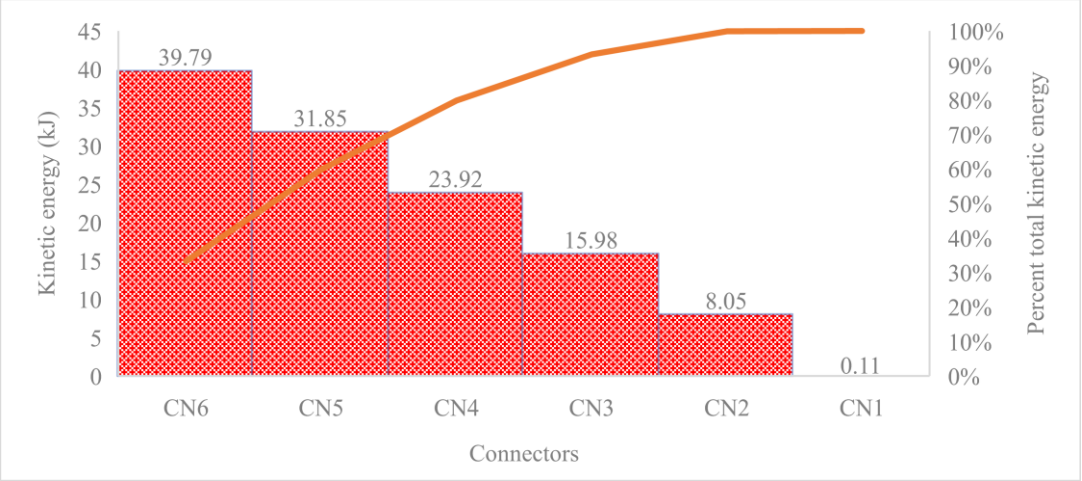

Figure 4.3: Kinetic Energy Variation in Connectors at 2500 rpm

Table A.8 and Table A.9 show the results of head losses due to friction in connectors and tubes of the hybrid recuperative heat exchanger respectively. Figure 4.7 and Figure 4.8 are plots of frictional head losses and friction factors and their variation with Reynolds number in connectors and tubes. Figure 4.9 is a plot of Reynolds number variation with volumetric flow rates in connectors and tubes. In Figure 4.7, the values of frictional head loss are higher as compared to the friction factor as applied in connectors of the heat exchanger. For this reason, frictional head loss was plotted on the primary vertical axis and the friction factor was plotted on the secondary vertical axis. The two plots were made with Reynolds number on the primary horizontal axis. It can be observed that for all the connectors, the frictional head loss increased with increasing Reynolds number an observation equally true for the tubes as plotted in Figure 4.8.

In addition, the frictional head loss increased from connector number one to six, with connector number six posting the highest value of 71 m. The high head loss is attributed to the variation of the longitudinal distance from the exhaust manifold from which it can be shown that connector number six was 16.3 m away. The friction factor graph in Figure 4.7 shows that with increasing Reynolds number, its values were decreased. This is explained by higher velocities of exhaust gas that led to higher Reynolds number as the gas flowed through connectors of the heat exchanger. In Figure 4.8, the values of frictional head loss in tubes were lower in comparison to the

friction factor. It was imperative that friction factor should be plotted on the primary vertical axis as frictional head loss took the secondary vertical axis so that Reynolds number values were plotted on the primary horizontal axis. The graph of friction factor shows a decreasing trend in Figure 4.8, with increased Reynolds number which in turn increase with increased velocities as the engine speed is increased.

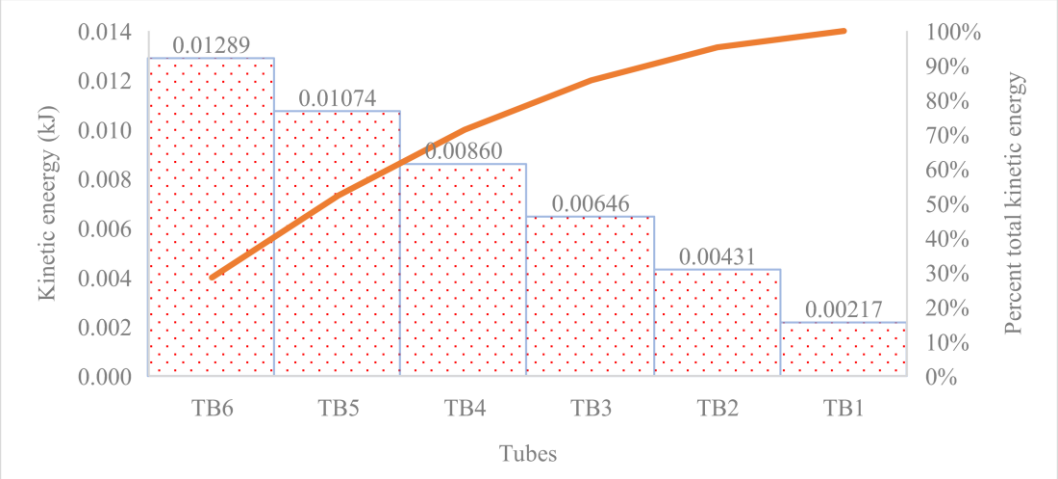

Figure 4.4: Kinetic Energy Variation In Tubes at 2500 rpm

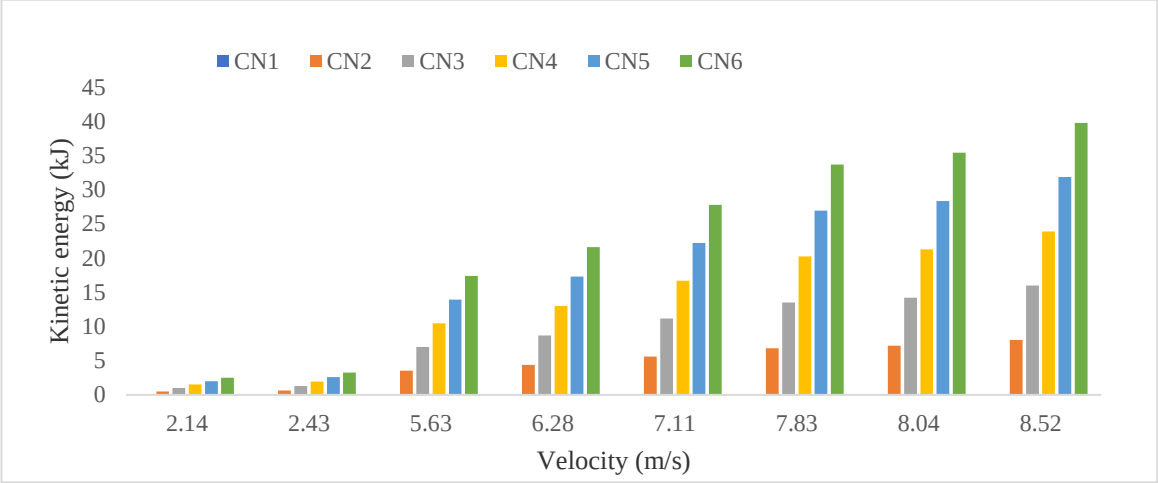

Figure 4.5: Connectors' Kinetic Energy Variation with Velocity

This is synonymous with what has been reported in Figure 4.7. Frictional head loss in tubes were comparatively low relative to those reported for connectors. At the optimal engine operation speed of 2500 rpm, coinciding with a Reynolds number of 1368, tube number one had the lowest value of frictional head loss at 0.00055 m and tube number six had the highest value reported at 0.00225 m. The two tubes were 14.2 m apart with tube number one being 4.6 m away from the exhaust manifold and tube number six at 18.8 m away for similar comparison.

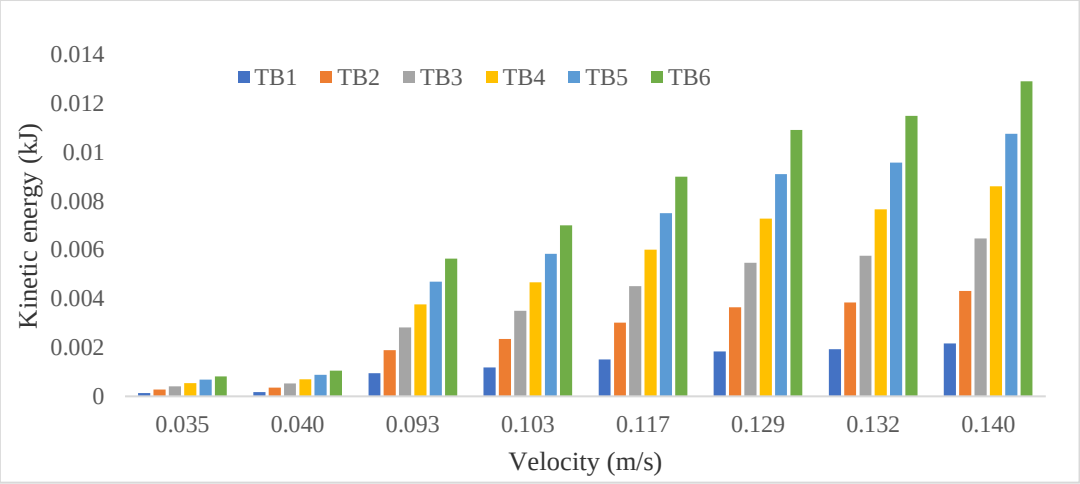

Figure 4.6: Tubes' Kinetic Energy Variation with Velocity

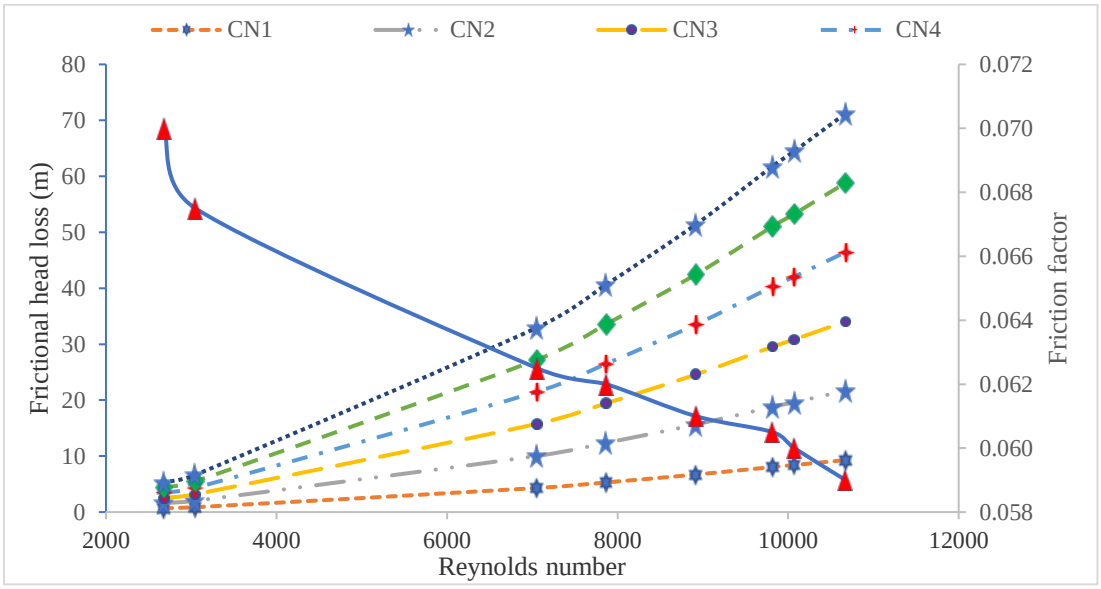

Figure 4.7: Connectors' Frictional Head Loss and Friction Factor Variations

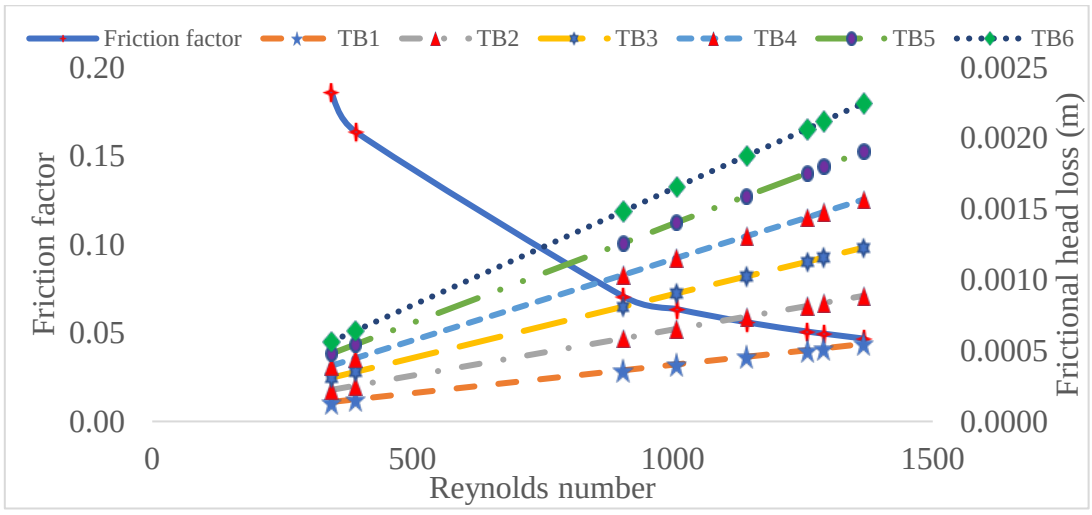

Figure 4.8: Friction Factor and Frictional Head Loss Variations in Tubes

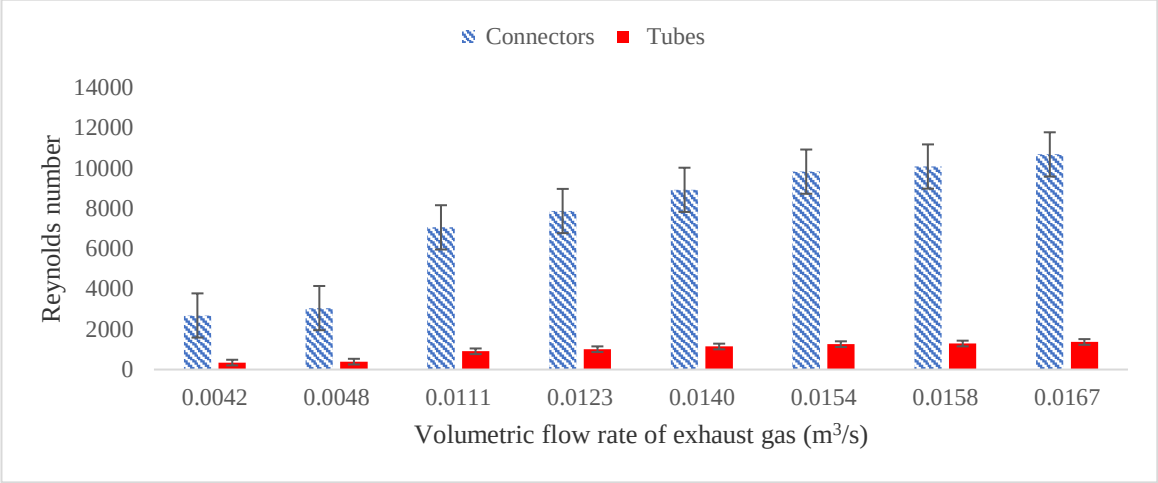

Figure 4.9: Reynolds Number Variation with Volumetric Flow Rate of Exhaust Gas in Connectors and Tubes

4.2 Development of the Hybrid Recuperative Heat Exchanger and Performance Evaluation Using Experimental Temperature and Moisture Evaporation Data

A labeled portion of the developed heat exchanger is shown in Figure 4.10. The percent internal uncertainty for experimental measurements of relative humidity (γ) was 4.1% and 17.5% for temperature (T) observations. The approximation based on linearization of partial vapour pressure over temperature ranges between 25-55℃ gave results of the constants G_1 as 397.53 and G_2 as 7926.9 with an R^2 of 0.9683. The results of linear regression analysis for the values of y and x in Equation (3.87) which correspond to Equation (3.86) show that with an R^2 of 0.9854, the constants C and n were obtained as 0.2183 and 0.2927 respectively.

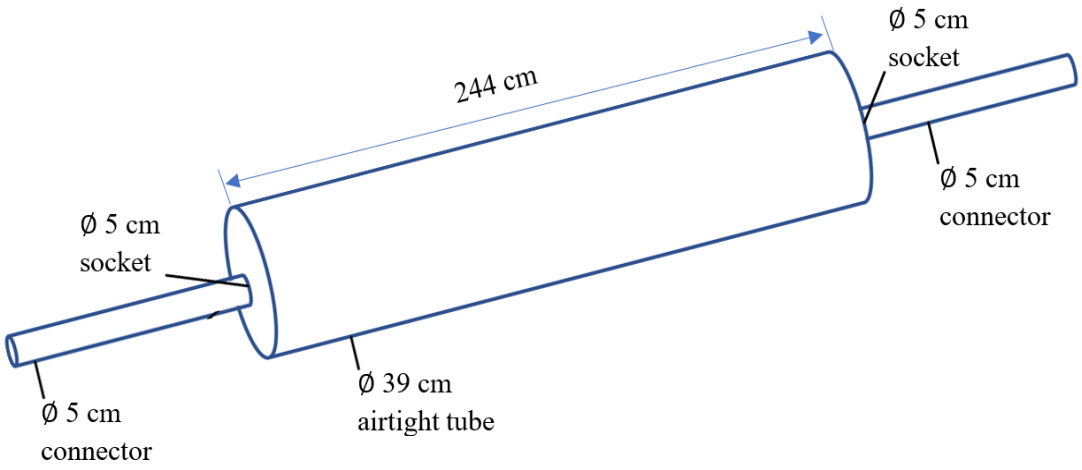

Figure 4.10: Schematic Diagram of Hybrid Recuperative Heat Exchanger Portion

The constants C and n were considered further for obtaining the values of convective heat transfer coefficients which were then used to evaluate the evaporative heat transfer coefficients and the results plotted in Figure 4.11. It can be observed from Figure 4.11 that the values of convective heat transfer coefficients (h_b) range between 2.48 and 2.55 W/m^{2}·°C and those of evaporative heat transfer coefficients (h_e) are between 0.95 and 36.81 W/m^{2}·°C for the considered drying period.

The percent variation ranged between 0.4 and 2.8% in convective heat transfer coefficients when the minimum value of (h_b) was compared with the others. In both cases, the minimum values of heat transfers were obtained for the time interval of one hour after drying had commenced. The maximum values were observed after 6 hours of drying time for evaporative heat transfer coefficients and 8 hours for convective heat transfer coefficients.

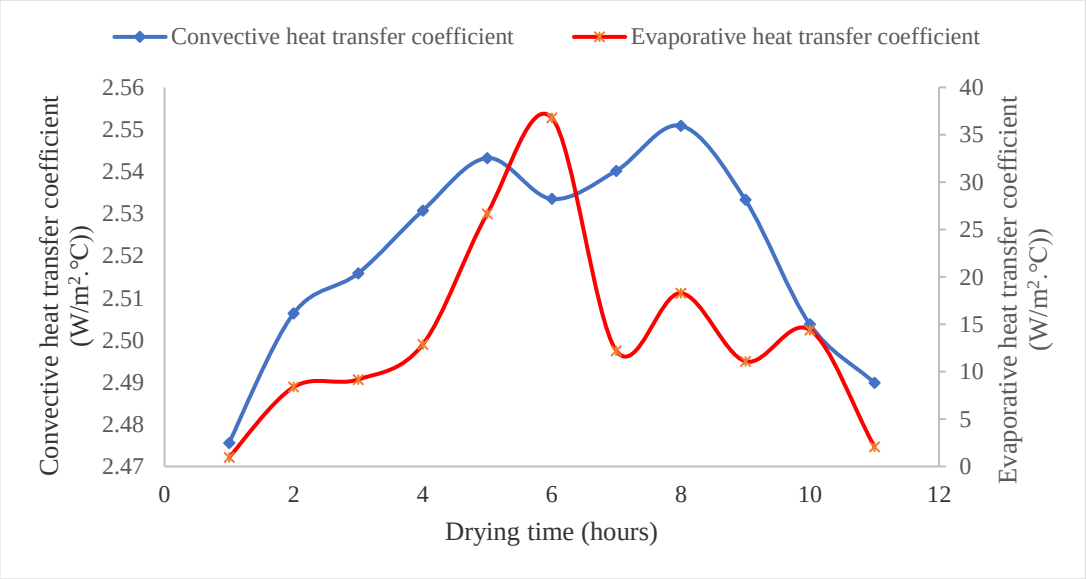

Figure 4.11: Variation of Heat Transfer Coefficients with Drying Time for Black Nightshade Seeds

4.2.1 Solar Drying Mode

Experimental and predicted results of changes in evaporated moisture, greenhouse dryer air temperature, black nightshade seeds temperature, and air relative humidity which all occur simultaneously to make drying a continuous process are summarized in Table A.10. The results of moisture evaporated (experimental and predicted) and relative humidity are plotted in Figure 4.12 from which the model's performance based on RMSE was found as 0.6455. The rate of heat utilized for solar mode of drying ranged from 37 to 683 J/m^2·s and peaked after 8 hours of drying when convective heat transfer coefficient was 2.55 W/m^2·°C and evaporative heat transfer coefficient was 18.29 W/m^2·°C.

Moisture evaporated and relative humidity decreased with increasing drying time. In Figure 4.12 relative humidity increased with increasing drying time after 8 hours of drying. Residual plots of predicted moisture evaporated are shown in Figure 4.13 with five positive data points, one on the residual equal to zero line, and six are observed on the negative side. A correlation coefficient of 0.9999 was obtained for predicted versus experimental moisture evaporated shown in Figure 4.14. From a two-tailed t-test of two samples while assuming equal variances at 0.05 level of significance,

experimental moisture evaporated data had a mean of 4.18 g when the predicted had a mean of 3.87 g ($t_{calc} = 0.9080$, $t_{crit} = 2.0860$). Thus, there was enough evidence to retain the null hypotheses that there is no difference in the means between predicted and experimental observations of moisture evaporated and it was concluded with 95% confidence that the model is useful in predicting moisture evaporated from black nightshade seeds. The solver converged to a solution after all the constraints were satisfied with iterations performed for which the objective function (minimum sums of squares of residuals) did not move significantly. From the iterations performed, the model parameters Ω_0, Ω_1, Ω_2, Ω_3, Ω_4, and Ω_5 were quantified.

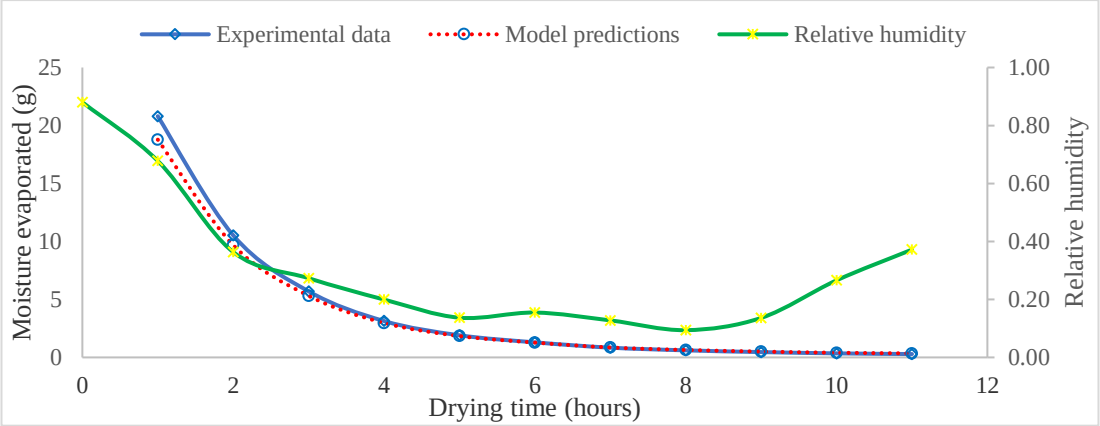

Figure 4.12: Moisture Evaporated and Relative Humidity in Solar Mode of Drying

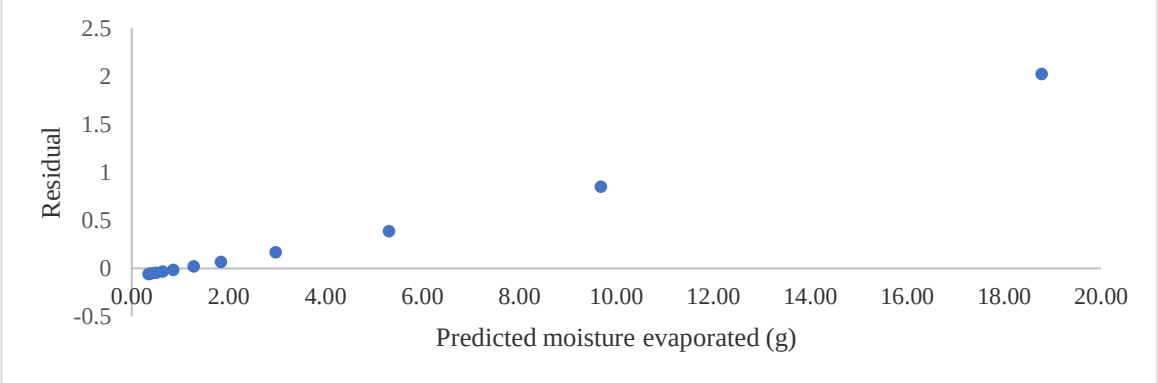

Figure 4.1: Residual Plots of Predicted Moisture Evaporated in Solar Mode of Drying

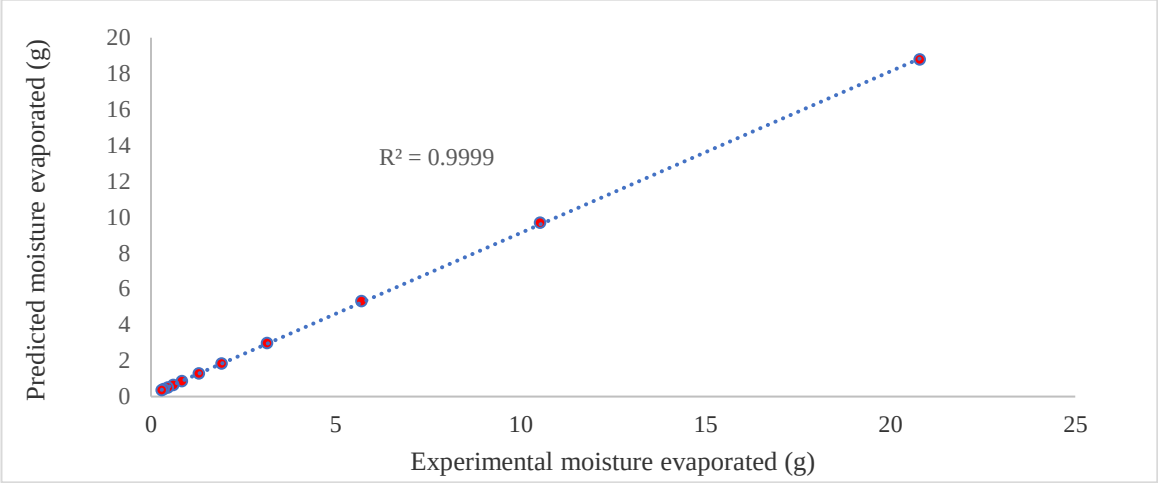

Figure 4.14: Correlation between Predicted and Experimental Moisture Evaporated in Solar Mode of Drying

The experimental and predicted black nightshade seeds temperatures against drying time are plotted in Figure 4.15 from which the results of the model's performance based on RMSE was found as 2.1409. The plot shows that there is an increasing nonlinear relationship between drying time and black nightshade seeds temperature for the first eight hours of drying and thereafter, a decreasing nonlinear relationship is observed for the rest of the drying period. The corresponding residual versus fits plot for the data set with black nightshade seeds temperature as the response and drying time as the predictor is shown in Figure 4.16. The residual plots show nonlinearity and an indication of cyclic behaviour. Figure 4.17 is a goodness of fit plot of the predicted temperatures against experimental observations which show a correlation coefficient of 0.9936.

The predicted black nightshade seeds temperature show agreement with experimental observations and from Figure 4.16, none of the data points fell directly on the residual equal to zero line. The residuals depart from the zero line in a systematic manner with most of the data points concentrated between 30 and 60℃ and are positive for five values and negative for seven values. From a two-tailed t-test of two samples while assuming equal variances at 0.05 level of significance, experimental black nightshade temperature data had a mean of 38.56℃ when the predicted data had a mean of 38.75℃ ($t_{calc} = 0.9745$, $t_{crit} = 2.0739$). Thus, there was enough evidence to retain

the null hypotheses that there is no difference in the means between predicted and experimental observations of black nightshade seeds temperatures and it was concluded with 95% confidence that the model is useful in predicting the temperature of the seeds. Model parameters ξ_0, ξ_1, and ξ_2 were quantified to show the main effects of screening and characterizing black nightshade seeds temperature prediction model. The model parameters ξ_3 quantified the interaction (cross product) term between drying time and experimental temperature data, ξ_4 quantified the first leading term with the second degree on drying time factor, ξ_5 quantified the second order term corresponding to black nightshade seeds experimental temperature and ϖ was the random error term that accounted for experimental error in the system. Experimental and predicted greenhouse dryer room air temperatures against drying times are plotted in Figure 4.18 from which the results of the model's performance based on RMSE was found as 2.1257.

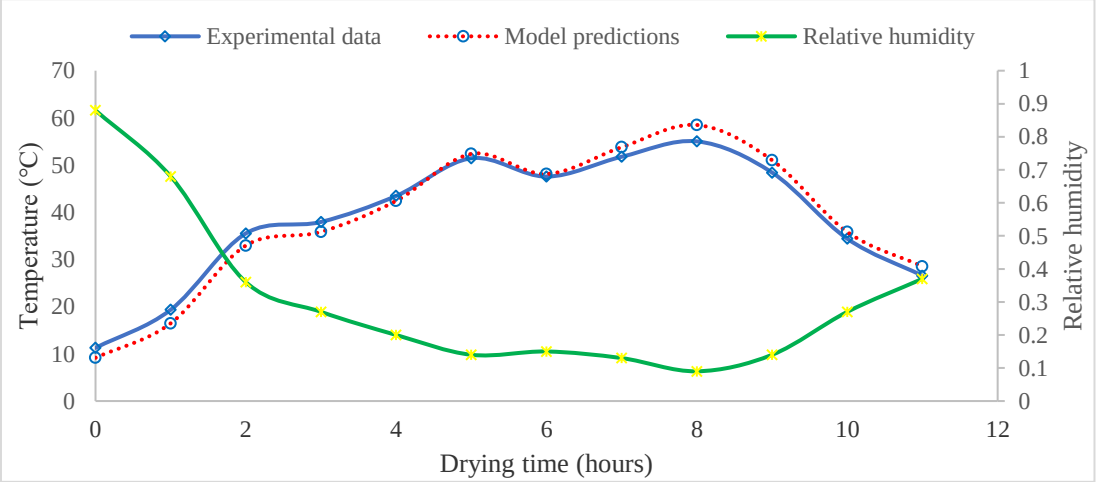

Figure 4.15: Black Nightshade Seeds Temperature and Relative Humidity in Solar Mode of Drying

The plot shows that there is an increasing nonlinear relationship between drying time and greenhouse dryer room air temperature for the first eight hours of drying and thereafter, a decreasing nonlinear relationship is observed for the rest of the drying period. The corresponding residual plot of greenhouse dryer room air predicted temperature is shown in Figure 4.19.

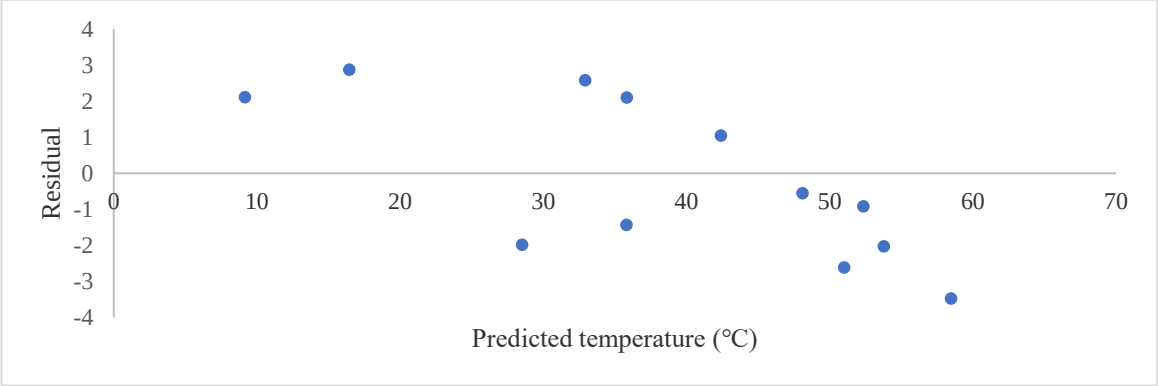

Figure 4.16: Residual Plots of Black Nightshade Seeds Predicted Temperature in Solar Mode of Drying

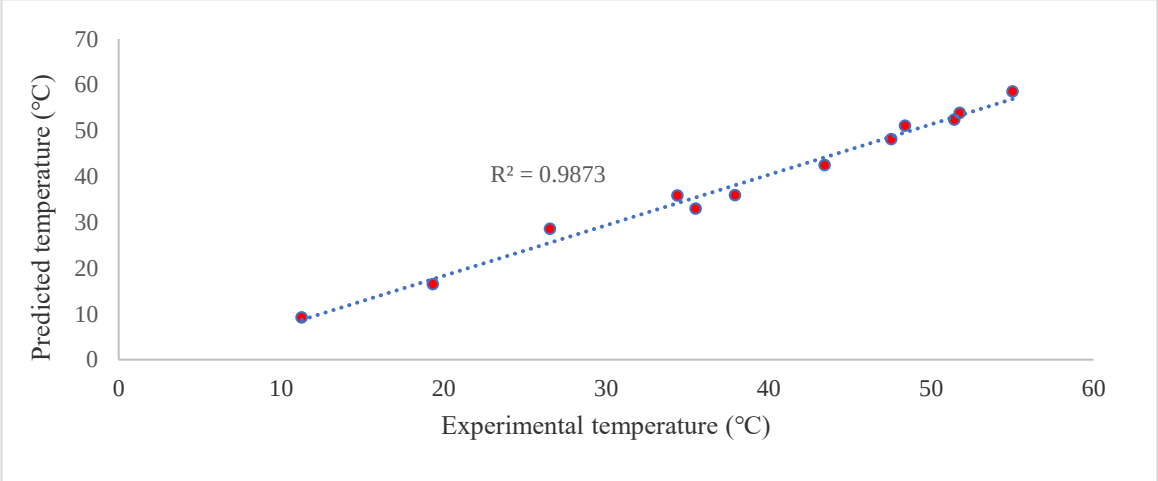

Figure 4.17: Correlation between Predicted and Experimental Black Nightshade Seeds Temperature in Solar Mode of Drying

The plot show nonlinearity and indication of cyclic behaviour. Observations from Figure 4.20 show a correlation coefficient of 0.9873. With reference to Figure 4.19, none of the data points fell directly on the residual equal to zero line. The residuals depart from the zero line in a systematic manner with most of the positive data points concentrated between 35 and 60°C. A two-tailed t-test of two samples while assuming equal variances at 0.05 level of significance, show that both predicted and experimental greenhouse dryer room air temperature data had an equal mean of 41.6°C ($t_{calc} = 0.9993$, $t_{crit} = 2.0739$). Thus, there was enough evidence to retain the null

hypotheses that there is no difference in the means between predicted and experimental observations of greenhouse dryer room air temperatures and it was concluded with 95% confidence that the model is useful in predicting room air temperature of the greenhouse dryer. From iterations, the model parameters ζ_0, ζ_1, and ζ_2 were quantified to show the main effects of screening and characterizing the greenhouse dryer room air temperature prediction model. The model parameters ζ_3 quantified the interaction (cross product) term between drying time and experimental temperature data, ζ_4 quantified the first leading term with the second degree on drying time factor, ζ_5 quantified the second order term corresponding to greenhouse dryer room air experimental temperature and ϱ was the random error term that accounted for the experimental error in the system.

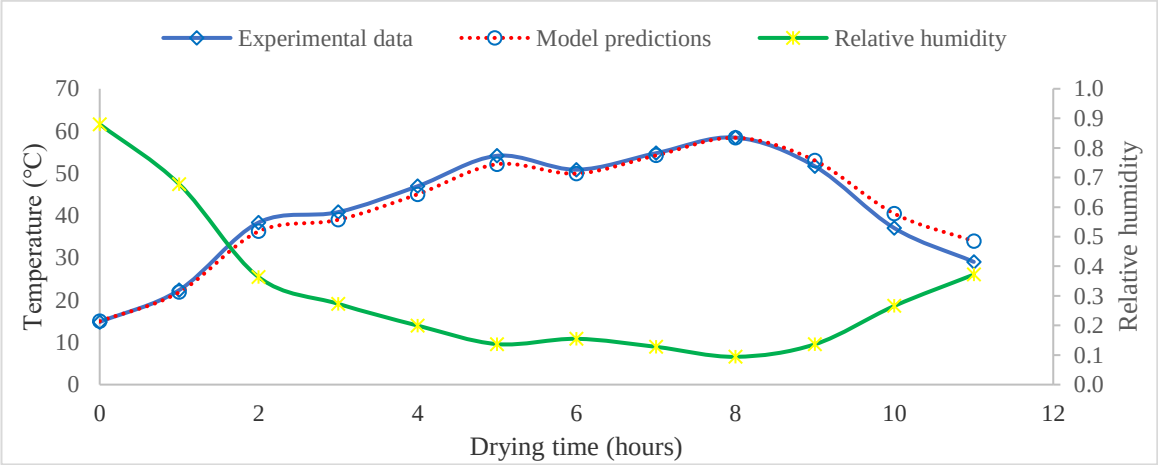

Figure 4.18: Greenhouse Dryer Room Air Temperature and Relative Humidity in Solar Mode of Drying

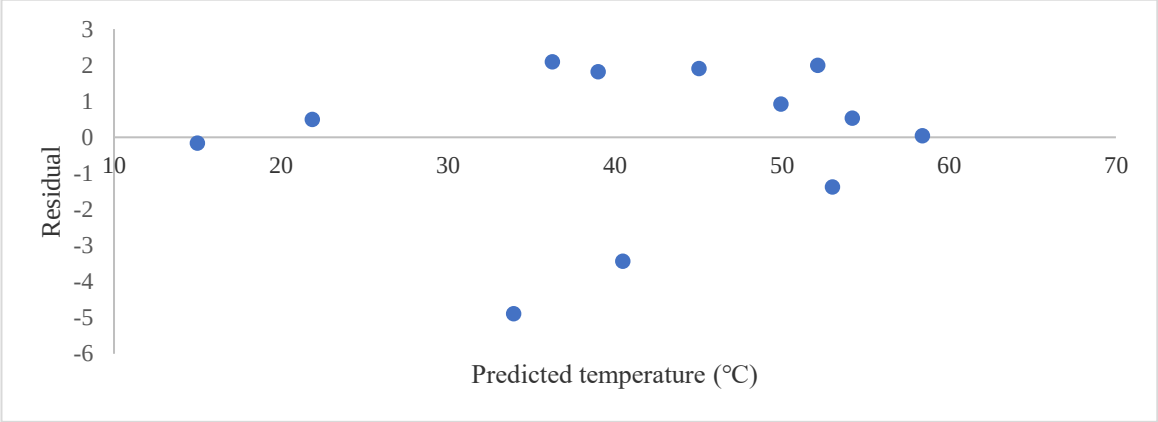

Figure 4.19: Residual Plots of Greenhouse Dryer Room Air Predicted Temperature in Solar Mode of Drying

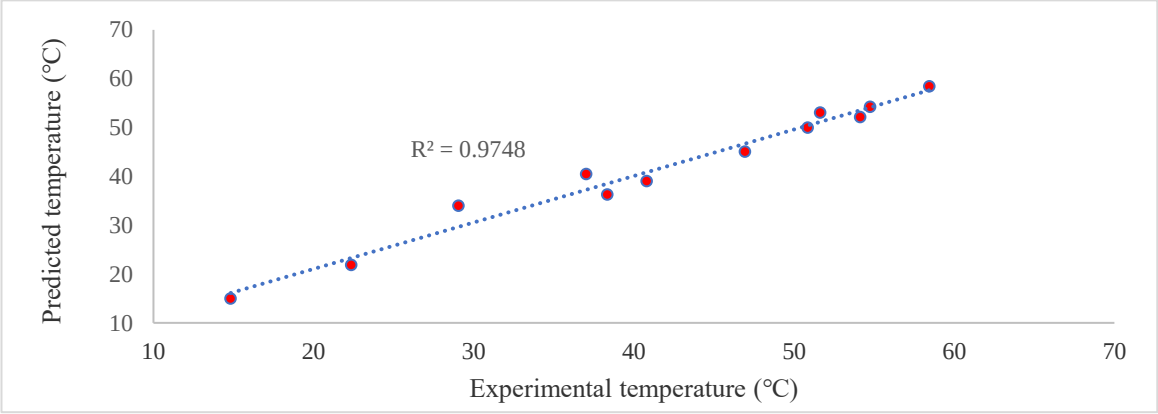

Figure 4.20: Correlation between Predicted and Experimental Greenhouse Dryer Room Air Temperature in Solar Mode of Drying

4.2.2 Heat Exchanger Performance in Solar-Exhaust Gas Mode of Drying

To analyse heat exchanger performance, Figure 4.21 illustrates the comparison of drying time between solar and solar-exhaust gas modes of drying. The heat exchanger provided additional heat energy for quicker drying of black nightshade seeds. Drying took 10 hours in solar-exhaust gas mode as compared to 11 hours in solar mode of drying. Temperature and relative humidity variations during the experiment are

presented in Figure 4.22. In solar mode of drying, temperature inside the dryer ranged between 14.82 and 58.46℃. In solar-exhaust gas mode of drying, the range was observed from 34.49 to 61.97℃.

The heat exchanger raised the dryer temperature by an average of 11.78℃ when temperature differences between inside and outside were compared in solar-exhaust gas mode of drying. In Figure 4.22, the lowest temperature difference between inside and outside the dryer, was observed on the 4^{th} hour of drying as 4.28℃. The highest temperature difference of 21.25℃ was observed on the 2^{nd} and 3^{rd} hours of drying. In summary, temperatures inside the dryer were higher than the corresponding outside temperatures throughout the drying period because the cover material used in the dryer harnessed solar energy to raise the temperature while at the same time heat energy recovered from exhaust gas of a diesel engine kept the temperatures high. Inside relative humidity was low as compared to the outside relative humidity for the first four hours of dying. The combination of high temperature and low relative humidity in a dryer increased the ability of drying air to carry away moisture. Table A.11 is a summary of experimental and predicted results of changes in evaporated moisture, greenhouse dryer room air temperature, black nightshade seeds temperature, and air relative humidity in solar-exhaust gas mode of drying.

The results of moisture evaporated (experimental and predicted) and relative humidity are plotted in Figure 4.23 from which the model's performance based on RMSE was found to be 0.5186. The rate of heat utilized for solar-exhaust gas mode of drying ranged from 40.49 to 685.94 $J/m^2.s$ and peaked after 8 hours of drying when convective heat transfer coefficient for black nightshade seeds was 2.55 $W/m^2.℃$ and evaporative heat transfer coefficient was 18.29 $W/m^2.℃$. Moisture evaporated and relative humidity decreased with increasing drying time.

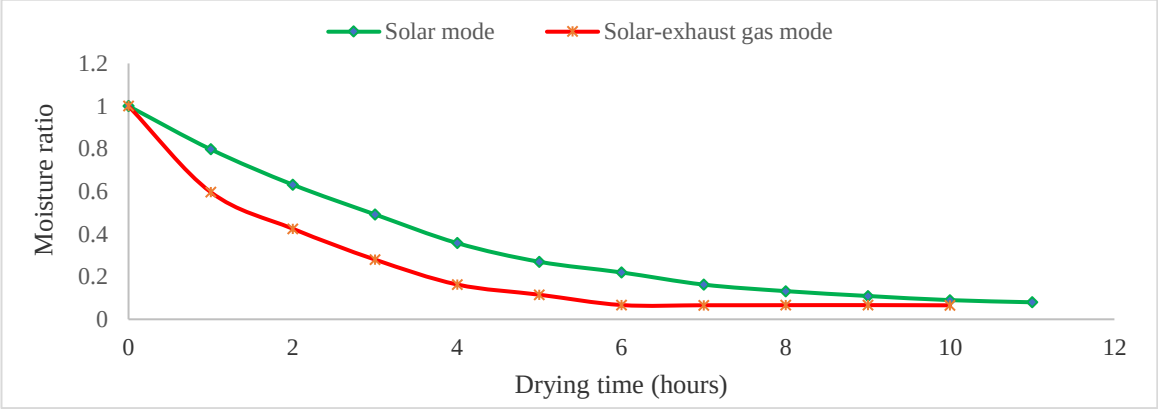

Figure 4.21: Drying Time Comparison between Solar and Solar-Exhaust Gas Modes of Drying

Residual plots of predicted moisture evaporated are illustrated in Figure 4.24 with five positive data points, and six clustered on residual equal to zero line. A correlation coefficient of one was obtained for predicted versus experimental moisture evaporated as shown in Figure 4.25. From a two-tailed t-test of two samples while assuming equal variances at 0.05 level of significance, experimental moisture evaporated data had a mean of 3.93 g when the predicted had a mean of 3.66 g ($t_{calc} = 0.9106$, $t_{crit} = 2.1001$). Thus, there was enough evidence to retain the null hypotheses that there is no difference in the means between predicted and experimental observations of moisture evaporated and it was concluded with 95% confidence that the model is useful in predicting moisture evaporated from black nightshade seeds. The solver converged to a solution after all the constraints were satisfied with iterations performed for which the objective function (minimum sums of squares of residuals) did not move significantly. From the iterations performed, the model parameters $\Omega_0, \Omega_1, \Omega_2, \Omega_3, \Omega_4$, and Ω_5 were quantified for solar-exhaust gas mode of drying.

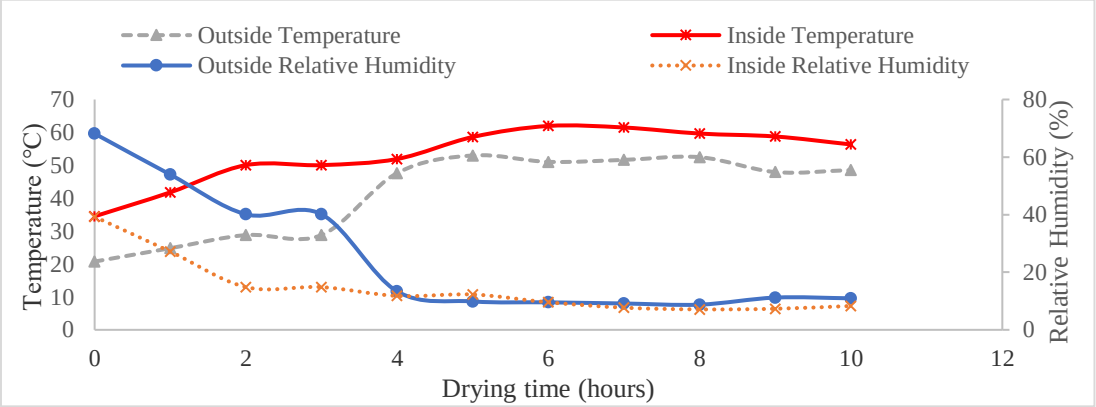

Figure 4.22: Temperature and Relative Humidity Variations in Solar-Exhaust Gas Mode of Drying

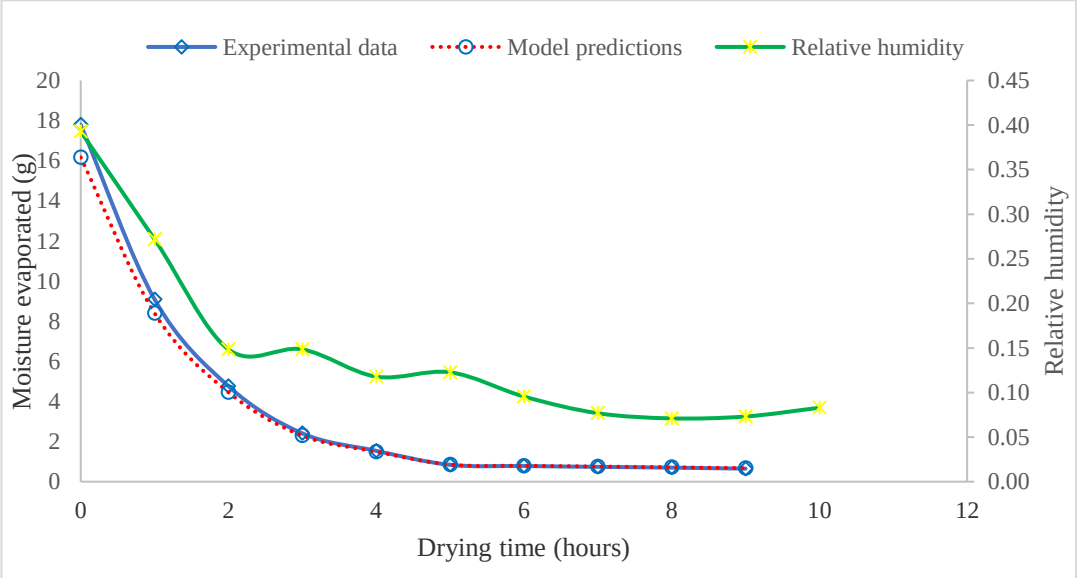

Figure 4.23: Moisture Evaporated and Relative Humidity in Solar-Exhaust Gas Mode of Drying

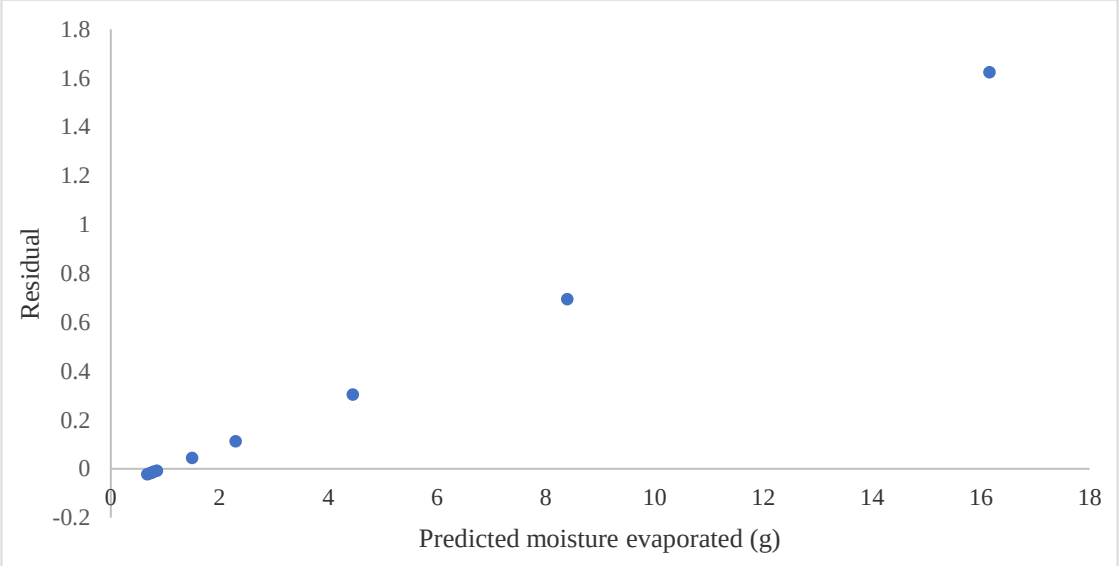

Figure 4.24: Residual Plots of Predicted Moisture Evaporated in Solar-Exhaust Gas Mode of Drying

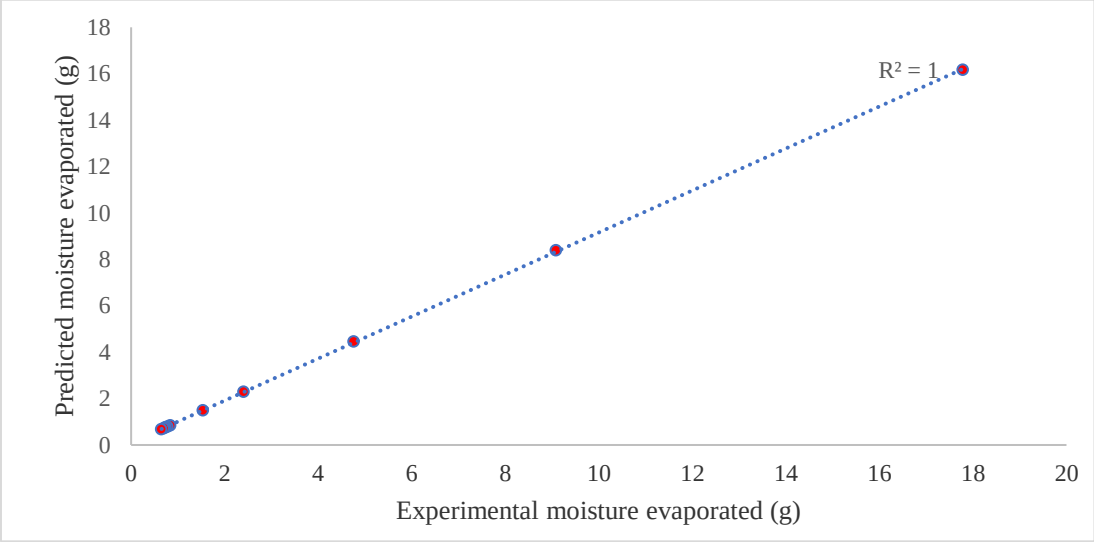

Figure 4.25: Correlation between Predicted and Experimental Moisture Evaporated in Solar-Exhaust Gas Mode of Drying

The experimental and predicted black nightshade seeds temperatures against drying time are plotted in Figure 4.26 from which the results of the model's performance based on RMSE was found as 1.9524. The plot shows that there is an increasing

nonlinear relationship between drying time and black nightshade seeds temperature for the first eight hours of drying and thereafter, a decreasing nonlinear relationship is observed for the rest of the drying period. The corresponding residual versus fits plot for the data set with black nightshade seeds temperature as the response and drying time as the predictor is shown in Figure 4.27. The residual plots show nonlinearity and an indication of cyclic behaviour. Figure 4.28 is a goodness of fit plot of the predicted temperatures against experimental observations which show a correlation coefficient of 0.9947. The predicted black nightshade seeds temperature show agreement with experimental observations and from Figure 4.27, none of the data points fell directly on the residual equal to zero line. The residuals depart from the zero line in a systematic manner with most of the data points concentrated between 45 and 60℃ and are positive for six values and negative for five values. From a two-tailed t-test of two samples while assuming equal variances at 0.05 level of significance, experimental black nightshade seeds temperature data had a mean of 53.48℃ when the predicted data had a mean of 53.03℃ ($t_{calc} = 0.9142, t_{crit} = 2.0860$). Thus, there was enough evidence to retain the null hypotheses that there is no difference in the means between predicted and experimental observations of black nightshade seeds temperatures and it was concluded with 95% confidence that the model is useful in predicting the temperature of the seeds. Model parameters ξ_0, ξ_1, and ξ_2 were quantified to show the main effects of screening and characterizing black nightshade seeds temperature prediction model. The model parameters ξ_3 quantified the interaction (cross product) term between drying time and experimental temperature data, ξ_4 quantified the first leading term with the second degree on drying time factor, ξ_5 quantified the second order term corresponding to black nightshade seeds experimental temperature and ϖ was the random error term that accounted for experimental error in the system. Experimental and predicted greenhouse dryer room air temperatures against drying time are plotted in Figure 4.29 from which the results of the model's performance based on RMSE was found as 1.7836.

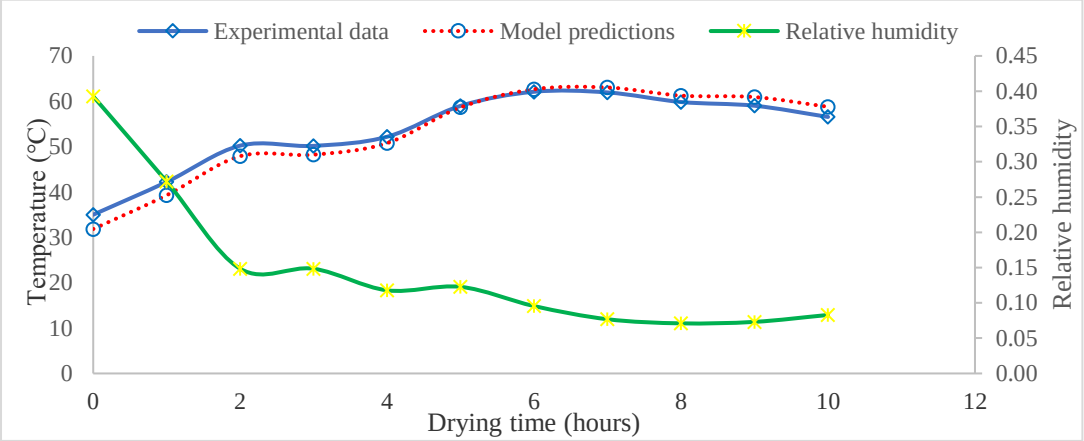

Figure 4.2: Black Nightshade Seeds Temperature and Relative Humidity in Solar-Exhaust Gas Mode of Drying

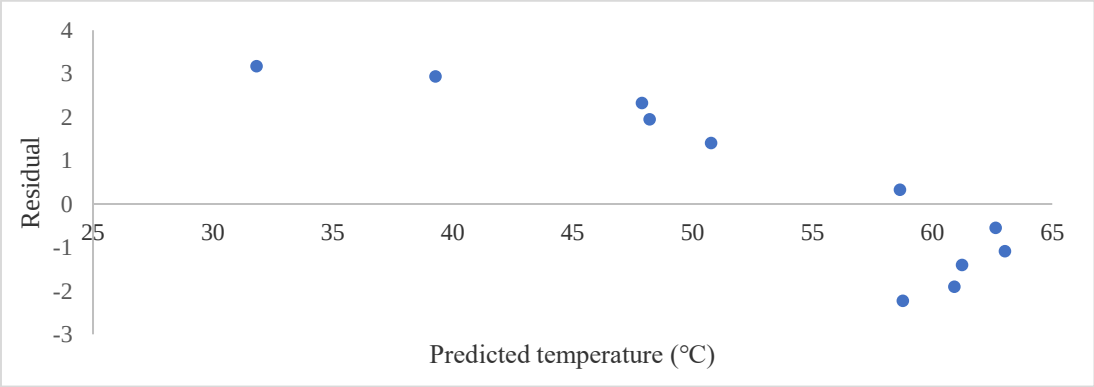

Figure 4.27: Residual Plots of Black Nightshade Seeds Predicted Temperature in Solar-Exhaust Gas Mode of Drying

The plot shows that there is an increasing nonlinear relationship between drying time and greenhouse dryer room air temperature for the first eight hours of drying and thereafter, a decreasing nonlinear relationship is observed for the rest of the drying period. The corresponding residual plot of greenhouse dryer room air predicted temperature is shown in Figure 4.30. The plot show nonlinearity and indication of cyclic behaviour. Observations from Figure 4.31 show a correlation coefficient of 0.9967. With reference to Figure 4.30, none of the data points fell directly on the residual equal to zero line. The residuals depart from the zero line in a systematic manner with most of the data points concentrated between 45 and 60℃. Seven data

points are positive while four are negative. A two-tailed t-test of two samples while assuming equal variances at 0.05 level of significance, show that experimental and predicted greenhouse dryer room air temperature data had means of 53.19℃ and 52.21℃, respectively ($t_{calc} = 0.8103$, $t_{crit} = 2.0860$).

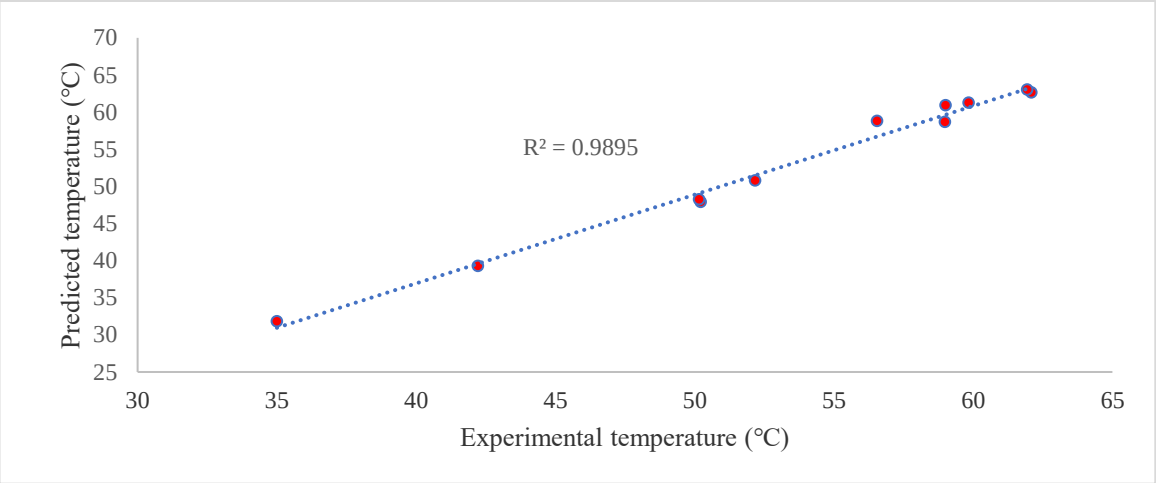

Figure 4.28: Correlation between Predicted and Experimental Black Nightshade Seeds Temperature in Solar-Exhaust Gas Mode of Drying

Thus, there was enough evidence to retain the null hypotheses that there is no difference in the means between predicted and experimental observations of greenhouse dryer room air temperatures and it was concluded with 95% confidence that the model is useful in predicting room air temperature of the greenhouse dryer. Lad *et al*. (2023) successfully and efficiently maintained drying chamber temperature between 50 and 55℃ in an indirect solar dryer for food quality preservation when phase change material was used.

Lad *et al*. (2023) further reported average solar radiation of 660 W/m^2, average day temperature of 40℃ and average night temperatures of 30℃ which are consistent with the findings of the current study done in Kenya—a region with tropical climatic conditions characterized by high temperature and direct sunlight. From iterations, the model parameters ζ_0, ζ_1, and ζ_2 were quantified to show the main effects of screening and characterizing the greenhouse dryer room air temperature prediction model.

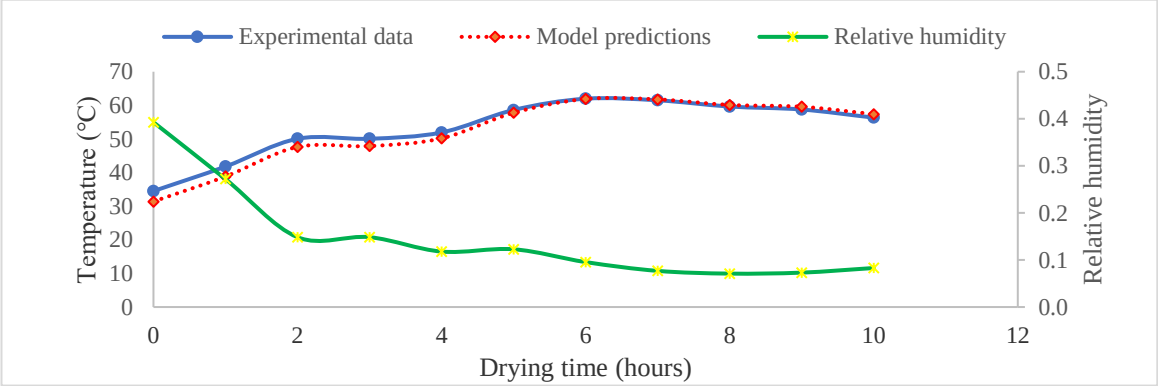

Figure 4.29: Greenhouse Dryer Room Air Temperature and Relative Humidity in Solar-Exhaust Gas Mode of Drying

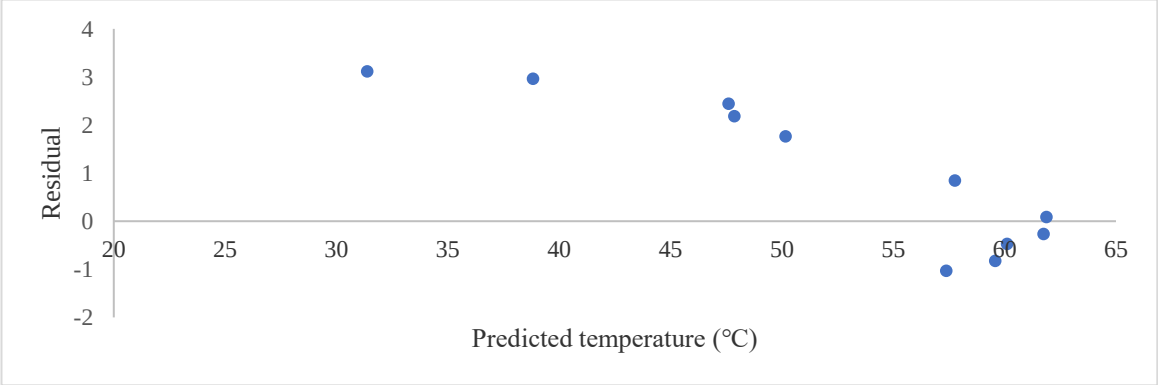

Figure 4.30: Residual Plots of Greenhouse Dryer Room Air Predicted Temperature in Solar-Exhaust Gas Mode of Drying

The model parameters ζ_3 quantified the interaction (cross product) term between drying time and experimental temperature data, ζ_4 quantified the first leading term with the second degree on drying time factor, ζ_5 quantified the second order term corresponding to greenhouse dryer room air experimental temperature and ϱ was the random error term that accounted for the experimental error in the system.

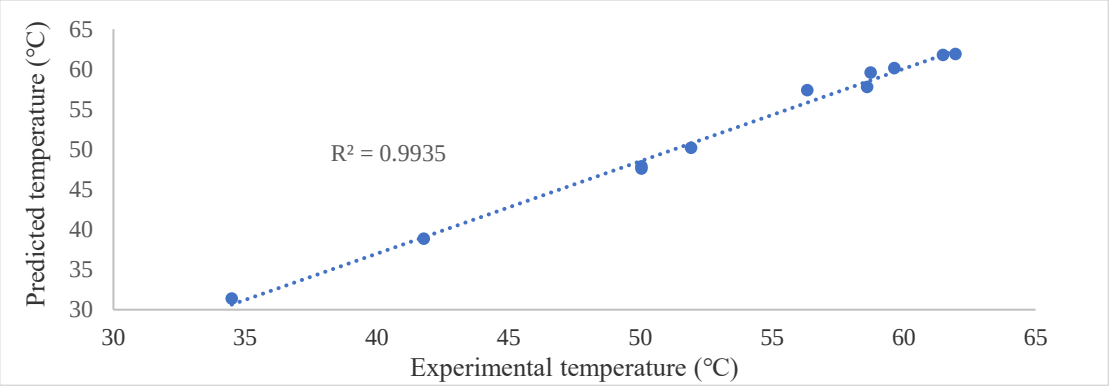

Figure 4.31: Correlation between Predicted and Experimental Greenhouse Dryer Room Air Temperature in Solar-Exhaust Gas Mode of Drying

4.2.3 Heat Exchanger Performance in Exhaust Gas Mode of Drying

Comparison of drying time for solar, solar exhaust gas, and exhaust gas modes of drying is illustrated in Figure 4.32. The heat exchanger provided the required heat energy to dry black nightshade seeds in 14 hours in exhaust gas mode of drying. Referring to Figure 4.33 and considering outside and inside temperatures of this mode of drying, the average hourly rise in temperature inside the dryer was 8.04℃ with a minimum rise of 3.7℃ and a maximum of 9.41℃ when exhaust gas was utilized to provide heat energy. Heat energy recovered from exhaust gas of a diesel engine kept the temperatures inside the dryer higher than outside. However, relative humidity inside the dryer were higher than those outside because water vapour from the open cooling system of a diesel engine kept the dryer moist. In a study by Ndirangu *et al*. (2020), the system performance of a developed multipurpose solar-biomass greenhouse dryer improved when solar energy was backed up with biomass energy. The drying increased by about 18 to 19% using the solar-biomass mode compared to both natural and forced convection modes. In conclusion, the authors recommended more tests to be undertaken to fully analyze the dryer's performance, especially in optimizing additional heat energy to achieve desired temperatures.

Table A.12 is a summary of experimental and predicted results of changes in evaporated moisture, greenhouse dryer room air temperature, black nightshade seeds temperature, and air relative humidity in exhaust gas mode of drying. The results of

moisture evaporated (experimental and predicted) and relative humidity are plotted in Figure 4.34 from which the model's performance based on RMSE was found as 0.2453. The rate of heat utilized for exhaust gas mode of drying ranged from 21.69 to 668.11 J/m^2·s and peaked after 8 hours of drying when convective heat transfer coefficient was 2.55 W/m^2·°C and evaporative heat transfer coefficient was 18.29 W/m^2·°C. Moisture evaporated and relative humidity decreased with increasing drying time. Residual plots of predicted moisture evaporated are shown in Figure 4.35 with all the 15 data points observed as negative. A correlation coefficient of 0.9999 was obtained for predicted versus experimental moisture evaporated shown in Figure 4.36. From a two-tailed t-test of two samples while assuming equal variances at 0.05 level of significance, experimental moisture evaporated data had a mean of 3.47 g when the predicted had a mean of 3.67 g ($t_{calc} = 0.9333$, $t_{crit} = 2.0556$).

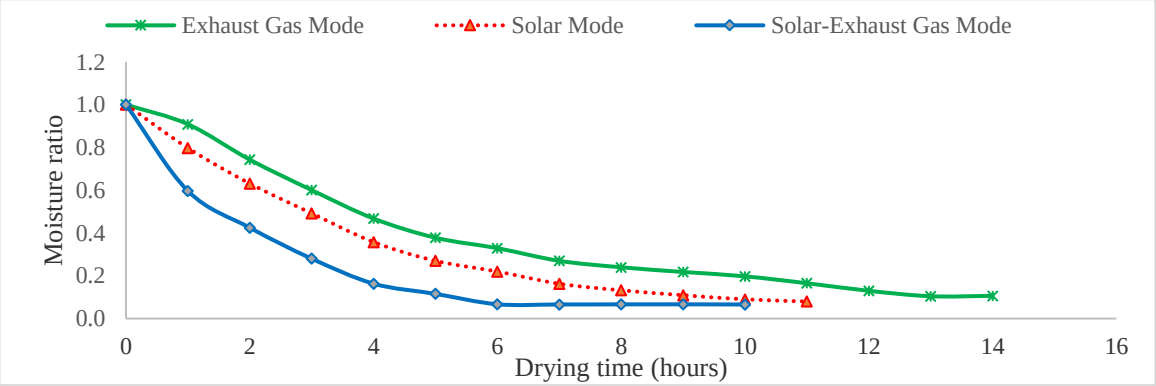

Figure 4.32: Drying Time Comparison for Solar, Solar-Exhaust Gas, and Exhaust Gas Modes of Drying

Thus, there was enough evidence to retain the null hypotheses that there is no difference in the means between predicted and experimental observations of moisture evaporated and it was concluded with 95% confidence that the model is useful in predicting moisture evaporated from black nightshade seeds. From the iterations performed, the model parameters Ω_0, Ω_1, Ω_2, Ω_3, Ω_4, and Ω_5 were quantified for exhaust gas mode of drying. The experimental and predicted black nightshade seeds temperatures against drying time are plotted in Figure 4.37 from which the results of the model's performance based on RMSE was found as 0.4859. The plot shows that there is an increasing nonlinear relationship between drying time and black nightshade

seeds temperature for the first eight hours of drying and thereafter, a decreasing nonlinear relationship is observed for the rest of the drying period.

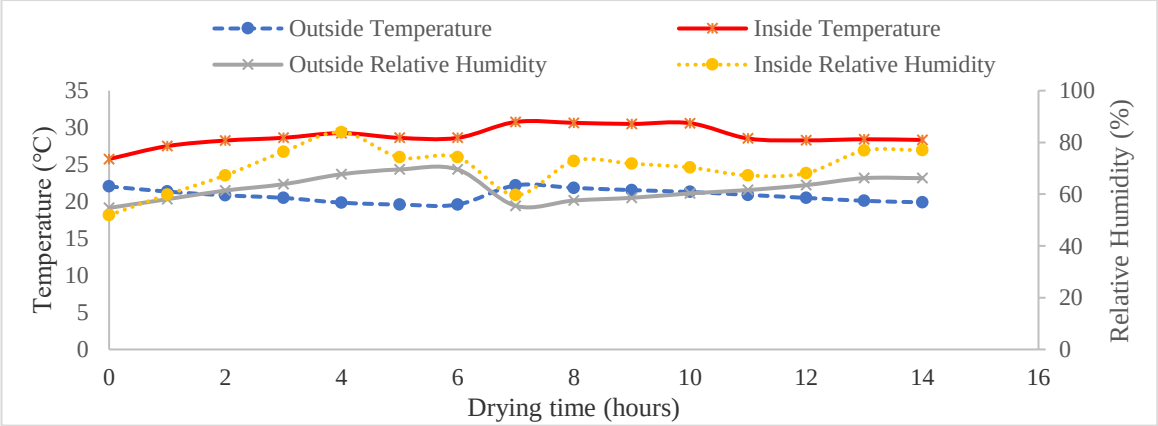

Figure 4.33: Relative Humidity and Temperature Variations with Drying Time in Exhaust Mode

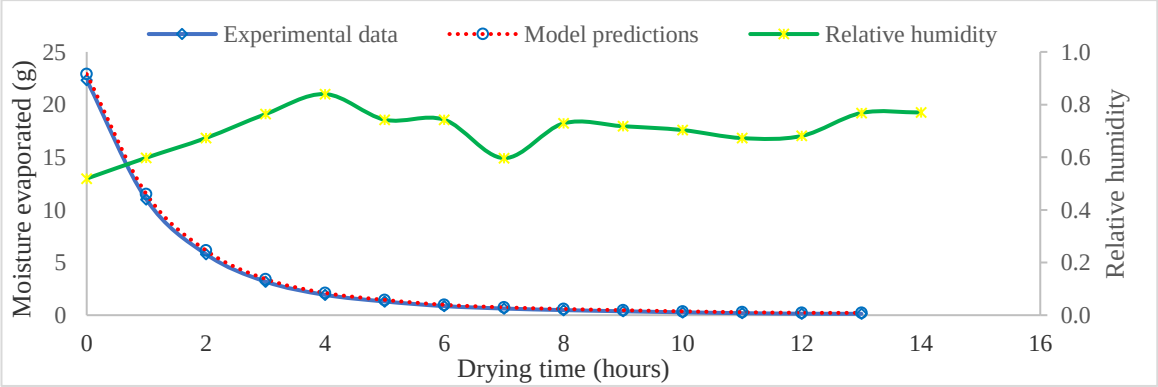

Figure 4.34: Moisture Evaporated and Relative Humidity in Exhaust Gas Mode of Drying

The corresponding residual versus fits plot for the data set with black nightshade seeds temperature as the response and drying time as the predictor is shown in Figure 4.38. The residual plots show nonlinearity and an indication of cyclic behaviour. Figure 4.39 is a goodness of fit plot of the predicted temperatures against experimental observations which show a correlation coefficient of 0.9620.

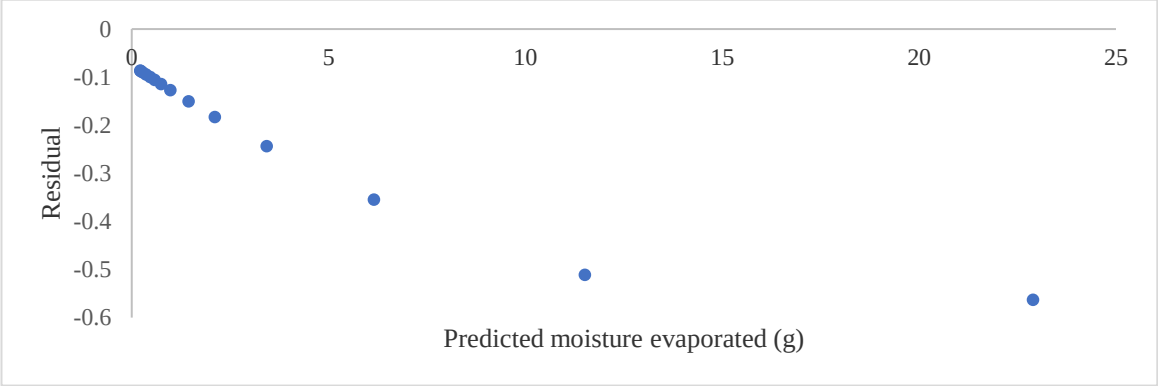

Figure 4.35: Residual Plots of Predicted Moisture Evaporated in Exhaust Gas Mode of Drying

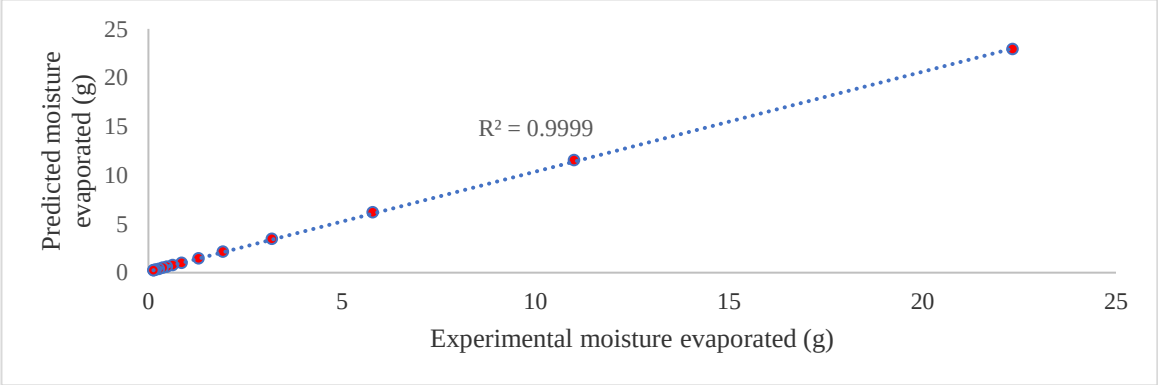

Figure 4.36: Correlation Between Predicted and Experimental Moisture Evaporated in Exhaust Gas Mode of Drying

The predicted black nightshade seeds temperature show agreement with experimental observations and from Figure 4.38, none of the data points fell directly on the residual equal to zero line. The residuals depart from the zero line in a systematic manner with most of the data points concentrated between 27 and 30℃ and are positive for ten values and negative for five values. From a two-tailed t-test of two samples while assuming equal variances at 0.05 level of significance, experimental black nightshade seeds temperature data had a mean of 29.33℃ when the predicted data had a mean of 29.15℃ ($t_{calc} = 0.7537$, $t_{crit} = 2.0484$). Thus, there was enough evidence to retain the null hypotheses that there is no difference in the means between predicted and experimental observations of black nightshade seeds temperatures and it was concluded with 95% confidence that the model is useful in predicting the temperature

of the seeds. Model parameters ξ_0, ξ_1, and ξ_2 were quantified to show the main effects of screening and characterizing black nightshade seeds temperature prediction model. The model parameters ξ_3 quantified the interaction (cross product) term between drying time and experimental temperature data, ξ_4 quantified the first leading term with the second degree on drying time factor, ξ_5 quantified the second order term corresponding to black nightshade seeds experimental temperature data and ϖ was the random error term that accounted for experimental error in the system.

Experimental and predicted greenhouse dryer room air temperatures against drying time are plotted in Figure 4.40 from which the results of the model's performance based on RMSE was found as 0.3392. The plot shows that there is an increasing nonlinear relationship between drying time and greenhouse dryer room air temperature for the first eight hours of drying and thereafter, a decreasing nonlinear relationship is observed for the rest of the drying period. The corresponding residual plot of greenhouse dryer room air predicted temperature is shown in Figure 4.41. The plot show nonlinearity and indication of cyclic behaviour. Observations from Figure 4.42 show a correlation coefficient of 0.9925. With reference to Figure 4.41, none of the data points fell directly on the residual equal to zero line. The residuals depart from the zero line in a systematic manner with most of the data points concentrated between 28 and 31℃. Two data points are positive while 14 are negative. A two-tailed t-test of two samples while assuming equal variances at 0.05 level of significance, show that experimental and predicted greenhouse dryer room air temperature data had means of 28.85℃ and 29.1℃, respectively ($t_{calc} = 0.632,\ t_{crit} = 2.048$). Thus, there was enough evidence to retain the null hypotheses that there is no difference in the means between predicted and experimental observations of greenhouse dryer room air temperatures and it was concluded with 95% confidence that the model is useful in predicting room air temperature of the greenhouse dryer.

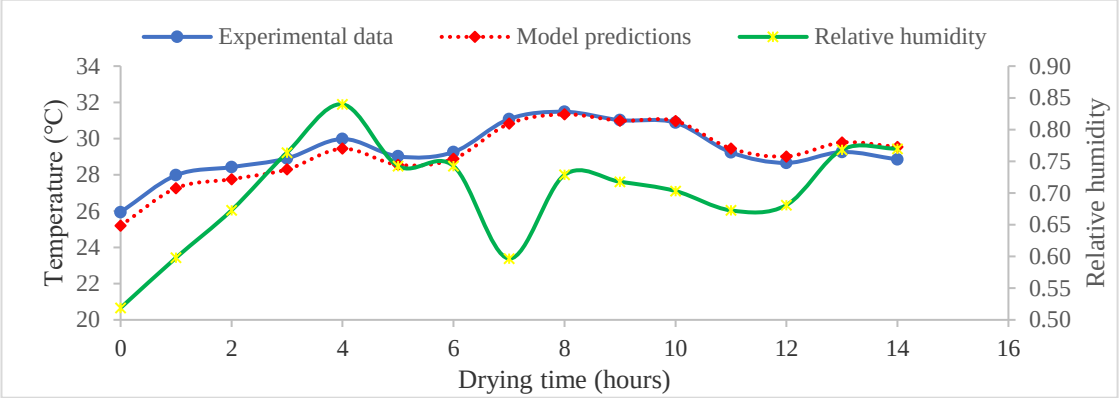

Figure 4.37: Black Nightshade Seeds Temperature and Relative Humidity in Exhaust Gas Mode of Drying

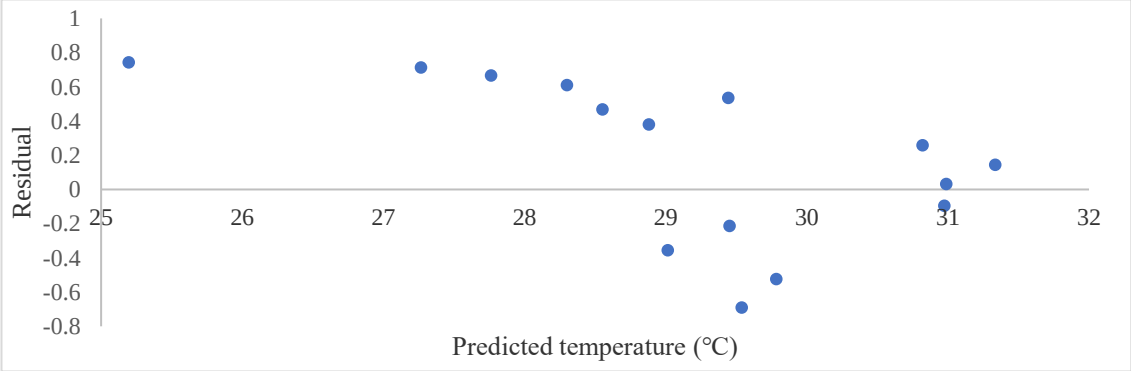

Figure 4.38: Residual Plots of Black Nightshade Seeds Predicted Temperature in Exhaust Gas Mode of Drying

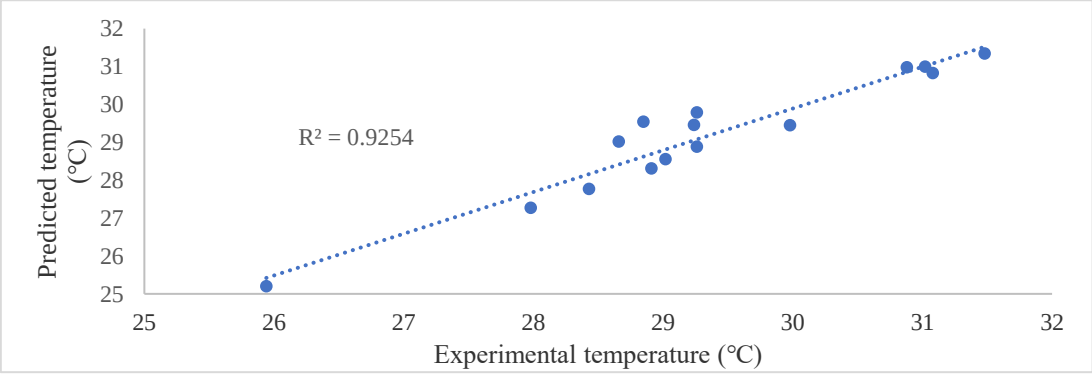

Figure 4.39: Correlation between Predicted and Experimental Black Nightshade Seeds Temperature in Exhaust Gas Mode of Drying

From iterations, the model parameters ζ_0, ζ_1, and ζ_2 were quantified to show the main effects of screening and characterizing the greenhouse dryer room air temperature prediction model. The model parameters ζ_3 quantified the interaction (cross product) term between drying time and experimental temperature data, ζ_4 quantified the first leading term with the second degree on drying time factor, ζ_5 quantified the second order term corresponding to greenhouse dryer room air experimental temperature and ϱ was the random error term that accounted for the experimental error in the system.

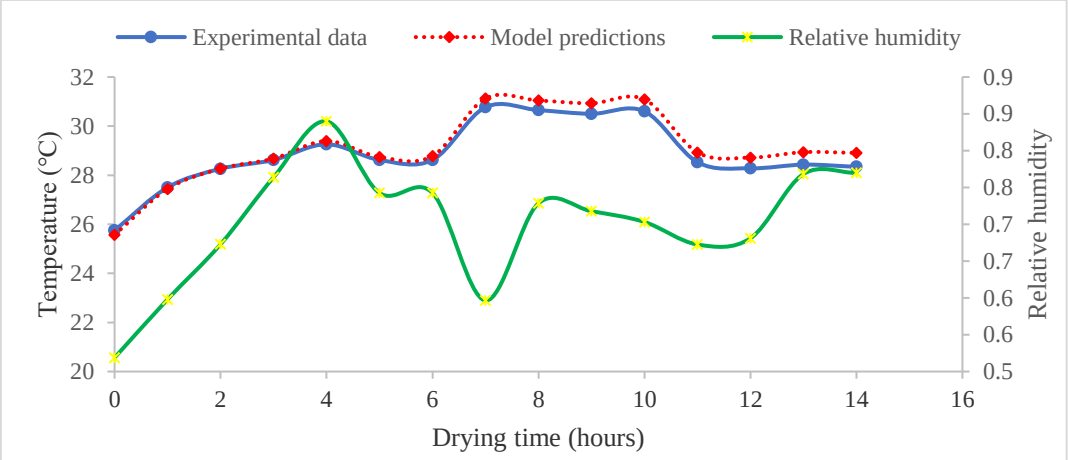

Figure 4.40: Greenhouse Dryer Room Air Temperature and Relative Humidity in Exhaust Gas Mode of Drying

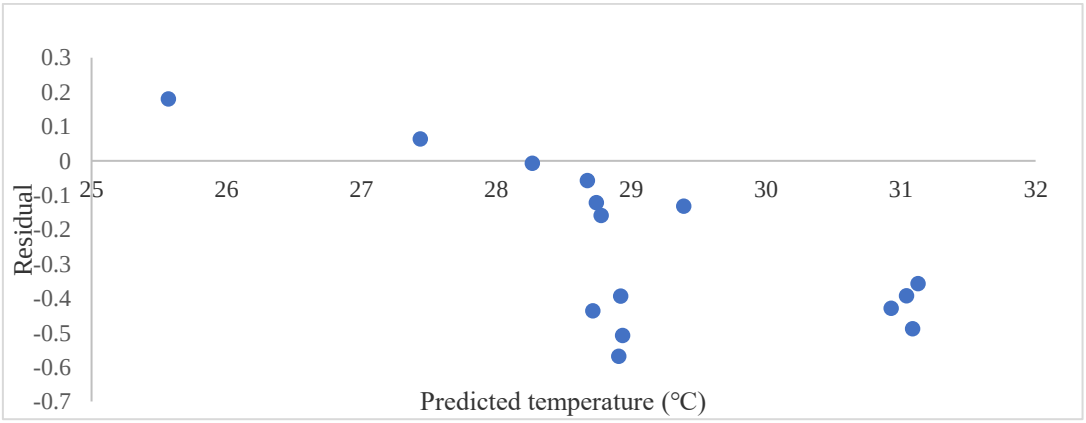

Figure 4.41: Residual Plots of Greenhouse Dryer Room Air Predicted Temperature in Exhaust Gas Mode of Drying

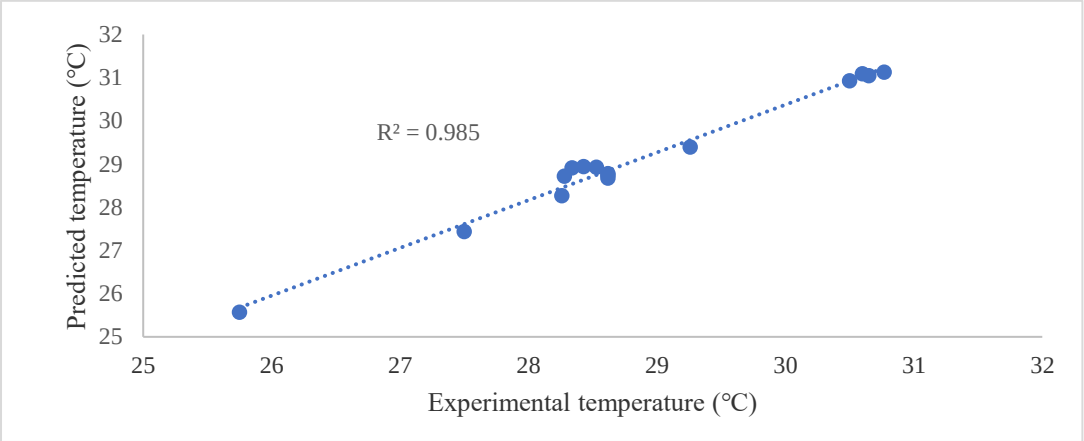

Figure 4.42: Correlation between Predicted and Experimental Greenhouse Dryer Room Air Temperature in Exhaust Gas Mode of Drying

4.2.4 Summary of Model Parameters

A summary of the model parameters estimated from experimental data responses, random error term that accounts for experimental inaccuracies in the system and RMSE that measures the mean difference values predicted by the models and the actual values are given in Table A.13 (Appendix A). The data was used to show how the models performed in the three drying modes.

4.3 Evaluation of the Thin Layer Drying Models for Simulating Drying Kinetics of Black Nightshade Seeds

Three sets of experiments were conducted by varying the drying modes—solar, solar-exhaust gas, and exhaust gas. In solar mode, Table A.14 summarizes the data for the average hourly relative humidities, and temperatures—both inside and outside the dryer. Figure 4.43 is a plot of variations of the parameters in Table A.14 with drying time of black nightshade seeds. From Figure 4.43 temperatures inside the dryer were higher than the corresponding outside temperatures throughout the drying period and this is because the cover material used in the dryer harnessed solar energy to keep the temperatures high. Previous authors (Kiburi *et al*., 2020b; Ronoh *et al*., 2020; Kiburi

et al., 2017; Ronoh *et al.*, 2012; Ozbek and Dadali, 2007) have reported that a combination of high temperature and low relative humidity in a dryer can increase the ability of drying air to perform well. In this mode, the temperature inside the dryer was observed to be high when the relative humidity inside the dryer was low.

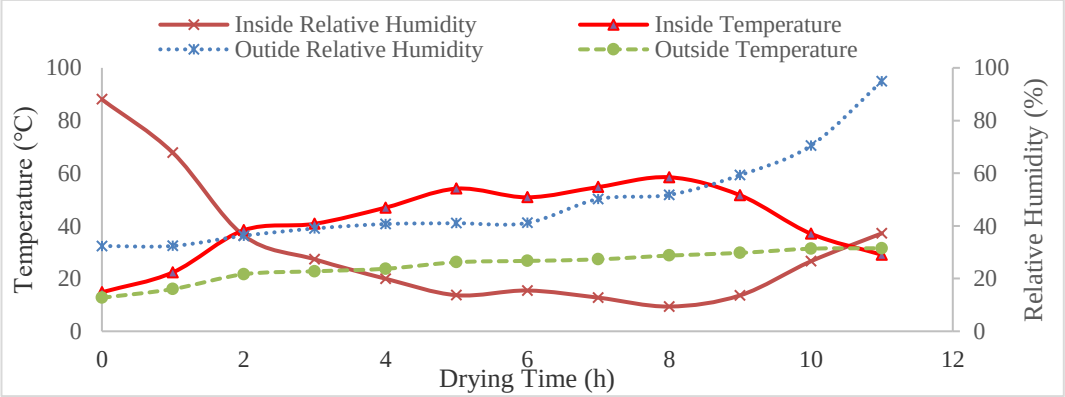

Figure 4.43: Variations of Dryer Parameters with Drying Time in Solar Mode

This phenomenon occurred as illustrated in Figure 4.43 for the drying time between 2-11 hours. In solar-exhaust gas mode, Table A.15 summarizes the data for the average hourly relative humidities, and temperatures both inside and outside the dryer. Figure 4.22 is a plot of variations of the parameters in Table A.15 with drying time of black nightshade seeds. From Figure 4.22 temperatures inside the dryer were higher than the corresponding outside temperatures throughout the drying period and this is because the cover material used in the dryer harnessed solar energy to raise the temperature while at the same time heat energy recovered from exhaust gas of a diesel engine kept the temperatures high. Inside relative humidity was low as compared to the outside relative humidity for the first four hours of dying. It is within these hours that fast rate of moisture loss from the product were observed (Figure 4.45; Figure 4.32). The relative humidity trend for the remaining hours of drying showed relative equality but were still low for the drying air to be effective in drying a combination of high temperature and low relative humidity in a dryer can increase the ability of drying air to carry away moisture. In summary, for this mode, the temperature inside the dryer was observed to be high when the relative humidity inside the dryer was low as illustrated in Figure 4.22 for the entire drying period. In exhaust gas mode, Table A.16 summarizes the data for the average hourly relative humidities, and temperatures both

inside and outside the dryer. Figure 4.33 is a plot of variations of the parameters in Table A.16 with drying time of black nightshade seeds.

From Figure 4.33 temperatures inside the dryer were higher than the corresponding outside temperatures throughout the drying period and this is because heat energy recovered from exhaust gas of a diesel engine kept the temperatures high. However, relative humidity inside the dryer were higher than those outside because water vapour from the open cooling system of a diesel engine kept the dryer moist. Increase in relative humidity inside the dryer was not suitable for quick drying, therefore, the drying period for the mode was 14 hours, a longer period as compared to solar-exhaust gas drying mode where the product was dried in 10 hours (Figure 4.32). With reference to the outside and inside temperatures of this mode of drying, the average hourly rise in temperature inside the dryer was 8.04℃ with a minimum rise of 3.7℃ and a maximum of 9.41℃ when exhaust gas was utilized to provide heat energy.

The results of mass change of black nightshade seeds with time are presented in Tables A.17, A.18 and A.19 for the corresponding drying modes. Figures 4.44, 4.45 and 4.46 illustrate the results of variation of moisture content and drying rate with drying time of black nightshade seeds during solar, solar-exhaust gas, and exhaust gas modes of drying respectively. Fast rates of moisture loss were observed within the first four hours and thereafter the rates slowed down. Similar trends of drying rates have been observed by Ronoh *et al*., (2020) who reported that the drying process can be divided into three periods: a short primary increasing, a fairly constant and a falling drying rate. From Figures 4.44 to 4.46 it can be observed that the falling rate period clearly dominated the drying process of black nightshade seeds. Such a dominant falling rate period is attributed to diffusion mechanisms that control drying of agricultural produce. Continuous decrease in drying rate with decreasing moisture content—increasing drying time—was observed in all the drying modes. Similar observations have been reported by authors who have previously dried agricultural produce (Kiburi *et al*., 2020b; Ronoh *et al*., 2020; Kiburi *et al*., 2017; Olanipekun *et al*., 2015; Ronoh *et al*., 2012; Chowdhury *et al*., 2011).

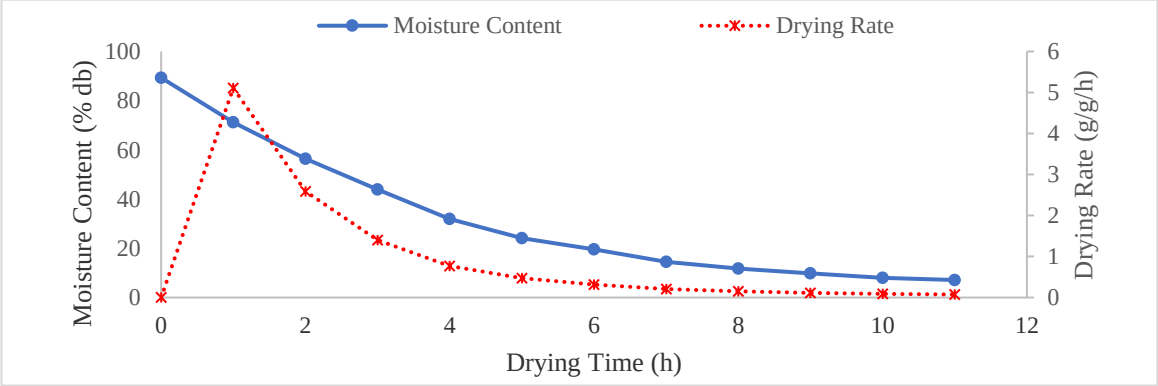

Figure 4.44: Moisture Content and Drying Rate Variations with Drying Time in Solar Mode

Figure 4.32 illustrates the comparison of drying time for the three modes of drying. Moisture ratio variation with time show that the solar-exhaust gas mode of drying took the shortest time at 10 hours. This was followed by solar mode of drying at 11 hours and finally exhaust gas mode of drying took the longest at 14 hours. These drying times can be explained by the relative humidity and temperature variations, inside and outside the dryer, with time as presented in Tables A.14 to A.16 and illustrated in Figures 4.43, 4.22 and 4.33. Tables 4.1, 4.2 and 4.3 show the coefficients, constants and RMSE values for thin layer drying models selected for this work in solar, solar-exhaust gas, and exhaust gas modes respectively. From Table 4.1, it can be observed that Page model with the lowest RMSE value was the most appropriate in describing drying kinetics of black nightshade seeds when the dryer was operated on solar mode.

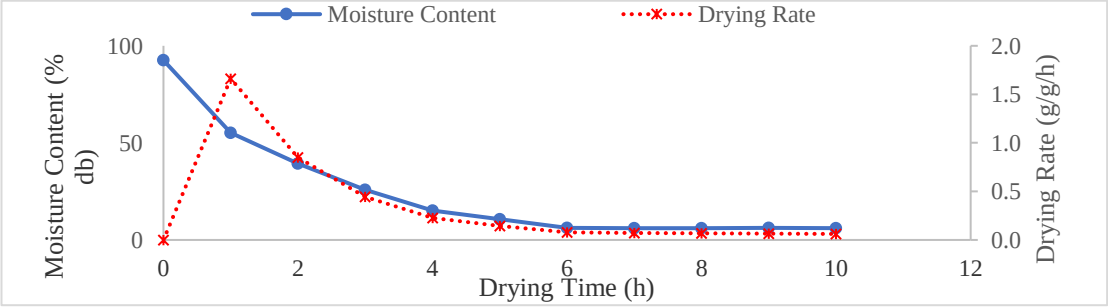

Figure 4.45: Moisture Content and Drying Rate Variations with Drying Time in Solar-Exhaust Gas Mode

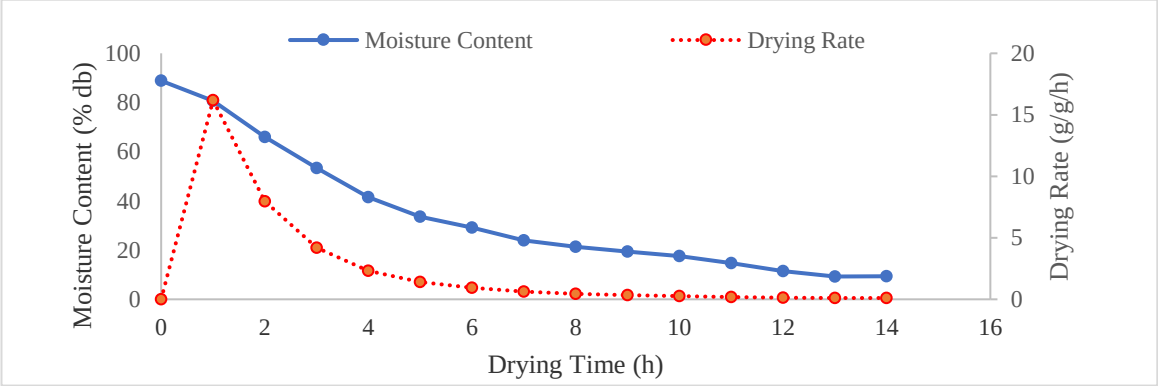

Figure 4.46: Moisture Content and Drying Rate Variations with Drying Time in Exhaust Gas Mode

Similar results for suitability of Page model in characterizing agricultural produce have been reported during thin layer drying studies of various food materials, including jackfruit slices (Ronoh *et al*., 2020), tomato slices (Oyerinde, 2016), pineapple (Olanipekun *et al*., 2015), banana (Da Silva *et al*., 2014), chili (Tunde-Akintunde, 2011), rapeseed (Han & Keum, 2011), amaranth (Ronoh *et al*., 2009), sultana grapes (Yaldiz *et al*., 2001). From Table 4.2, in solar-exhaust gas mode of drying, Logarithmic model had the lowest value of RMSE compared to the other three thin layer drying models. Accordingly, Logarithmic model was selected to best characterize the thin layer drying of black nightshade seeds in the mode. Similarly, from Table 4.3, in exhaust gas mode Logarithmic model with the lowest RMSE value was the most appropriate in describing the drying kinetics of the seeds. Tables A.20, A.21 and A.22 show the experimental and predicted moisture ratios by thin layer drying models selected for this work in solar, solar-exhaust gas, and exhaust gas modes respectively. Figure 4.47 illustrates the Newton model fitting to experimental data in solar mode of drying while Figure 4.48 shows the residual plots as a variation with the model's predictions. Residual plots were performed to show the model's appropriateness in describing the drying kinetics of black nightshade seeds in solar mode of drying.

Table 4.1: Thin Layer Drying Models' Coefficients, Constants and RMSE for Solar Mode

Model	Coefficients and Constants	R^2	RMSE
Newton	k = 0.2478	0.9982	0.01329
Page	k = 0.2319, n = 1.0435	**0.9985**	**0.01147**
Logarithmic	k.= 0.2539, a = 1.0104, c = 0.0042	0.9982	0.01235
Henderson and Pabis	k = 0.2512, a = 1.0133	0.9982	0.01240

From Figure 4.48, considering a band width of ± 0.015, Newton model had 8 out of the possible 12 data points for the predicted moisture ratio close to the residual line. Out of 12 predicted data points, 1 fell directly on the residual line. However, for this model, out of the four thin layer drying models considered in this mode of drying, it was fourth in performance.

Table 4.2: Thin Layer Drying Models' Coefficients, Constants and RMSE for Solar-Exhaust Gas Mode

Model	Coefficients and Constants	R^2	RMSE
Newton	k = 0.4354	0.9937	0.0293
Page	k = 0.5057, n = 0.8586	0.9943	0.0221
Logarithmic	k = 0.4949, a = 0.9502, c = 0.0444	0.9964	0.0172
Henderson and Pabis	k = 0.4256, a = 0.9777	0.9926	0.0284

Figure 4.49 illustrates the Page model fitting to experimental data in solar mode of drying while Figure 4.50 shows the residual plots as a variation with the model's predictions. Residual plots were performed to show the model's appropriateness in describing drying kinetics of black nightshade seeds in solar mode of drying. Unlike other thin layer drying models considered in this mode, Page model, from Figure 4.50, had 10 out of the possible 12 predicted data points for moisture ratio close to the residual line within a band width of ± 0.015. Out of the 12 predicted data points, 2 fell directly on the residual line, therefore, this model was the most appropriate in

describing thin layer drying of black nightshade seeds when drying was performed in solar mode.

Table 4.3: Thin Layer Drying Models' Coefficients, Constants and RMSE for Exhaust Gas Mode

Model	Coefficients and Constants	R^2	RMSE
Newton	k = 0.1748	0.9914	0.0273
Page	k = 0.1653, n = 1.0305	0.9914	0.0269
Logarithmic	k = 0.2011, a = 1.0001, c = 0.0423	**0.9933**	**0.0232**
Henderson and Pabis	k = 0.1802, a = 1.0285	0.9921	0.0254

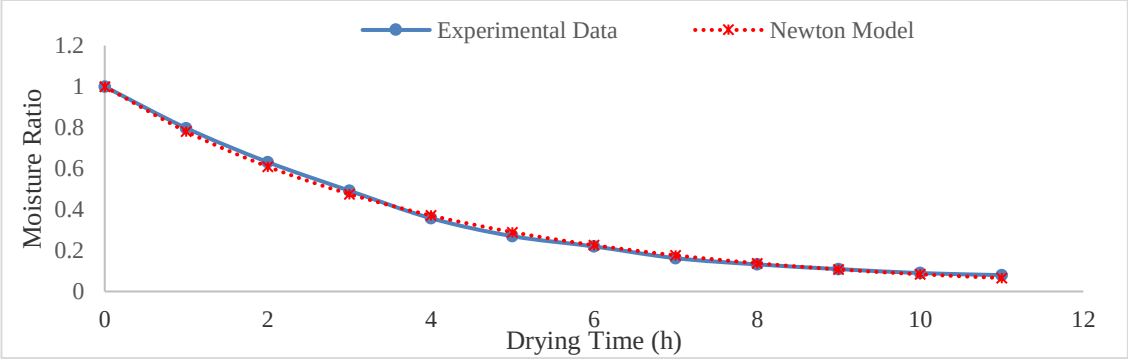

Figure 4.47: Newton Model Fitting to Experimental Data in Solar Mode of Drying

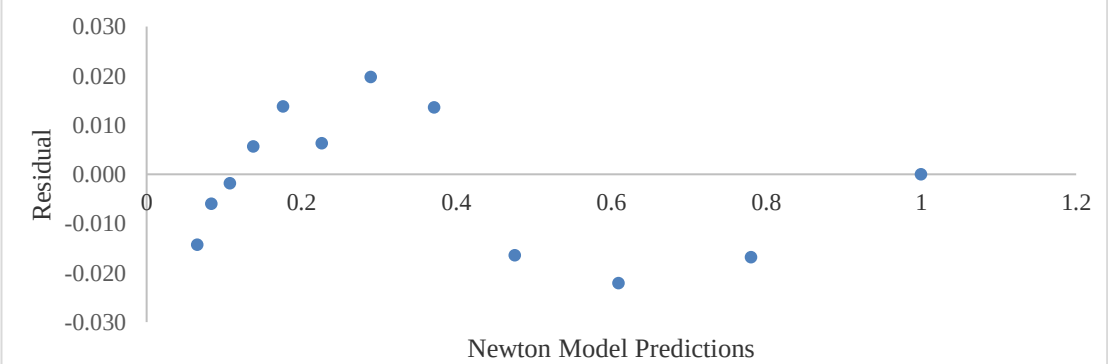

Figure 4.48: Newton Model Predictions and Residual Plots in Solar Mode of Drying

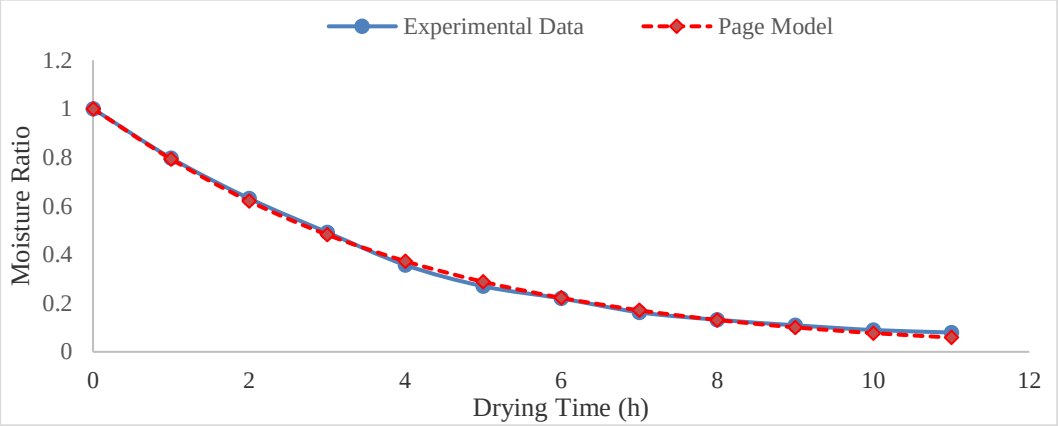

Figure 4.49: Page Model Fitting to Experimental Data in Solar Mode of Drying

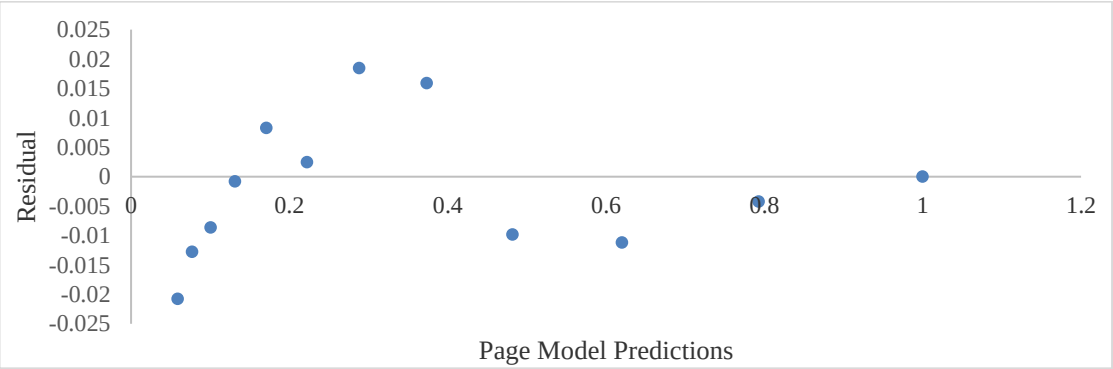

Figure 4.50: Page Model Predictions and Residual Plots in Solar Mode of Drying

Figure 4.51 illustrates Logarithmic model fitting to experimental data in solar mode of drying while Figure 4.52 shows the residual plots as a variation with the model's predictions. Residual plots were performed to show the model's appropriateness in describing the drying kinetics of black nightshade seeds in solar mode of drying. From Figure 4.52, considering a band width of ± 0.015, Logarithmic model had 9 out of the possible 12 data points for the predicted moisture ratio close to the residual line. Out of 12 predicted data points, none fell directly on the residual line. However, for this model, out of the four thin layer drying models considered in this mode of drying, it was second in performance.

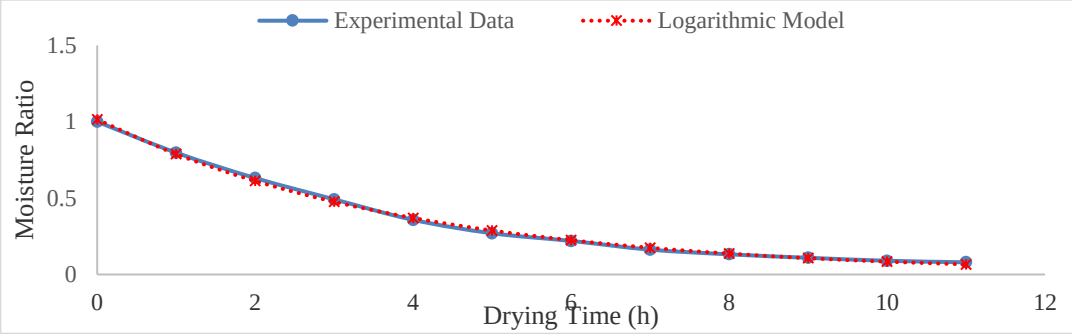

Figure 4.51: Logarithmic Model Fitting to Experimental Data in Solar Mode of Drying

Figure 4.53 illustrates Henderson and Pabis model fitting to experimental data in solar mode of drying while Figure 4.54 shows the residual plots as a variation with the model's predictions. Residual plots were performed to show the model's appropriateness in describing the drying kinetics of black nightshade seeds in solar mode of drying. From Figure 4.54 the performance of Henderson and Pabis was almost similar to Logarithmic model when the product was dried in solar mode. Considering a band width of ± 0.015, Henderson and Pabis model had 9 out of the possible 12 data points for the predicted moisture ratio close to the residual line. Out of 12 predicted data points, none fell directly on the residual line. However, for this model, out of the four thin layer drying models considered in this mode of drying, it was third in performance.

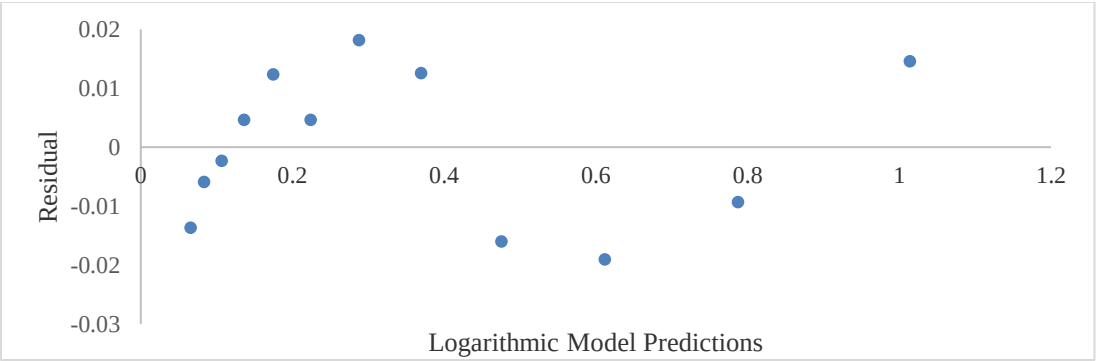

Figure 4.52: Logarithmic Model Predictions and Residual Plots in Solar Mode of Drying

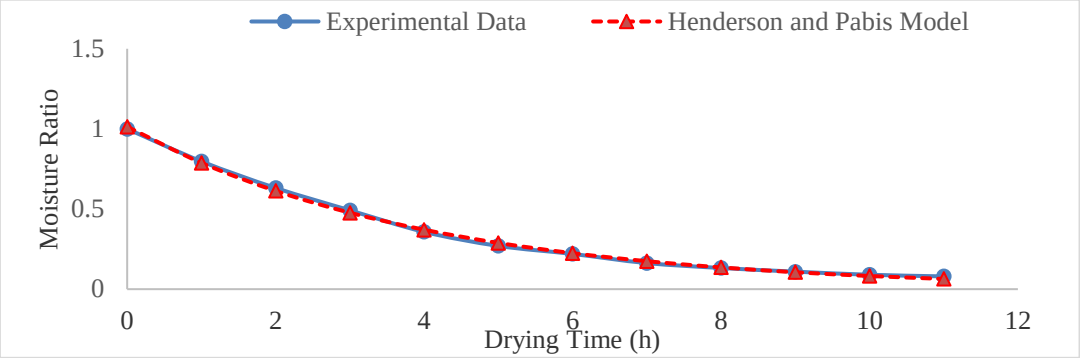

Figure 4.53: Henderson and Pabis Model Fitting to Experimental Data in Solar Mode of Drying

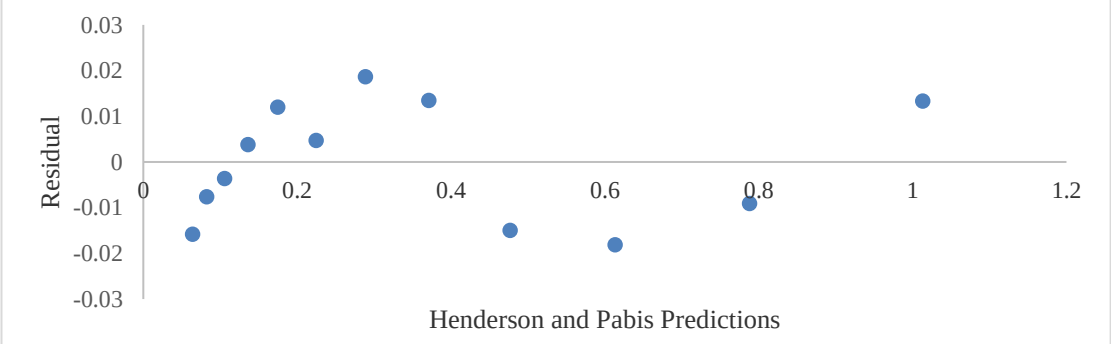

Figure 4.54: Henderson and Pabis Model Predictions and Residual Plots in Solar Mode of Drying

Figure 4.55 illustrates Newton model fitting to experimental data in solar-exhaust gas mode of drying while Figure 4.56 shows the residual plots as a variation with the model's predictions. Residual plots were performed to show the model's appropriateness in describing the drying kinetics of black nightshade seeds in solar-exhaust gas mode of drying. From Figure 4.56, considering a band width of ± 0.015, Newton model had 6 out of the possible 11 data points for the predicted moisture ratio close to the residual line. Out of 11 predicted data points, 1 fell directly on the residual line. However, for this model, out of the four thin layer drying models considered in this mode of drying, it was fourth in performance because 4 out of 11 of the predicted values were outside the band width of ± 0.03.

Figure 4.57 illustrates Page model fitting to experimental data in solar-exhaust gas mode of drying while Figure 4.58 shows the residual plots as a variation with the model's predictions. Residual plots were performed to show the model's appropriateness in describing drying kinetics of black nightshade seeds in solar-exhaust gas mode of drying. From Figure 4.58, considering a band width of ±0.015, Page model had 4 out of the possible 11 data points for the predicted moisture ratio close to the residual line. Out of 11 predicted data points, 1 fell directly on the residual line. However, for this model, out of the four thin layer drying models considered in this mode of drying, it was second in performance because 2 out of 11 of the predicted values were outside the band width of ±0.03.

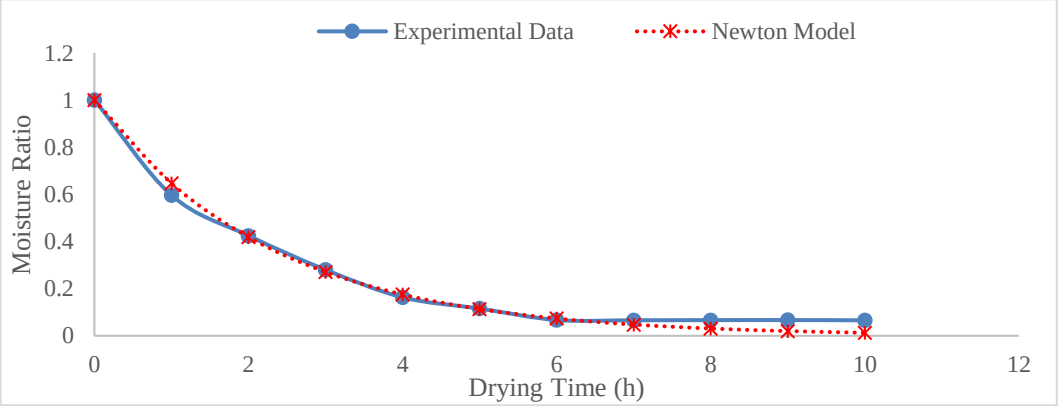

Figure 4.55: Newton Model Fitting to Experimental Data in Solar-Exhaust Gas Mode of Drying

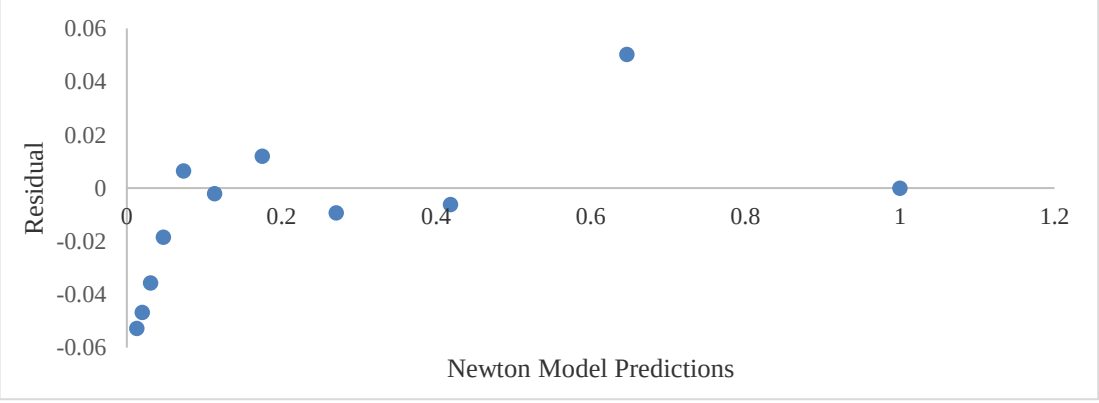

Figure 4.56: Newton Model Predictions and Residual Plots in Solar-Exhaust Gas Mode of Drying

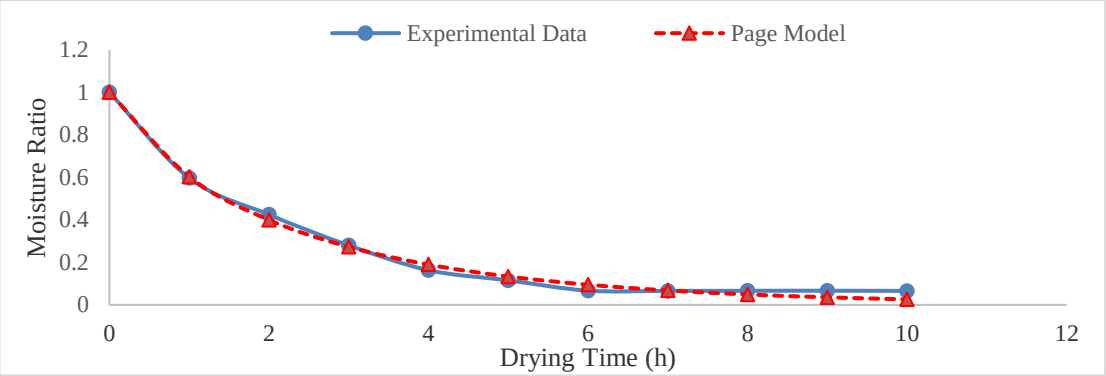

Figure 4.57: Page Model Fitting to Experimental Data in Solar-Exhaust Gas Mode of Drying

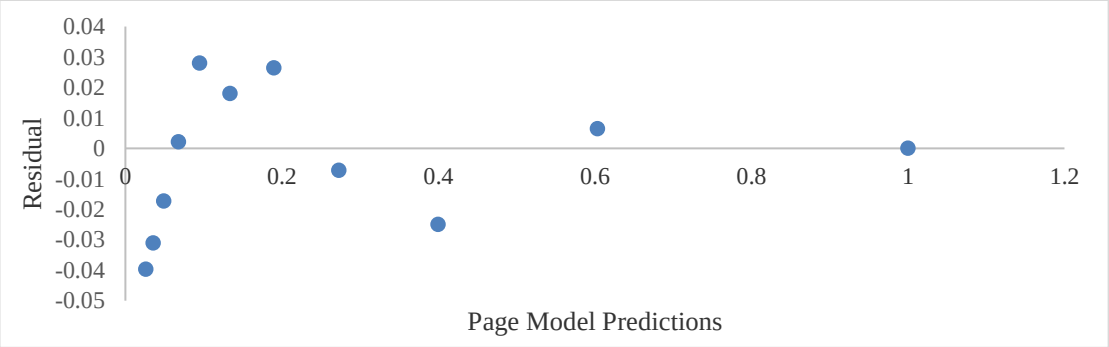

Figure 4.58: Page Model Predictions and Residual Plots in Solar-Exhaust Gas Mode of Drying

Figure 4.59 illustrates Logarithmic model fitting to experimental data in solar-exhaust gas mode of drying while Figure 4.60 shows the residual plots as a variation with the model's predictions. Residual plots were performed to show the model's appropriateness in describing the drying kinetics of black nightshade seeds in solar-exhaust gas mode of drying. Unlike other thin layer drying models considered in this mode, Logarithmic model, from Figure 4.60, had 6 out of the possible 11 predicted data points for moisture ratio close to the residual line within a band width of $\pm$0.015.

Out of the 11 predicted data points, none fell directly on the residual line, however, this model was the most appropriate in describing thin layer drying of black nightshade seeds when drying was performed in solar-exhaust mode because none out of 11 of the predicted values were outside the band width of ±0.03.

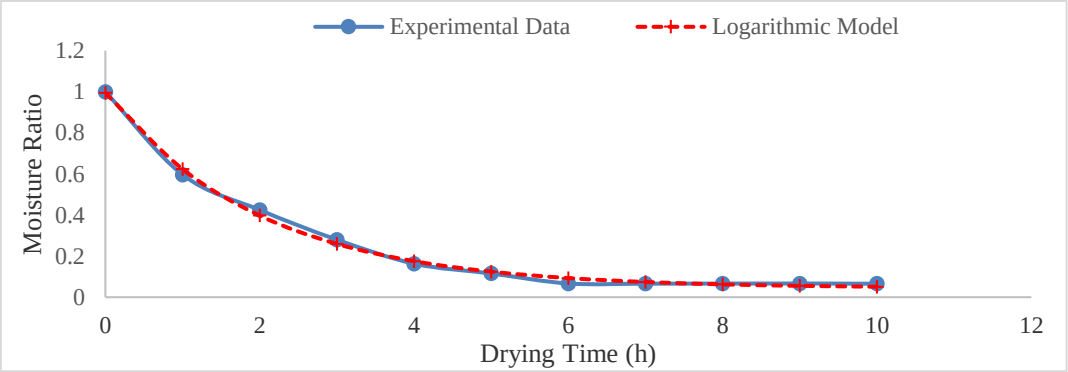

Figure 4.59: Logarithmic Model Fitting to Experimental Data in Solar-Exhaust Gas Mode of Drying

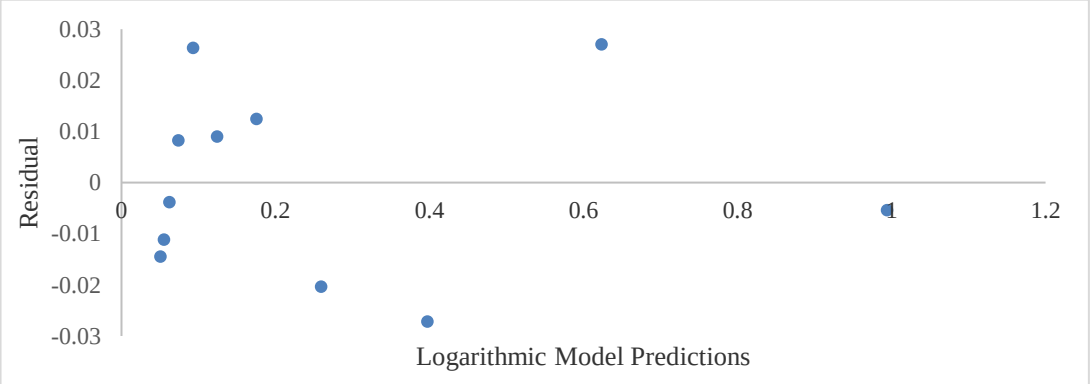

Figure 4.60: Logarithmic Model Predictions and Residual Plots in Solar-Exhaust Gas Mode of Drying

Figure 4.61 illustrates Henderson and Pabis model fitting to experimental data in solar-exhaust gas mode of drying while Figure 4.62 shows the residual plots as a variation with the model's predictions. Residual plots were performed to show the model's appropriateness in describing the drying kinetics of black nightshade seeds in solar-exhaust gas mode of drying. From Figure 4.62, considering a band width of ±0.015, Henderson and Pabis model had 5 out of the possible 11 data points for the predicted moisture ratio close to the residual line.

Out of 11 predicted data points, 1 fell directly on the residual line. However, for this model, out of the four thin layer drying models considered in this mode of drying, it was third in performance because 4 out of 11 of the predicted values were outside the band width of ±0.03. Figure 4.63 illustrates the Newton model fitting to experimental data in exhaust gas mode of drying while Figure 4.64 shows the residual plots as a variation with the model's predictions. Residual plots were performed to show the model's appropriateness in describing the drying kinetics of black nightshade seeds in exhaust gas mode of drying. From Figure 4.64, considering a band width of ±0.015, Newton model had 6 out of the possible 15 data points for the predicted moisture ratio close to the residual line. Out of 15 predicted data points, 2 fell directly on the residual line.

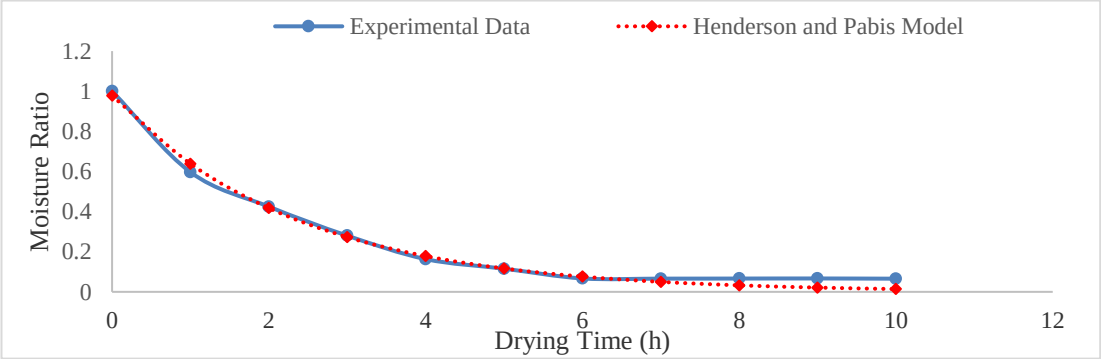

Figure 4.61: Henderson and Pabis Model Fitting to Experimental Data in Solar-Exhaust Gas Mode of Drying

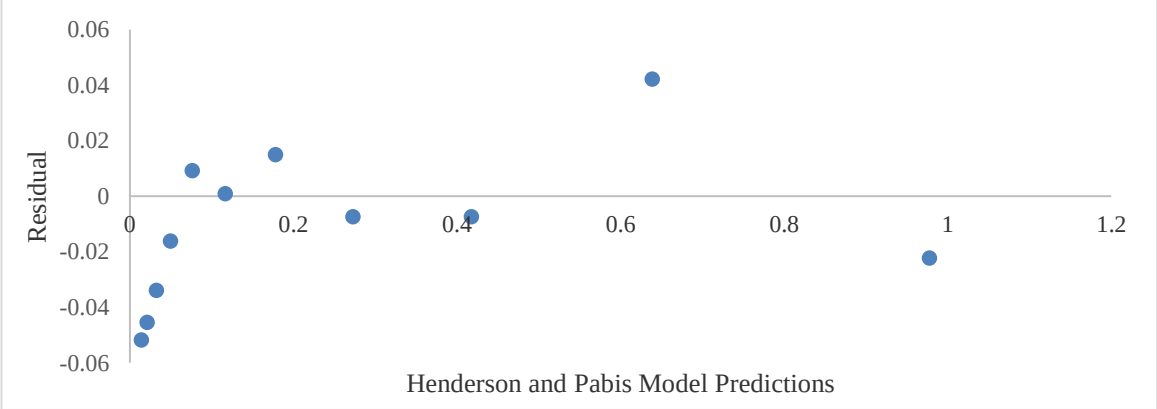

Figure 4.62: Henderson and Pabis Model Predictions and Residual Plots in Solar-Exhaust Gas Mode of Drying

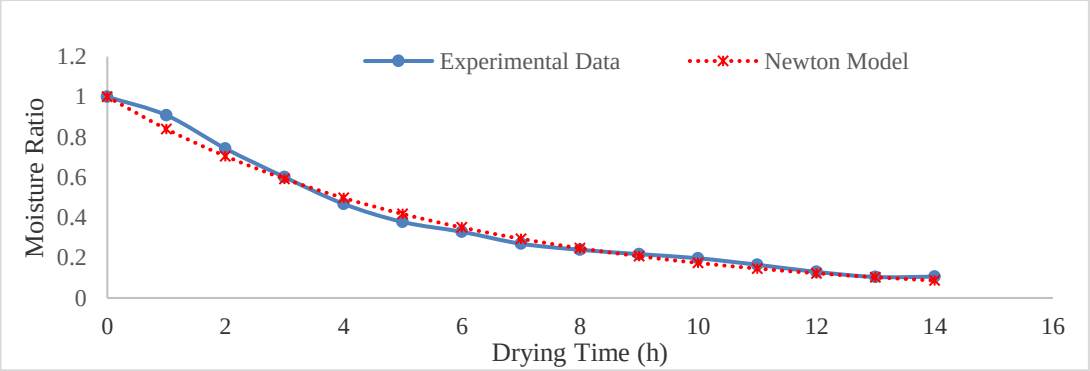

Figure 4.63: Newton Model Fitting to Experimental Data in Exhaust Gas Mode of Drying

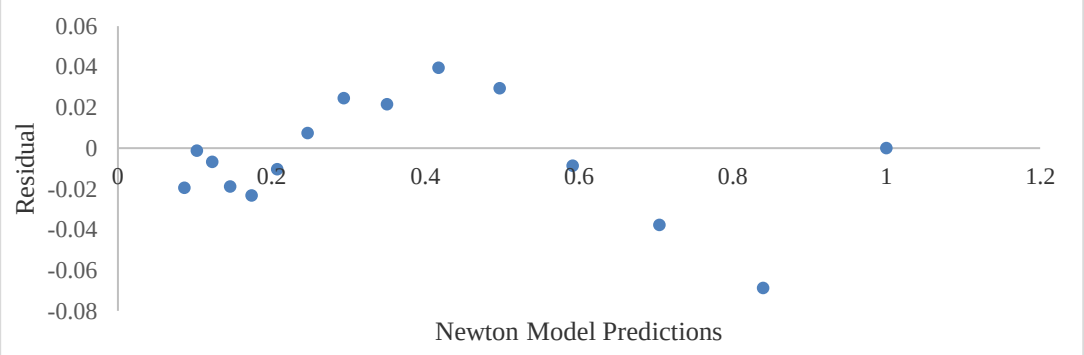

Figure 4.64: Newton Model Predictions and Residual Plots in Exhaust Gas Mode of Drying

However, for this model, out of the four thin layer drying models considered in this mode of drying, it was fourth in performance because 3 out of 15 of the predicted values were outside the band width of ± 0.03. Figure 4.65 illustrates the Page model fitting to experimental data in exhaust gas mode of drying while Figure 4.66 shows the residual plots as a variation with the model's predictions. Residual plots were performed to show the model's appropriateness in describing the drying kinetics of black nightshade seeds in exhaust gas mode of drying. This model performed almost

similar to Newton model based on the residual plots. From Figure 4.64, considering a band width of ±0.015, Page model had 6 out of the possible 15 data points for the predicted moisture ratio close to the residual line. Out of 15 predicted data points, 2 fell directly on the residual line. However, for this model, out of the four thin layer drying models considered in this mode of drying, it was third in performance because 3 out of 15 of the predicted values were outside the band width of ±0.03.

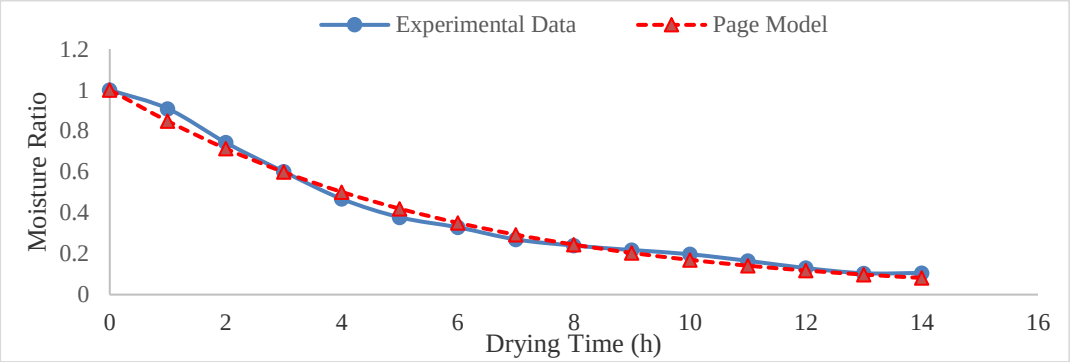

Figure 4.65: Page Model Fitting to Experimental Data in Exhaust Gas Mode of Drying

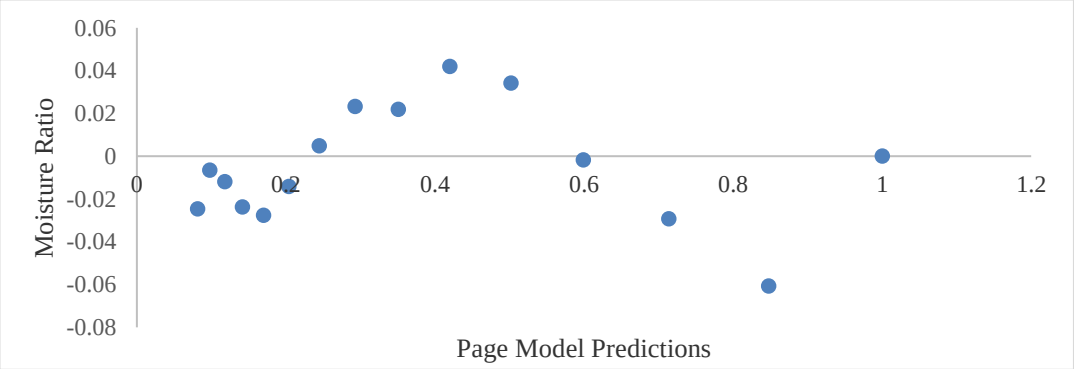

Figure 4.66: Page Model Predictions and Residual Plots in Exhaust Gas Mode of Drying

Figure 4.67 illustrates Logarithmic model fitting to experimental data in exhaust gas mode of drying while Figure 4.68 shows the residual plots as a variation with the model's predictions. Residual plots were performed to show the model's appropriateness in describing the drying kinetics of black nightshade seeds in exhaust gas mode of drying. Unlike other thin layer drying models considered in this mode,

Logarithmic model, from Figure 4.68, had 8 out of the possible 15 predicted data points for moisture ratio close to the residual line within a band width of ±0.015. Out of the 15 predicted data points, none fell directly on the residual line, however, this model was the most appropriate in describing thin layer drying of black nightshade seeds when drying was performed in exhaust mode because 2 out of 15 of the predicted values were outside the band width of ±0.03. Figure 4.69 illustrates Henderson and Pabis model fitting to experimental data in exhaust gas mode of drying while Figure 4.70 shows the residual plots as a variation with the model's predictions. Residual plots were performed to show the model's appropriateness in describing the drying kinetics of black nightshade seeds in exhaust gas mode of drying.

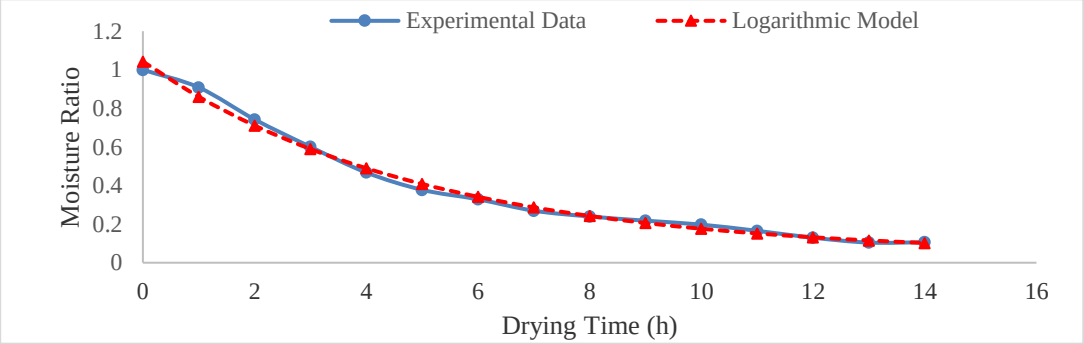

Figure 4.67: Logarithmic Model Fitting to Experimental Data in Exhaust Gas Mode of Drying

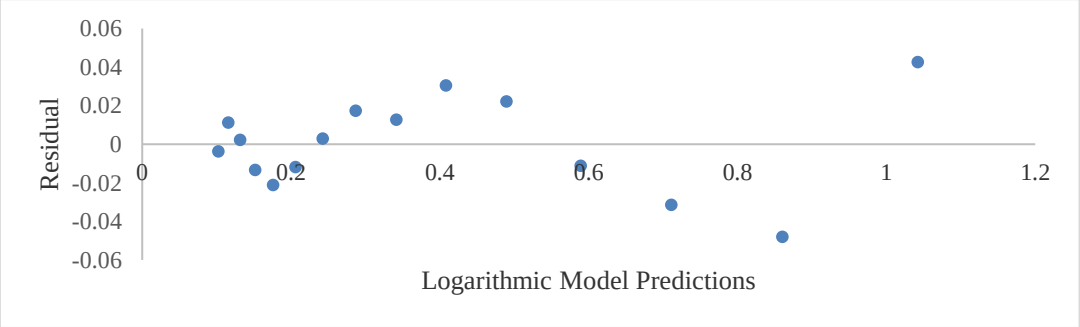

Figure 4.68: Logarithmic Model Predictions and Residual Plots in Exhaust Gas Mode of Drying

From Figure 4.70, considering a band width of ±0.015, Page model had 5 out of the possible 15 data points for the predicted moisture ratio close to the residual line. Out

of 15 predicted data points, none fell directly on the residual line. However, for this model, out of the four thin layer drying models considered in this mode of drying, it was second in performance because 3 out of 15 of the predicted values were outside the band width of ± 0.03.

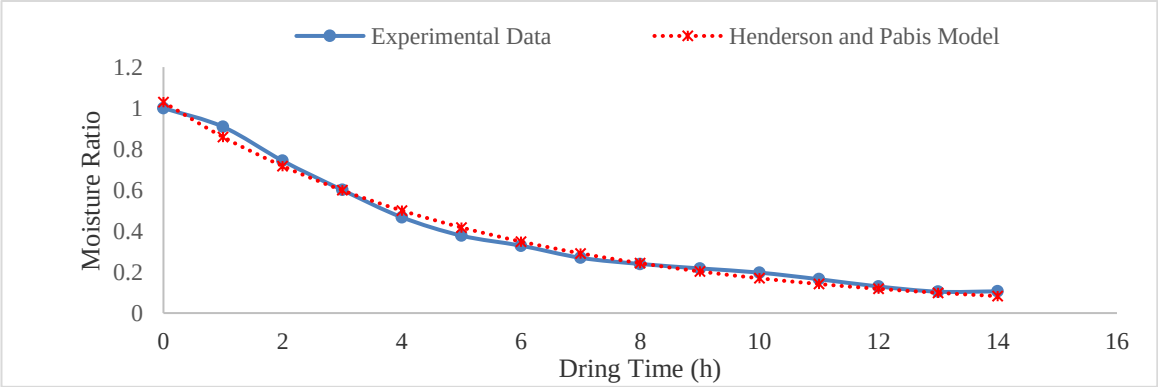

Figure 4.69: Henderson and Pabis Model Fitting to Experimental Data in Exhaust Gas Mode of Drying

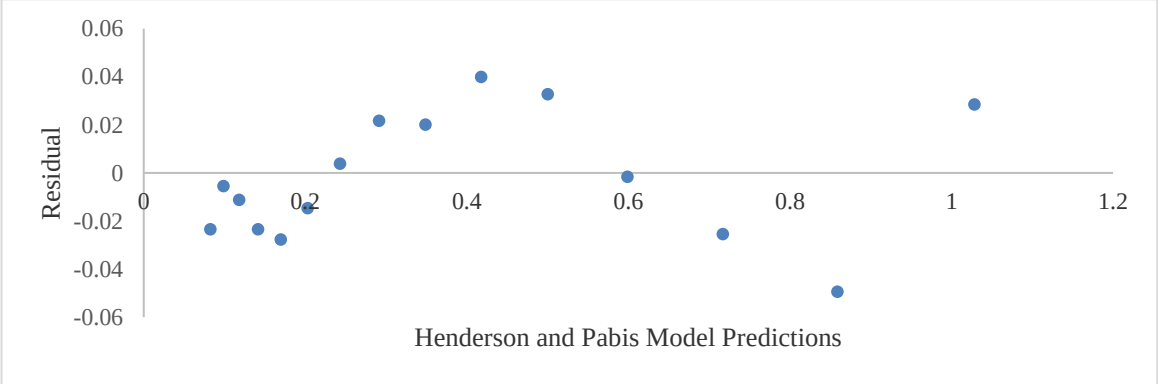

Figure 4.70: Henderson and Pabis Model Predictions and Residual Plots in Exhaust Gas Mode of Drying

4.4 Determination of the Influence of Solar-Exhaust Gas Greenhouse Drying Modes on Viability of Black Nightshade Seeds

4.4.1 Sampling Results

The results of accessible population of black nightshade berries comprised of four strata, such that: $N_1 = 50$, $N_2 = 100$, $N_3 = 150$ and $N_4 = 200$. The respective

standard deviations of the diameters of the berries were: $\sigma_1 = 0.6815\ mm$, $\sigma_2 = 0.6994\ mm$, $\sigma_3 = 0.7223\ mm$ and $\sigma_4 = 0.8200\ mm$. A desirable sample size of 40 black nightshade berries was optimally allocated to the four strata using disproportionate sampling design as: $n_1 = 4$, $n_2 = 7$, $n_3 = 12$ and $n_4 = 17$ with a 99% precision of $E_1 = 0.24\ mm$, $E_2 = 0.18\ mm$, E_3 =0.16 mm and $E_4 = 0.17\ mm$. The accessible berries' population mean diameter was, $\mu = 6.83\ mm$ with a standard deviation of, $\sigma = 0.7552\ mm$. The mean number of seeds in a berry in this study were 54 seeds—comparable with a study done by Schippers (1998) where seed count in a berry was reported to be between 20-60 seeds. Figure 4.71 shows a scatter plot of the variations of seeds count with berries diameter. It reveals a linear relationship with a coefficient of determination, R^2 = 0.8328. The size in diameter of black nightshade berries was found to be directly related to the number of seeds in a berry at harvest on maturity. The maximum berry size in diameter was reported as 7.99 mm from an accessible population of 500 berries. From the same population, the minimum size in the form of diameter was recorded at 5.28 mm.

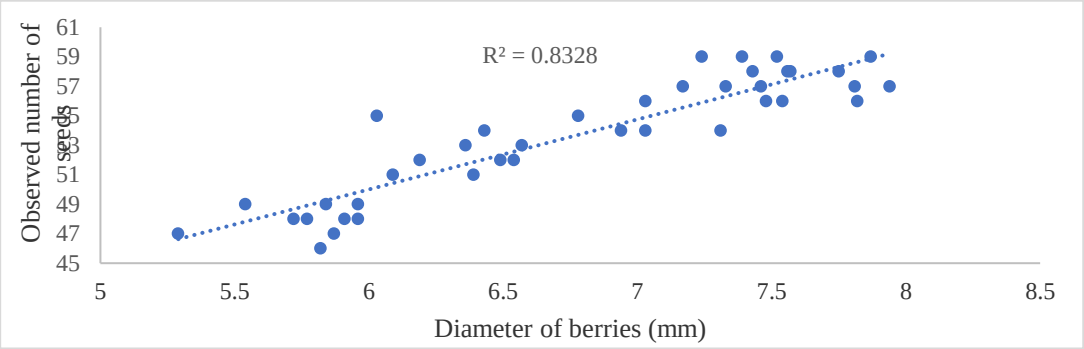

Figure 4.71: Scatter Plot of Seeds' Count Variation with Berries' Diameter

Results of regression analysis revealed that the number of seeds (N_s) on the y-axis was positively correlated with the diameter of berries (D_b) on the x-axis. A linear regression model was developed from the data and is presented in Equation (4.1) which is applicable for diameters ranging from 5 to 8 mm.

$$N_s = 21.5207 + 4.7469D_b \qquad (4.1)$$

In Equation (4.1), N_s is the number of seeds in a berry, 21.5207 is the intercept (a_0), of the model, 4.7469 is the slope (a_1), of the regression model, D_b is the diameter of a berry. From the coefficient of determination, over 83% of the total variability in seed count was accounted for by the model, showing that, there exists a strong positive linear relationship between the number of seeds in a berry and the diameter of black nightshade berries. This implied that the number of seeds could be estimated from a berry's diameter ranging from 5 to 8 mm with reasonable certainty. The t-distribution similar to the t-test was used as the test statistic for the regression model's intercept and slope. Making statistical inferences at the 0.05 level of significance ($\alpha = 0.05$), it was concluded that the true value of the intercept of the regression model lied in the interval 19.1191 to 23.9223 and similarly the true slope lied in the interval 4.4032 to 5.0905. The value of the t-distribution calculated from the data was more than the critical value of the t-distribution for a two tailed test with $\alpha = 0.05$: ($t_{calc} = 18.6082$, $t_{crit} = 2.074$) for the intercept and ($t_{calc} = 27.9584$, $t_{crit} = 2.074$) for the slope. Thus, there was enough evidence to reject the null hypotheses that the intercept and slope were equal to zero and it was concluded with 95% confidence that berries diameter is useful in predicting the number of seeds in a berry of black nightshade. The RMSE for the seed count model was 2 seeds. A plot of the residuals against the independent variable (berries' diameter) is shown in Figure 4.72. It was observed from Figure 4.72 that the seed count model gave a scattered residual plot, and this led to a conclusion that the model was able to explain the variation in the experimental data. The covariance was constant with a band width of most values at ± 2.

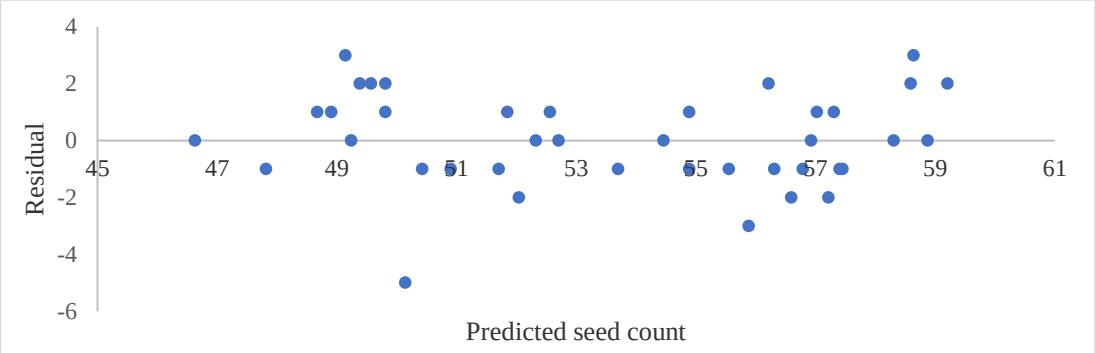

Figure 4.72: Residual Plot of Seed Count Data for Black Nightshade Berries

4.4.2 Standard Germination Test Results

The results of standard germination test are presented in Figure 4.73. The ANOVA results showed that at 0.05 level of significance $F_{cal} = 17 > F_{crit} = 3.68$. Thus, at least one of the drying modes was significantly different from the other. Fishers least significant difference (LSD) was determined as 5.1%. The difference between the means of germination percentage of solar drying mode compared to solar-exhaust gas mode of drying were not significantly different at 3.7%. Exhaust gas drying mode had a difference of 12.5% when its mean germination percentage was compared to solar mode of drying. Moreover, a 16.2% difference in means of germination percentage was recorded when solar-exhaust gas mode of drying was compared to exhaust gas mode. The highest mean germination percentage was recorded at 89% for exhaust gas drying mode because black nightshade seeds were subjected to temperatures ranging from 25.75 to 30.77°C. These temperatures were lower when compared to those of the other two modes of drying: solar (14.82-58.46°C) and solar-exhaust gas (34.49-61.97°C).

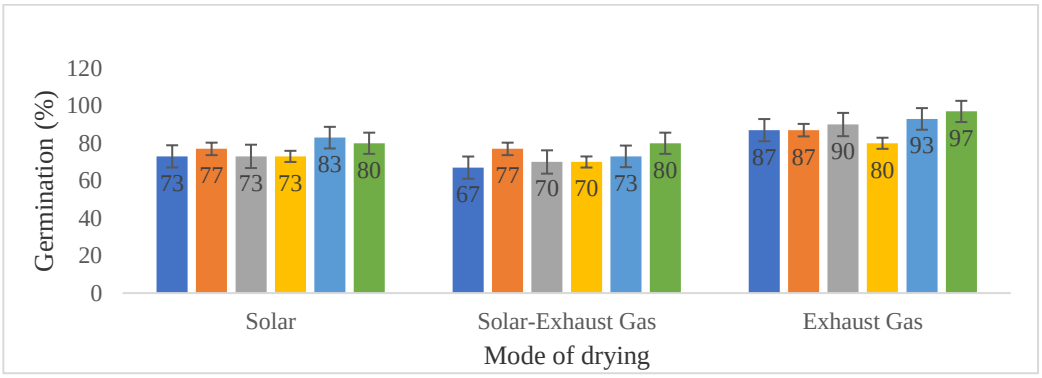

Figure 4.73: Six Replications of Mean Germination Tests on Black Nightshade Seeds' Viability

A number of authors have recommended low drying temperatures for seeds. Moreno *et al*. (2022) has recommended 35-40℃ for drying amaranth seeds in order to ensure viability. The authors reported an unacceptable decrease in amaranth seeds germination rate from 85 to 23% due to increased drying temperatures in microwave drying and forced convection drying using hot air in an electric oven. A slight decrease of germinability was observed in beech seeds dried at 30℃ when Pukacka and Wójkiewicz (2003) dried the seeds at 15 and 30℃. The previous study reviewed 15-20℃ as the recommended temperature of drying beech seeds and contrasted broadleaved species to conifers specifically on their inability to withstand high drying temperatures. Xie *et al*. (2022) have reported germination rates of up to 88% while drying peanut pods used for seeds through hot air drying technique. Soares *et al*. (2016) in a study aimed at evaluating the drying kinetics of barley grains in conventional and intermittent drying methods reported that drying at 40℃ resulted in the highest values of germination energy and germination index.

4.4.3 Germination Models Fitting

Modified Sharp's model and modified Giner's model have been commonly used in predicting germination percentage of seeds during drying process. Consequently, in the present study, experimental data of standard germination test were used to fit the two models using data collected from exhaust gas mode of drying. This mode of drying was chosen because black nightshade seeds dried under it had the highest germination percentages. The patterns from Sharp's model and Giner's model were used in R

statistical software (*mosaic* collection of packages) to obtain the values of RMSEs, and constants as presented in Table 4.4. Figure 4.74 shows the performance of the modified Sharp's model against experimental germination data. Figure 4.75 is correlation between the observed and predicted germination percentages when modified Sharp's model was used. Figure 4.76 is a plot of residuals resulting from the predictions of modified Sharp's model.

Table 4.4: Germination Models' Parameters

Model	R^2	RMSE	Constants
Modified Sharp's Model $G_t = G_0 - \frac{t}{10^{(C_0 - C_1 log M_i - C_2 T - C_3 T^2)}}$	0.6853	6.4519	$C_0 = 30.874$ $C_1 = 0.0163$ $C_2 = 0.0229$ $C_3 = 0.0101$
Modified Giner's Model $\frac{G_t}{G_0} = exp\left[-\left(exp\left(-\frac{E_a}{RT_a} + Z_1 + Z_2 M_i\right)\right)t\right]$	0.6896	6.1554	$E_a = 7.034 \times 10^3$ $Z_1 = 2.64 \times 10^{28}$ $Z_2 = 1.88 \times 10^{28}$

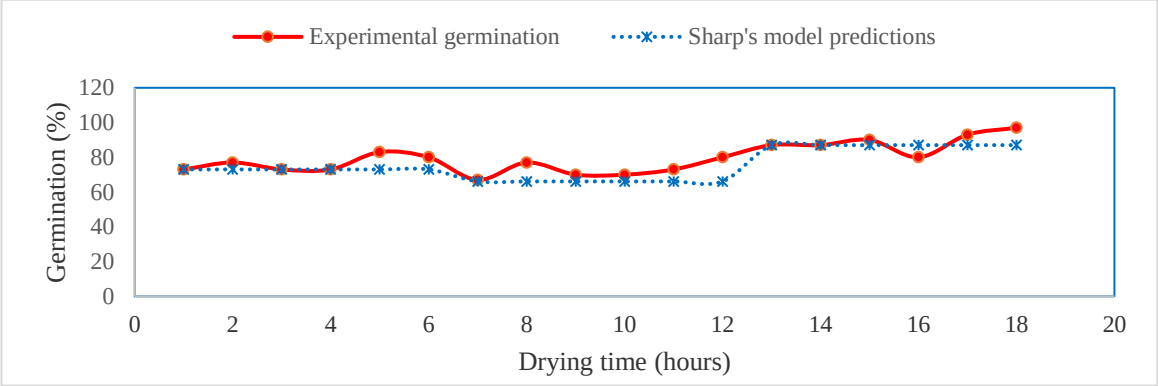

Figure 4.74: Modified Sharp's Model Performance Compared to Experimental Data

Figure 4.77 shows the performance of modified Giner's model against experimental germination data. Figure 4.78 is correlation between the observed and predicted germination percentages when modified Giner's model was used. Figure 4.79 is a plot of residuals resulting from the predictions of modified Giner's model. The survival analysis procedures with life tables, logistic regression, and accelerated failure are the most informative analyses for seed germination studies (Scott *et al.*, 1984). In this regard, the statistical procedure selected to evaluate the models' parameters shown in Table 4.4 best tested the hypothesis posed by the experiments in the current study.to provide as much ancillary information as possible. Graphical evaluation of percent germination shown in Figures 4.74 to 4.79 was a useful step in analysis to promote stand establishment through the use of exhaust gas energy to dry black nightshade seeds.

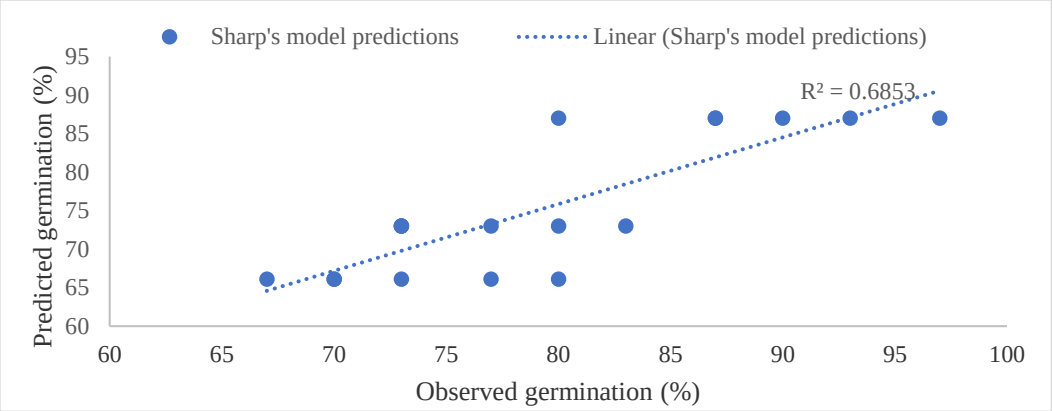

Figure 4.75: Correlation between Observed and Predicted Germination Percentages Using Modified Sharp's Model

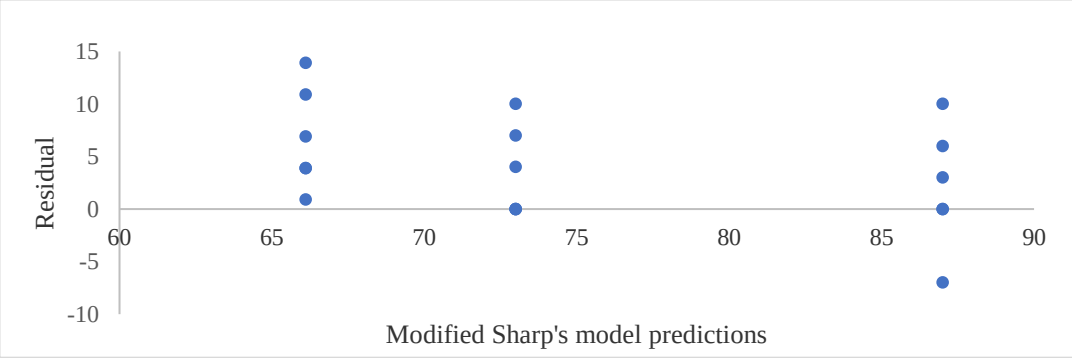

Figure 4.76: Residual Plots of Modified Sharp's Model Predictions

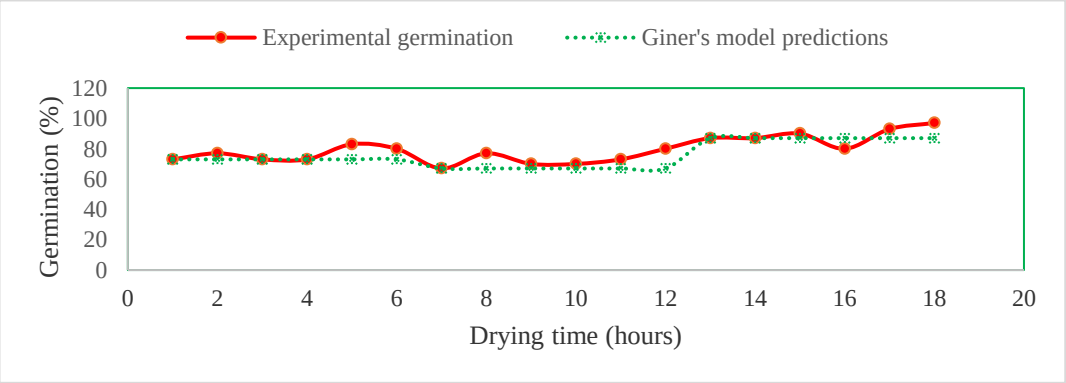

Figure 4.3: Modified Giner's model performance compared to experimental data

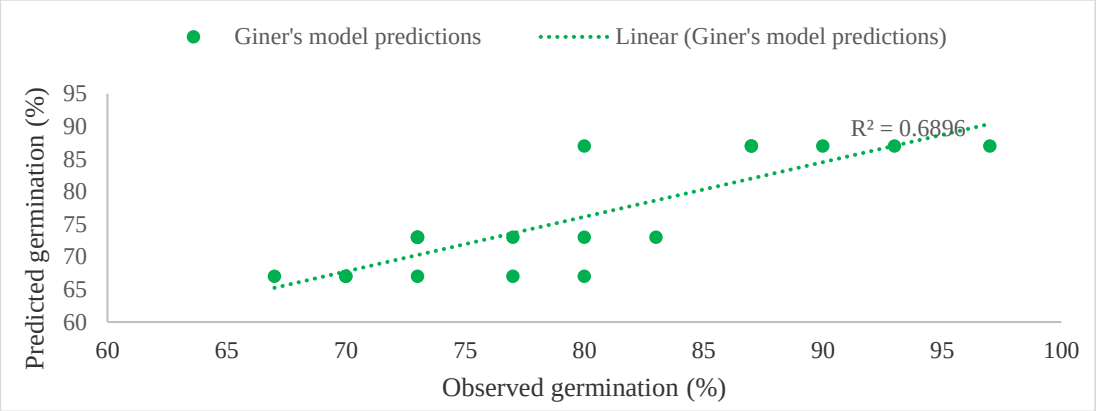

Figure 4.78: Correlation between Observed and Predicted Germination Percentages Using Modified Giner's Model

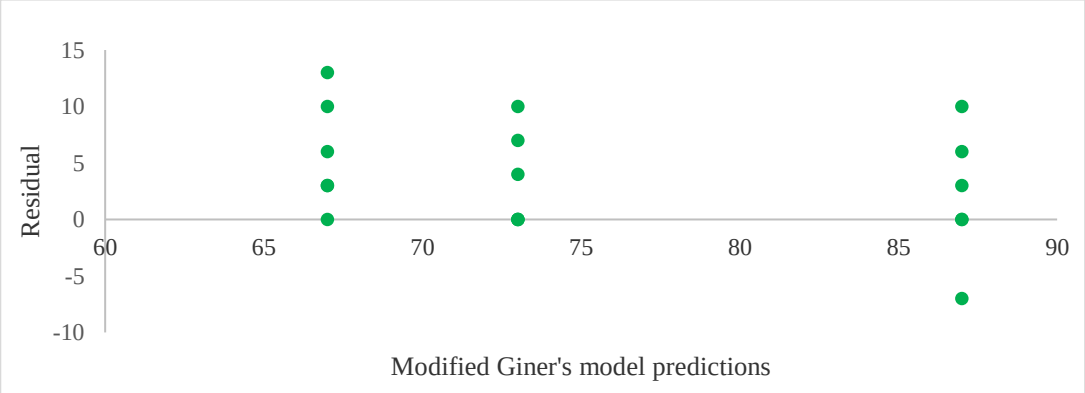

Figure 4.79: Residual Plots of Modified Giner's Model Predictions

CHAPTER FIVE

CONCLUSIONS AND RECOMMENDATIONS

5.1 Conclusions

The specific conclusions drawn from this study are as follows:

(1) It is feasible to predict the temperature of black nightshade seeds, greenhouse dryer room air temperature and moisture evaporated from black nightshade seeds based on the developed second order and exponential decay models. The three proposed thermal models for temperature and moisture evaporation performed better with low RMSEs (0.4859, 0.2453, and 0.3392) in exhaust gas mode compared to the other modes of drying.

(2) The concept of using a heat exchanger in a solar-exhaust gas dryer was successfully applied in the recovery of exhaust gas energy from a diesel engine heat energy that under normal circumstances is wastefully released to the environment. The heat exchanger raised the dryer temperature by an hourly average of 11.78℃ in solar-exhaust gas mode and 8.04℃ when temperature differences between inside and outside were compared in exhaust gas mode of drying. The rate of heat energy utilized for the three modes of drying were: solar (37.33 to 683.3 $J/m^2 \cdot s$), solar-exhaust gas (40.49 to 685.94 $J/m^2 \cdot s$), and exhaust gas (21.69 to 668.11 $J/m^2 \cdot s$).

(3) The page model was the most appropriate in describing thin layer drying of black nightshade seeds when drying was performed in solar mode (highest R^2 of 0.9985 and lowest RMSE of 0.0115). In solar-exhaust gas mode, Logarithmic model was the best model obtained for predicting thin layer drying of black nightshade seeds (highest R^2 of 0.9964 and lowest RMSE of 0.0172). In exhaust gas mode of drying, the Logarithmic model was found to be the most suitable in describing thin layer drying of black night shade seeds (highest R^2 of 0.9933 and lowest RMSE of 0.0232).

(4) Exhaust gas mode of drying was found to be the most suitable mode of drying black nightshade seeds because it produced the highest mean germination rate

of 89%. Modified Giner's model predicted germination changes of black nightshade seeds more accurately than modified Sharp's model.

5.2 Recommendations

5.2.1 Recommendations from this Study

The recommendations drawn from this study are as follows:

(1) It is recommended that products dried using exhaust gas mode can be further dried using solar mode to achieve safe moisture levels for storage. This combination shortens the solar hours required for drying and will ensure continuity of drying during peak demand.
(2) Use of diesel engines to power hammer mills in Kenya is known to produce regulated and unregulated emissions which are hazardous to public health. However, the released pollutants contain heat energy in their composition, and it is therefore necessary that the solution studied in this work be extended to the recovery of waste heat energy from hammer mills operated on diesel engines in Kenya.
(3) Generally, the drying rate of black nightshade seeds increased with increase in temperature—as observed in solar-exhaust gas drying mode—and decreased with increase in relative humidity—as depicted in exhaust gas drying mode whose experiments were performed when solar radiation was low, and humidity inside the dryer was high due to the presence of water vapour evaporating from the open cooling system of a diesel engine. Placing the diesel engine outside the dryer is therefore recommended.
(4) Exhaust gas mode of drying was recommended as the most suitable mode of drying black nightshade seeds. The models described in this study have potential use as seeds management protocols in quantifying seeds in berries and assessing germination.

5.2.2 Recommendations for Further Research

The following are recommendations for further studies:

(1) Some of the assumptions made when diesel exhaust gas was used as a working fluid in the heat exchanger included: the existence of steady operating conditions, negligible potential energy, and use of air properties for exhaust gas. It is recommended that the study be carried out without the assumptions in place.

(2) The energy in this study was not stored. It is recommended that a method to store the continuously produced heat energy from exhaust gas and solar energy may be studied.

(3) It was noted that exhaust gas particles adhere to the wall of the heat exchanger, and this may increase thermal resistance over a prolonged period of time, therefore, further research is recommended to find solutions capable of reversing or controlling the phenomenon.

(4) To write the energy balance equations, the assumptions made were: thin layer drying is adopted, heat capacity of greenhouse dryer cover and wall material is neglected, no stratification in greenhouse dryer air temperature, absorptivity of air is neglected, and greenhouse dryer is east-west oriented. It is recommended that thermal models for prediction of black nightshade seeds temperature and moisture evaporation be developed using energy balance equations for a solar-exhaust gas greenhouse dryer without the assumptions.

REFERENCES

Adesusi, O. M., Adetunji, O. R., Kuye, S. I., Musa, A. I., Erinle, T. J., Gbadamosi-Olatunde, O. B., & Ipadeola, S. O. (2023). A Comprehensive Review of the Materials Degradation Phenomena in Solid-Liquid Phase Change Materials for Thermal Energy Storage. *International Journal of Thermofluids*, 100360.

Aflakpui, G. K., Gregory, P. J., & Froud-Williams, R. J. (1998). Effect of temperature on seed germination rate of Striga hermonthica (Del.) Benth. *Crop Protection*, *17*(2), 129-133.

Agudelo, A. F., García-Contreras, R., Agudelo, J. R., & Armas, O. (2016). Potential for exhaust gas energy recovery in a diesel passenger car under European driving cycle. *Applied Energy*, *174*, 201-212.

Akhter, Md. S., Nabi, Md. N., & Afroz, Z. (2007). Recovery of waste heat from engine exhaust for utilization in a paddy dryer. *Paper presented at the proceeding of International Conference on Mechanical Engineering 2007 (ICME2007) 29- 31 December 2007, Dhaka, Bangladesh*, 1-5.

Akowuah, J. O., Maier, D., Opit, G., McNeill, S., Amstrong, P., Campabadal, C., & Obeng-Akrofi, G. (2018). Drying temperature effect on kernel damage and viability of maize dried in a solar biomass hybrid dryer. *Open Journal of Applied Sciences*, *8*(3.112), 506-517.

Alamayreh, M. I., & Alahmer, A. (2023). Design a solar harvester system capturing light and thermal energy coupled with a novel direct thermal energy storage and nanoparticles. *International Journal of Thermofluids*, *18*, 100328.

Alklaibi, A. M., & Lior, N. (2021). Waste heat utilization from internal combustion engines for power augmentation and refrigeration. *Renewable and Sustainable Energy Reviews*, *152*, 111629.

Al-Muhtaseb, A. H., McMinn, W. A. M. & Magee T. R. A. (2004). Water sorption isotherms of starch powders. Part 1: Mathematical description of experimental data. *Journal of Food Engineering, 61*, 297-306.

Anderson, R. B. (1946). Modifications of the B.E.T. equation. *Journal of American Chemical Society, 68*, 686–691.

Anwar, S. I., & Tiwari, G. N. (2001). Convective heat transfer coefficient of crops in forced convection drying—an experimental study. *Energy Conversion and Management, 42*(14), 1687-1698.

Aritesty, E., & Wulandani, D. (2014). Performance of the rack type-greenhouse effect solar dryer for wild ginger (*Curcuma xanthorizza* Roxb.) drying. *Energy Procedia, 47*, 94-100.

Armstead, J. R., & Miers, S. A. (2014). Review of waste heat recovery mechanisms for internal combustion engines. *Journal of Thermal Science and Engineering Applications, 6*(1), 14-20.

ASAE, (1996). ASAE D245.5: 1996. Moisture relationship of plant-based agricultural products. *ASAE Standards* (43rd ed.). St. Joseph, MI, USA: American Society of Agricultural Engineers.

Aviara, N. A., Ajibola, O. O., & Oni, S. A. (2004). Sorption equilibrium and thermodynamic characteristics of soya bean. *Biosystems Engineering, 87*(2), 179-190.

Aviara, N. A., Ajibola, O. O., Aregbesola, O. A., & Adedeji, M. A. (2006). Moisture sorption isotherms of sorghum mal at 40 and 50 ℃. *Journal of Stored Products Research, 42*(3), 290-301.

Azaizia, Z., Kooli, S., Elkhadraoui, A., Hamdi, I., & Guizani, A. (2017). Investigation of a new solar greenhouse drying system for peppers. *International Journal of Hydrogen Energy, 42* (13), 8818-8826.

Bakhtavar, M. A., Afzal, I., & Basra, S. M. A. (2019). Moisture adsorption isotherms and quality of seeds stored in conventional packaging materials and hermetic Super Bag. *Plos One*, *14*(2), e0207569.

Barrett, S., Ndegwa, W., & Maggio, G. (2021). The value of local climate and weather information: an economic valuation of the decentralized meteorological provision in Kenya. *Climate and Development*, *13*(2), 173-188.

Baskin, C. C., Thompson, K., & Baskin, J. M. (2006). Mistakes in germination ecology and how to avoid them. *Seed Science Research*, *16*(3), 165-168.

Basunia, M. A., & Abe, T. (2001). Moisture desorption isotherms of medium-grain rough rice. *Stored Products Research*, *37*, 205-219.

Brunauer, S., Emmet, P. H., & Teller, E. (1938). Adsorption of gases in multimolecular layers. *Journal of the American Chemical Society*, *60*, 309-315.

Budelsky, R. A., & Galatowitsch, S. M. (1999). Effects of moisture, temperature, and time on seed germination of five wetland Carices: implications for restoration. *Restoration Ecology*, *7*(1), 86-97.

Cai, W., Wei, R., Xu, L., & Ding, X. (2022). A method for modelling greenhouse temperature using gradient boost decision tree. *Information Processing In Agriculture*, *9*(3), 343-354.

Chadha, M. L., Oluoch, M. O., & Silue, D. (2006). Promoting indigenous vegetables for health, food security, and income generation in Africa. In *XXVII International Horticultural Congress-IHC2006: International Symposium on Horticultural Plants in Urban and Peri-Urban 762*, 253-262.

Chaichan, M. T. (2018). Combustion and emission characteristics of E85 and diesel blend in conventional diesel engine operating in PPCI mode. *Thermal Science and Engineering Progress*, *7*, 45-53.

Chao, E., Tian, J., Fan, L., & Zhang, T. (2022). Drying methods influence the physicochemical and functional properties of seed-used pumpkin. *Food Chemistry*, *369*, 130937.

Chaudhari, A. D., & Salve, S. P. (2014). A review of solar dryer technologies. *International Journal of Research in Advent Technology*, *2*(2), 218-232.

Chauhan, P. S., & Kumar, A. (2018). Thermal modeling and drying kinetics of gooseberry drying inside north wall insulated greenhouse dryer. *Applied Thermal Engineering*, *130*, 587-597.

Chauhan, P. S., & Kumar, A., (2016). Performance analysis of greenhouse dryer by using insulated north-wall under natural convection mode. *Energy Reports. 2*, 107-116.

Chauhan, P. S., Kumar, A., & Gupta, B. (2017). A review on thermal models for greenhouse dryers. *Renewable and Sustainable Energy Reviews*, *75*, 548-558.

Chauhan, P. S., Kumar, A., & Nuntadusit, C. (2018a). Thermo-environomical and drying kinetics of bitter gourd flakes drying under north wall insulated greenhouse dryer. *Solar Energy*, *162*, 205-216.

Chauhan, P. S., Kumar, A., Nuntadusit, C., & Banout, J. (2018b). Thermal modeling and drying kinetics of bitter gourd flakes drying in modified greenhouse dryer. *Renewable Energy*, *118*, 799-813.

Chen, C. (1988). *A study of equilibrium relative humidity for yellow-dent corn kernels.* Unpublished Ph.D. Thesis. St Paul, USA: University of Minnesota.

Chen, C. C., & Morey, R. V. (1989). Comparison of four EMC/ERH equations. *Transactions of the American Society of Agricultural Engineers*, *32*, 983-990.

Chirife, J., & Iglesias, H. A. (1978). Equations for fitting water sorption isotherms of foods. Part I-A review. *Journal of Food Technology, 13,* 159-174.

Choab, N ., Allouhi, A ., El Maakoul, A ., Kousksou, T ., Saadeddine, S ., & Jamil, A. (2019). Review on greenhouse microclimate and application: Design parameters, thermal modeling and simulation, climate controlling technologies. *Solar Energy*, *191*, 109-137.

Chowdhury, M. M. I., Bala, B. K., & Haque, M. A. (2011). Mathematical modelling of thin layer drying of jackfruit leather. *Journal of Food Processing and Preservation*, *35*(6), 797-805.

Chowdhury, N., Ghosh, A., & Chandra, G. (2008). Mosquito larvicidal activities of Solanum villosum berry extract against the dengue vector Stegomyia aegypti. *BMC Complementary and Alternative Medicine*, *8*(1), 1-8.

Chung, D. S., & Pfost, H. B. (1967). Adsorption and desorption of water vapour by cereal grains and their products. Part II: Development of the general isotherm equation. *Transactions of the ASAE, 10*, 549-557.

Coradi, P. C., Maldaner, V., Lutz, É., da Silva Daí, P. V., & Teodoro, P. E. (2020). Influences of drying temperature and storage conditions for preserving the quality of maize postharvest on laboratory and field scales. *Scientific Reports*, *10*(1), 22006.

Covell, S., Ellis, R. H., Roberts, E. H., & Summerfield, R. J. (1986). The influence of temperature on seed germination rate in grain legumes: I. A comparison of chickpea, lentil, soyabean and cowpea at constant temperatures. *Journal of Experimental Botany*, *37*(5), 705-715.

Croft, M. M. (2016). *The role of African leafy vegetables in food security,y* Unpublished PhD dissertation, USA: Purdue University.

Da Silva, W. P., e Silva, C. M., Gama, F. J., & Gomes, J. P. (2014). Mathematical models to describe thin-layer drying and to determine drying rate of whole

bananas. *Journal of the Saudi Society of Agricultural Sciences*, *13*(1), 67-74.

Dai, L., Li, S., DuanMu, L., Li, X., Shang, Y., & Dong, M. (2015). Experimental performance analysis of a solar assisted ground source heat pump system under different heating operation modes. *Applied Thermal Engineering*, *75*, 325-333.

Daniels, M. (2003). Contemporary statistical models for the plant and soil sciences. Oliver Schabenberger and Francis J. Pierce.

Dantas, B. F., Moura, M. S., Pelacani, C. R., Angelotti, F., Taura, T. A., Oliveira, G. M., ... & Seal, C. E. (2020). Rainfall, not soil temperature, will limit the seed germination of dry forest species with climate change. *Oecologia*, *192*(2), 529-541.

De Boer, J. H. (1953). *The dynamical character of adsorption*. Oxford: Clarendon Press.

De Groote, H., & Kimenju, S. C. (2008). Comparing consumer preferences for color and nutritional quality in maize: Application of a semi-double-bound logistic model on urban consumers in Kenya. *Food Policy*, *33*(4), 362-370.

De Poures, M. V., Damodharan, D., Gopal, K., Augustin, V. C., & Swaminathan, M. R. (2022). Prediction of emissions and performance of a diesel engine fueled with waste cooking oil and C8 oxygenate blends using response surface methodology. *Journal of Cleaner Production*, 133323.

De Vitis, M., Hay, F. R., Dickie, J. B., Trivedi, C., Choi, J., & Fiegener, R. (2020). Seed storage: maintaining seed viability and vigor for restoration use. *Restoration Ecology*, *28*, S249-S255.

Degwale, A., Tesfa, T., Meseret, B., & Fantaw, S. (2023). Seed extraction methods affect the physiological quality of tomato seed and developing seedlings. *International Journal of Vegetable Science*, *29*(1), 16-24.

Dhahad, H. A., Chaichan, M. T., & Megaritis, T. (2019). Performance, regulated and unregulated exhaust emission of a stationary compression ignition engine fueled by water-ULSD emulsion. *Energy*, *181*, 1036-1050.

Dong, R., Lu, Z., Liu, Z., Nishiyama, Y., & Cao, W. (2009). Moisture distribution in a rice kernel during tempering drying. *Journal of Food Engineering*, *91*(1), 126-132.

Dube, P., Heijman, W. J., Ihle, R., & Ochieng, J. (2018). The potential of traditional leafy vegetables for improving food security in Africa. In *Establishing Food Security and Alternatives to International Trade in Emerging Economies*, IGI Global, 220-243.

Edmonds, J. M., & Chweya, J. A. (1997). *Black nightshades: Solanum nigrum L. and related species* (Vol. 15). *Bioversity International*. *45*(1), 13-30.

Eichsteller, M., Njagi, T., & Nyukuri, E. (2022). The role of agriculture in poverty escapes in Kenya Developing a capabilities approach in the context of climate change. *World Development*, *149*, 1-14.

Ekhuya, N. A., Wesonga, J. M., & Abukutsa-Onyango, M. O. (2018). Production, processing, and storage techniques of African nightshade (Solanum spp.) seeds and their correlations with farmers' characteristics in Western Kenya. *African Journal of Food, Agriculture, Nutrition and Development*, *18*(2), 13338-13351.

Ellis, R. H., & Roberts, E. H. (1980). Improved equations for the prediction of seed longevity. *Annals of Botany*, *45*(1), 13-30.

Ellis, R. H., Simon, G., & Covell, S. (1987). The influence of temperature on seed germination rate in grain legumes: III. A comparison of five faba bean genotypes at constant temperatures using a new screening method. *Journal of Experimental Botany*, *38*(6), 1033-1043.

El-Maarouf-Bouteau, H. (2022). The Seed and the metabolism regulation. *Biology*, *11*(2), 168.

ElMasry, G., Mandour, N., Ejeez, Y., Demilly, D., Al-Rejaie, S., Verdier, J., & Rousseau, D. (2022). Multichannel imaging for monitoring chemical composition and germination capacity of cowpea (*Vigna unguiculata*) seeds during development and maturation. *The Crop Journal*, *10*(5), 1399-1411.

Feldsine, P., Abeyta, C., & Andrews, W. H. (2002). AOAC International methods committee guidelines for validation of qualitative and quantitative food microbiological official methods of analysis. *Journal of AOAC International*, *85*(5), 1187-1200.

Feru, E., Kupper, F., Rojer, C., Seykens, X. L. J., Scappin, F., Willems, F. P. T., & Steinbuch, M. (2013). Experimental validation of a dynamic waste heat recovery system model for control purposes. In *SAE 2013 World Congress and Exhibition, 16-18 April 2013, Detroit, MI, USA*. SAE International, 1-13.

Finocchiaro, M. A. (2012). *Galileo and the art of reasoning: Rhetorical foundation of logic and scientific method* (Vol. 61). London: Springer Science & Business Media.

Gaede, J., & Meadowcroft, J. (2016). A question of authenticity: Status quo bias and the International Energy Agency's World Energy Outlook. *Journal of Environmental Policy & Planning*, *18*(5), 608-627.

Gal, S. (1981). Recent developments in techniques for obtaining complete sorption isotherms. In L. B. Rockland & G. F. Stewart (Eds.), *Water activity: Influence on Food Quality*. New York: Academic Press.

Garcia, J. L., De la Plaza, S., Navas, L. M., Benavente, R. M., & Luna, L. (1998). Evaluation of the feasibility of alternative energy sources for greenhouse heating. *Journal of Agricultural Engineering Research*, *69*(2), 107-114.

Giner, S. A., Lupano, C. E., & Anon, M. C. (1991). A model for estimating loss of wheat seed viability during hot-air drying. *Cereal Chemistry*. *45*(1), 13-30.

Guggenheim, E. A. (1966). *Applications of statistical mechanics*. Oxford: Clarendon Press.

Halsey, G. (1948). Physical adsorption on non-uniform surfaces. *Journal of Chemical Physics, 16*, 931-937.

Han, J. W., & Keum, D. H. (2011). Thin layer drying characteristics of rapeseed (Brassica napus L.). *Journal of Stored Products Research*, *47*(1), 32-38.

Harrington, J. F. (1959). *Drying, storage, and packaging seed to maintain germination and vigor.* Oxford: Clarendon Press.

Hathal, M. M., Al-Jadir, T., Al-Sheikh, F., Edan, M. S., Haider, M. J., Rsool, R. A., ... & Badawy, T. (2023). Thermal performance characterization of a thermal energy storage tank with various phase change materials. *International Journal of Thermofluids*, *18*, 100322.

He, W., Su, Y., Wang, Y. Q., Riffat, S. B., & Ji, J. (2012). A study on incorporation of thermoelectric modules with evacuated-tube heat-pipe solar collectors. *Renewable Energy*, *37*(1), 142-149.

Henderson, S. M. (1952). A basic concept of equilibrium moisture. *Agricultural Engineering, 33*, 29-32.

Hii, C. L., Law, C. L., & Cloke, M. (2009). Modeling using a new thin layer drying model and product quality of cocoa. *Journal of Food Engineering*, *90*(2), 191-198.

Hodson, T. O. (2022). Root-mean-square error (RMSE) or mean absolute error (MAE): When to use them or not. *Geoscientific Model Development*, *15*(14), 5481-5487.

Hong, T. D., Linington, S., & Ellis, R. H. (1996). *Seed storage behavior: A compendium*. Oxford: Clarendon Press.

Huang, Y. T., Wu, W., Zou, W. X., Wu, H. P., & Cao, D. D. (2020). Drying temperature affects rice seed vigor via gibberellin, abscisic acid, and antioxidant enzyme metabolism. *Journal of Zhejiang University. Science. B*, *21*(10), 796.

Iguaz, A., & Virseda, P. (2007). Moisture desorption isotherms of rough rice at high temperatures. *Journal of Food Engineering*, *79*(3), 794-802.

Ingold, K. (2017). How to create and preserve social capital in climate adaptation policies: A network approach. *Ecological economics*, *131*, 414-424.

International Seed Testing Association. (1985). International rules for seed testing. Rules 1985. *Seed Science and Technology*, *13*(2), 299-513.

Ismaili, S. E., Maurady, A., Lachkar, M., Britel, M. R., & Bakali, A. H. (2023). Effect of temperature and different pre-treatments on seed germination of Stachys mouretii Batt. & Pit. *Journal of Applied Research on Medicinal and Aromatic Plants*, *32*, 100438.

Jadhao, J. S., & Thombare, D. G. (2013). Review on exhaust gas heat recovery for IC engine. *International Journal of Engineering and Innovative Technology*, *2*(12), 93-100.

Jain, D., & Tiwari, G. N. (2004a). Effect of greenhouse on crop drying under natural and forced convection I: Evaluation of convective mass transfer coefficient. *Energy Conversion and Management*, *45*(5), 765-783.

Jain, D., & Tiwari, G. N. (2004b). Effect of greenhouse on crop drying under natural and forced convection II. Thermal modelling and experimental validation. *Energy Conversion and Management*, *45*(17), 2777-2793.

Janssens, J. P., & Cloudt, R. (2013). High temperature heat exchanger for Rankine cycle-based exhaust waste heat recovery. In *Advanced Microsystems for Automotive Applications*. London: Springer, Heidelberg.

Jarso, J. F. (2012). The East African Community and the climate change agenda: An inventory of the progress, hurdles, and prospects. *Sustainable Development Law & Policy*, *12*(2), 6-15.

Javaid, M. M., Mahmood, A., Alshaya, D. S., AlKahtani, M. D., Waheed, H., Wasaya, A., ... & Fiaz, S. (2022). Influence of environmental factors on seed germination and seedling characteristics of perennial ryegrass (Lolium perenne L.). *Scientific Reports*, *12*(1), 9522.

Jayas, D. S., & Mazza, G. (1993). Comparison of five three-parameter equations for the description of adsorption data of oats. *Transactions of the ASAE*, *36*, 119-125.

Jayendra, K. A., Singh, R. R. B., Patil, G. R., & Patel, A. A. (2005). Effect of temperature on moisture desorption isotherms of Kheer. *Lebensmittel-Wissenschaft und technology*, *38*, 303-310.

Jiang, Y., Zhang, H., Zhang, H., Zhao, X., Liu, H., Sun, C., & Sun, J. (2014). Tsmart-galsblock: A toolkit for modelling, validation, and synthesis of multi-clocked embedded systems. In *Proceedings of the 22nd ACM SIGSOFT International Symposium on Foundations of Software Engineering*, 711-714.

Jittanit, W., Srzednicki, G., & Driscoll, R. (2009). Germination models for seeds dried in fluidised and spouted bed dryers. *Seed Science and Technology*, *37*(1), 180-191.

Jittanit, W., Srzednicki, G., & Driscoll, R. (2010). Corn, rice, and wheat seed drying by two-stage concept. *Drying Technology*, *28*(6), 807-815.

Jnyana, R. P., Santosh, K. H., & Mahanta, P. (2015). Effect of waste heat recovery on drying characteristics of sliced ginger in a natural convection dryer. *Procedia Engineering*, *105*, 145-152.

Jobst, L. J., Heine, C., Auerswald, M., & Moshagen, M. (2021). Effects of multivariate non-normality and missing data on the root mean square error of approximation. *Structural Equation Modelling: A Multidisciplinary Journal*, 28(6), 1-8.

Jouhara, H., & Ezzuddin, H. (2013). Thermal performance characteristics of a wraparound loop heat pipe (WLHP) charged with R134A. *Energy*, *61*, 128-138.

Jouhara, H., & Meskimmon, R. (2014). Heat pipe based thermal management systems for energy-efficient data centres. *Energy*, *77*, 265-270.

Jouhara, H., & Olabi, A. G. (2018). Industrial waste heat recovery. *Energy*, *160*, 1-2.

Jouhara, H., Almahmoud, S., Brough, D., Guichet, V., Delpech, B., Chauhan, A., ... & Serey, N. (2021a). Experimental and theoretical investigation of the performance of an air to water multi-pass heat pipe-based heat exchanger. *Energy*, *219*, 119624.

Jouhara, H., Almahmoud, S., Chauhan, A., Delpech, B., Bianchi, G., Tassou, S. A., ... & Arribas, J. J. (2017a). Experimental and theoretical investigation of a flat heat pipe heat exchanger for waste heat recovery in the steel industry. *Energy*, *141*, 1928-1939.

Jouhara, H., Anastasov, V., & Khamis, I. (2009). Potential of heat pipe technology in nuclear seawater desalination. *Desalination*, *249*(3), 1055-1061.

Jouhara, H., Bertrand, D., Axcell, B., Montorsi, L., Venturelli, M., Almahmoud, S., ... & Chauhan, A. (2021b). Investigation on a full-scale heat pipe heat exchanger in the ceramics industry for waste heat recovery. *Energy*, *223*, 120037.

Jouhara, H., Chauhan, A., Nannou, T., Almahmoud, S., Delpech, B., & Wrobel, L. C. (2017b). Heat pipe based systems-Advances and applications. *Energy*, *128*, 729-754.

Jouhara, H., Khordehgah, N., Almahmoud, S., Delpech, B., Chauhan, A., & Tassou, S. A. (2018). Waste heat recovery technologies and applications. *Thermal Science and Engineering Progress*, *6*, 268-289.

Jouhara, H., Żabnieńska-Góra, A., Khordehgah, N., Ahmad, D., & Lipinski, T. (2020). Latent thermal energy storage technologies and applications: A review. *International Journal of Thermofluids*, *5*, 100039.

Kalogirou, S. A. (2004). Solar thermal collectors and applications. *Progress in Energy and Combustion Science*, *30*(3), 231-295.

Kamga, R. T., Kouamé, C., Atangana, A. R., Chagomoka, T., & Ndango, R. (2013). Nutritional evaluation of five African indigenous vegetables. *Journal of Horticultural Research*, *21*(1), 99-106.

Kanali, C., Kituu, G., Mutwiwa, U., Mung'atu, J., Ronoh, E., Njuguna, S., & Mulamu, L. (2017). Energy efficient rural food processing utilising renewable energy to improve rural livelihoods in Kenya. *RE4Food Project Report, Kenya: Jomo Kenyatta University of Agriculture and Technology (JKUAT)*.

Karamarkovic, V., Marasevic, M., Karamarkovic, R., & Karamarkovic, M. (2013). Recuperator for waste heat recovery from rotary kilns. *Applied Thermal Engineering*, *54*(2), 470-480.

Kaya, A., & Aydın, O. (2009). An experimental study on drying kinetics of some herbal leaves. *Energy Conversion and Management*, *50*(1), 118-124.

Kesgin, U. (2005). Study on the design of inlet and exhaust system of a stationary internal combustion engine. *Energy Conversion and Management*, *46*(13-14), 2258-2287.

Khaeim, H., Kende, Z., Jolánkai, M., Kovács, G. P., Gyuricza, C., & Tarnawa, Á. (2022). Impact of temperature and water on seed germination and seedling growth of maize (Zea mays L.). *Agronomy*, *12*(2), 397.

Khaliq, A., Almohammadi, B. A., Alharthi, M. A., Siddiqui, M. A., & Kumar, R. (2021). Investigation of a combined refrigeration and air conditioning system based on two-phase ejector driven by exhaust gases of natural gas fueled homogeneous charge compression ignition engine. *Journal of Energy Resources Technology*, *143*(12), 120911.

Kiburi, F. G., Kanali, C. L., Kituu, G. M., Ajwang, P. O., & Ronoh, E. K. (2020a). Performance evaluation and economic feasibility of a solar-biomass hybrid greenhouse dryer for drying Banana slices. *Renewable Energy Focus*, *34*, 60-68.

Kiburi, F. G., Kanali, C. L., Kituu, G. M., Ajwang, P. O., & Ronoh, E. K. (2020b). Quality evaluation of four banana cultivars dried in a greenhouse dryer operated under different energy modes. *African Journal of Horticultural Science*, *17*, 53-66.

Kiburi, F. G., Mutwiwa, U. N., Ronoh, E. K., Chemain, N., & Yegon, H. K. (2017). Evaluating the performance of dehumidified solar dryer in drying of pumpkin slices (*Cucurbita pepo*). *African Journal of Horticultural Science*, *11*, 72-81.

Kilcik, A. (2005). Regional sun–climate interaction. *Journal of atmospheric and solar-terrestrial physics*, *67*(16), 1573-1579.

Kiyan, M., Bingöl, E., Melikoğlu, M., & Albostan, A. (2013). Modelling and simulation of a hybrid solar heating system for greenhouse applications using Matlab/Simulink. *Energy Conversion and Management*, *72*, 147-155.

Kosky, P., Balmer, R. T., Keat, W. D., & Wise, G. (2015). *Exploring engineering: an introduction to engineering and design*. New York: Academic Press.

Krichen, K., Ghorbel, M. A., & Chaieb, M. (2023). Modeling the influence of temperature, salt and osmotic stresses on seed germination and survival capacity of Stipa tenacissima L. *Plant Biosystems-An International Journal Dealing with all Aspects of Plant Biology*, *157*(2), 325-338.

Kruiswyk, R. W., Fairbanks, J., & Maronde, C. (2008). An engine system approach to exhaust waste heat recovery. In *Diesel Engine-Efficiency and Emissions Research (DEER) Conference, Dearborn, Michigan*.

Kumar, A., & Tiwari, G. N. (2006). Thermal modelling of a natural convection greenhouse drying system for jaggery: An experimental validation. *Solar energy*, *80*(9), 1135-1144.

Kurata, K., & Takakura, T. (1991). Underground storage of solar energy for greenhouses heating. I. Analysis of seasonal storage system by scale and numerical models. *Transactions of the ASAE*, *34*(2), 563-0569.

Laban, M. C., Anthony, W. K., & Elias, O. B. (2021). Driving youth participation in agriculture: A synopsis of the influence of existing agricultural policies in selected counties in Kenya. *International Journal of Academic Research in Business and Social Sciences*, *11*(9), 991-1015.

Lad, P., Kumar, R., Saxena, R., & Patel, J. (2023). Numerical investigation of phase change material assisted indirect solar dryer for food quality preservation. *International Journal of Thermofluids*, *18*, 100305.

Lin, Y., Chong, C. H., Ma, L., Li, Z., & Ni, W. (2022). Quantification of waste heat potential in China: A top-down Societal Waste Heat Accounting Model. *Energy*, *261*, 125194.

Lingayat, A., Chandramohan, V. P., & Raju, V. R. K. (2017). Design, development, and performance of indirect type solar dryer for banana drying. *Energy Procedia*, *109*, 409-416.

Liu, J. P., Fu, J. Q., Ren, C. Q., Wang, L. J., Xu, Z. X., & Deng, B. L. (2013). Comparison and analysis of engine exhaust gas energy recovery potential through various bottom cycles. *Applied Thermal Engineering*, *50*(1), 1219-1234.

Liu, S., Yin, H., Pickard, M., & Ai, Y. (2020). Influence of infrared heating on the functional properties of processed lentil flours: A study focusing on tempering period and seed size. *Food Research International*, *136*(1), 59-68.

López-Flores, F. J., Rubio-Castro, E., & Ponce-Ortega, J. M. (2022). Incorporating machine learning for thermal engines modeling in industrial waste heat recovery. *Chemical Engineering Research and Design*, *181*, 239-252.

Luijten, J. (2005). Bioenergy Options for a Cleaner Environment: In Developed and Developing Countries. *Agricultural Systems*, *83*(3), 329-331.

Ma, Z., Huang, H., Huang, Z., Guo, D., Saeed, M., Jiang, C., ... & Wei, S. (2021). Germination response of black nightshade (Solanum nigrum) to temperature and the establishment of a thermal time model. *Weed Science*, *69*(6), 695-703.

Mahmoud, M., Naher, S., Ramadan, M., Abdelkareem, M. A., Jaber, H., & Olabi, A. G. (2023). Investigation of a ground-cooled organic Rankine cycle for waste heat recovery. *International Journal of Thermofluids*, *18*, 100348.

Manzela, A. A., Hanriot, S. M., Cabezas-Gómez, L., & Sodré, J. R. (2010). Using engine exhaust gas as energy source for an absorption refrigeration system. *Applied energy*, *87*(4), 1141-1148.

Maruoka, N., Mizuochi, T., Purwanto, H., & Akiyama, T. (2004). Feasibility study for recovering waste heat in the steelmaking industry using a chemical recuperator. *ISIJ International*, *44*(2), 257-262.

McCormack, J. H. (2004). Seed processing and storage: principles and practices of seed harvesting, processing, and storage: *An organic seed production manual for seed growers in the Mid-Atlantic and Southern US, 1*(2), 1-28.

Menon, E. S. (2014). *Transmission pipeline calculations and simulations manual*. Gulf Professional Publishing.

Mishra, S., Verma, S., Chowdhury, S., & Dwivedi, G. (2021). Analysis of recent developments in greenhouse dryer on various parameters - a review. *Materials Today: Proceedings*, *38*, 371-377.

Mitrevski, V., Lutovska, M., Mijakovski, V., Pavkov, I., Babic, M., & Radojcin, M. (2015). Adsorption isotherms of pear at several temperatures. *Thermal Science*, *19*(3), 1119-1129.

Mohite, A. M., Mishra, A., & Sharma, N. (2016). Equilibrium moisture content and drying behaviour of tamarind seed under thin layer condition. *International Journal of Seed Spices*, *6*(2), 18-22.

Moody, L. F. (1944). Friction factors for pipe flow. *Transactions of ASME*, *66*, 671-684.

Morales, R. S., Rigola, J., Rodriguez, I., & Oliva, A. (2012). Numerical resolution of the liquid vapour two phase flow by means of the two-fluid model and a pressure-based method. *International Journal of Multiphase Flow, 43*(3.111), 118-130.

Moreno, Á. H., Aguirre, Á. J., Maqueda, R. H., Jiménez, G. J., & Miño, C. T. (2022). Effect of temperature on the microwave drying process and the viability of amaranth seeds. *Biosystems Engineering*, *215*, 49-66.

Murr, R., El Achkar, G., Faraj, J., El Hage, H., Castelain, C., & Khaled, M. (2023). Using solar air heating for fruit drying: Thermo-economic and environmental studies. *International Journal of Thermofluids*, *18*, 100366.

Najib, T., Heydari, M. M., & Meda, V. (2022). Combination of germination and innovative microwave-assisted infrared drying of lentils: effect of physicochemical properties of different varieties on water uptake, germination, and drying kinetics. *Applied Food Research*, *2*(1), 100040.

Nakhauka, E. B. (2009). Agricultural biodiversity for food and nutrient security: The Kenyan perspective. *International Journal of Biodiversity and Conservation*, *1*(7), 208-214.

Natesan, V. T., Mani, P., Prasad, T. S., Krishna, J. M., & Sekar, S. (2020). Applications of thin layer modelling techniques and advances in drying of agricultural products. In *AIP Conference Proceedings* AIP Publishing LLC. *2311(1)*, 1-11.

Ndeda, J. O. H., Rabiu, A. B., & Ngoo, L. M. (2013). *Solar radiative variability forcing of climate change on seasonal to decadal scales in Kenya*, Unpublished PhD dissertation, Juja: JKUAT.

Ndegwa, D. W., & Kinyua, J. M. (2018). Strategic measures employed by the National Drought Management Authority for drought mitigation in Kenya.*International Journal of Management and Commerce Innovations* *6*(1), 802-812.

Ndirangu, S. N., Ronoh, E. K., Kanali, C. L., Mutwiwa, U. N., & Kituu, G. M. (2020). Design and performance evaluation of an improved solar-biomass greenhouse dryer for drying of selected crops in Western Kenya. *Agricultural Engineering International: CIGR Journal*, *22*(3), 219-229.

Nguyen, T. K., Mondor, M., & Ratti, C. (2018). Shrinkage of cellular food during air drying. *Journal of Food Engineering*, *230*, 8-17.

Ogulata, R. T. (2004). Utilization of waste-heat recovery in textile drying. *Applied Energy*, 79(1), 41-49.

Olanipekun, B. F., Tunde-Akintunde, T. Y., Oyelade, O. J., Adebisi, M. G., & Adenaya, T. A. (2015). Mathematical modeling of thin-layer pineapple drying. *Journal of Food Processing and Preservation, 39*(6), 1431-1441.

Oliveira, E. G. D., Rosa, G. D. S., Moraes, M. A. D., & Pinto, L. A. D. A. (2009). Moisture sorption characteristics of microalgae Spirulina platensis. *Brazilian Journal of Chemical Engineering, 26*, 189-197.

Ondieki, M. J., Aguyoh, J. N., & Opiyo, A. (2011). Variations in growth and yield characteristics of three black nightshade species grown under high altitude conditions. *Agriculture and Biology Journal of North America, 2*(3), 401-406.

Onwude, D. I., Hashim, N., Janius, R. B., Nawi, N. M., & Abdan, K. (2016). Modeling the thin layer drying of fruits and vegetables: A review. *Comprehensive Reviews in Food Science and Food Safety, 15*(3), 599-618.

Oswin, C. R. (1946). The kinetic of package life. III Isotherm. *Journal of Chemical Industry, London, 65*, 419-421.

Oyerinde, A. S. (2016). Modelling of thin layer drying kinetics of tomato (Lycopersicon esculentum Mill) slices under direct sun and air assisted solar dryer. *International Journal of Engineering and Applied Sciences, 3*(5), 257660.

Özbek, B., & Dadali, G. (2007). Thin-layer drying characteristics and modelling of mint leaves undergoing microwave treatment. *Journal of Food Engineering, 83*(4), 541-549.

Pagano, A. M., & Mascheroni, R. H. (2005). Sorption isotherms for amaranth grains. *Journal of Food Engineering, 67*(4), 441-450.

Pan, M., Zheng, Z., Huang, R., Zhou, X., Huang, H., Pan, J., & Chen, Z. (2019). Reduction in PM and NOX of a diesel engine integrated with n-octanol fuel addition and exhaust gas recirculation. *Energy, 187*, 115946.

Pati, J. R., Hotta, S. K., & Mahanta, P. (2015). Effect of waste heat recovery on drying characteristics of sliced ginger in a natural convection dryer. *Procedia Engineering, 105*, 145-152.

Perea-Moreno, A.J., Juaidi, A., & Manzano-Agugliaro, F., (2016). Solar greenhouse dryer system for wood chips improvement as biofuel. *Journal of Cleaner Production, 135*, 1233-1241.

Perry, R. H., and Green, D. W., (1997). *Perry's Chemical Engineers' Handbook*. 7th edition. McGraw-Hill, New York.

Phartyal, S. S., Thapliyal, R. C., Nayal, J. S., Rawat, M. M. S., & Joshi, G. (2003). The influences of temperatures on seed germination rate in Himalayan elm (*Ulmus wallichiana*). *Seed Science and Technology*, *31*(1), 83-93.

Poovizhi, M., & Sujatha, K. (2020). Improvement in seed germination by priming treatments in Black nightshade (Solanum nigrum L.). *Journal of Applied and Natural Science*, *12*(2), 8.

Popli, S., Rodgers, P., & Eveloy, V. (2012). Trigeneration scheme for energy efficiency enhancement in a natural gas processing plant through turbine exhaust gas waste heat utilization. *Applied Energy, 93*, 624-636.

Prakash, O., & Kumar, A. (2013). Historical review and recent trends in solar drying systems. *International Journal of Green Energy, 10* (7), 690-738.

Prakash, O., & Kumar, A. (2014a). Design, development, and testing of a modified greenhouse dryer under conditions of natural convection. *Heat Transfer Research, 45*(5), 433-451.

Prakash, O., & Kumar, A. (2014b). Solar greenhouse drying: a review. *Renewable and Sustainable Energy Review, 29*, 905-910.

Prakash, O., Kumar, A., & Laguri, V. (2016). Performance of modified greenhouse dryer with thermal energy storage. *Energy Reports, 2*, 155-162.

Pruim, R. J., Kaplan, D. T., & Horton, N. J. (2017). The mosaic package: helping students to 'think with data' using R. *The R Journal*, *9*(1), 77-102.

Pukacka, S., & Wójkiewicz, E. (2003). The effect of the temperature of drying on viability and some factors affecting storability of Fagus sylvatica seeds. *Acta Physiologiae Plantarum*, *25*, 163-169.

Quoilin, S., Aumann, R., Grill, A., Schuster, A., Lemort, V., & Spliethoff, H. (2011). Dynamic modelling and optimal control strategy of waste heat recovery using organic Rankine cycles. *Applied Energy, 88*(6), 2183-2190.

R Core Team (2023). R: A language and Environment for Statistical Computing. R Foundation for Statistical Computing, Vienna, Austria. Retrieved from https://www.R-project.org/.

Rapp, B. E. (2016). *Microfluidics: modeling, mechanics, and mathematics*. New Jersey: William Andrew.

Ratti, C. (1994). Shrinkage during drying of foodstuffs. *Journal of Food Engineering*, *23*(1), 91-105.

Reed, R. C., Bradford, K. J., & Khanday, I. (2022). Seed germination and vigor: ensuring crop sustainability in a changing climate. *Heredity, 128*(6), 450-459.

Roberts, E. H. (1972). Storage environment and the control of viability. *Viability of Seeds*, 14-58.

Rockland, L. B. (1969). Water activity and storage stability. *Food Technology, 23*, 1241-1248.

Rolke, W., & Gongora, C. G. (2021). A chi-square goodness-of-fit test for continuous distributions against a known alternative. *Computational Statistics, 36*(3), 1885-1900.

Ronoh, E. K., C. L. Kanali, J. T. Mailutha, & D. Shitanda. (2010). Thin layer drying characteristics of amaranth grains in a natural convection solar tent dryer. *The Kenya Journal of Mechanical Engineering, 6*(2), 1-12.

Ronoh, E. K., Kanali, C. L., Mailutha, J. T., & Shitanda, D. (2009). Modeling thin layer drying of amaranth seeds under open sun and natural convection solar tent dryer. *Agricultural Engineering International: the CIGR Ejournal. Manuscript*, *1420*(XI). November 2009.

Ronoh, E. K., Ndirangu, S. N., Kiburi, F. G., Kipsang, M. J., & Rutto, E. J. (2020). Evaluation of thin layer drying models for simulating drying kinetics of jackfruit slices in a solar greenhouse dryer. *African Journal of Horticultural Science*, *17*, 31-42.

Ronoh, E.K., Kanali, C.L., Mailutha, J.T. and Shitanda, D. (2012). Evaluation of solar energy dryer systems on drying behaviour and quality attributes of amaranth grains. *International Journal of Energy Science, 2*(5), 189-194.

Rubaiyat, S. N. H., & Bari, S. (2010). *Waste heat recovery using shell and tube heat exchanger from the exhaust of an automotive engine*, Unpublished PhD dissertation, Bangladesh: Bangladesh Society of Mechanical Engineers.

Saipari, E., Goswami, A. M., & Dadlani, M. (1998). Effect of seed drying on germination behaviour in citrus. *Scientia Horticulturae, 73*(2-3), 185-190.

Samapundo, S., Devlieghere, F., Meulenaer, B., Atukwase, A., Lamboni, Y. and Debevere, J. M. (2007). Sorption isotherms and isosteric heats of sorption of whole yellow dent corn. *Journal of Food Engineering, 79*, 168-176.

Samuels, J. (2015). Biodiversity of food species of the Solanaceae family: A preliminary taxonomic inventory of subfamily *Solanoideae*. *Resources*, *4*(2), 277-322.

San Marin, M. B., Mate, J. I., Fernandez, T., & Virseda, P. (2001). Modelling adsorption equilibrium moisture characteristics of rough rice. *Drying Technology*, *19*(3-4), 681-690.

Sangamithra, A., Swamy, G. J., Prema, R. S., Priyavarshini, R., Chandrasekar, V., & Sasikala, S., (2014). An overview of a polyhouse dryer. Renew. *Renewable and Sustainable Energy Reviews*, *40*, 902-910.

Sathiamurthi, P. (2011). Design and development of waste heat recovery system for air conditioning. *Unit European Journal of Scientific Research*, *54*(1), 102-110.

Sawant, P., Warstler, M., & Bari, S. (2018). Exhaust tuning of an internal combustion engine by the combined effects of variable exhaust pipe diameter and an exhaust valve timing system. *Energies*, *11*(6), 1545.

Scherr, S. J., Shames, S., & Friedman, R. (2012). From climate-smart agriculture to climate-smart landscapes. *Agriculture & Food Security*, *1*(1), 1-15.

Schippers, R. (1998). Notes on huckleberry, Solanum scabrum and related black nightshade species. *Natural Resource Institute, University of Greenwich.* Retrieved from http://www. dfid. gov. uk/r4d/pdf/outputs/R6964a.

Scott, S. J., Jones, R. A., & Williams, W. (1984). Review of data analysis methods for seed germination 1. *Crop Science*, *24*(6), 1192-1199.

Sethi, V. P., & Sharma, S. K. (2008). Survey and evaluation of heating technologies for worldwide agricultural greenhouse applications. *Solar Energy*, *82*(9), 832-859.

Sharma, A., Chen, C. R., & Lan, N. V. (2009). Solar-energy drying systems: a review *Renewable and Sustainable Energy Review, 13* (6-7), 1185-1210.

Sharp, J. R. (1982). A review of low temperature drying simulation models. *Journal of Agricultural Engineering Research*, *27*(3), 169-190.

Shepard, D. (2021). UN Communications on Climate Change: Letting People Know the Facts. In *World Scientific Encyclopedia of Climate Change: Case Studies of Climate Risk, Action, and Opportunity 3*, 15-20.

Siddiqui, M. A., Khaliq, A., & Kumar, R. (2021). Proposal and analysis of a novel cooling-power cogeneration system driven by the exhaust gas heat of HCCI engine fueled by wet-ethanol. *Energy*, *232*, 120954.

Simal, S., Femenia, A., Castell-Palou, A. and Rosselló, C. (2007). Water desorption thermodynamic properties of pineapple. *Journal of Food Engineering*, *80*, 1293-1301.

Soares, M. A. B., Jorge, L. M. D. M., & Montanuci, F. D. (2016). Drying kinetics of barley grains and effects on the germination index. *Food Science and Technology*, *36*, 638-645.

Sopade, P. A., & Ajisegiri, E. S. (1994). Moisture sorption study on Nigerian foods: maize and sorghum. *Journal of Food Process Engineering*, *17*(1), 33-56.

Speiss, W. E. L., & Wolf, W. (1987). Critical evaluation of methods to determine moisture sorption isotherms. In L. B. Rokcland & L. R. Beuchat (Eds.), *Water activity: Theory and applications to foods*. New York: Marcel Dekker Inc.

Srinivasan, G., & Muthukumar, P. (2021). A review on solar greenhouse dryer: Design, thermal modelling, energy, economic and environmental aspects. *Solar Energy*, *229*, 3-21.

Sun, Da-Wen (1999). Comparison and selection of EMC/ERH isotherm equations for rice. *Journal of Stored Products Research*, *35*, 249-264.

Sun, Da-Wen, & Byrne, C. (1998). Selection of EMC/MRH isotherms for rapeseeds. *Journal of Agricultural Engineering Research*, *69*, 307-315.

Sun, Da-Wen, & Woods, J. L. (1994). Low temperature moisture transfer characteristics of barley: thin-layer models and equilibrium isotherms. *Journal of Agricultural Engineering Research, 54*(4), 273-283.

Sun, Da-Wen, & Woods, J. L. (1997a). Simulation of heat and moisture transfer process during drying and in deep grain beds. *Drying Technology, 15*, 2479-2508.

Sun, Da-Wen, & Woods, J. L. (1997b). Deep bed simulation of the cooling of stored grain with ambient air: a test bed for ventilation control strategies. *Journal of Stored Products Research, 33*, 299-312.

Tang, R., Gao, W., Yu, Y., & Chen, H. (2009). Optimal tilt-angles of all-glass evacuated tube solar collectors. *Energy*, *34*(9), 1387-1395.

Tavousi, E., Perera, N., Flynn, D., & Hasan, R. (2023). Heat transfer and fluid flow characteristics of the passive method in double tube heat exchangers: a critical review. *International Journal of Thermofluids,* 100282.

Tawalbeh, M., Khan, H. A., Al-Othman, A., Almomani, F., & Ajith, S. (2023). A comprehensive review on the recent advances in materials for thermal energy storage applications. *International Journal of Thermofluids*, 100326.

Thakar, R., Bhosle, S., & Lahane, S. (2018). Design of heat exchanger for waste heat recovery from exhaust gas of diesel engine. *Procedia Manufacturing*, *20*, 372-376.

Thompson, T. L., Peart, R. M., & Foster, G. H. (1968). Mathematical simulation of corn drying – a new model. *Transaction of the ASAE, 24*(3), 582-586.

Thuy, N. X., Choudhary, M. A., & Hampton, J. G. (1999). The effects of high drying temperature and tempering on development of stress cracks and germination of maize seed (Zea mays L.). *Seed Science and Technology*, *27*(2), 507-515.

Tiwari, G. N., Kumar, S., & Prakash, O. (2004). Evaluation of convective mass transfer coefficient during drying of jaggery. *Journal of food engineering*, *63*(2), 219-227.

Tiwari, S., Tiwari, G. N., & Al-Helal, I. M. (2016). Development and recent trends in greenhouse dryer: A review. *Renewable and Sustainable Energy Review*, *65*, 1048-1064.

Tolaba, M. P., Peltzer, M., Enriquez, N., & Pollio, M. A. (2004). Grain sorption equilibria of quinoa grains. *Journal of Food Engineering, 61*, 365-371.

Toneatti, L., Deluca, C., Fraleoni Morgera, A., Piller, M., & Pozzetto, D. (2022). Waste to Energy Onboard Cruise Ships: A New Paradigm for Sustainable Cruising. *Journal of Marine Science and Engineering*, *10*(4), 480.

Travlos, I., Gazoulis, I., Kanatas, P., Tsekoura, A., Zannopoulos, S., & Papastylianou, P. (2020). Key factors affecting weed seeds' germination, weed emergence, and their possible role for the efficacy of false seedbed technique as weed management practice. *Frontiers in Agronomy*, *2*, 1.

Uluko, H., Kanali, C. L., Mailutha, J. T., & Shitanda, D. (2006). A finite element model for the analysis of temperature and moisture distribution in a solar grain dryer. *The Kenya Journal of Mechanical Engineering*, *2*(1), 47-56.

Van der Berg, C. (1984). Description of water activity of foods for engineering purposes by means of the GAB model of sorption. In B. M. McKeenna (Ed.), *Engineering and foods*. New York: Elsevier Science Publishers.

Wahile, G. S., Malwe, P. D., & Kolhe, A. V. (2020). Waste heat recovery from exhaust gas of an engine by using a phase change material. *Materials Today: Proceedings*, *28*, 2101-2107.

Wang, L. W., Wang, R. Z., Wu, J. Y., Wang, K., & Wang, S. G. (2004). Adsorption ice makers for fishing boats driven by the exhaust heat from diesel engine:

choice of adsorption pair. *Energy Conversion and Management*, *45*(13-14), 2043-2057.

Wang, L. W., Wang, R. Z., Lu, Z. S., & Chen, C. J. (2006a). Studies on split heat pipe type adsorption ice-making test unit for fishing boats: choice of heat pipe medium and experiments under unsteady heating sources. *Energy Conversion and Management*, *47*(15-16), 2081-2091.

Wang, L. W., Wang, R. Z., Wu, J. Y., Xu, Y. X., & Wang, S. G. (2006b). Design, simulation, and performance of a waste heat driven adsorption ice maker for fishing boat. *Energy*, *31*(2-3), 244-259.

Wang, T., Zhang, Y., Zhang, J., Shu, G., & Peng, Z. (2013). Analysis of recoverable exhaust energy from a light-duty gasoline engine. *Applied Thermal Engineering*, *53*(2), 414-419.

Waqas, M., Korres, N. E., Khan, M. D., Nizami, A. S., Deeba, F., Ali, I., & Hussain, H. (2019). Advances in the concept and methods of seed priming. *Priming and pretreatment of seeds and seedlings: Implication in plant stress tolerance and enhancing productivity in crop plants*, 11-41.

Weisser, H. (1985). Influence of temperature on sorption equilibria. In: D. Simantos & J. L. Multon (Eds.), *Properties of water in foods in relation to quality and stability* (95-118). Dordrecht, The Netherlands: Martinus Nijhoff Publishers.

Whitehouse, K. J., Hay, F. R., & Lusty, C. (2020). Why seed physiology is important for genebanking. *Plants*, 9(5), 584.

Wilberforce, T., & Muhammad, I. (2023). Dynamic modelling and analysis of Organic Rankine Cycle power units for the recovery of waste heat from 110kW Proton Exchange Membrane Fuel cell system. *International Journal of Thermofluids*, 100280.

Wolf, W., Speiss, W. E. L., & Jung, G. (1985). Standardization of isotherm measurements (cost project 90 and 90 bis). In D. Simantos & J. L. Multon (Eds.), *Properties of water in foods in relation to quality and stability* (661-679). Dordrecht, The Netherlands: Martinus Nijhoff Publishers.

Xie, Y., Lin, Y., Li, X., Yang, H., Han, J., Shang, C., ... & Lu, F. (2023). Peanut drying: Effects of various drying methods on drying kinetic models, physicochemical properties, germination characteristics, and microstructure. *Information Processing in Agriculture*, *10*(4), 447-458.

Yadoo, A., & Cruickshank, H. (2012). The role for low carbon electrification technologies in poverty reduction and climate change strategies: A focus on renewable energy mini grids with case studies in Nepal, Peru, and Kenya. *Energy Policy*, *42*, 591-602.

Yaldiz, O., Ertekin, C., & Uzun, H. I. (2001). Mathematical modeling of thin layer solar drying of sultana grapes. *Energy*, *26*(5), 457-465.

Yi, F., Wang, Z., Baskin, C. C., Baskin, J. M., Ye, R., Sun, H., ... & Huang, Z. (2019). Seed germination responses to seasonal temperature and drought stress are species-specific but not related to seed size in a desert steppe: Implications for effect of climate change on community structure. *Ecology and Evolution*, *9*(4), 2149-2159.

Zhang, Z., Liu, H., Yue, Z., Li, Y., Liang, H., Kong, X., ... & Yao, M. (2023). Effects of intake high-pressure compressed air on thermal-work conversion in a stationary diesel engine. *International Journal of Green Energy*, *20*(3), 338-351.

Zhang, Z., Liu, H., Yue, Z., Wu, Y., Kong, X., Zheng, Z., & Yao, M. (2022). Effects of multiple injection strategies on heavy-duty diesel energy distributions and emissions under high peak combustion pressures. *Frontiers in Energy Research*, *10*, 857077.

Zheng, Z., Xia, M., Liu, H., Wang, X., & Yao, M. (2018). Experimental study on combustion and emissions of dual fuel RCCI mode fuelled with biodiesel/n-butanol, biodiesel/2, 5-dimethylfuran and biodiesel/ethanol. *Energy*, *148*, 824-838.

Zheng, Z., Yue, L., Liu, H., Zhu, Y., Zhong, X., & Yao, M. (2015). Effect of two-stage injection on combustion and emissions under high EGR rate on a diesel engine by fuelling blends of diesel/gasoline, diesel/n-butanol, diesel/gasoline/n-butanol, and pure diesel. *Energy Conversion and Management*, *90*, 1-11.

APPENDICES

Appendix I: Tables

Table A.1: Basic parameters of diesel engine used in this study

Item	Content
IC engine type	Single cylinder
Bore (mm)	75
Stroke (mm)	80
Displacement (L)	0.353
Compression ratio	21:1
Specific fuel consumption (kg/kWh)	0.2802
Maximum Speed (rpm)	2500
Mean effective pressure (kN/m^2)	576
Valve clearance (mm)	Inlet valve 0.15-0.25; Exhaust valve 0.25-0.35
Fuel tank capacity (L)	4
Rated power (kW)	4.4
Injection pressure (kN/m^2)	$1.42 \times 10^4 \pm 5 \times 10^2$
Cooling mode	Water cooled
Intake mode	Naturally aspirated

Table A.2: Physical properties of air (P=101.13 kPa)

T	ρ	h	s	C_P	μ	k
-13.15	1.340	260.0	6.727	1.006	1.65×10^{-5}	0.0231
6.85	1.245	280.2	6.802	1.006	1.75×10^{-5}	0.0247
26.85	1.161	300.3	6.871	1.007	1.85×10^{-5}	0.0263
76.85	0.995	350.7	7.026	1.009	2.08×10^{-5}	0.0301
126.85	0.871	401.2	7.161	1.014	2.30×10^{-5}	0.0336
176.85	0.774	452.1	7.282	1.021	2.51×10^{-5}	0.0371
226.85	0.696	503.4	7.389	1.030	2.70×10^{-5}	0.0404
326.85	0.580	607.5	7.579	1.051	3.06×10^{-5}	0.0466
526.85	0.435	822.5	7.888	1.099	3.70×10^{-5}	0.0577
726.85	0.348	1046.8	8.138	1.141	4.24×10^{-5}	0.0681
926.85	0.290	1278	8.349	1.175	4.73×10^{-5}	0.0783
1126.85	0.249	1515	8.531	1.207	5.27×10^{-5}	0.0927

Table A.3: Suitability of galvanized iron as fabricating material

Property	Value
Specific heat capacity (kJ/kg.℃)	0.4605
Thermal conductivity (W/m.℃)	59
Melting point (℃)	1536.85
Density kg/m^3	7849
Thickness (mm)	1.6

Table A.4: Dimensional properties of connectors, tubes, and exhaust gas mass

Property	CN1	CN2	CN3	CN4	CN5	CN6	TB1	TB2	TB3	TB4	TB5	TB6
Distance from exhaust manifold (m)	2.1	5.0	7.8	10.7	13.5	16.3	4.6	7.4	10.3	13.1	15.9	18.8
Volume (m^3)	0.004	0.3	0.6	0.9	1.2	1.5	0.3	0.6	0.9	1.2	1.5	1.8
Mass of exhaust gas (kg)	0.003	0.2	0.4	0.7	0.9	1.1	0.2	0.4	0.7	0.9	1.1	1.3

Table A.5: Exhaust gas residence time in connectors and tubes

DES (rpm)	Q_{ex}(m^3/s)	Elapsed time for exhaust gas to fill connectors and tubes of heat exchanger (seconds)											
		CN1	CN2	CN3	CN4	CN5	CN6	TB1	TB2	TB3	TB4	TB5	TB6
750	0.0042	1.00	71	140	210	279	349	70	140	210	279	349	418
1000	0.0048	0.88	62	123	185	246	307	62	123	184	246	307	368
1250	0.0111	0.38	27	53	80	106	133	27	53	80	106	133	159
1500	0.0123	0.34	24	48	72	95	119	24	48	71	95	119	143
1750	0.0140	0.30	21	42	63	84	105	21	42	63	84	105	126
2000	0.0154	0.27	19	38	57	76	95	19	38	57	76	95	114
2250	0.0158	0.27	19	37	56	74	93	19	37	56	74	93	111
2500	0.0167	0.25	18	35	53	70	88	18	35	53	70	88	105

Table A.6: Exhaust gas properties corresponding to engine speed

DES (rpm)	T_{ex}(℃)	$\dot{m}_{ex}$(kg/h)	$\dot{Q}_{ex}$(m^3/s)	V_{cn} (m/s)	V_{tb} (m/s)	Re_{cn}	Re_{tb}	Nu_{cn}	Nu_{tb}	$\dot{A}_{ex}$ (kJ/h)
750	197.19	11.32	0.0042	2.14	0.035	2681	344	14	3.66	2082.32
1000	213.47	12.87	0.0048	2.43	0.040	3048	391	16	3.66	2591.28
1250	238.54	29.79	0.0111	5.63	0.093	7055	905	31	3.66	6795.84
1500	325.07	33.21	0.0123	6.28	0.103	7865	1008	34	3.66	10645.96
1750	352.94	37.65	0.0140	7.11	0.117	8917	1143	37	3.66	13190.24
2000	359.82	41.46	0.0154	7.83	0.129	9819	1259	40	3.66	14829.75
2250	356.98	42.53	0.0158	8.04	0.132	10073	1291	41	3.66	15083.44
2500	357.36	45.07	0.0167	8.52	0.140	10674	1368	43	3.66	16002.56

Table A.7: Kinetic energy of exhaust gas within the heat exchanger

V_{CN} (m/s)	V_{TB} (m/s)	Kinetic energy (kJ)											
		CN1	CN2	CN3	CN4	CN5	CN6	TB1	TB2	TB3	TB4	TB5	TB6
2.14	0.035	0.007	0.51	1.01	1.51	2.01	2.51	0.00014	0.00027	0.00041	0.00054	0.00068	0.00081
2.43	0.040	0.009	0.66	1.30	1.95	2.60	3.24	0.00018	0.00035	0.00053	0.00070	0.00088	0.00105
5.63	0.093	0.050	3.52	6.98	10.45	13.92	17.38	0.00095	0.00188	0.00282	0.00376	0.00469	0.00563
6.28	0.103	0.062	4.37	8.68	12.99	17.30	21.60	0.00118	0.00234	0.00351	0.00467	0.00583	0.00700
7.11	0.117	0.079	5.62	11.15	16.69	22.23	27.77	0.00151	0.00301	0.00451	0.00600	0.00750	0.00899
7.83	0.129	0.096	6.81	13.53	20.24	26.96	33.67	0.00184	0.00365	0.00546	0.00728	0.00909	0.01091
8.04	0.132	0.101	7.17	14.23	21.30	28.36	35.43	0.00193	0.00384	0.00575	0.00766	0.00957	0.01148
8.52	0.140	0.114	8.05	15.98	23.92	31.85	39.79	0.00217	0.00431	0.00646	0.00860	0.01074	0.01289

Table A.8: Major head losses in connectors

Re_{CN}	f_{CN}	Frictional head loss in connectors (m)					
		CN1	CN2	CN3	CN4	CN5	CN6
2681	0.1860	0.7	1.6	2.5	3.5	4.4	5.3
3048	0.1637	0.9	2.0	3.2	4.3	5.5	6.6
7055	0.0707	4.3	10	16	21	27	33
7865	0.0635	5.3	12	19	27	34	41
8917	0.0560	6.7	16	25	34	42	51
9819	0.0508	8.1	19	30	40	51	62
10073	0.0496	8.4	20	31	42	53	65
10674	0.0468	9.3	22	34	46	59	71

Table A.9: Major head losses in tubes

Re_{TB}	f_{TB}	Frictional head loss in tubes (m)					
		TB1	TB2	TB3	TB4	TB5	TB6
344	0.0700	0.00014	0.00022	0.00031	0.00039	0.00048	0.00056
391	0.0675	0.00016	0.00025	0.00035	0.00045	0.00054	0.00064
905	0.0625	0.00036	0.00059	0.00081	0.00104	0.00126	0.00148
1008	0.0620	0.00040	0.00065	0.00090	0.00116	0.00141	0.00166
1143	0.0610	0.00046	0.00074	0.00103	0.00131	0.00159	0.00188
1259	0.0605	0.00050	0.00082	0.00113	0.00144	0.00175	0.00207
1291	0.0600	0.00052	0.00084	0.00116	0.00148	0.00180	0.00212
1368	0.0590	0.00055	0.00089	0.00123	0.00157	0.00191	0.00225

Table A.10: Experimental and predicted data from forced convection solar drying mode

Drying Time (hours)	Experimental T_r (°C)	Predicted T_r (°C)	Experimental T_b (°C)	Predicted T_b (°C)	Experimental m_{ev} (g)	Predicted m_{ev} (g)	γ_v (%)
0	14.82	14.98	11.27	9.16	0	0	0.88
1	22.36	21.87	19.34	16.47	20.80	18.78	0.68
2	38.35	36.26	35.52	32.95	10.53	9.68	0.36
3	40.81	38.99	37.95	35.85	5.70	5.31	0.27
4	46.94	45.04	43.47	42.42	3.14	2.97	0.2
5	54.14	52.15	51.45	52.37	1.91	1.84	0.14
6	50.85	49.93	47.56	48.12	1.30	1.28	0.15
7	54.75	54.22	51.77	53.79	0.84	0.86	0.13
8	58.46	58.41	55.02	58.50	0.61	0.64	0.09
9	51.64	53.02	48.41	51.03	0.46	0.51	0.14
10	37.03	40.46	34.39	35.82	0.35	0.40	0.27
11	29.05	33.93	26.55	28.54	0.29	0.35	0.37

Table A.11: Experimental and predicted data from forced convection solar-exhaust gas drying mode

Drying Time (hours)	Experimental T_r (℃)	Predicted T_r (℃)	Experimental T_b (℃)	Predicted T_b (℃)	Experimental m_{ev} (g)	Predicted m_{ev} (g)	γ_v (%)
0	34.49	31.38	35.00	31.83	0	0	0.39
1	41.79	38.83	42.22	39.29	17.79	16.17	0.27
2	50.05	47.61	50.22	47.90	9.09	8.40	0.15
3	50.05	47.87	50.17	48.23	4.76	4.46	0.15
4	51.93	50.17	52.18	50.78	2.41	2.30	0.12
5	58.61	57.77	58.99	58.66	1.54	1.50	0.12
6	61.97	61.89	62.10	62.65	0.84	0.85	0.10
7	61.49	61.76	61.95	63.04	0.78	0.79	0.08
8	59.64	60.12	59.84	61.25	0.74	0.76	0.07
9	58.75	59.58	59.02	60.93	0.70	0.72	0.07
10	56.34	57.38	56.55	58.78	0.65	0.67	0.08

Table A.12: Experimental and predicted data from forced convection exhaust gas drying mode

Drying Time (hours)	Experimental T_r (°C)	Predicted T_r (°C)	Experimental T_b (°C)	Predicted T_b (°C)	Experimental m_{ev} (g)	Predicted m_{ev} (g)	γ_v (%)
0	25.75	25.57	25.94	25.20	0	0	0.52
1	27.50	27.44	27.98	27.27	22.33	22.89	0.60
2	28.26	28.27	28.43	27.76	11.00	11.51	0.67
3	28.62	28.68	28.91	28.30	5.80	6.15	0.76
4	29.26	29.39	29.98	29.45	3.19	3.43	0.84
5	28.62	28.74	29.02	28.55	1.93	2.11	0.74
6	28.62	28.78	29.26	28.88	1.30	1.45	0.74
7	30.77	31.13	31.08	30.82	0.86	0.99	0.60
8	30.65	31.04	31.48	31.34	0.63	0.74	0.73
9	30.50	30.93	31.02	30.99	0.48	0.59	0.72
10	30.60	31.09	30.88	30.98	0.37	0.47	0.70
11	28.53	28.92	29.24	29.45	0.27	0.36	0.67
12	28.28	28.72	28.66	29.02	0.19	0.28	0.68
13	28.43	28.94	29.26	29.78	0.14	0.23	0.77
14	28.34	28.91	28.85	29.54	0.13	0.22	0.77

Table A.13: Models, drying modes, RMSE and model parameters

Model	Solar drying mode	Solar-exhaust gas drying mode	Exhaust gas drying mode
Black nightshade seeds temperature	$RMSE = 2.1409$	$RMSE = 1.9524$	$RMSE = 0.4859$
	$\xi_0 = 0.0495$	$\xi_0 = 0.1424$	$\xi_0 = 0.2382$
	$\xi_1 = 0.0426$	$\xi_1 = 0.0739$	$\xi_1 = 0.0145$
	$\xi_2 = 0.7515$	$\xi_2 = 0.8237$	$\xi_2 = 0.9100$
	$\xi_3 = 0.0002$	$\xi_3 = 0.0046$	$\xi_3 = 0.0005$
	$\xi_4 = 0.0385$	$\xi_4 = 0.0151$	$\xi_4 = 0.0053$
	$\xi_5 = 0.0047$	$\xi_5 = 0.0022$	$\xi_5 = 0.0016$
	$\varpi = 0.0495$	$\varpi = 0.1670$	$\varpi = 0.2433$
Moisture evaporated	$RMSE = 0.6455$	$RMSE = 0.5186$	$RMSE = 0.2453$
	$\Omega_0 = 0.0797$	$\Omega_0 = 0.0699$	$\Omega_0 = 0.0795$
	$\Omega_1 = 10.1707$	$\Omega_1 = 9.7564$	$\Omega_1 = 10.1707$
	$\Omega_2 = 0.9382$	$\Omega_2 = 0.8458$	$\Omega_2 = 0.9382$
	$\Omega_3 = 331.9957$	$\Omega_3 = 328.6183$	$\Omega_3 = 347.7691$
	$\Omega_4 = 0.0382$	$\Omega_4 = 0.0428$	$\Omega_4 = 0.0399$
	$\Omega_5 = 0.0729$	$\Omega_5 = 0.0660$	$\Omega_5 = 0.0761$
Greenhouse dryer room air temperature	$RMSE = 2.1257$	$RMSE = 1.7836$	$RMSE = 0.3392$
	$\zeta_0 = 1.1590$	$\zeta_0 = 0.2070$	$\zeta_0 = 0.2017$
	$\zeta_1 = 0.2880$	$\zeta_1 = 0.0460$	$\zeta_1 = 0.0154$
	$\zeta_2 = 0.8505$	$\zeta_2 = 0.8199$	$\zeta_2 = 0.9079$
	$\zeta_3 = 0.0052$	$\zeta_3 = 0.0030$	$\zeta_3 = 0.0001$
	$\zeta_4 = 0.0158$	$\zeta_4 = 0.0139$	$\zeta_4 = 0.0018$
	$\zeta_5 = 0.0002$	$\zeta_5 = 0.0023$	$\zeta_5 = 0.0028$
	$\varrho = 1.1824$	$\varrho = 0.1552$	$\varrho = 0.1504$

Table A.14: Average hourly data of the dryer parameters in solar mode

Drying Time (hours)	Outside RH (%)	Inside RH (%)	Outside Temperature (℃)	Inside Temperature (℃)
0	32.37	88.03	12.72	14.82
1	32.40	67.78	16.03	22.36
2	36.27	36.35	21.65	38.35
3	39.02	27.32	22.77	40.81
4	40.72	19.97	23.73	46.94
5	41.02	13.70	26.22	54.14
6	41.13	15.48	26.72	50.85
7	50.20	12.77	27.30	54.75
8	51.78	9.40	28.75	58.46
9	59.30	13.63	29.75	51.64
10	70.52	26.59	31.35	37.03
11	94.88	37.19	31.52	29.05

Table A.15: Average hourly data of the dryer parameters in solar-exhaust gas mode

Drying Time (hours)	Outside RH (%)	Inside RH (%)	Outside Temperature (℃)	Inside Temperature (℃)
0	68.15	39.27	20.75	34.49
1	53.93	27.19	24.80	41.79
2	40.13	14.84	28.80	50.05
3	40.13	14.84	28.80	50.05
4	13.35	11.78	47.65	51.93
5	9.88	12.27	53.00	58.61
6	9.55	9.55	51.05	61.97
7	9.15	7.68	51.65	61.49
8	8.75	7.10	52.48	59.64
9	11.20	7.31	47.95	58.75
10	10.95	8.29	48.55	56.34

Table A.16: Average hourly data of the dryer parameters in exhaust gas mode

Drying Time (hours)	Outside RH (%)	Inside RH (%)	Outside Temperature (℃)	Inside Temperature (℃)
0	54.70	51.88	22.05	25.75
1	58.05	59.80	21.35	27.50
2	61.40	67.28	20.85	28.26
3	63.85	76.37	20.50	28.62
4	67.70	83.98	19.85	29.26
5	69.55	74.25	19.60	28.62
6	69.55	74.25	19.60	28.62
7	55.50	59.66	22.20	30.77
8	57.55	72.85	21.85	30.65
9	58.60	71.77	21.55	30.50
10	60.30	70.31	21.30	30.60
11	61.60	67.25	20.90	28.53
12	63.50	68.10	20.50	28.28
13	66.20	76.82	20.10	28.43
14	66.20	76.98	19.90	28.34

Table A.17: Change in mass of black nightshade seeds during solar mode of drying

Time (h)	Mass (g)	Moisture Content (% db)	Drying Rate (g/g/h)	Moisture Ratio
0	50.00	89.34	0	1
1	29.20	71.2329	5.1106	0.7973
2	18.67	56.4006	2.5872	0.6313
3	12.97	43.9476	1.4005	0.4919
4	9.83	31.9430	0.7715	0.3575
5	7.92	24.1162	0.4693	0.2699
6	6.62	19.6375	0.3194	0.2198
7	5.78	14.5329	0.2064	0.1627
8	5.17	11.7988	0.1499	0.1321
9	4.71	9.7665	0.1130	0.1093
10	4.36	8.0275	0.0860	0.0899
11	4.07	7.1253	0.0713	0.0798

Table A.18: Change in mass of black nightshade seeds during solar-exhaust gas mode of drying

Time (h)	Mass (g)	Moisture Content (% db)	Drying Rate (g/g/h)	Moisture Ratio
0	50.00	92.57	0	1
1	32.21	55.2313	1.6626	0.5966
2	23.12	39.3166	0.8495	0.4247
3	18.36	25.9259	0.4449	0.2801
4	15.95	15.1097	0.2252	0.1632
5	14.41	10.6870	0.1439	0.1154
6	13.57	6.1901	0.0785	0.0669
7	12.79	6.0985	0.0729	0.0659
8	12.05	6.1411	0.0692	0.0663
9	11.35	6.1674	0.0654	0.0666
10	10.70	6.0748	0.0607	0.0656

Table A.19: Change in mass of black nightshade seeds during exhaust gas mode of drying

Time (h)	Mass (g)	Moisture Content (% db)	Drying Rate (g/g/h)	Moisture Ratio
0	50.00	88.84	0	1
1	27.67	80.7011	16.1812	0.9084
2	16.67	65.9868	7.9710	0.7428
3	10.87	53.3579	4.2029	0.6006
4	7.68	41.5365	2.3116	0.4675
5	5.75	33.5652	1.3986	0.3778
6	4.45	29.2135	0.9420	0.3288
7	3.59	23.9554	0.6232	0.2696
8	2.96	21.2838	0.4565	0.2396
9	2.48	19.3548	0.3478	0.2179
10	2.11	17.5355	0.2681	0.1974
11	1.84	14.6739	0.1957	0.1652
12	1.65	11.5152	0.1377	0.1296
13	1.51	9.2715	0.1014	0.1044
14	1.38	9.4203	0.0942	0.1060

Table A.20: Experimental and predicted moisture ratios data in solar mode of drying

Time (h)	Experimental	Newton	Page	Logarithmic	Henderson and Pabis
0	1	1	1	1.0145	1.0133
1	0.7973	0.7805	0.7931	0.7880	0.7882
2	0.6313	0.6092	0.6201	0.6122	0.6131
3	0.4919	0.4755	0.4821	0.4758	0.4769
4	0.3575	0.3711	0.3734	0.3701	0.3710
5	0.2699	0.2897	0.2884	0.2880	0.2886
6	0.2198	0.2261	0.2223	0.2244	0.2245
7	0.1627	0.1765	0.1709	0.1750	0.1746
8	0.1321	0.1377	0.1313	0.1367	0.1358
9	0.1093	0.1075	0.1007	0.1070	0.1057
10	0.0899	0.0839	0.0771	0.0839	0.0822
11	0.0798	0.0655	0.0590	0.0660	0.0639

Table A.21: Experimental and predicted moisture ratios data for solar-exhaust mode of drying

Time (h)	Experimental	Newton	Page	Logarithmic	Henderson and Pabis
0	1	1	1	0.9945	0.9777
1	0.5966	0.6470	0.6031	0.6236	0.6388
2	0.4247	0.4186	0.3997	0.3975	0.4174
3	0.2801	0.2708	0.2728	0.2596	0.2727
4	0.1632	0.1752	0.1896	0.1756	0.1782
5	0.1154	0.1134	0.1334	0.1244	0.1164
6	0.0669	0.0733	0.0949	0.0931	0.0761
7	0.0659	0.0475	0.0680	0.0741	0.0497
8	0.0663	0.0307	0.0490	0.0625	0.0325
9	0.0666	0.0199	0.0356	0.0554	0.0212
10	0.0656	0.0129	0.0259	0.0511	0.0139

Table A.22: Experimental and predicted moisture ratios data for exhaust mode of drying

Time (h)	Experimental	Newton	Page	Logarithmic	Henderson and Pabis
0	1	1	1	1.0425	1.0285
1	0.9084	0.8397	0.8476	0.8602	0.8589
2	0.7428	0.7050	0.7134	0.7112	0.7173
3	0.6006	0.5920	0.5988	0.5894	0.5990
4	0.4675	0.4970	0.5017	0.4897	0.5003
5	0.3778	0.4173	0.4197	0.4082	0.4178
6	0.3288	0.3504	0.3508	0.3415	0.3489
7	0.2696	0.2942	0.2929	0.2870	0.2914
8	0.2396	0.2471	0.2444	0.2424	0.2433
9	0.2179	0.2074	0.2037	0.2060	0.2032
10	0.1974	0.1742	0.1697	0.1762	0.1697
11	0.1652	0.1462	0.1414	0.1518	0.1417
12	0.1296	0.1228	0.1177	0.1318	0.1184
13	0.1044	0.1031	0.0979	0.1155	0.0988
14	0.1060	0.0866	0.0814	0.1022	0.0825

Appendix II: Plates

Plate B.1: Outside view of the solar-exhaust gas greenhouse dryer

Plate B.2: Inside view of the solar-exhaust gas greenhouse dryer

Plate B.3: Freshly harvested black nightshade berries

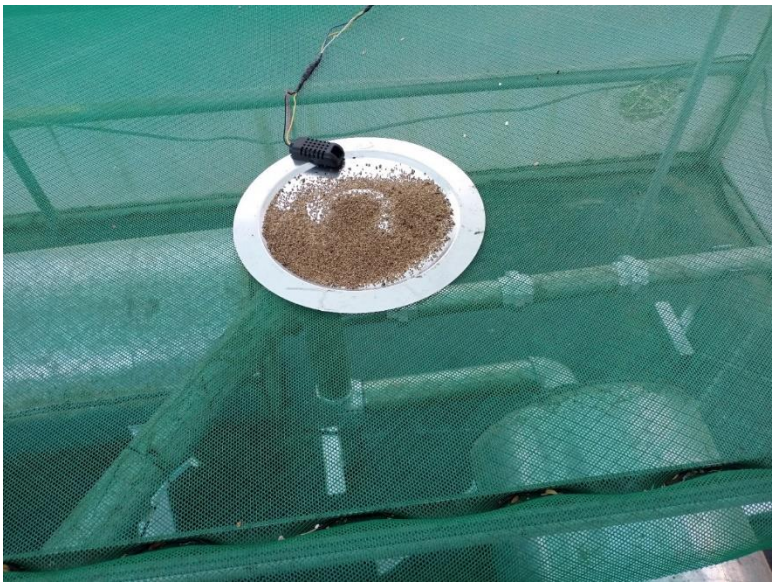

Plate B.4: Thin layer drying of black nightshade seeds on a drying tray

Plate B.5: Weighing black nightshade seeds

Plate B.6: Research engine test setup in thermofluids laboratory, JKUAT

Plate B.7: Location of thermocouple temperature sensors for exhaust gas

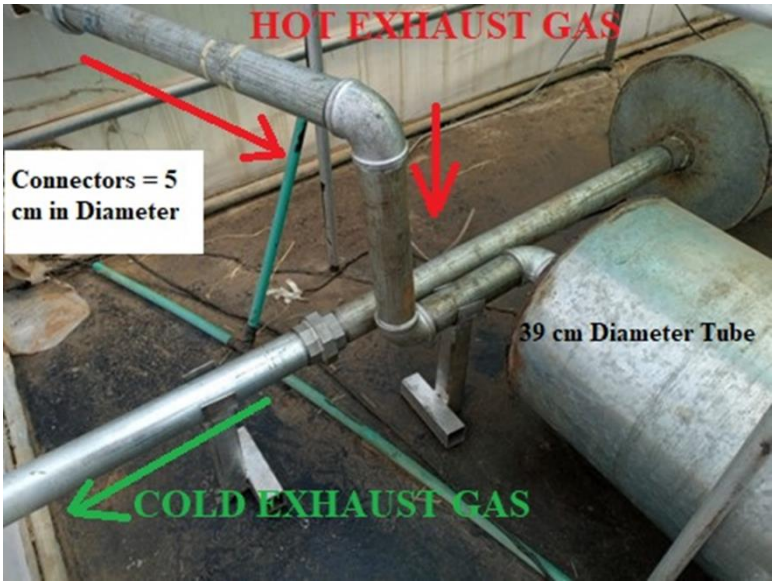

Plate B.8: Exhaust gas flow in connectors and tubes of hybrid recuperative heat exchanger

Plate B.9: Black nightshade (*solanum villosum*) vegetable crop

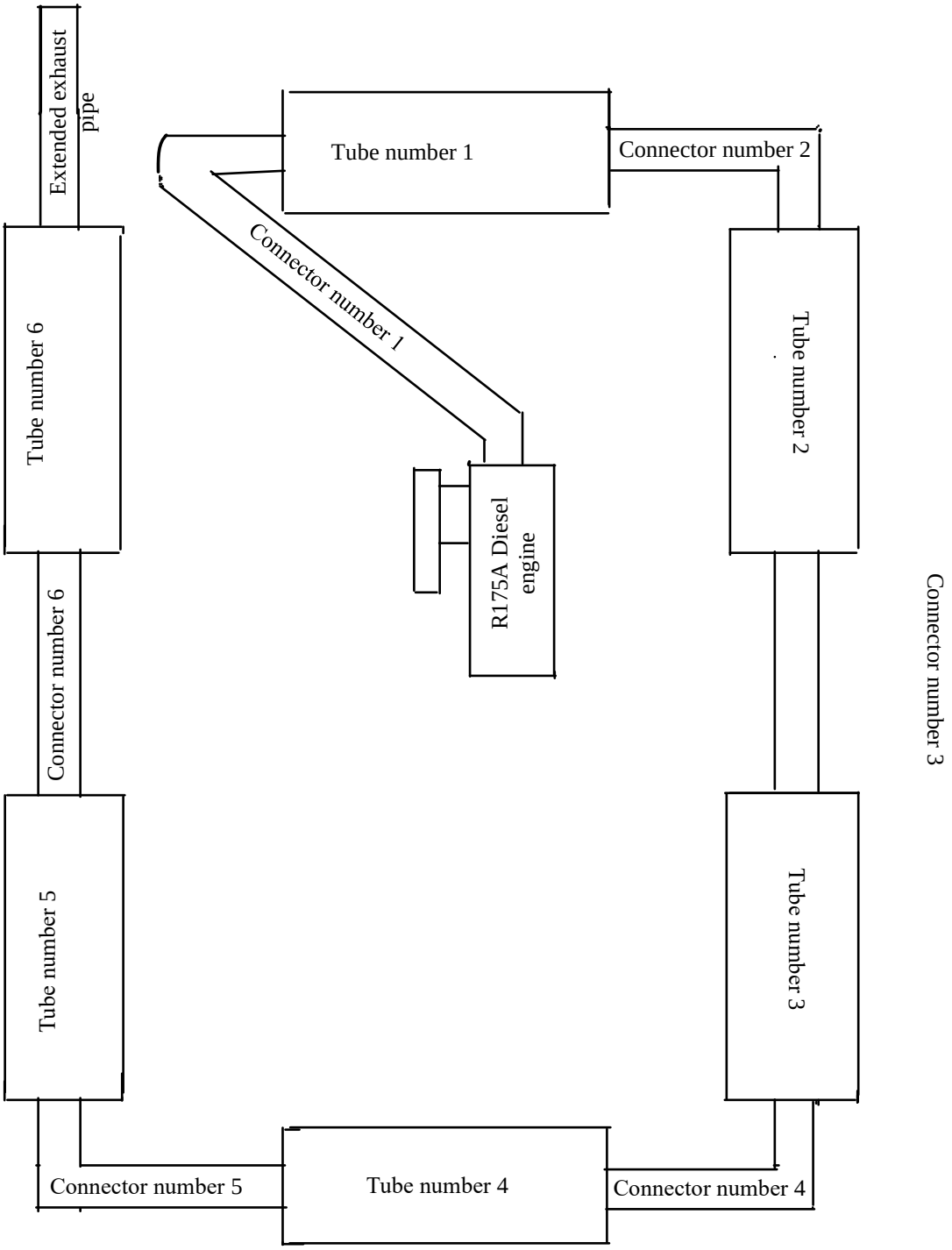

Plate B.10: Schematic diagram showing the layout of the diesel engine and heat exchanger

Appendix III: List of Published Papers from this Study

[1] Orido, G. O., Ronoh, E. K., Ajwang, P. O., & Gathitu, B. B. (2024). Fluid-thermal characteristics of solar-exhaust gas powered dryer: An experimental validation. *Results in Engineering*, 102205.

[2] Orido, G. O., Ronoh, E. K., Ajwang, P. O., & Gathitu, B. B. (2023). Performance Assessment of Hybrid Recuperative Heat Exchanger for Diesel Engine Generated Exhaust Gas. *International Journal of Thermofluids*, 19, August 2023, 100392.

[3] Orido, G. O., Ronoh, E. K., Ajwang, P. O., & Gathitu, B. B. (2023). Evaluation of Thin Layer Models for Simulating Drying Kinetics of Black Nightshade Seeds in a Solar-Exhaust Gas Greenhouse Dryer. *Bioprocess Engineering*, *7*(1), 10-31.

[4] Orido, G. O., Ronoh, E. K., Ajwang, P. O., & Gathitu, B. B. (2023). Influence of Solar-Exhaust Gas Greenhouse Drying Modes on Viability of Black Nightshade Seeds. *Journal of Chemical, Environmental and Biological Engineering*, *7*(2), 44-56.